Spring 2015

Nonviral gene delivery to the liver

Samuel Thomas Crowley
University of Iowa

NONVIRAL GENE DELIVERY TO THE LIVER

by

Samuel Thomas Crowley

A thesis submitted in partial fulfillment
of the requirements for the Doctor of
Philosophy degree in Pharmacy (Medicinal and Natural Products Chemistry)
in the Graduate College of
The University of Iowa

May 2015

Thesis Supervisor: Professor Kevin G. Rice

Graduate College
The University of Iowa
Iowa City, Iowa

CERTIFICATE OF APPROVAL

PH.D. THESIS

This is to certify that the Ph.D. Thesis of

Samuel Thomas Crowley

has been approved by the Examing Committee
for the thesis requirement for the Doctor of Philosophy
degree in Pharmacy (Medicinal and Natural Products Chemistry) at
the May 2015 graduation

Thesis Committee: _____
Kevin G. Rice, Thesis Supervisor

_____
Jonathan A. Doorn

_____
Robert J. Kerns

_____
David L. Roman

_____
Janice M. R. Staber

This thesis is dedicated to the trees that were sacrificed in the making of this document.

ACKNOWLEDGMENTS

I would like to thank Dr. Kevin Rice for his support and guidance during my graduate school career and the preparation of this thesis. I would also like to thank the other members of the Rice Lab for providing me with the peptides that made this research possible. I also thank the University of Iowa, the College of Pharmacy, the Center for Biocatalysis and Bioprocessing, and the American Foundation for Pharmaceutical Education for financial support.

I am also grateful for my wife, Kaitlin, whose support throughout graduate school has been necessary. She was also very helpful in checking this thesis for grammar and spelling mistakes. I would also like to thank my family, especially my father, who reminded me that graduate school could have been a lot worse.

ABSTRACT

Diseases of the liver have a large impact on human health. Genetic disorders, metabolic disorders, alcoholism, cancer, or infections can all impair liver function. If serious enough, a liver transplant may be necessary, a major surgical procedure which requires life-long immune suppression and relies on the availability of donor livers.

Gene therapy is being intensively studied as a potential method to treat many disorders, including disorders of the liver. While viral gene therapy has seen some success, possible side effects make it risky, so nonviral gene delivery vectors are being developed. Unfortunately, these nonviral vectors do not yet have the efficiency of the viral vectors.

Nonviral gene delivery vectors face many challenges in vivo. The vectors must protect DNA from nucleases while it moves through the bloodstream, they must avoid nonspecific uptake, they must be enter the correct cells, and must enter the nucleus before the DNA can be expressed. If any step of this process fails, there will be very little, if any, expression, and it may be impossible to determine what went wrong.

One impediment to nonviral gene delivery research is the transition from in vitro studies to in vivo studies. The cancer derived cell lines most often used for in vitro transfections are rapidly dividing, which makes nuclear entry much easier than in the whole animal. While primary cells would be a more accurate model of the in vivo environment, the number of cells that can be obtained from tissues is small, and primary cells usually cannot be cultured for long. This limits the number of experiments that can be done with each preparation of cells. To overcome this, we have miniaturized transfection assays, including the transfection of mouse primary hepatocytes with luciferase in 384 well plates. Because fewer cells are needed, more experiments can be performed with each liver preparation.

Another issue introduced by the differences between in vitro and in vivo research is circulatory stability. In vitro, large particles with strong positive charges are desired, because they sink down onto the cells and are attracted to the negatively charged cellular membranes. However, in vivo these particles will aggregate serum proteins and become lodged in narrow capillary beds in the lungs or other organs, often causing toxicity. While this behavior can usually be overcome through PEGylation, improving a particle's circulatory half-life will still improve its chances of finding the correct target. Scavenger receptors found on liver nonparenchymal cells are very efficient at removing negatively charged particles from the bloodstream. We have shown that dosing large amounts of PEGylated polyacridine DNA polyplex can saturate the scavenger receptors and improve circulatory half-life. We have also shown that large doses of PEGylated peptide, with or without acridine groups, can inhibit scavenger receptor uptake through the formation of peptide-protein nanoparticles. By inhibiting scavenger receptor uptake, DNA can be successfully hydrodynamically stimulated at times up to 12 hours post-delivery, demonstrating a longer circulatory half-life and suggesting a mechanism to explain how delayed hydrodynamic stimulation can achieve full level gene expression in the liver after the DNA has had time to circulate throughout the whole animal.

Once a nonviral vector finds its target cell, it must still enter the cell through endocytosis and then escape the endosome before it becomes digested in the lysosome. Before the DNA cargo can be expressed, it must enter the nucleus. Nuclear entry in nondividing cells is a major barrier to efficient gene delivery. One method to over come this barrier is to avoid the need for nuclear entry altogether by delivering mRNA instead of DNA. mRNA can produce protein in the cytoplasm by finding a ribosome and initiating translation. However, it is even less stable in the

bloodstream than DNA. We have produced an mRNA construct capable of high-level expression in the liver through hydrodynamic delivery. The PEGylated polyacridine peptides used to protect DNA were applied to mRNA and shown to enhance expression, allowing a 1 μg dose of mRNA peptide polyplex to produce higher expression than an equal dose of DNA. The peptides were also shown to provide some protection against nuclease digestion in serum. This suggests that efficient, if transient, protein expression can be achieved through peptide protected mRNA delivery.

However, DNA delivery is still desired for longer term expression, and the nuclear entry of DNA is still a problem. In an effort to help facilitate nuclear entry, the membrane disrupting enzyme phospholipase A2 was modified in several ways. The enzyme was conjugated with DNA binding peptides, nuclear localization peptides, and hepatocyte targeting oligosaccharides. Additionally, mutant forms of the enzyme were prepared in bacterial expression systems to achieve site-specific conjugation. Unfortunately, none of these efforts produced a useful tool for nuclear entry.

The research presented in this thesis represents some progress toward the goal of nonviral gene delivery to the liver. Hopefully, some of this work will be useful in the development of new treatments and therapies to improve human health.

PUBLIC ABSTRACT

Gene therapy has the potential to treat many diseases and disorders, including genetic disorders, diabetes, cancer, viral infections, and more. However, gene therapy requires that DNA is efficiently delivered to the correct cells in the correct tissue in the body. This is not easy, because enzymes in the blood and other fluids can destroy unprotected DNA on its way to these cells. Several chemicals have been created to bind to DNA and protect it during delivery.

A particularly effective group of these chemicals are known as PEGylated polyacridine peptides. These peptides have positive charges that bind to the negative charges on DNA, and acridine structures that fit in between the base pairs of the DNA double helix, allowing much tighter binding. The long polyethylene glycol, or PEG, chains attached to these peptides help to keep dangerous enzymes away from the DNA while it's moving through the blood.

This work not only further studied how PEGylated polyacridine peptides protect DNA, but also studied how they might be used to protect and deliver messenger RNA, or mRNA. mRNA is the chemical that carries information from DNA to make proteins, and may be used to treat some diseases like DNA can. However, mRNA is much harder to protect than DNA. Despite this challenge, low doses of protected mRNA were given to mice, and were able to produce more protein than an equal dose of DNA.

TABLE OF CONTENTS

LIST OF TABLES

LIST OF FIGURES

1 Gene Therapy for the Liver

1.1 Abstract

The liver is an incredibly important organ, vital to the metabolism of many compounds and the production of blood proteins. As such, several diseases and disorders can affect the liver and harm human health. Many of these are genetic, and could potentially be treated by a gene therapy. This chapter presents an overview of liver anatomy, several genetic disorders of the liver, and the development of nonviral gene delivery methods.

1.2 Anatomy and Function of the Liver

The liver has long been recognized as an important and unique organ. Greek myth describes how Prometheus stole fire from the gods and was punished by being tied to a rock, where a vulture would eat his liver, only to have it regenerate and be eaten again every day[1]. Assyrians, Babylonians, Hittites, and Etruscans all attempted to divine the future by studying the livers of sacrificed animals[2]. Many clay models of livers have been found in archeological sites throughout the Mediterranean and Middle East[3].

1.2.1 Gross Anatomy of the Liver

Clearly, our knowledge of the liver has greatly improved since ancient times. The liver is the primary filter of ingested material. It removes and metabolizes metals, environmental toxins, and pharmaceuticals. It scavenges bacteria and other particles from the blood[4]. It produces most of the proteins found in the blood, including albumin, transferrin, and clotting factors. The liver

is also important for glucose homeostasis, storing excess glucose as glycogen, and releasing it from glycogen when blood sugar is low[5].

The liver is the largest internal organ of the body, weighing about 1500g in the average adult human, approximately 2.5% of total body weight[6]. The organ is divided into 4 lobes. The anterior view of the liver shows the right and left lobes, divided by the falciform ligament (**Fig. 1-1**). From the posterior view, the caudal and quadrate lobes are also visible. The liver is located directly below the diaphragm, and is attached to the diaphragm by the coronary ligament. It receives nutrient rich blood from the gut through the portal vein, and oxygenated blood from the hepatic artery. The blood eventually leaves through the hepatic veins, which emerge from all four lobes, and attach to the inferior vena cava[5].

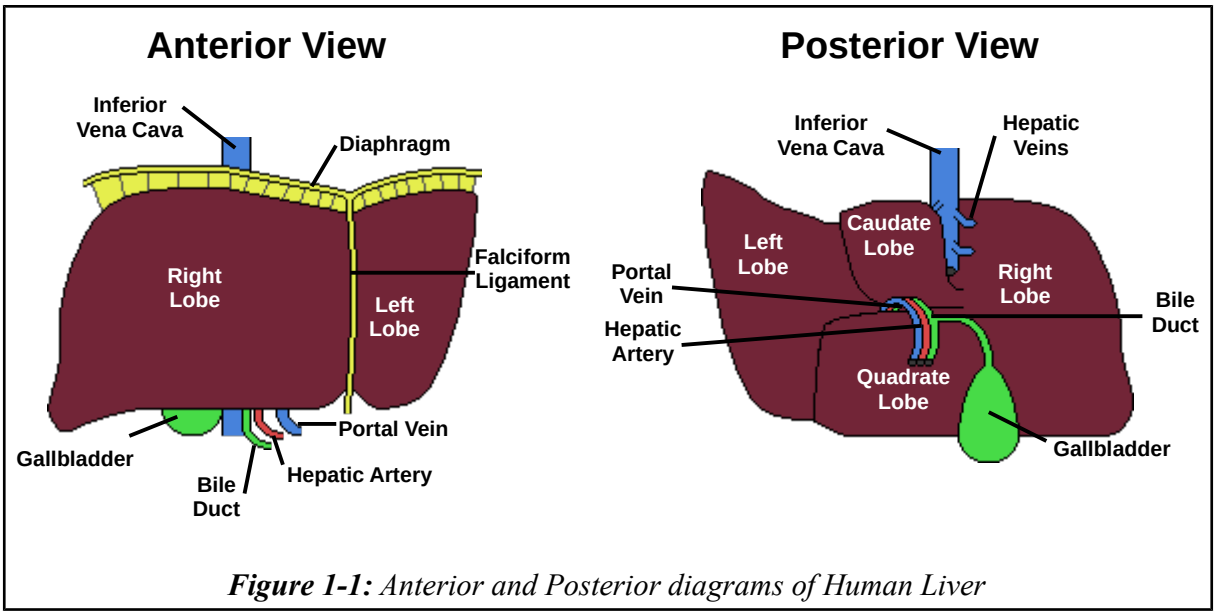

Figure 1-1: *Anterior and Posterior diagrams of Human Liver*

1.2.2 The Liver Lobules

The hepatic artery, portal vein, and bile duct form a structure known as the portal triad, which also contains lymphatic vessels and extensions of the vagus nerve. This structure branches throughout the liver tissue. The blood from the portal venules and arterioles flows through

specialized capillaries called sinusoids, eventually entering a central vein. The central veins flow into interlobular veins and eventually into the hepatic veins[5] (**Fig 1-2**).

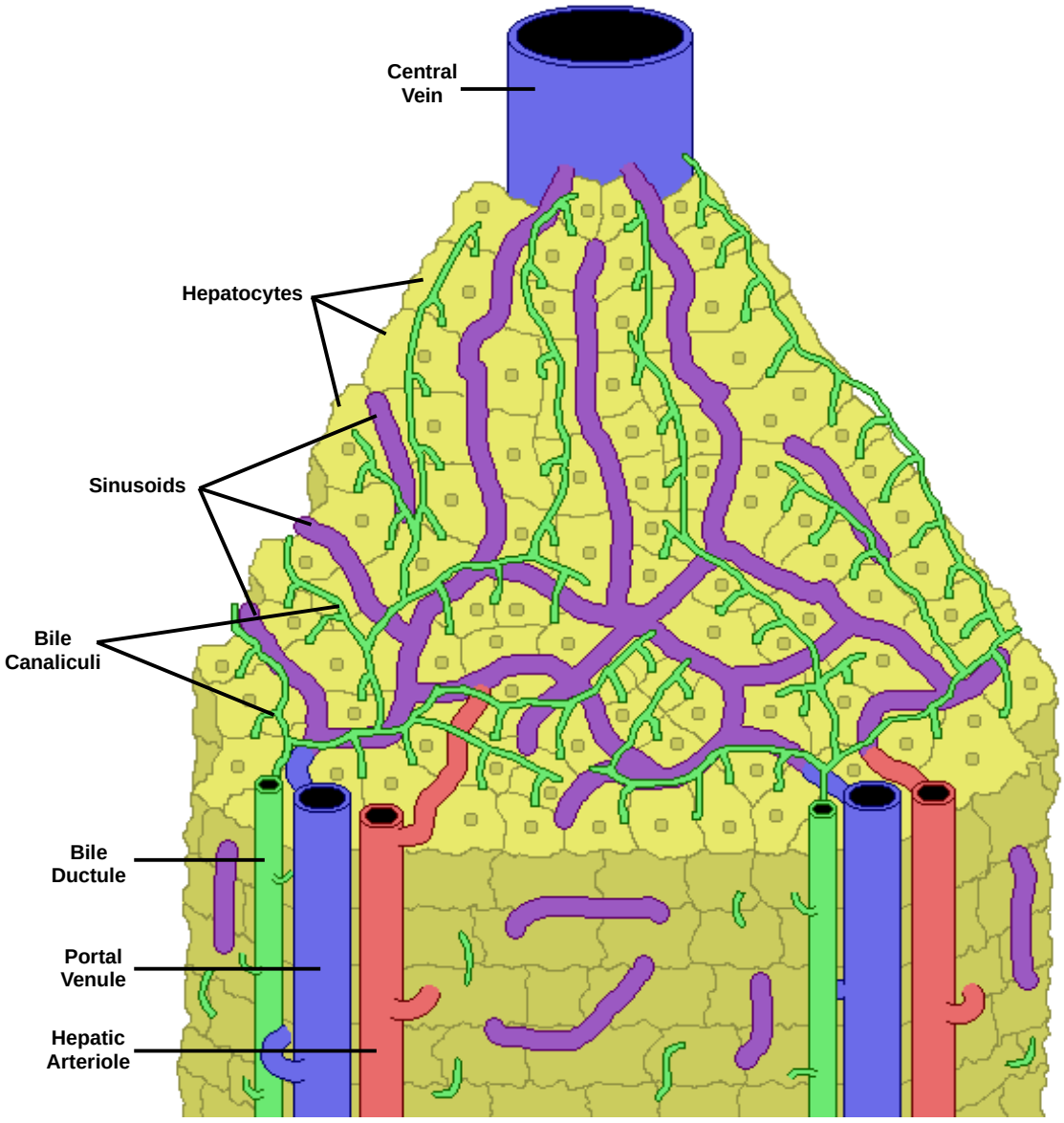

Figure 1-2: *Detailed Diagram of Liver Lobule, showing network of Sinusoids and Bile Canaliculi.*

The pattern of portal triads, central veins, and the sinusoids that connect them, organize the liver into functional units known as lobules. Although lobules are not clearly separated in the liver, lobules can be defined by three different systems (**Fig. 1-3**). The Classical Lobule is a roughly hexagonal structure with the central vein at its center, and portal triads at each point. The Portal Lobule is a triangular structure that places the portal triad at the middle with a central vein at each point. Finally, the Acinus, is a diamond structure with two portal triads and two central veins. The Acinus is used to organize the liver according to oxygenation, with the cells nearer to the portal triad receiving more oxygen than the tissues nearer the central veins[5].

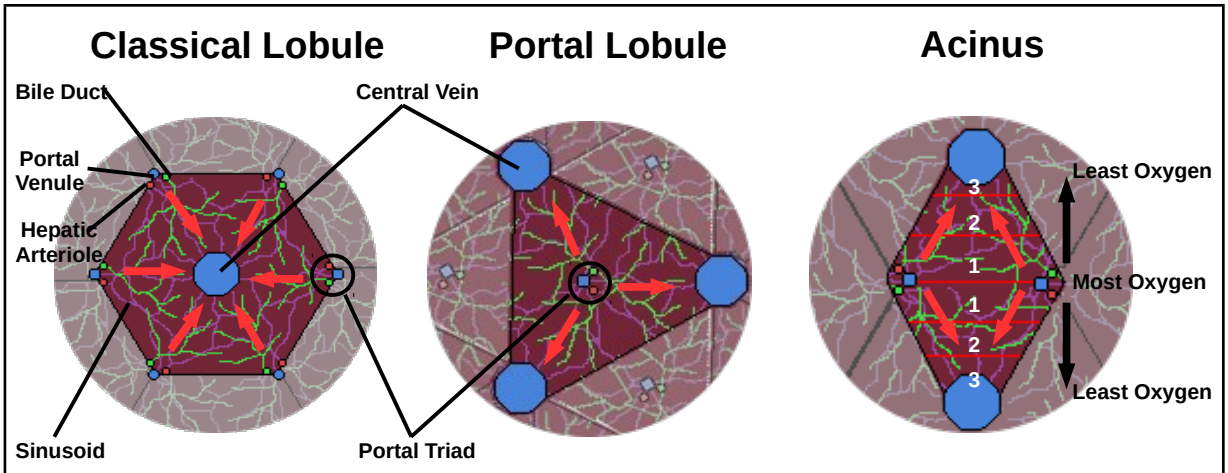

Figure 1-3: *Models of liver lobule organization.* Classical model is centered on the central vein. Portal model is centered on portal triad. The acinus is used to organize the lobule into three zones based on levels of oxygen, with highest levels in periportal region and lowest in centrilobular region.

The Acinus has become the preferred functional unit of the liver because of several differences across the structure. The periportal region not only has higher oxygen concentration than the centribolular region, but different enzyme activities as well. For example, periportal hepatocytes tend to prefer sulfation of molecules, while centribolular hepatocytes prefer glucuronidation. Additionally, chemicals that damage the liver affect different regions of the

Acinus. For instance, allyl alcohol and iron overload will cause more damage to periportal tissues, whereas carbon tetrachloride and acetominophen do more damage to the centrilobular tissues[4].

1.2.3 Cellular Anatomy of the Liver

The liver is made of several cell types (**Fig. 1-4**). Hepatocytes, or parenchymal cells, make up 60% of cell population and 80% of liver volume, and are responsible for carrying out most of the liver's functions. Hepatocytes are arranged into plates, usually about 1 cell thick. Sinusoids contact at least 2 sides of each hepatocyte. The surface of the hepatocyte adjacent to the sinusoid is the basal membrane, while the surface that contacts other hepatocytes is the lateral membrane. When two hepatocytes contact each other, they form a narrow channel called a bile canaliculus, where bile is secreted and moved towards bile ductules. The surface exposed to the

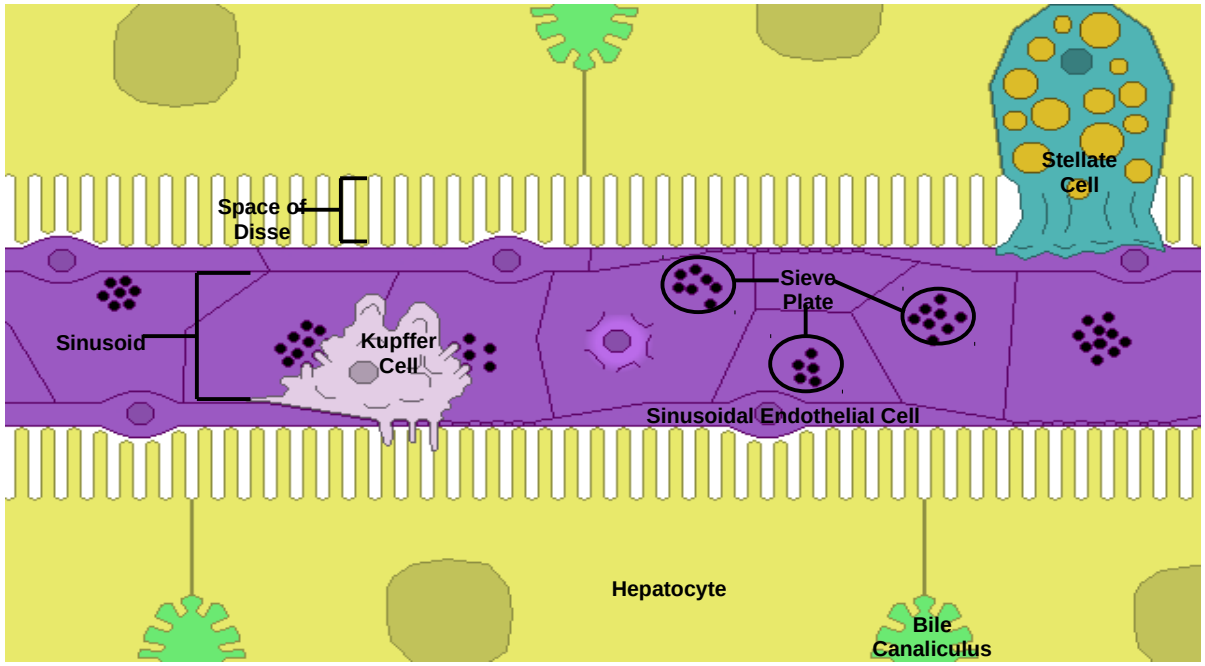

Figure 1-4: *Diagram of Liver Sinusoid with liver cells*

bile canaliculus is the apical membrane. The basal and apical membranes have many microvilli that increase surface area available for exchanging materials across the membranes.

Hepatocytes often have 2 nuclei, though single nuclei are also common. These nuclei are also often polyploidal, and increase in size in proportion to their ploidy. The genomic DNA inside the nuclei is also almost entirely euchromatic, indicating that most of the genome is being transcribed. Hepatocytes also have prominent nucleoli, the sites of ribosome synthesis. These adaptations allow hepatocytes to make large amounts of ribosomes, mRNA, and protein. Hepatocytes also have extensive networks of rough endoplasmic reticulum, smooth endoplasmic reticulum, and golgi complexes, allowing them to shuttle proteins back and forth from basal and apical membranes. To power these processes, hepatocytes have many mitochondria, as many as 2000 per cell. Periportal hepatocytes have larger mitochondria than centrilobular hepatocytes, to take advantage of the additional oxygen.

Sinusoidal endothelial cells make up about half of the non-parenchymal cells. They line the sinusoid similarly to the endothelial cells around normal capillaries. However, unlike capillaries, they lack a basement membrane and have holes, known as fenestrae, which are arranged in groups called sieve plates. There is a gap between the sinusoidal endothelial cells and hepatocytes known as the Space of Disse, or the perisinusoidal space. The fenestrae allow direct access between the sinusoidal lumen and Space of Disse so that plasma proteins and small particles can quickly move between both spaces[3].

The size of fenestrae varies between species, humans have an average diameter of 104 nm, while mice have diameters close to 140 nm[7]. Fenestrae diameter can be dynamically controlled by rings of actin around each fenestration[5]. Particles slightly larger than the fenestrae

diameter can be pushed through by "forced sieving," where a large blood cell squeezes through the sinusoid and stretches the sinusoidal endothelium[8]. Additionally, the periportal sinusoid has fewer fenestrae, but they are larger. The centrilobular sinusoid has more fenestrae, but they are smaller. When the larger surface area of the centrilobular sinusoid is taken into account, the centrilobular sinusoidal endothelium has greater porosity than its periportal counterpart[5]. As individuals age, the number of fenestrae decreases, and the sinusoids begin to more closely resemble capillaries[9]. Liver cirrhosis and other diseases can also trigger this process, known as capillarization, where fenestrae disappear and a basement membrane is built[10].

The sinusoidal endothelial cells themselves play important roles in capturing particles from the bloodstream. They have very high endocytotic capacity, and are often refered to as "Scavenger" endothelial cells. They can pinocytize particles less than 200 nm in diameter[11]. They also express many high affinity receptors such as FC, transferrin, scavenger, mannose, galactose, apo-E, and C-III receptors[5]. Sinusoidal endothelial cells are responsible for capturing damaged and degraded proteins such as oxidized low density lipoproteins, protein turnover byproducts, and some advanced glycation end products. These cells also capture up to 90% of adenovirus I[8]. Pinocytotic vesicles take up 45% of Sinusoidal endothelial cell volume, and another 14% is taken up by lysozomes, further indicating their high capacity to capture and destroy material from the blood[5].

Another important cell type is the Kupffer cell. Kupffer cells are the largest population of fixed macrophages in the body, and reside inside the sinusoidal lumen. They are attached to the sinusoid surface, and often reach through fenestrae with microvilli and other processes. This allows them direct access to the Space of Disse as well as interaction with hepatocytes and

stellate cells[5]. Kupffer cells also capture particles from the bloodstream, but typically capture larger particles than sinusoidal endothelial cells can[11]. Kupffer cells are more abundant in periportal sinusoids, and often cluster at sinusoidal junctions[5].

Stellate cells are located inside the Space of Disse, and primarily act as fat storage cells. They have large lipid droplets that accumulate retinoids, such as vitamin A and other fat-soluble vitamins. They may play a role in controlling bloodflow through the sinusoids. They have long processes that reach around the sinusoidal wall and are closely associated with nerve fibers and express smooth muscle fibers. It is believed that they can squeeze a sinusoid and restrict flow. Liver damage, including alcohol abuse, can lead to stellate cells becoming "activated," causing them to express collagen and other extracellular matrix proteins. This leads to liver fibrosis and eventually cirrhosis[5].

Other cell types found in the liver include cholangiocytes, which are epithelial cells that line the bile ducts. In small bile ducts, the cholangiocytes are cubical, but in larger ducts they become columnar and secrete mucous[9]. Pit cells are natural killer cells derived from large granular lymphocytes which become captured and take up residence in the liver. Pit cells are important in immunity and have been shown to kill cancer cells[5].

Disorder	Gene	Protein	Inheritance	Prevalence	OMIM
Genetic Cholestasis					
PFIC1	ATP8B1	FIC1		1/50,000 to 1/100,000	211600
PFIC2	ABCB11	Bile Salt Export Pump			601847
PFIC3	ABCB4	Multi Drug Resistance 3			602347
Alagille Syndrome	JAG1	JAG-1	AD	1/100,000	118450
	NOTCH2	NOTCH-2	AD		610205
Metal Storage Disorders					
Hereditary Hemochromatosis					
Type 1	HFE	Hemochromatosis Modifier	AR	1/300 to 1/500	235200
Type 2A	HJV	Hemojuvelin	AR		602390
Type 2B	HAMP	Hepcidin	AR		613313
Type 3	TFR2	Transferrin Receptor 2	AR		604250
Type 4	SLC404A1	Ferroportin	AD		606069
Wilson's Disease	ATP7B	Copper-Transport P-Type ATPase	AR	30/1,000,000	277900
Urea Cycle Disorders				1/30,000 Cumulative	
NAGS Deficiency	NAGS	N-Acetyl Glutamate Synthetase	AR		237310
CPS-1 Deficiency	CPS	Carbamoyl Phosphate Synthetase	AR	1/200,000 to 1/800,000	237300
OTC Deficiency	OTC	Ornithine Transcarbamylase	XR	1/40,000 to 1/80,000	311250
Arginiosuccinic Aciduria	ASL	Argininosuccinate Lyase	AR	1/150,000	608310
Argininemia	ARG	Arginase	AR	1/1,100,000	608313
Citrullinemia	ASS	Argininosuccinate Synthetase	AR	1/100,000	215700
Glycogen Storage Disease				1/20,000 to 1/50,000	
Type 0	GYS2	Glycogen Synthase			240600
Type I	G6PC	Glucose-6-Phosphatase	AR	1/100,000 to 1/300,000[a]	232200

Type III	AGL	Glycogen Debranching Enzyme	AR	1/100,000[b]	232400
Type IV	GBE1	Glycogen Branching Enzyme	AR		232500
Type VI	PYGL	Liver Glycogen Phosphorylase	AR		232700
Type IX	PHKA2	Phosphorylase Kinase	XR, AR		306000
Type XI	LDHA	Glucose Transporter	AR	1/500*[c]	612933
Type XII	ALDOA	Aldolase A	AR		611881
Crigler-Najjar Syndrome					
Type 1	UGT1A1	UDP glucoronosyltransferase	AR	< 1/5,000,000	218800
Type 2	UGT1A1	UDP glucoronosyltransferase	AR		606785
Clotting Diseases					
Hemophilia A	F8	Clotting Factor VIII	XR	1/5,000 Males	306700
Hemophilia B	F9	Clotting Factor IX	XR	1/30,000 Males	306900
Hemophilia C	F11	Clotting Factor XI	AR	1/200[d]	612416
Von Willebrand Disease	VWF	Von Willebrand Factor	AR, AD	1/20 to 1/100*	193400
Organic Acid Metabolism Disorders					
Phenylketonuria	PAH	Phenylalanine Hydroxylase	AR	1/10,000	261600
Tyronsinemia					
Type 1	FAH	Fumarylacetoacetate Hydrolase	AR	1/2,000	276700
Type 2	TAT	Tyrosine Aminotransferase	AR		276600
Type 3	HPD	4-Hydroxyphenylpyruvate Dioxygenase	AR		276710
Alkaptonuria	HGD	Homogentisate 1,2-Dioxygenase	AR	1/250,000 to 1/1,000,000[e]	203500
Homocystinuria					
	CBS	Cystathionine β-Synthase	AR	1/60,000 to 1/350,000	236200
	MTHFR	Methylene Tetrahydrofolate Reductase	AR		236250
	MTR	Methionine Synthase	AR		250940
	MTRR	Methionine Synthase Reductase	AR		236270
Maple Syrup Urine Disease				1/185,000	248600
Type IA	BCKDHA	Branched Chain Ketoacid Dehydrogenase			

Type IB	BCKDHB				
Type II	DBT	Dihydrolipoamide Branched Chain Transacylase			
Isovaleric acidemia	IVD	Isovaleryl-CoA Dehydrogenase			243500
3-Methylcrotonylglycinuria	MCCC1	3-α-Methylcrotonyl-CoA Dehydrogenase		1/50,000	210200
Propionic Acidemia				1/100,000	606054
Type I	PCCA	Propionyl CoA Carboxylase			
Type II	PCCB	Propionyl CoA Carboxylase			
Methylmalonic Acidemia	MUT	Methylmalonyl CoA Mutase			251000
Heme Metabolism Disorders					
Acute Intermittent Porphyria	HMBS	Hydroxymethylbilane Synthase	AD	1/50,000	176000
Erythropoietic Protoporphyria	FECH	Ferrocheletase	AR, AD	1/75,000 to 1/200,000	177000
Familial Hypercholesterolemia	LDLR	Low Density Lipoprotein Receptor	AD	1/500*	143890
Cystic Fibrosis	CFTR	Cystic Fibrosis Conductance Regulator	AR	1/3,700[f]	251000
Gaucher Disease	GBA	B-Glucocerebrosidase	AR		230800
Galactosemia	GALT	Galactose-1-phosphate uridylyltransferase	AR	1/50,000f	230400
α-1- Antitrypsin Deficiency	SERPINA1	α-1- Antitrypsin	AR	1/2,000 to 1/5,000	613490
Familial Amyloid Polyneuropathy	TTR	Transthyretin	AD		105210
Hemolytic Uremic Syndrome-1	CFH	Complement Factor H	AR, AD		235400
Primary Hyperoxaluria Type 1	AGXT	Alanineglyoxylateaminotransferase	AR		259900

* Frequency for heterozygotes, a 1/20,000 for Ashkenazi Jews, b 1/5,000 for North African Jews, c Frequency in Japanese, d Frequency in Ashkenazi Jews, e 1/19,000 in former Czechoslovakia and Dominican Republic, f Frequency in Caucasians

Data Taken from OMIM database.

Table 1-1: *Partial list of genetic disorders of the liver.*

1.3 Genetic Disorders of the Liver

Given the liver's central role in homeostasis, liver health is necessary for general health. Several diseases affect the liver, including genetic disorders, hepatitis virus, cirrhosis, and hepatocellular carcinoma. Monogenic disorders, those caused by a problem in a single gene, can often be treated by liver transplantation. They are also candidates for potential gene therapies, and will be discussed here.

1.3.1 Clotting Disorders

One of the most well known genetic disorders of the liver is hemophilia. Hemophilia is commonly thought of as a blood disease, and is characterized by an inability to form clots. Historically, hemophiliacs often died at young ages due to minor injuries, simply because they did not stop bleeding. Hemophiliacs often suffer from spontaneous bleeding into joints and muscle tissues, eventually causing severe arthritis and joint damage. Early treatment attempts included blood transfusions from healthy humans, or even animals such as sheep, and killed about half of all patients due to mismatched blood types[13]. Studies into blood coagulation eventually revealed that a series of proteins in the blood were responsible for forming clots (**Fig. 1-5**), and that loss of specific clotting factors led to hemophilia.

The coagulation cascade is triggered when blood vessels are damaged. When blood is exposed to collagen, the Extrinsic Pathway is triggered. Factor XII is activated, which activates Factor XI, which in turn activates Factor IX. Factor IX binds to activated Factor VIII to form a complex known as Tenase, which activates Factor X.

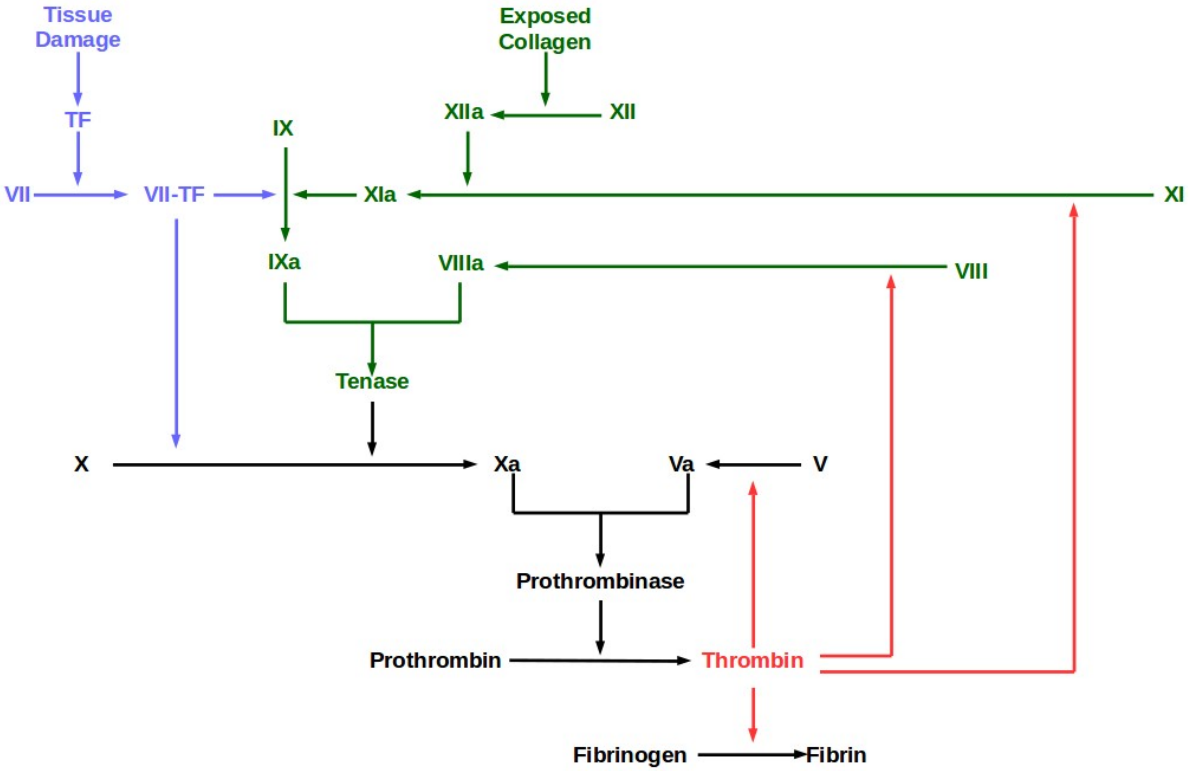

Figure 1-5: *Diagram of Clotting Cascade.* The Extrinsic Pathway is marked in green. The Intrisic Pathway is marked in blue. The Common Pathway is marked in black. Thrombin amplifies the coagulation process by activating Factors V, VIII, and XI. Hemophila A is the loss of Factor VIII, Hemophila B is loss of Factor IX. The rare hemophila C is loss of Factor XI.

The Intrinsic Pathway is triggered by damage that exposes Factor VII to Tissue Factor, TF. The VII-TF complex activates both Factor IX and Factor X. The Intrinsic pathway is more important for blood clotting than the Extrinsic pathway. Once Factor X is activated, it binds to an activated Factor V, forming a Prothrombinase complex. Prothrombinase activates Prothrombin to Thrombin. Thrombin converts Fibrinogen to Fibrin, which crosslinks platelets in the clot. Thrombin also amplifies the coagulation process by activating Factors V, VIII, and XI. This amplification is very important for proper clotting.

Hemophilia A is caused by any mutation or deletion of the Factor VIII gene. This is an X-linked disorder, so almost all patients are male. Hemophilia B is caused by mutation of Factor IX

gene, and is also X-linked, but rarer than A. Hemophilia C is much rarer than type A or B and is caused by mutation of Factor XI gene, but is autosomal. A related disorder is Von Willebrand disease, which is caused by loss of Von Willebrand Factor, a protein that binds to Factor VIII and helps stabilize it in the bloodstream. All of these proteins are produced in the liver[14].

Current treatment for hemophilia is prophylactic administration of concentrated clotting factors. Recombinant clotting factors are preferred to prevent potential contamination by HIV, Hepatitis C, and other pathogens found in human plasma[13]. However, prophylactic treatment is very expensive, often costing $100,000 - $300,000 per year, and can be complicated by formation of "inhibitors", neutralizing antibodies against the clotting factors[15].

Many researchers are considering gene therapy for hemophilia treatment. Hemophilia is often considered an "easy" target for gene therapy because most spontaneous bleeding can be stopped with just 5% of the normal expression of clotting factors, though supplementation with exogenous clotting factors may still be needed to stop bleeding from injuries[14]. A few hemophilia gene therapy clinical trials have been performed over the last two decades. A 1996 Chinese study took fibroblasts from two patient's skin, transfected them with Factor IX cDNA, then re-implanted them into the patients[16]. A similar study from 2001 transfected fibroblasts with Factor VIII gene, and implanted them in the fat inside the omentum[17]. A 2003 study used a retroviral vector carrying Factor VIII gene[18]. However, none of these studies produced significant or long term expression of either factor.

More recent trials using adeno-associated virus serotype 2 were able to achieve measurable amounts of Factor IX expressed in the liver, but an immune response against the transfected hepatocytes eliminated expression[19]. When AAV serotype 8 was used, Factor IX was

able to be expressed at 10-12% of normal levels for about 2 months before the immune response reduced expression. If corticosteroids were used, expression could be maintained at 6%, allowing many of the patients to forgo prophylactic treatment[20]. However, success rates are still unreliable and immune responses force the use of immunosuppression. Factor VIII gene delivery with AAV is more difficult because the Factor VIII gene is very large. Removing the large B domain can produce a mutant Factor VIII protein with greater stability than the wild type protein[21], however the shorter gene is still 4.4 kb after introns are excised, and the AAV genome is normally 4.6 kb. Replication deficient AAV genomes built with Factor VIII genes are often significantly larger than 5 kb, which reduces encapsidation efficiency, requiring a much larger amount of virus to be delivered and making immune response a much more serious problem[22].

1.3.2 α-1-Antitrypsin Deficiency

α-1-antitrypsin deficiency is another genetic disorder of the liver. α-1-antitrypsin is produced by the SERPINA1 gene in the liver and secreted into the bloodstream. Once in the blood, it binds to and inhibits neutrophil elastase through suicide inhibition. This is especially important for the lungs, where neutrophil elastase can damage lung tissue. It is a relatively common autosomal codominant disorder, with frequency estimated at 1 in 2000-5000 people depending on location, but is often not diagnosed. α-1-antitrypsin deficiency causes early onset emphysema and sometimes liver disease. The emphysema is made worse by smoking or lung infection, which causes increased levels of neutrophil elastase. The liver damage is caused by certain α-1-antitrypsin mutants that accumulate in hepatocytes instead of being secreted. Other mutants cause intracellular degradation, which still leads to lung disease, but not liver disease.

Current treatment involves intravenous infusion of concentrated α-1-antitrypsin purified from pooled human plasma, which carries some risk of contamination[23]. A 2004 human clinical trial attempted to deliver functional α-1-antitrypsin gene by intramuscular injection of AAV2 virus carrying the gene[24]. However, results from this study are not expected until 2021 (clinicaltrials.gov identifier NCT00377416).

1.3.3 Metal Storage Disorders

Metal storage disorders, such as hereditary hemochromatosis and Wilson's Disease, are autosomal recessive disorders that cause excessive accumulation of metals in tissues. Hereditary hemochromatosis is the excessive build up of iron, mostly in the liver, but also accumulates in the heart, gonads, pituatary gland, pancreas, joints, and skin. If left untreated, it can lead to cirrhosis, heart disease, diabetes, and joint damage. If detected early, regular phlebotomy can be used to remove excess iron from the blood and keep iron concentration at safe levels[25].

Iron metabolism and homeostasis is complex and still not fully understood (**Fig. 1-6**). Dietary iron in the form of Fe^{3+} is reduced by Duodenal Cytochrome B, DcytB, in the small intestine to Fe^{2+}. Fe^{2+} is taken up by enterocytes through the Divalent Metal Transporter 1, DMT1. Once inside the cell, Fe^{2+} is reversibly stored in ferritin. Fe^{2+} is exported into the bloodstream by Ferroportin, FPN. Once in the bloodstream, Fe^{2+} is oxidized back to Fe^{3+} by hephaestin or ceruloplasmin. Circulatory Fe^{3+} is stored inside transferrin. Most transferrin bound iron is taken up by erythroblasts, the precursors to red blood cells, and used to synthesize hemoglobin, which accounts for 80% of the body's iron content.

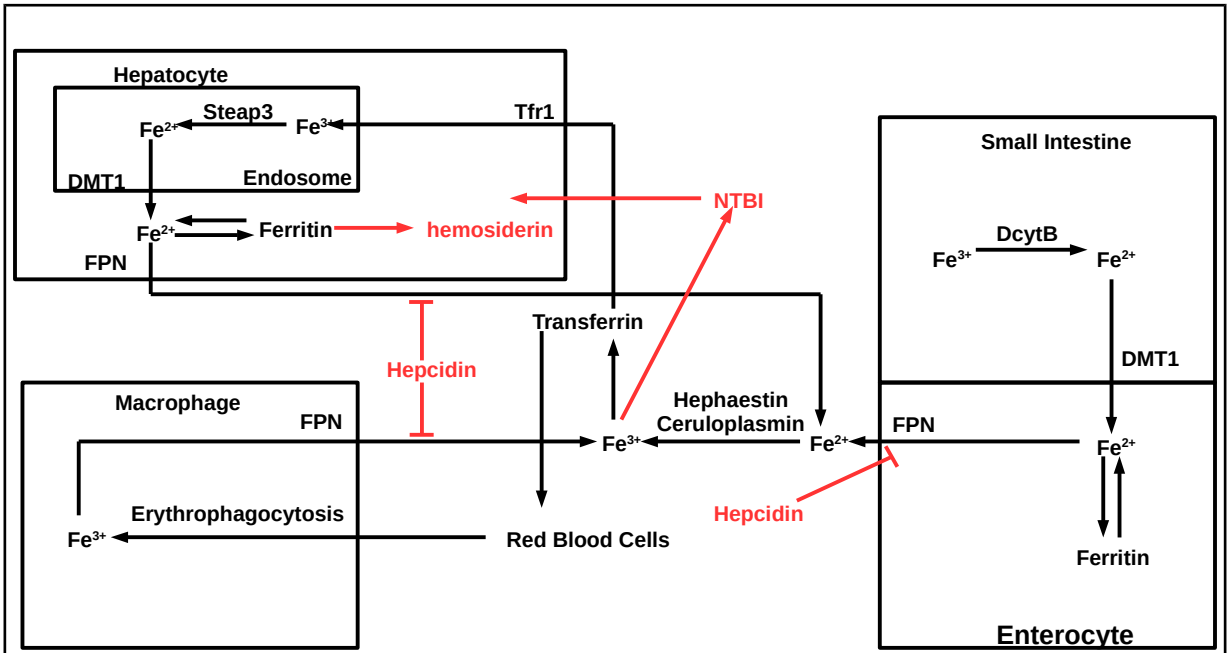

Figure 1-6: *Diagram of Iron Homeostasis showing interaction of enterocytes, macrophages, and hepatocytes.* Pathways active during iron overload are shown in red.

When red blood cells age, they are taken up by liver or spleen macrophages and degraded through erythrophagocytosis. The macrophages efficiently recycle the iron back into the bloodstream through ferroportin. The liver also serves as a major storage site for iron, taking up transferrin through the Transferrin Receptor 1, Tfr1, and internalizing it into endosomes. Endosome acidification causes the Fe^{3+} to dissociate from transferrin, and is reduced to Fe^{2+} by endosomal reductases including Steap3. Fe^{2+} is transported into the cytoplasm by the Divalent Metal Transporter 1, and stored in ferritin. When serum iron levels are low, the hepatocytes export iron through ferroportin[26].

When iron levels are high, the liver expresses a peptide hormone called hepcidin, which binds to ferroportin and causes it to be internalized and degraded. This causes serum iron levels to decrease by inhibiting the export of iron from enterocytes, macrophages, and hepatocytes. Most importantly, the iron trapped in enterocytes is lost as the cells are recycled. Iron that enters

the bloodstream through enterocytes cannot be naturally removed from the body. Under conditions of iron overload, transferrin cannot store all serum iron, which results in the accumulation of Non-Transferrin Bound Iron, NTBI, which is mostly Iron Citrate, and is eventually captured by hepatocytes. If intracellular iron levels overcome a heptacyte's ferritin reserves, iron will accumulate as hemosiderin, an insoluble mixture of degraded ferritin and ferric hydroxide. Once sequesterd inside hemosiderin, iron cannot be readily mobilized[26].

Iron overload, if left untreated, leads to the accumulation of iron in several tissues around the body, including the liver, pancreas, heart, and skin. As iron concentrations increase, reactive oxygen species become more dangerous. The Fenten and Haber-Weiss reactions catalyze the generation of dangerous hydroxyl radicals, which damage DNA, proteins, and membranes. Iron overload has been linked to insulin resistance, type 2 diabetes, and increased odds of hepatocellular carcinoma. Patients with hereditary hemochromatosis are 100 – 200 fold more likely to develop hepatocellular carcinoma.

Treatment of hereditary hemochromatosis is usually done using phlebotomy. Regular blood draws increase the body's demand for iron to replace the lost hemoglobin, which slowly pulls excess iron from hepatocytes. Iron chelators are also used to reduce serum iron levels. However, not all tissue damage can be reversed as iron levels decrease, and hereditary hemochromatosis is often not diagnosed until significant tissue damage has occurred, and often after a patient is too old for a liver transplant[27].

Hereditary hemochromatosis is usually caused by mutations in the HFE gene, which produces a transmembrane protein that interacts with Transferrin Receptor 2 and regulates expression of hepcidin. Mutations in HFE are autosomal recessive, and 1 in 8 Americans carry a

faulty copy[26]. Although there have been no studies addressing gene therapy solutions for hereditary hemochromatosis, the central role of hepcidin in iron homeostasis suggests a potential for treating the illness by transient overexpression of hepcidin in the liver. Expression must be transient to prevent anemia. Transient hepatocyte expression of ferroportin could also help to export excess iron from the liver and speed up phlebotomy therapy. Long term treatment might be achieved by persistent expression of a working HFE gene in most cases of hereditary hemochromatosis.

Wilson's disease is an autosomal recessive disorder of copper metabolism, resulting in the accumulation of copper in the liver, brain, and cornea. Wilson's Disease is caused by a mutation in the ATP7B gene, which encodes an ATPase that helps transport copper through the hepatocyte golgi network and into the bile. When this protein is mutated, copper cannot be secreted into the bile. Wilson's disease is usually diagnosed between ages 5 and 40, and has a wide range of severity. The disease can present as acute liver failure or as chronic liver disease. Accumulation of copper in the brain can lead to neurological issues including tremors, drooling, and speech problems. Personality changes caused by brain damage are often confused with normal puberty related changes in behavior. Approximately 98% of patients with neurological symptoms also have Kayser-Fleischer rings, brown deposits of copper visible in the cornea. These rings are less common in patients who only have liver symptoms. Treatment of Wilson's Disease is typically done with British Anti-lewisite, d-penicillamine, trientine, or ammonium tetrathriomolybdate, which work through a combination of chelation and induction of metallothionein to inhibit copper uptake in the intestine. However, side effects often cause patients to discontinue use of some therapies. If acute liver failure occurs, liver transplantation is necessary[25]. Expression of a

correct form of ATP7B in hepatocytes could restore normal copper metabolism and provide a cure for the disease.

1.3.4 Crigler-Najjar Syndrome

Crigler-Najjar syndrome is a rare autosomal recessive disorder of bilirubin metabolism with fewer than 1 in 5 million humans affected. The disease is caused by loss of functional uridine glucuronosyl transferase, UGT1A1. Without UGT1A1, bilirubin cannot be glucuronidated and cannot be excreted. As bilirubin accumulates, it causes jaundice and eventually neurological damage known as kernicterus[27]. Type I Crigler-Najjar syndrome is the complete loss of UGT1A1 activity and is more severe. Type II Crigler-Najjar syndrome retains some UGT1A1 activity, and induction of UGT1A1 by phenobarbitol usually increases enzyme activity enough to safely control bilirubin levels. The type I disorder is treated through phototherapy to convert bilirubin to isomers which can be excreted into bile. However, phototherapy must be applied for about 12 hours a day. At puberty, the skin thickens and becomes darker, and the surface area to volume ratio decreases, reducing the effectiveness of phototherapy. About 40% of type I patients require liver transplantation during childhood, with 27% of these patients developing kernicterus[28].

The Gunn rat has been used as a model of Crigler-Najjar syndrome for several years. Lentiviral vectors have been used to deliver functional UGT1A1 genes to Gunn rat livers, and succesfully treat the disease[29]. Hepatocyte transplantation has been attempted in humans, with some success, but benefits only lasted for about three years[30]. Hepatocytes have also been extracted from Crigler-Najjar patients and transfected ex vivo using lentiviral vectors and

transplanted into mouse livers with expression detectable at least 26 weeks after transplantation. This could lead to the reimplantation of a patient's own hepatocytes after gene transfer therapy to treat the illness without a full liver transplant[31].

1.3.5 Urea Cycle Disorders

Urea cycle disorders are a group of genetic disorders that affect the urea cycle, the biochemical process that converts ammonia to urea for removal from the body (**Fig. 1-7**). The cycle begins inside the mitochondria when carbamyl phosphate synthetase, CPS-1, combines bicarbonate, ammonia, and ATP to make carbamyl phosphate. Ornithine transcarbamylase, OTC, attaches the carbamyl group to ornithine to produce citruline. Citruline is transported out of the mitochondria and combined with aspartate to form argininosuccinate by argininosuccinate synthase, ASS. Argininosuccinate is converted to arginine and fumarate by argininosuccinate lyase, ASL. Arginine is converted to urea and ornithine by arginase. The ornithine is transported back into the mitochondria to start the cycle over again. This process occurs almost exclusively in hepatocytes, with some activity in the kidney[27,28,32].

The loss of any one of these enzymes results in a urea cycle disorder. The severity varies greatly between individuals, from fatal neonatal forms to nearly asymptomatic forms that usually go unnoticed. All enzyme deficiencies are autosomal recessive, except ornithine transcarbamylase deficiency, which is X-linked dominant. Early onset disease is very dangerous, often presenting within hours of birth. Failure to detoxify ammonia leads to hyperammonemia. Hyperammonemia can cause neurological problems ranging from irritability and lethargy, to coma and death. Arginase deficiency is normally less serious, but still causes spasticity and

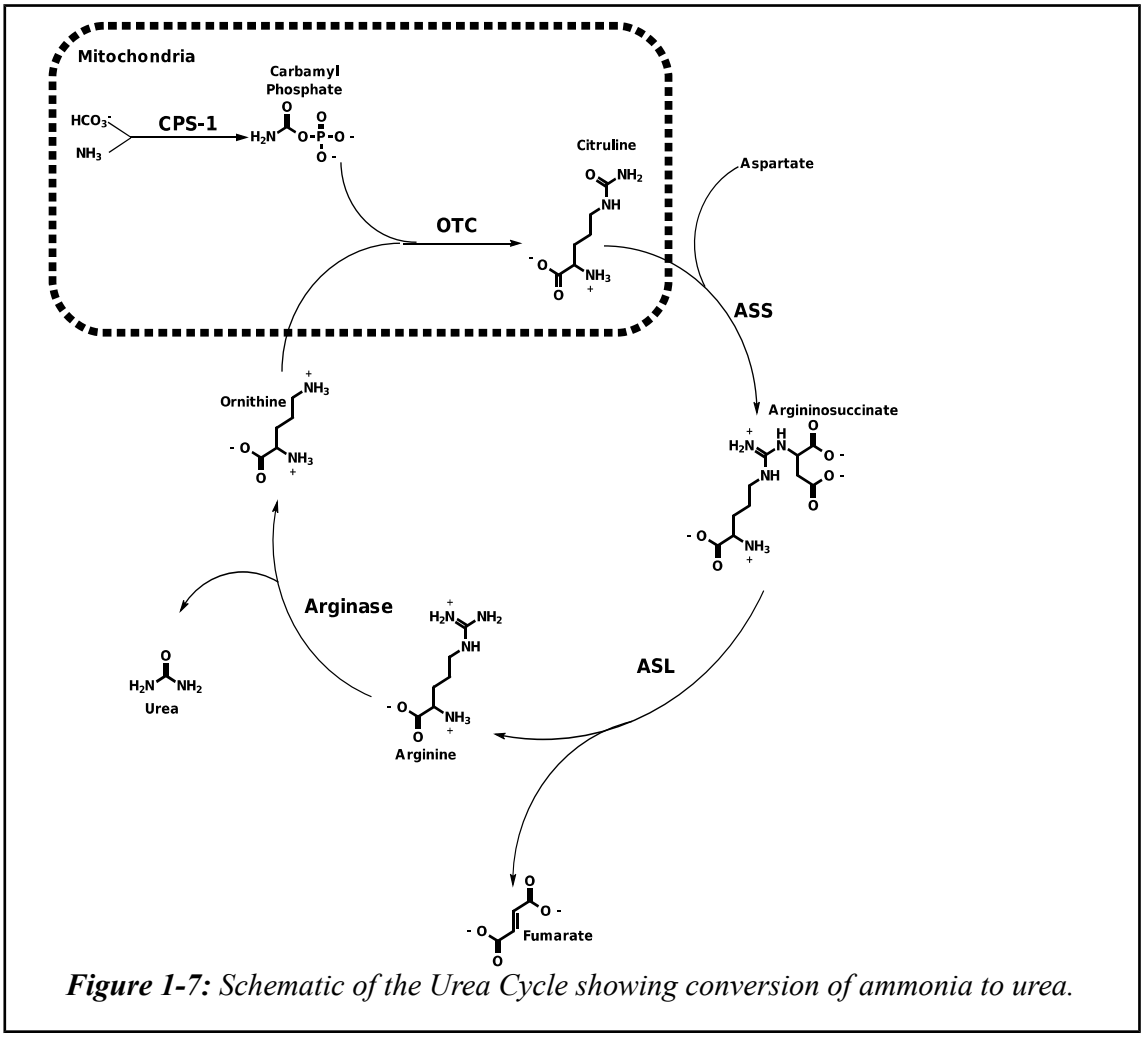

Figure 1-7: *Schematic of the Urea Cycle showing conversion of ammonia to urea.*

mental retardation.

Treatment of urea cycle disorders involves careful high calorie diets with very little, if any, protein, and essential amino acid supplementation. Nitrogen scavengers such as benzoate and phenylbutyrate are also used. In hyperammonaemic crises, where ammonia levels spike, dialysis is used. However, liver transplantation is almost always eventually necessary, with earlier replacement leading to better prevention of neurological damage[27,28,32].

A 2002 clinical trial to treat ornithine transcarbamylase deficiency using a type 5 adenoviral vector showed no clinical improvement. Unfortunately, one patient died during the

study, due to an extreme innate immune reaction against the viral vector[33].

1.3.6 Amino Acid Metabolism Disorders and Organic Acidemias

When amino acids are not properly catabolized, metabolic byproducts can accumulate in several tissues and can cause a wide range of symptoms. Most are autosomal recessive, and incidence tends to be rare. Non amino organic acids are excreted in urine, and detection of these acids is a common tool for diagnosis. As metabolites accumulate in the liver, brain, kidneys, pancreas, and other organs, tissue becomes damaged. Many of these disorders cause serious neurological damage, and if left untreated can cause mental retardation, coma, or death. Most treatment involves careful diets that manage the disorder by strictly limiting the intake of the offending amino acid, but compliance is often poor. Since the liver is usually responsible for most of the missing metabolic activity, liver transplantation has been useful for many organic acidemias, but often fails to correct all symptoms in other organs[27,28].

1.3.6.1 Phenylalanine and Tyrosine Metabolism Disorders

Phenylketonuria is the failure to convert phenylalanine to tyrosine due to a deficiency of phenylalanine hydroxylase (**Fig 1-8**). Phenylketonuria is an autosomal recessive disorder with global incidence of about 1 in 10,000 births, though this rate varies greatly between locations and ethnicities. If left untreated, excess phenylalanine builds up in the brain and causes neurological damage. Excess phenylalanine appears to be directly toxic to the brain through unknown mechanisms, and indirectly toxic because it competes with other amino acids for transport across the blood-brain barrier. This reduces the concentrations of those amino acids in the brain and

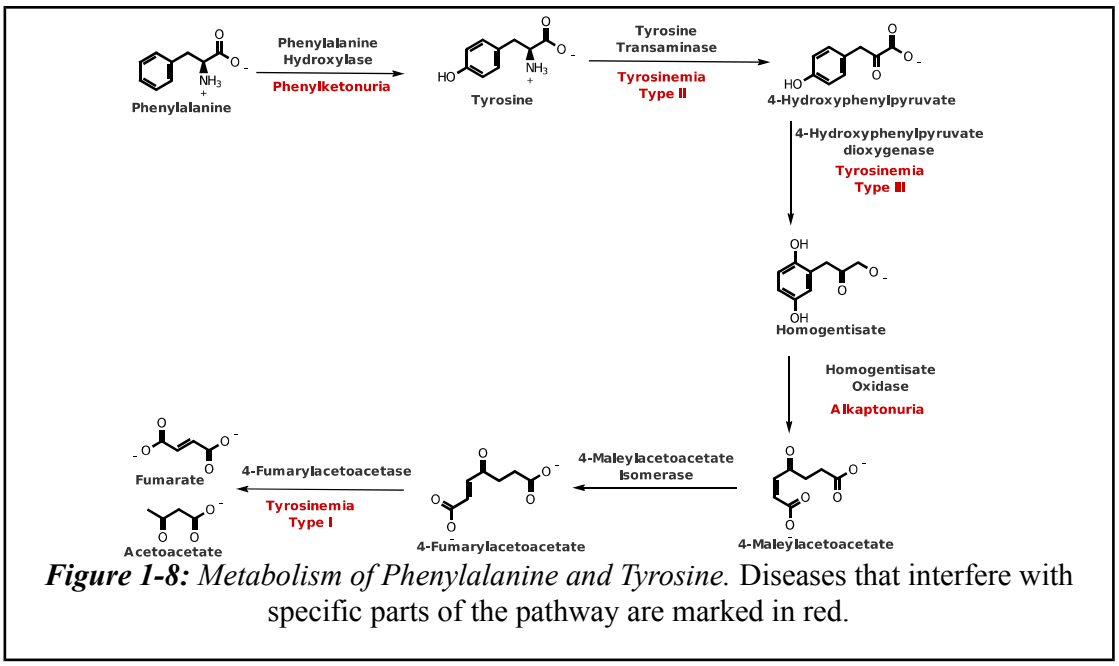

Figure 1-8: *Metabolism of Phenylalanine and Tyrosine.* Diseases that interfere with specific parts of the pathway are marked in red.

interferes with protein and neurotransmitter production.

If left untreated, phenylketonuria causes severe mental retardation, with an IQ < 40. Additionally, melanin is not synthesized at normal levels, so skin, hair, and eyes are all lighter than normal. Phenylacetate is excreted in the urine, making it smell like mice.

Early diagnosis is critical for proper treatment of phenylketonuria. It is estimated that 1 IQ point is lost for every week the disease goes undiagnosed. Treatment involves a phenylalanine restricted diet and monitoring phenylalanine levels. The diet is very strict, and should be continued throughout the patient's lifetime. When treatment is started early and carefully followed, the patient can expect normal development. The improved survival of phenylketonuriacs has allowed female patients to have children. Pregnancy requires even stricter control of phenylalanine levels to prevent birth defects in the developing fetus. Control is complicated because if the fetus has functional phenylalanine hydroxylase, it will start metabolizing phenylalanine as its liver develops, further reducing maternal phenylalanine

levels[34,35].

Although phenylketonuria can be managed through proper diet, gene therapy research has been done on the disease in mouse models. A 2011 study used AAV8 virus carrying the phenylalanine hydroxylase gene to treat phenylalanine hydroxylase knockout mice. These mice not only had normal phenylalanine metabolism restored, but levels of neurotransmitters returned to normal. Levels remained normal throughout the 8-week duration of the study[36]. A 2013 study used minicircle DNA carrying phenylalanine hydroxylase delivered through hydrodynamic tail vein injection. This corrected phenylalanine levels for at least 180 days after dosing. The treated mice also showed repigmentation because melanin synthesis was restored once phenylalanine could be metabolized correctly[37]. Gene therapy could replace the strict diet and greatly improve the phenylketonuriac's quality of life.

A related disorder, Tyrosinemia, is an autosomal recessive disorder of tyrosine catabolism. Tyrosinemia type 1 is a deficiency of Fumarylacetoacetate hydrolase, which catalyzes the final step of tyrosine catabolism (**Fig. 1-8**). This causes buildup of fumarylacetoacetate and malelylacetoacetate, which can cause hepatocytes and kidney tubular epithelial cells to undergo apoptosis. These metabolites can alkylate DNA, and greatly increase the odds of developing hepatocellular carcinoma. Treatment includes a phenylalanine and tyrosine restricted diet along with 2-(2-nitro-4-trifluoromethylbenzoyl)-1-3-cycloexenedione, or NTBC. NTBC inhibits the second step of tyrosine metabolism and prevents accumulation of fumarylacetoacetate and malelylacetoacetate. If this treatment starts within the first 6 months of life, the risk of hepatocellular carcinoma is greatly reduced. Patients must still be closely monitored for signs of liver damage, and liver transplant is still necessary in 12% of cases.

However, liver transplantation does not correct metabolism in the kidneys, and a combined liver kidney transplant may be needed[27].

Tyrosinemia type II is caused by a deficiency of tyrosine aminotransferase. Although there is no liver damage, tyrosinemia type II does cause eye and skin lesions. Eye lesions are caused by tyrosine crystal deposits in the cornea, and typically leads to photophobia and eye pain. Skin lesions are hyperkeratinized plaques on the palms of the hand and soles of the feet, with yellow thickening. As the patient ages, the elbows, knees, and ankles can show these plaques as well. Some patients have also shown developmental delay, but predicting which patients will have neurological damage is not precise. A diet without phenylalanine and tyrosine not only halts progression of the illness, but resolves the skin and eye symptoms within weeks[38].

Tyrosinemia type III is the rarest tyrosinemia, with fewer than 6 patients identified as of 2006. This form is caused by deficiency of 4-Hydroxyphenlypyruvate Dioxygenase, which normally converts 4-hydroxyphenylpyruvate to homogentisate. The known patients did not show liver damage or eye or skin lesions. At least 3 of the patients had mental retardation[38].

Alkaptonuria is another disorder of tyrosine metabolism, due to deficiency of functional Homogentisate 1,2-Dioxygenase, leading to accumulation of homogentisic acid. Its symptoms include dark brown to black urine, joint and cartilage damage, stones in the kidneys, gallbladder, prostate, and salivary glands, and damage to the heart valves. Alkaptonuria is treated with NTBC similarly to type I tryosinemia[39].

1.3.6.2 Methionine and Cysteine Metabolism Disorders

Cysteine is produced from methionine through a homocysteine intermediate (**Fig. 1-9**). Homocysteine can be converted back into methionine through 2 pathways, through methionine synthase or through betaine methyltransferase. Deficiencies of the enzymes involved in methionine regeneration can lead to homocistinuria, the build up of excess homocysteine, as well as deficiencies of methionine and cysteine. The symptoms of these disorders are usually slow to develop, but affect many organs. Eye abnormalities and blindness are common. Skeletal abnormalities similar to Marfan syndrome also occur, including osteoporosis and spontaneous vertebral crush fractures. About two thirds of patients have mental defects, with smaller portions with seizures. Blood clots are the main cause of death for patients, causing heart attacks and

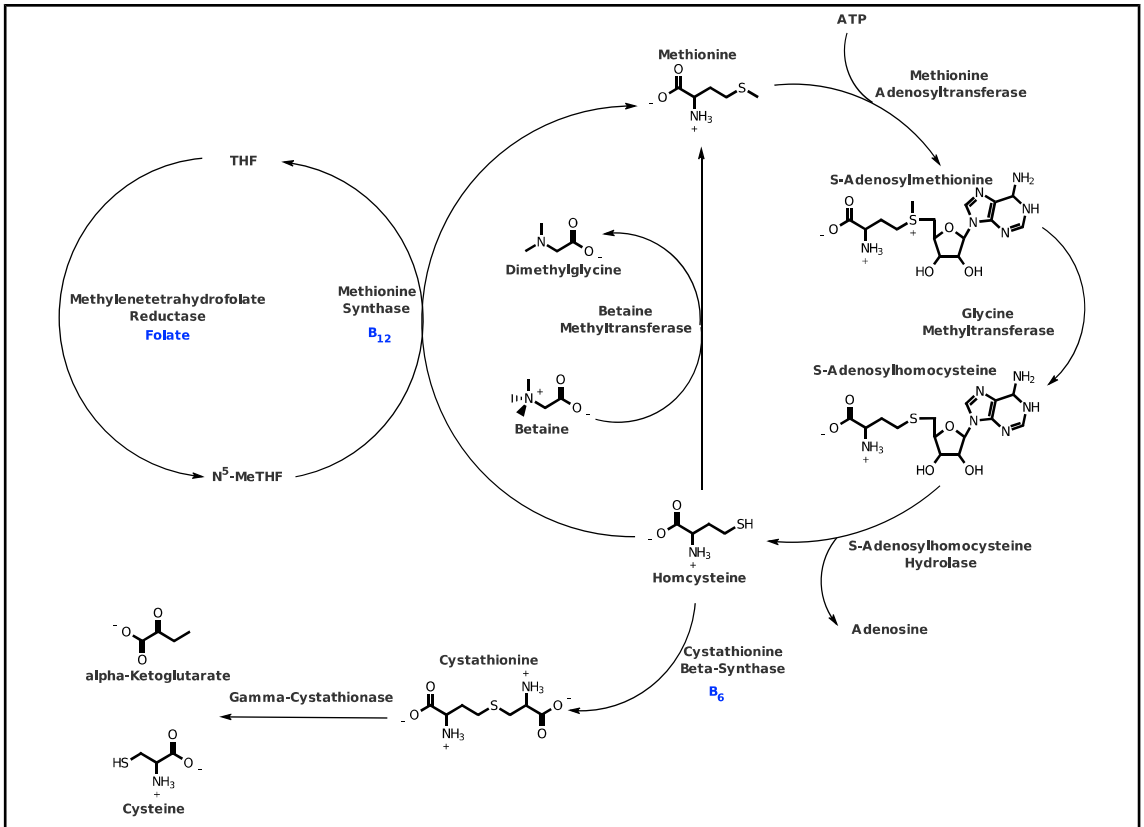

Figure 1-9: *Diagram of Methionine Metabolism and Cysteine Synthesis.*

strokes. Clots have been found in blood vessels of the kidneys, the gut, and limbs as well. Treatment includes a strict low protein diet supplemented with methionine free amino acids. Patients must also take high doses of vitamins B_6, B_{12}, folic acid, and betaine, which are cofactors or reagents in converting homocysteine to either cysteine or methionine[32].

1.3.6.3 Maple Syrup Urine Disease

Maple syrup urine disease is the failure to properly metabolize leucine, isoleucine, and valine due to a deficiency of Branched Chain Ketoacid dehydrogenase. These amino acids and their α-keto acid and hydroxyacid derivatives accumulate. The characteristic maple syrup smell is caused by the buildup of some of these compounds, and can be found in the urine, but usually more strongly in the ear canal. Toxic metabolites accumulate in the brain and cause neurological symptoms such as seizures, lethargy, and alternating hypotonia and muscle rigidity. If not promptly treated, the illness will quickly progress to coma and death. Treatment is based on a diet with very little, if any, leucine, isoleucine, or valine[32]. Liver transplantation has been shown to manage the disease[23].

1.3.6.4 Isovaleric Acidemia

A related disorder is isovaleric acidemia. Isovaleryl-CoA is produced during leucine catabolism and is normally metabolized by isovaleryl-CoA dehydrogenase. The disorder has similar symptoms and treatment to maple syrup urine disease, but produces a foul sweaty foot odor[32].

1.3.6.5 3-Methylcrotonylglycinuria

Another related disorder, 3-Methylcrotonylglycinuria, characterized by a 3-α-methylcrotonyl-CoA carboxylase deficiency, prevents conversion of 3-methylcrotonyl-CoA to 3-methylglutaconyl-CoA. This disorder is the most common of the organic acidemias, with a frequency of about 1 in 50,000 births. The enzyme requires biotin as a cofactor, so biotin deficiencies must be excluded first. However, only 10% of homozygotes actually develop symptoms. Those who are symptomatic usually have mild neurological problems, but a few will develop serious potentially fatal illness during infancy.[32]

1.3.6.6 Propionic Aciduria

Propionic aciduria is the build up of propionyl-CoA from breakdown of isoleucine, threonine, methionine, valine, odd numbered fatty acids, and cholesterol, and is contributed to from gut bacteria. Propionyl-CoA carboxylase normally degrades propionyl-CoA to methylmalonyl-CoA. Symptoms and treatment are similar to other organic acidemias, but may also cause secondary urea cycle disorders. To reduce propionyl-CoA uptake from gut bacteria, regular treatment with metronidazole and colistin is used[32]. The disease usually presents during infancy, with acidosis, hyperammonemia, pancreatitis, and eventually heart disease and neurological damage. Few survive beyond their teenage years, even with treatment. Treatment has not improved the neurological outcomes[28]. Liver transplantation has improved the quality of life for some patients, though it cannot correct the metabolic errors in other tissues[27].

1.3.6.7 Methylmalonic Aciduria

Methylmalonic aciduria is a related disorder caused by deficiency of Methylmalonyl-CoA Mutase, which converts methylmalonyl-CoA to succinyl-CoA, which is fed into the Krebs cycle. Because methylmalonyl-CoA is the product of propionyl-CoA carboxylase, the symptoms are similar to propionic aciduria. This disorder can interfere with mitrochondrial energy production due to shortages of succinyl-CoA and the urea cycle. Clinically, it can be difficult to distinguish methylmalonic aciduria from propionic aciduria[32]. Methylmalonic aciduria is difficult to treat through liver transplantation, due to incorrect metabolism that remains in the kidneys and brain. Patients who undergo combined liver and kidney transplantation fare better, but still require medication and a somewhat restricted diet[27].

1.3.7 Glycogen Storage Disorders

Glycogen storage disorders are a class of genetic disorders that cause errors in glycogen metabolism, usually leading to accumulation of glycogen in liver, skeletal muscles, and occasionally heart, kidney, and other tissues. Glycogen storage disorders have a wide range of severity, from almost asymptomatic to fatal neonatal forms. Most forms are currently treated by dietary management, including increased protein to promote gluconeogenesis, and either a feeding tube to deliver glucose to infants at night, or uncooked cornstarch in older children to prevent hypoglycemia.

Hepatocytes that accumulate glycogen often swell up and take on a “plant cell” appearance. If untreated, glycogen storage disorders of the liver can lead to hypoglycemia, and excess levels of lactic acid, uric acid, triglycerides, and cholesterol. Complications from these

may cause kidney stones and gout. The majority of patients develop hepatic adenomas by their thirties, with some of these developing into hepatocellular carcinoma. Other types, such as type 2 also known as Pompe's Disease, lead to muscle weakness and heart failure, often causing death within 1 year of birth, though liver deformity is rare. Pompe's Disease can be treated with acid-alpha-glucosidase enzyme replacement therapy[40].

Several studies have used adeno-associated viral vectors to treat glycogen storage disorder type 1 in mouse models[41]. A canine model of type 1 glycogen storage disease also showed promsing results by using AAV to deliver the glucose-6-phosphatase gene[42]. Gene therapy trials for Pompe's Disease have been done in mice and humans using AAV directed towards cardiac muscle[43,44]. However, if enzyme replacement therapy provides some alleviation of symptoms, the liver could be used to produce acid-alpha-glucosidase and secrete it into the blood, acting as enzyme replacement therapy.

1.4 Gene Delivery to the Liver

In vivo gene delivery is typically classified into two broad categories, viral and nonviral. Viral gene delivery uses a viral vector, usually a replication deficient adenovirus, adeno-associated virus, or lentiviral vector. So far, viral vectors have had more clinical success than nonviral vectors, including one therapy approved in Europe. UniQure's Glybera uses an AAV1 vector to deliver the gene for LPL to treat lipoprotein lipase deficiency[45]. However, viral vectors present many challenges, such as high cost of production, immune response, limited genome capacity, and the potential for insertional mutagenesis. Immune response is an important aspect, if neutralizing antibodies against the vector are developed, repeated dosing of the vector may not

be possible. In rare cases, immune response can be very severe, even fatal[29]. Nonviral vectors are much less expensive to produce, have much larger cargo capacities, and should be less likely to induce an immune response.

1.4.1 Barriers to Nonviral Gene Delivery

However, nonviral gene delivery faces many barriers to successful delivery (**Fig. 1-10**). The first of these barriers is survival in the bloodstream. Serum nucleases can destroy DNA[46], scavenger receptors can capture DNA nanoparticles[47], and certain DNA condensing agents can aggregate serum proteins and cause toxicity[48,49]. DNA nanoparticles must be delivered to specific tissues and cell types, which is most easily accomplished using a targeting ligand towards a specific receptor. Once bound, the receptor must be internalized through endocytosis, compartmentalizing the receptor and DNA nanoparticle in an endosome. Because endosomes are often sent to lysosomes to break down their contents, the DNA nanoparticle must escape the endosome and enter the cytoplasm. Once in the cytoplasm, the DNA must move into the nucleus before it can be expressed. Nuclear entry can be achieved by passing through the Nuclear Pore Complex, NPC. However, the NPC has a size limit of 39 nm[50], too small for most DNA nanoparticles, so other methods of nuclear entry may be necessary.

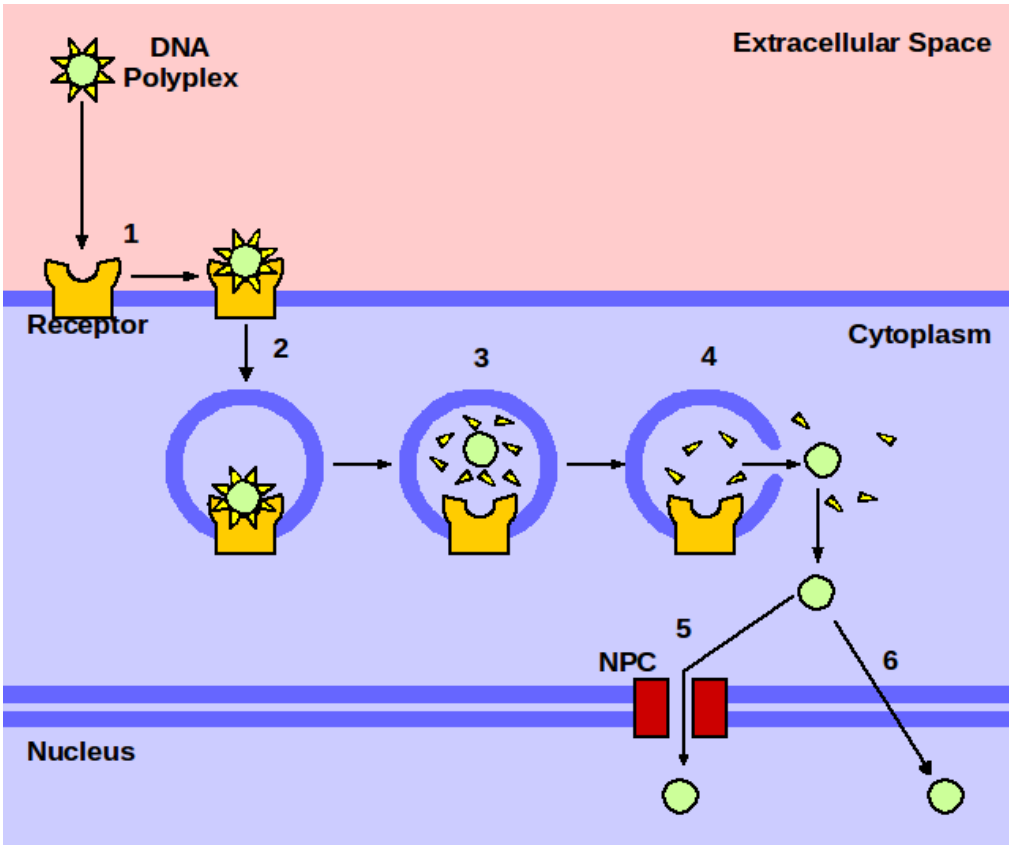

Figure 1-10: *Barriers to Nonviral Gene Delivery.* A DNA polyplex must bind to a receptor by a targeting ligand in step 1. The bound receptor is internalized through endocytosis in step 2. As the endosomal pH decreases, the polyplex can undergo structural changes, triggering endosmal escape mechanisms in step 4. Once in the cytoplasm, the DNA plasmid must enter the nucleus, either through the nuclear pore complex shown in 5, or through some other mechanism as shown in 6.

1.4.1.1 Circulatory Stability

Stability in the bloodstream is critically important to DNA delivery. If the DNA nanoparticle is not stable in circulation, it will not have sufficient time to locate its target in the body before it becomes degraded and no longer capable of being transcribed. Unprotected DNA is rapidly destroyed by nucleases[46], and several compounds have been used to help protect it. Cationic lipids and cationic polymers have been utilized to condense DNA into nanoparticle sized lipoplexes or polyplexes. Once condensed, DNA is far more resistant to nuclease degradation.

Cationic lipids have been extensively studied for use in DNA delivery[51,52]. The cationic head group binds to the anionic phosphate backbone of DNA and packages the DNA into layers of lipid bilayers[53]. Several conformations of DNA-lipid complex are possible, including liposomes that trap DNA in an aqueous interior, aggregates of micelles bound to DNA, and lamellar structures with DNA intercalated between the layers. The types of lipids and formulation methods used determine which structures are produced. While cationic lipids are commonly used to transfect cultured cells in vitro, they have not had as much success in vivo. Lipoplexes are susceptible to disintigration when exposed to serum[54], and can bind serum proteins in the blood, altering their behavior. Lipoplexes are known to aggregate in vivo, and these aggregates can accumulate in the liver, spleen, and lungs, possibly causing toxicity[55,56].

To alleviate these toxicity issues, several lipids have been developed with ionizable head groups with pKa of 7 or less. These lipids form lipoplexes with near neutral charges in the blood, and reduces their interaction with proteins and cellular membranes[57,58]. PEGylated lipids are also used to prevent aggregation, but can also hinder the lipoplex's ability to bind to target cells and release their DNA[59]. Therefore, PEGylated lipids are often designed to be exchangeable[60], with shorter lipid chains so that they can be inserted into the outer layer of the lipoplex after formulation with DNA. In the circulation, the PEGylated lipids eventually dissociate, which restores interaction with cellular membranes.

Cationic polymers, such as polyethyleneimine (PEI), polylysine, chitosan, and PAMAM have also been used for gene delivery[61–65], again with better success in vitro than in vivo. Cationic polymers are available in either linear, branched, or dendrimer forms. Similarly to the cationic lipoplexes, cationic polyplexes can aggregate in the bloodstream, causing embolisms

and toxicity. Again, PEGylation is often used to make these polymers safe for in vivo use.

PEI in particular has proven useful as an in vitro transfection agent. The polymer has many primary, secondary, and tertiary amines that can be positively charged and bind DNA, condensing it into complexes with diameters of 30 – 1000 nm. Shorter linear PEIs do not bind DNA as tightly, and form larger particles, while larger linear PEIs (22 kDa) bind more tightly and form smaller particles. Branched PEIs are even better at DNA binding, and form even smaller particles[66]. However, PEI is cytotoxic, and its toxicity tends to correlate with its affinity for DNA[67]. Chemical modifications that reduce its toxicity, such as the addition of PEG, also often reduce its ability to bind DNA and make it a less effective transfection agent.

1.4.1.2 Cellular Targeting and Uptake

Delivery of DNA to the proper tissue is important for treating disease. The interaction between DNA nanoparticles and the cellular surface is still not fully understood, however cell surface proteins are believed to be important. For example, many viruses are known to use heparan sulfate proteoglycans to bind to cells, especially syndecans[68]. Syndecans are single transmembrane domain proteins that interact with the cytoskeleton through actin, and are localized to filopodia, thin cellular extensions into the extracellular space. Viruses bind to these proteins and are pulled to the cell surface, where they are internalized. Lipoplexes and polyplexes have also been shown to bind to filopodia and get pulled to the cellular surface[69].

Once bound to the cellular surface, lipoplexes or polyplexes may be internalized by several mechanisms. Internalization may occur through clathrin-coated pits, caveolae, and macropinocytosis. The preferred method seems to be size dependent, where particles with

diameters around 100 nm being taken up by caveolae, particles around 250 nm being taken up by clathrin-coated pits, and particles larger than approximately 500 nm being taken up through macropinocytosis[70]. These pathways are not mutually exclusive, and the size ranges have some significant overlap. However, there is evidence to indicate that some internalization mechanisms are more effective at successful DNA delivery than others. For example, caveolae mediated endocytosis may avoid lysosomes and therefore avoid degradation[71]. However, material internalized through this pathway is usually targeted to caveosomes, which have a neutral pH rather than the acidic pH found in maturing endosomes. It is also possible, in vitro, to promote one internalization pathway over others using inhibitors. For example, chlorpromazine inhibits clathrin-coated pit mediated endocytosis, while nystatin and fillipin III inhibit caveolae mediated endocytosis by sequestering cholesterol, and wortmannin and amiloride inhibit macropinocytosis[72]. However, intracellular trafficking is complicated, and how lipoplexes or polyplexes are transferred from compartment to compartment is far from fully understood.

Targeting ligands have also been used to direct lipoplexes and polyplexes to specific tissues. Targeted receptors are often those upregulated in cancer cells, so that the DNA can be delivered to tumors and treat the cancer. This has the additional benefits that rapidly dividing cancer cells are easier to transfect due to simpler nuclear entry[73], and nanoparticles tend to accumulate in tumors due to the enhanced permeability and retention, EPR, effect[74,75].

One commonly targeted receptor is the transferrin receptor, which is upregulated in many cancers and binds the iron carrying protein transferrin[76]. Once bound, the receptor-transferrin complex is internalized into an endosome. Transferrin has been incorporated into several gene delivery systems, including lipoplexes and polyplexes[77,78]. Transferrin bound DNA nanoparticles

have been used to deliver genes such as the tumor suppressor p53[79,80] to prostate cancer cells in animal experiments, with some success. Antibodies against the transferrin receptor have also been used to target nanoparticles[81].

Another ligand commonly used to target cancer cells is folate. Again, the folate receptor is upregulated on many cancer cells, and folate has been used to deliver other anti-cancer agents to cancer cells[82]. Folate has been attached to PEI to form targeted polyplexes, and these polyplexes have had some success at treating cancer in mouse models[83]. While many studies have directly attached folate to PEI, other studies have attached folate to PEI through a PEG linker[84], to better present the ligand to the folate receptor.

Peptide based targeting ligands have also seen some use. The RGD peptide has been recognized as a cell recognition signal that interacts with integrin proteins on the surface of many cells[85]. The arginine-glycine-aspartate domain is often cyclized to properly present the peptide for binding. The cyclic RGD peptide was attached to PEI through a PEG linker to deliver the polyplex to intracranial xenografts in a mouse model of glioblastoma, increasing median survival time[86]. Other peptides have been used to target other tissues, such as the angiogenic vessel-homing peptide, APRPG, also linked to PEI through a PEG linker. Anti-VEGF siRNA delivered with this PEI was able to reduce the growth of microvessels and decrease tumor volume[87]. Another peptide used to deliver particles across the blood-brain barrier is called RVG, and was derived from a rabies virus glycoprotein[88]. The RVG peptide binds to the acetylcholine receptor on neurons. PEI was linked to RVG through a reducible disulfide bond and used to deliver red fluorescent protein DNA to the brain by tail vein injection, though fluorescence was only 1.3 fold higher than control.

Epidermal growth factor, EGF, a 53 amino acid peptide that binds the EGF receptor to stimulate cell growth has also been used. EGF was attached to modified branched PEI with PEG and a melittin derivative to lyse cellular membranes[89]. This PEI was used to deliver polyIC to nude mice with tumor xenografts, and was able to eliminate glioblastoma, breast, and skin cancer tumors in mice. Mutations in human epidermal growth factor receptor 2, HER2, are responsible for many breast and ovarian cancers, which often overexpress the receptor. The MC-10 oligopeptide, with sequence MARAKE, binds HER2, and was attached to a PEI-cyclodextrin derivative[90]. This system was used to deliver IFN-α expressing plasmid DNA to mouse xenograft models, and suppressed tumor growth.

Cartilage is a difficult tissue to deliver drugs to, given its dense extracellular matrix and lack of blood vessels. However, phage display was used to identify a "chondrocyte affinity peptide", CAP, with sequence DWRVIIPPRPSA. This peptide was covalently linked to PEI and used to successfully deliver GFP and luciferase genes to rabbit knee joints[91]. However, these polyplexes had to be injected into the knee joint.

1.4.1.3 Endosomal Escape

After the DNA nanoparticle is internalized into an endosome, it must escape into the cytoplasm before the DNA can be useful. Different mechanisms for endosomal escape have been utilized, but the ultimate goal is to disrupt the endosomal membrane and release the contents into the cytoplasm. Cationic lipids are believed to disrupt the endosome by interacting with the anionic lipids of the endosomal membrane to form ion pairs with a relatively small head group and wide hydrophobic tail region. This shape promotes the formation of an H_{II} inverted

hexagonal phase, which destabilizes membrane bilayers[92]. The use of helper lipids can promote the H_{II} phase, and dioleoylphosphatidylethanolamine, DOPE, is a very common helper lipid[51]. Another result of lipid ion pairing is releasing DNA from the cationic lipids, allowing the free plasmid to enter the cytoplasm. Some research indicates that when cationic lipids bind too tightly, the DNA is not expressed as efficiently, most likely because the lipids are still bound and the transcriptional machinery cannot access the DNA[93,94].

However, not all cationic lipid formulations benefit from a helper lipid or rely on the H_{II} phase. Gemini cationic lipids have two head groups, often with ionizable groups with pKas in the 5 – 7 range[95–97]. At neutral pH, the head groups are not fully charged, and the lipids form a stable bilayer. As the endosome is acidified, the head groups gain 1 or more charges, and electrostatic repulsion causes the head group to expand. This creates a lipid with a head group larger than its hydrophobic tail and promotes the H_I micelle phase, which can also disrupt membrane bilayers. DOPE strongly inhibits the H_I phase, most likely because the DOPE adopts a small head group, large tail group shape, which complements the gemini lipid's large head group, small tail group shape, stabilizing the bilayer phase[98].

Cationic polymers disrupt endosomes through a different mechanism, known as the "Proton Sponge Effect"[61,99,100]. The polymers usually have primary, secondary, or tertiary amines, or imidazole rings, with apparent pKas in the 5 – 7 range. As the endosome acidifies, the polymer buffers the endosomal pH. This forces the endosomal proton pump to push more H^+ ions into the endosome, which are accompanied by Cl^- ions. The additional ions increase the osmotic pressure inside the endosome and water leaks through the membrane, swelling the endosome and eventually rupturing it. While the proton sponge model has been challenged[101,102],

evidence to support the proton sponge effect includes observations that inhibiting the proton pump with bafilomycin A1 inhibits PEI mediated transfection[103–105], and that endosomes in PEI or PAMAM treated cells are larger than in cells treated with polymers that don't buffer as well[106,107].

Calcium phosphate DNA nanoparticles are another transfection method often used for in vitro transfection. The Ca^{2+} ions bind to the phosphate backbone and condense the DNA. As phosphate ions are added, insoluble calcium phosphate particles precipitate, trapping the DNA. These particles are large and sink on to the cell surface, where they can be internalized. Once inside the endosome, the calcium phosphate matrix is broken down as the endosome acidifies. The released ions increase the osmotic pressure, pulling in water and bursting the endosome in a similar manner to the proton sponge effect[108,109]. While calcium phosphate transfection has remained a mostly in vitro method, attempts have been made to adapt it for in vivo use. By forming the calcium phosphate DNA nanoparticles in an emulsion, lipid coated calcium phosphate particles were formed with controlled size. These particles could be further modified with PEG and targeting ligands and showed some success at in vivo DNA and siRNA delivery[110–112].

Another method for disrupting the endosomal membrane is to use a fusogenic peptide. This method is used by many viruses and bacteria[100,113]. Many enveloped viruses have membrane bound peptides that reach into the endosomal membrane, pulling the viral and cellular membranes close to each other and triggering membrane fusion, releasing the viral cargo into the cytoplasm[114,115]. The influenza haemaglutinin protein N-terminal domain is one such peptide[116–118]. When the endosome is acidified, aspartate and glutamate residues become protonated and the peptide undergoes a confomational change to become an alpha helix, which inserts into the

endosomal membrane. This peptide was used to design the diINF-7 peptide, which has been studied with siRNA and protein delivery[119,120]. The influenza peptide also inspired the GALA and KALA peptides, cationic amphipathic peptides that also become helical under acidic conditions and have been shown to lyse membranes. These peptides have been tested with lipoplexes and polyplexes and shown to increase transfection in vitro[121–129].

Other membrane disrupting peptides work by forming a pore that quickly allows water into the endosome, swelling the endosome and bursting it through osmotic pressure[130–132]. These pore forming peptides also form amphipathic helices, with one hydrophobic side that faces into the membrane and one hydrophilic side that faces into an aqueous channel. The channel is formed when several peptides aggregate into a circle. An example of these pore forming membranes comes from bee venom, and is known as melittin[133,134]. The peptide has powerful membrane disruption activity, but is also toxic, and must be carefully controlled to make it safe in vivo. Melittin has been combined with lipoplexes and polyplexes to enhance both DNA and siRNA transfection[135–138]. Recently, melittin has been used to help with siRNA delivery by separately targeting it toward hepatocytes with N-acetylgalactosamine, which deactivated the melittin until endosomal pH became low enough to remove the sugar groups[139]. One problem with membrane disrupting peptides is getting enough peptides into an endosome to achieve an effective concentration. Conjugating the peptides to the DNA nanoparticles can help get enough peptides into an endosome, but makes the formulation more complicated and may make the peptides less efficient if they cannot dissociate from the DNA particle. Delivering the peptides separately avoids those problems, but introduces the problem of getting enough peptides into the same endosomes as the DNA.

An additional consideration is the timing of release. As endosomes mature, they move toward the perinuclear space. Eventually, most endosomes are merged with lysosomes to digest their contents. Clearly, DNA should be released before it becomes degraded in the lysosome, but if the cargo is released too soon, it will have to travel further to the nucleus. Because the cytoplasm is a crowded environment, particles larger than 30 nm have great difficulty diffusing through the cytoplasm[140,141]. One way to move the DNA toward the nucleus would be to take advantage of the microtubule network of the cytoskeleton using motor proteins[142–144]. However, simply releasing the DNA from the endosome when it is closer to the nucleus would make up most of that distance. Alternatively, if the DNA could be protected well enough, releasing it from inside the lysosome may also be possible.

1.4.1.4 Nuclear Entry

Before DNA can be transcribed and translated, it must enter the nucleus, where the transcriptional machinery is kept. The nucleus is surrounded by a double layered membrane known as the nuclear envelope, and is contiguous with the endoplasmic reticulum. The nuclear pore complex is perforated with several nuclear pore complexes, large transmembrane protein complexes that allow molecules to pass between the cytoplasm and nuclear space. While molecules smaller than approximately 5 nm can passively diffuse through the nuclear pore complex, molecules larger than that must be pulled through by active transport[50]. Even with active transport, molecules larger than 39 nm cannot fit through.

Active transport through the nuclear pore complex is usually facilitated by proteins called importins. Proteins meant for transport into the nucleus have a nuclear localizing sequence, or

NLS, peptide. The best studied NLS peptide sequence comes from the SV40 virus large T antigen protein and has sequence PKKKRKV[145,146]. In the cytoplasm, the NLS peptide is bound by importin α, which then binds importin β. The importin-NLS complex is then pulled toward the nuclear envelope and eventually binds to a nuclear pore complex. The importin-NLS complex is then pulled through the nuclear pore complex and into the nucleus. Once in the nucleus, Ran-GTP binds to importin β, displacing the importin α-NLS complex. The importin α releases the NLS peptide, and both importins are exported from the nucleus. Once in the cytoplasm, Ran GAP hydrolyzes the RAN-GTP to RAN-GDP, Ran-GDP falls off importin β and is imported back into the nucleus[147,148].

When plasmid DNA enters the cytoplasm, it does not efficiently enter the nucleus. When DNA was microinjected into the cytoplasm of nondividing COS-7 cells, only 0.1% of the DNA was measured in the nucleus[149]. Many attempts were made to link plasmid DNA to an NLS peptide to increase the amount of DNA entering the nucleus. Methods include pairing the cationic SV40 NLS peptide to DNA by electrostatic interactions[150,151], covalently linking the NLS peptide to cationic polymers[152], biotinylating the DNA and forming DNA-Streptavidin-NLS complexes[153], and covalently linking the NLS directly to the DNA itself[154,155]. These attempts met with limited success at best. A successful report of DNA nuclear entry used linearized DNA with hairpins ligated to each end[156]. The 3' hair pin was attached to an NLS peptide, and an improvement in transfection of almost 100 fold over normal plasmid DNA was reported. Unfortunately, attempts by other groups to replicate this finding have not proven as fruitful[157,158]. Some reasons for the failure of these methods could be that the cationic NLS peptide binds to the anionic DNA, and is not properly presented to the nuclear import machinery. The addition of

multiple NLS peptides may recruit multiple importin complexes, which might not move through the NPC efficiently. DNA polyplexes could be too large to move through the NPC on their own. Additionally, the large covalently attached NLS peptide may hinder the transcriptional machinery and prevent gene expression even if the plasmid were successfully imported.

Other research has suggested that the DNA itself may carry a sort of nuclear localizing sequence[73,159]. Because transcription factor proteins are all produced in the cytoplasm, but needed in the nucleus, they have NLS peptides. Some of these transcription factors have their NLS peptides in separate positions from their DNA binding sites. When a DNA plasmid has binding sites for these transcription factors, the proteins may bind to the DNA and still properly present their NLS peptide for importin α binding. One of these proposed DNA "Nuclear Targeting Sequences" is a 72 bp portion of the SV40 enhancer[160–166]. This sequence contains binding sites for several transcription factors, such as AP1, AP2, NF-κB, Oct1, and TEF-1, which are ubiquitously expressed. Not all transcription factor binding sites can act as Nuclear Targeting Sequences, these transcription factors may not be able to bind DNA and present their NLS peptides at the same time. Some transcription factors are only found in certain cell types, potentially allowing for cell type specific nuclear entry and expression[167–169]. However, much of this work remains controversial, and often relies on microinjecting the plasmid DNA into the cytoplasm rather than use of a transfection agent. Many DNA polyplexes or lipoplexes may bind too tightly to allow transcription factors to bind or to move through the NPC. Nuclear entry remains a difficult barrier to cross for effective non-viral gene delivery.

1.5 Our Efforts Toward Nonviral Gene Delivery

1.5.1 Delayed Hydrodynamic Stimulation and Bioluminescent Imaging

Direct hydrodynamic delivery is a method for efficiently delivering material to the livers of small animals[170,171]. The method involves dissolving a substance, usually plasmid DNA, in a large volume of nomal saline, typically 8 – 10% of a mouse's mass, within 5 – 10 seconds. This method has been used to deliver several substances to mouse livers, including DNA[172,173], mRNA[174,175], nanoparticles[176], viruses[177], and cancer cells[178]. The delivered material enters the liver due to the fenestrated sinusoids allowing the high pressure liquid into the liver. The liver swells up as the high pressure forces liquid and dissolved material into the hepatocytes. There is research being done to adapt the technique to larger animals, such as dogs, pigs, and nonhuman primates, but this requires surgical techniques to isolate the liver from the rest of the circulation[179–181]. Though hydrodynamic injection is safe enough for routine use in small animals in research labs, the technique might not ever be made safe enough for practical use in humans.

Our lab has adapted hydrodynamic delivery to test the stability of DNA polyplex formulations in circulation by separating the DNA and saline doses. Plasmid DNA polyplex is first injected into the tail vein of a mouse in a small volume, approximately 100 μL. The DNA is allowed to circulate for some time, then the large volume of normal saline is rapidly injected into the tail vein to complete the hydrodynamic delivery. This technique has proven useful for demonstrating that plasmid DNA remains intact in the bloodstream over time[182–185]. If the DNA is intact, expression after delayed hydrodynamic stimulation is equal to expression of an equal dose of DNA after direct hydrodynamic delivery.

After hydrodynamic delivery of a luciferase encoding plasmid, luciferase activity can be measured using bioluminescent imaging. Bioluminescent imaging uses a sensitive CCD camera to capture photons emitted from the liver of an anesthetized mouse, generating an image that shows where the photons are being emitted from. Our group calibrated the bioluminescent imaging assay so that it could be used quantitatively[186].

1.5.2 Disulfide Linked Cationic Peptides

One issue with cationic polymers is that the polymers are almost always heterogenous. The range and distribution of polymer sizes may affect the transfection efficiency in vitro or their pharmacodynamics, pharmacokinetics, or biodistribution in vivo. If the polymer needs to be chemically modified with targeting ligands or other functional groups, the ligands are added at essentially random positions. The polydispersity in size and ligand sites may create significant batch to batch variation and complicate transfection.

To overcome some of these issues, cationic peptides may be used instead of cationic polymers. Because peptides can be produced by solid phase peptide synthesis, they can be reliably made with controlled size and known structure. The 20 standard amino acids, and many more artificial ones, allow a wide variety of functional groups to be added. However, solid phase peptide synthesis can only produce peptides of limited size, and yields quickly fall off as length increases.

To compensate for the shorter lengths, several peptides can be linked together using disulfide bonds by adding a cysteine at each end. Our group has produced several sulfhydryl crosslinking cationic peptides for gene delivery[187–191]. The crosslinking peptides produced higher

levels of expression than their cysteine free non-crosslinking counterparts. The longer lengths achieved by linking several peptides together created higher affinity for DNA, and when the polyplexes entered cells, the disulfides were reduced, weakening the affinity and releasing the DNA. Peptides were produced with PEG and targeting oligosaccharides and were able to produce detectable expression of secreted alkaline phosphatase in mice for up to 12 days after infusion into the tail vein[189,190]. The fusogenic peptide melittin, which is cationic, was modified with additional lysines and terminal cysteines. When crosslinked on DNA, it was able to transfect cells in vitro and compete with PEI[191]. Similar formulations were dosed in vivo and hydrodynamically stimulated at 5 min after initial dose[182]. Even though the bioluminescent signal was 5000 fold less than direct hydrodynamic injection of plasmid DNA, it was still able to provide some protection in the blood.

However, even these peptides have quite a bit of polydispersity because the number of peptides that crosslink cannot be controlled. Methods to produce crosslinked peptides with controlled structure were developed. By protecting the C terminal cysteine with dithiopyridine group and attaching an FMOC protected thiazoladine group, peptides could be assembled under controlled conditions[192]. The N terminal FMOC thiazoladine could be deprotected with piperadine, followed by silver triflate to convert the thaizoladine to a cysteine with a free thiol, which could react with the dithiopyridine on the next peptide. This method was extended by using a modified thiazolidine to create a penicillamine instead of a cysteine after deprotection[193]. The penicillamine disulfide bonds are more stable than cysteine disulfide bonds so that the peptide structure falls apart in a more controlled manner upon reduction. By using acetamidomethyl groups as an orthogonal protection group, individual cysteines on a peptide

could be deprotected, allowing the convergent synthesis of large peptide structures[194].

The great diversity of sequences available through solid phase peptide synthesis allows for the creation of large peptide libraries that might be useful as transfection agents. By adding cysteines to each end of the peptide to allow sulfhydryl crosslinking, different peptides can be polymerized, making the possible number of compounds much much larger. A large library was produced with 256 crosslinking peptides, then peptides were mixed and crosslinked to produce larger libraries (unpublished data). Attempts were made to analyze these peptides for potential as transfection agents failed to produce any outstanding compounds.

1.5.3 Polyacridine Peptides

Cationic lipids and cationic polymers bind to DNA by purely electrostatic interactions. These interactions can be displaced by the presence of competing ions, such as salts, proteins, or the cellular surface. To provide another mechanism of binding and increase affinity for DNA under physiological conditions, intercalating acridine groups were added to a polylysine peptide. Acridines were added either by conjugating acridine to a finished polylysine peptide[195], or building the peptide using an acridine-lysine amino acid[196]. The latter method was determined to be more effective. These peptides could bind to and condense DNA efficiently, and could protect it in the bloodstream of mice for prolonged periods of time. By altering the spacing of the acridine groups and how PEG was attached to the peptides, DNA stability was improved enough to keep it intact in the bloodstream for up to 4 hours[184,185].

1.5.4 Fusogenic Peptides

To help improve endosomal escape, a modified polyacridine peptide was produced using arginines instead of lysines to space out the acridine residues, and melittin was attached to the peptide either through a reducible disulfide linkage or a nonreducible maleimide linkage[197]. These peptides were used to transfect cultured cells in vitro, and some were able to transfect as well as PEI. The reducible linkages produced expression up to 1000 fold greater than their maleimide counterparts. This demonstrated that efficient transfection was possible in vitro using fairly short peptides rather than long cationic polymers or crosslinked melittin systems, and emphasizes the importance of releasing the fusogenic melittin from the DNA binding peptide.

1.5.5 Targeted Delivery

To improve the specifity and uptake of our peptide based nonviral gene delivery systems, some targeting ligands have been attached to the DNA binding peptides. The most commonly used ligand in our group is the triantennary oligosaccharide from bovine fetuin, which binds with high affinity to the asialoglycoprotein receptor commonly found on hepatocytes and can be internalized[198]. Sulfhydryl crosslinking cationic peptides with triantennary oligosaccharides were prepared with plasmid DNA and delivered to mice[190]. The formulations with the targeting oligosaccharide showed greater specifity for hepatocytes than for Kupffer cells, while nontargeted formulations were taken up by both cell types by approximately 50%.

Cationic peptide formulations using various amounts of crosslinking melittin and crosslinking PEG peptides with 10% of crosslinking triantennary oligosaccharide glycopeptide were prepared with DNA and tested in vivo by hydrodynamic stimulation at 5 minutes post-

delivery[182]. Those formulations with triantennary oligosaccharide produced higher signal than a control formulation where the terminal galactose residues of the oligosaccharide had been removed. The triantennary oligosaccharide peptides were also able to improve the formulation's specifity for hepatocytes, where 60% of the dose was found in hepatocytes and 40% in Kupffer cells. When the control oligosaccharide was used, 62% of the dose was found in Kupffer cells.

The triantennary oligosaccharide has also been conjugated to polyacridine peptides to improve the hepatocyte targeting. However, replacing some of the PEGylated peptides with the triantennary peptides tended to harm the biodistribution properties without evidence of targeting (unpublished data). To help alleviate this issue, peptides have been produced with the triantennary oligosaccharide conjugated to the polyacridine peptide through a long PEG linker, which should better present the oligosaccharide to the receptor while preserving the biodistribution.

Another targeting oligosaccharide used by our group is a high mannose oligosaccharide purified from soybean agglutinin[196]. The oligosaccharide was conjugated to a polyacridine peptide and used to transfect CHO cells in vitro. The CHO cells were split into 2 groups, one expressing the dendritic cell SIGN receptor and one without. The receptor positive cells showed 100 fold higher expression than the receptor negative cells, indicating that the high mannose oligosaccharide could be used to target an in vivo delivery system to dendritic cells and be useful for DNA based vaccines.

A targeting peptide studied by our group was octreotide, a cyclic peptide often bound to radioisotopes and used to image tumors by binding to the somatostatin receptor[199]. The peptide was produced and conjugated to polyacridine peptides, but did not show any significant

improvement in transfection (unpublished data).

1.6 Research Objectives

Current treatment options for genetic disorders of the liver leave much to be desired. Some disorders, such as hemophilia, can be managed through enzyme replacement therapy, which is expensive. Others, such as phenylketonuria, can be managed with a very strict diet. Others must be treated with liver transplantation, which requires a donor liver and life-long immune suppression. Gene therapy has the potential to offer better treatment for these disorders and others.

However, the field of gene therapy is still in its infancy. Only one gene therapy, Glybera, has been approved for use. Viral gene therapies pose the potential threat of insertional mutagenesis, inflammatory responses, and neutralizing antibodies that may prevent recurring doses. Nonviral gene therapy is believed to have a better safety profile with lower costs and better quality control. Unfortunately, nonviral gene therapy has remained less efficient than viral gene therapy in vivo.

This thesis is meant to expand on the work of others to improve nonviral gene therapy to the liver, with the ultimate goal of creating a safe and efficient method to deliver DNA to the liver.

In chapter 2, the in vitro transfection of HepG2 cells and primary hepatocytes in small format 384 and 1536 well plates with PEI or calcium phosphate will be presented. Primary hepatocytes are closer to the in vivo conditions of the liver than cancer derived HepG2 cells, and transfection agents that transfect primary hepatocytes in culture may be better suited for in vivo

delivery. By performing the transfection in small volumes, more compounds can be tested with a given batch of cells, increasing the efficiency of the experiments, and allowing high throughput screening of transfection agents.

In chapter 3, the mechanism behind delayed hydrodynamic stimulation is explored, and the effect of scavenger receptors on polyplex uptake is elucidated. By better understanding how the DNA nanoparticles behave in circulation and how to extend their circulatory half-lives, better DNA delivery systems can be built. Longer circulation times give more opportunities for a targeted DNA nanoparticle to find its target and successfully deliver its cargo. Furthermore, concepts learned here may be applied to nanoparticles in general.

Chapter 4 presents the development of messenger RNA peptide polyplexes with PEGylated polyacridine peptides for in vivo delivery. Messenger RNA does not need to enter the nucleus to express protein, and mRNA delivery may be a good way to treat certain illnesses where long-term protein expression is not needed. A functional mRNA delivery system may also be a useful tool for developing better DNA delivery systems. However, overcoming the inherit instability of mRNA presents a significant challenge.

Chapter 5 presents efforts towards using the membrane disrupting enzyme phospholipase A2 to aid in nuclear entry or endosomal escape. While this work failed to produce a useful reagent to enhance gene delivery, several modifications were successfully made to the enzyme by chemical conjugation, and some progress was made toward genetic modification of the enzyme.

2 Miniaturization of Gene Transfection Assays in 384 and 1536 Well Microplates

In collaboration with Jing Li, Sanjib Khargharia, and Meng Wu

This research is also presented in Analytical Biochemistry, 470 (2015) 14 – 21.

2.1 Abstract

Miniaturization of in vitro transfection assays to 384 or 1536 well plates greatly reduces the cost of experiments while increasing the number of experiments that can be performed, compared to the more common 96 well plate assays. This efficiency is especially valuable for primary cells, which are usually obtained in limited numbers. Luciferase and GFP reporter gene transfer assays were developed to optimize conditions of cell density, DNA dose, ratio of DNA to transfection agent, and luciferin dose. HepG2, CHO, and NIH 3T3 cells were transfected with polyethyleneimine, PEI, in 384 and 1536 well plates. Optimal parameters for luciferase transfection of HepG2 cells in 384 well plates were 5000 cells per well, 250 ng of DNA PEI per well at N:P ratio of 9. In 1536 well plates, 1200 cells per well with 80 ng DNA PEI at N:P of 9. These conditions produced Z' of 0.53 in 384 well plates, high enough for use in high throughput screening assays. However, Z' in 1536 well plates was only 0.42, below the 0.5 threshold. Primary hepatocytes were extracted from mice and plated in 384 well plates. Primary cells were transfected with PEI and calcium phosphate nanoparticles. When using PEI, optimal conditions were 250 cells per well and 400 ng per well of DNA PEI at N:P of 7. When using calcium phosphate, optimal conditions were 250 cells per well with 250 ng DNA per well at Ca:P ratio of 200. While primary hepatocyte transfections had large variability, Z' factors were below zero, the number of cells used per well was very low, allowing a single animal to provide enough cells to

perform many more experiments than previously possible.

2.2 Introduction

High throughput screening has become an important tool in the discovery of new pharmaceutical agents. To facilitate measurements on hundreds to thousands of samples in reasonable amounts of time and at affordable costs, assays must be miniaturized to fit in small volumes while retaining accuracy and precision. Assays have typically been adapted for use in 96 well plates, but recent years have seen increased use of 384 and 1536 well plates[200,201]. In addition to smaller plates allowing more samples to be analyzed at smaller volumes, advances in robotics have allowed for automated plate handling, liquid pipetting, and measurement.

In vitro non-viral transfection of cultured cells have been very useful for biological research. Transfection agents including cationic lipids[202–204], polyethyleneimines[205,206], cyclodextrins[207,208], chitosan and polysaccharides[209], dendrimers[210–212], polylysines[213,214], and disulfide cross-linking peptides[187,188] have been studied using screening assays, but usually in 6 to 96 well plates. These assays often use luciferase or green fluorescent protein reporter genes, due to their relatively simple assays.

Most classes of transfection agents are amenable to combinatorial and parallel chemistry, allowing for the creation of large compound libraries. Assaying these large libraries becomes cumbersome and expensive without miniaturization to save time, materials, and cost. Several reports have utilized 384 well plates for screening of transfection agents[205,210,215–223], but did not report optimization parameters for cell culture and transfection. Even fewer reports are available for gene transfection assays in 1536 well plates[224–227]. In addition to DNA delivery vectors,

miniaturized assays have been reported for siRNA delivery vectors to demonstrate knockdown in stably transfected cells[205,210,215–223].

Most in vitro transfection assays use mammalian cancer cell lines, which divide rapidly and can be easily maintained in culture[228]. This allows for large numbers of cells to be grown and used in the large format 6 and 96 well plate assays. However, these cells may not behave like their in vivo counterparts. Rapidly dividing cultured cells are much easier to transfect than non-dividing primary cells because the nuclear envelope is disassembled every time the cell divides, allowing plasmid DNA to enter the nucleus and become expressed[229]. Transfection agents that work well for cancer cell lines often fail to efficiently transfect primary cells[230], making in vitro transfection assays unreliable when developing transfection agents for in vivo use.

However, primary hepatocyte transfection has been reported with calcium phosphate ($CaPO_4$) nanoparticles[231,232], cationic lipids[233–235], and galactose based cationic glycolipids[236,237]. It is hoped that in vitro transfection agents that work well in primary cells are more likely to function in vivo. Obtaining and preparing primary cells for in vitro transfection is difficult, with a single animal providing a limited number of cells. Primary cells usually do not divide and cannot be maintained in culture for more than a few days. Therefore, miniaturization of transfection assays is critical for getting as many experiments as possible from a single batch of cells[238].

We have optimized in vitro non-viral transfection assays in 384 and 1536 well plates for HepG2, CHO, and NIH 3T3 cells using PEI. Additionally, we have optimized transfection for primary hepatocytes in 384 well plates using PEI and $CaPO_4$ DNA nanoparticles. These results allow for transfection of many samples of cells at minimal cost.

2.3 Materials and Methods

2.3.1 Cell Culture

HepG2, NIH 3T3, and CHO cells (American Type Culture Collection, Manassas, VA) were maintained in 10 cm plates with DMEM/F12 media without phenol red (Gibco Life Technologies, Grand Island, NY, USA) supplemented with 10% FBS (Gibco Life Technologies, Grand Island, NY, USA) and 1% 10,000 units/mL Penicillin/ 10,000 µg/mL streptomycin (Gibco Life Technologies, Grand Island, NY, USA). FBS was heat deactivated at 50 °C for 30 min. Cells were passed twice a week.

2.3.2 Primary Hepatocyte Extraction

Primary hepatocyte culture media was prepared with 500 mL Williams E Medium (Gibco Life Technologies, Grand Island, NY, USA), 5 mL penicillin/streptomycin (Gibco Life Technologies, Grand Island, NY, USA), 2.5 mL gentamycin (Gibco Life Technologies, Grand Island, NY, USA), 0.2 mL fungizone (Gibco Life Technologies, Grand Island, NY, USA), 5 mL 200 mM L-glutamine (Sigma Aldrich, St. Louis, MO, USA), 5 mL non-essential amino acids (Gibco Life Technologies, Grand Island, NY, USA). Percoll buffer was prepared with 9 mL percoll (GE Healthcare, Uppsala, Sweden), 1 mL 10X Hank's Balanced Salt Solution (Gibco Life Technologies, Grand Island, NY, USA), and 0.2 mL PBS (Gibco Life Technologies, Grand Island, NY, USA).

Primary hepatocytes were obtained from ICR mice (Harlan Laboratories, Indianopolis, IN, USA) by collagenase perfusion method[239]. Briefly, mice were anesthetized with ketamine and xylazine and restrained. A U incision was cut in the abdomen and intestines were moved to

expose inferior vena cava and portal vein. A cannula was inserted into the inferior vena cava and 39°C Liver Perfusion Medium (Gibco Life Technologies, Grand Island, NY, USA) was pumped into the liver at 10 mL/min with a peristaltic pump for 10 min. Portal vein was cut to let fluid drain, and blood was flushed from the liver. Liver was then perfused with 39°C Liver Digest Medium (Gibco Life Technologies, Grand Island, NY, USA) for 10 min. As liver was digested, it swelled. Perfusion was stopped when gently touching the liver would leave an indentation. The liver was removed and placed in a 10 cm plate with primary hepatocyte culture media, the gallbladder was removed and the liver was cut into sections, releasing the hepatocytes.

The crude hepatocyte suspension was passed through a 100 µm mesh filter into two sterile 50 mL tubes. Tubes were centrifuged at 50xg for 2 min, sedimenting live hepatocytes while leaving dead hepatocytes and other liver cells in supernatant. Supernatant was discarded and pellet was suspended in 10 mL primary hepatocyte culture media. Then, 10 mL of percol buffer was added and mixture was centrifuged at 50xg for 3 min. Supernatant was discarded and pellet was resuspended in 20 mL primary hepatocyte media and centrifuged at 50xg for 2 min. Pellet was suspended in 10 mL primary hepatocyte media. An aliquot of cells were stained with trypan blue and counted on hemocytometer to determine cell density and viability.

2.3.3 Luciferase Calibration Curve

HepG2 cells were plated into a 384 black solid wall well plate (VWR, Radnor, PA, USA) at 5000 cells per well, using a BioTek Multiflo (BioTek, Winooski, VT) with 5 µL cassette in 26 µL media. Cell suspensions were gently stirred to prevent settling during plating. At 24 hr post plating, 30 µl of firefly luciferase (Roche, Mannheim, Germany) at 0.64 – 10,000 pg/µL was

added to triplicate wells using the 384 pin head on a Janus automated workstation (Perkin Elmer, Waltham, MA, USA), followed by addition of 10, 20, or 30 µL of ONE-Glo luciferin solution (Promega, Fitchburg, WI, USA).

HepG2 cells were plated into each well of a 1536 black solid wall well plate (VWR, Radnor, PA, USA) at 1200 cells per well, using the BioTek Multiflo with 1 µL cassette in 6 µL media. Then, 2 µL of luciferase at 4.6 – 10,000pg/µL was added with 384 pin head of Janus automated workstation, followed by addition of 1 – 3 µL ONE-Glo luciferin.

Both plates were centrifuged at 1000 RPM for 1 min and incubated at room temperature for 4 min, then bioluminescence was measured on a Wallac Envision 2104-0010 Mutlilabel Plate Reader (Perkin Elmer, Waltham, MA, USA) with an emission filter of 700 nm at height of 6.5 mm.

2.3.4 Luciferase In Vitro Transfection of HepG2 Cells in 384 and 1536 Well Plates

HepG2 cells were plated at 5000 cells per well in 384 well plates. At 48 hr after plating, gWiz-Luc luciferase expressing plasmid DNA (Aldevron, Fargo, ND, USA) was mixed with an equal volume of polyethyleneimine, PEI, in HEPES Buffered Mannitol, HBM (5 mM HEPES, 2.7 M mannitol, pH 7.5) at a nitrogen:phosphate , N:P, ratio of 9, followed by incubation at room temperature for 30 min. Finally, 250 ng of gWiz-Luc PEI polyplex in 5 µL HBM was added to each well of cells.

HepG2 cells were plated at 1200 cells per well in 1536 well plates. Then 80 ng of gWiz-Luc PEI polyplex in 2 µL HBM was added to each well.

At 48 hr post-transfection, 5, 10, 20, or 30 µL ONE-Glo luciferin was added to each well of the 384 well plate and 1, 2, or 3 µL was added to each well of the 1536 well plate. Plates were centrifuged, incubated, and measured as described above.

2.3.5 Optimization of Cell Seeding Number and DNA Dose

HepG2 cells were plated at 2500, 5000, 10,000, 15,000, or 20,000 cells per well in 384 well plates. gWiz-Luc plasmid DNA was prepared with PEI at N:P of 9, and added to cells at 100, 150, 200, 250, or 300 ng per well in volume of 5 µL.

HepG2 cells were plated at 600, 900, 1200, or 1500 cells per well in 1536 well plates. gWiz-Luc plasmid DNA was prepared with PEI at N:P of 9, and added to cells at 40, 60, 80, 100, and 120 ng per well in 2 µL.

At 48 hr post transfection 10 µL of ONE-Glo was added to each well of the 384 well plate, and 2 µL ONE-Glo was added to each well of the 1536 wellplate. Plates were centrifuged, incubated, and measured as above.

2.3.6 Optimization of N:P Ratio and Bioluminescence Acquisition Time

HepG2 cells were plated in each well of 384 well plates at 5000 cells per well. gWiz-Luc plasmid DNA was prepared with PEI at N:P ratios from 0 – 27. Then, 250 ng of DNA PEI polyplex was added to each well of the plate in 5 µL volume.

HepG2 cells were plated in each well of 1536 well plates at 1200 cells per well. gWiz-Luc plasmid DNA was prepared with PEI at N:P ratios of 0 – 26 and 75 ng DNA PEI polyplexes were added to each well in 2 µL volume.

At 48 hr post-transfection, 10 μL ONE-Glo was added to each well of the 384 well plate, and 3 μL ONE-Glo was added to each well of the 1536 well plate. Both plates were centrifuged as above, but the 384 well plate was measured at 5, 10, 25, and 60 min. The 1536 well plate was measured at 5, 10, 25, 45, and 60 min.

Optimization for NIH 3T3 and CHO cells were performed following the procedures outlined for HepG2 cells.

2.3.7 Whole Plate Transfections

HepG2 cells were plated in every well of 384 and 1536 well plates with optimized conditions. In 384 well plates, cells were plated at 5000 cells per well, with 250 ng gWiz-Luc PEI polyplex at N:P of 9 and measured 5 min after addition of ONE-Glo, 2 columns were left untransfected to measure background. In 1536 well plates, cells were plated at 1200 cells per well, with 80 ng of gWiz-Luc PEI polyplex at N:P of 9 and measured at 5 min after addition of ONE-Glo, 4 columns were left untransfected to measure background.

2.3.8 GFP Transfection

In 384 well plates, 10,000 HepG2 cells were plated per well, and transfected with 250 ng of gWiz-GFP plasmid DNA with PEI at N:P of 0, 2, 4, 6 8, 9, 10, 12, 14, 18, and 27. Fluorescence was measured at 48 and 72 hr post-transfection on a Wallac Envision plate reader with λ_{ex} = 480 nm and λ_{em} = 510 nm.

In 1536 well plates, 1500 HepG2 cells were plated per well and transfected with 60 ng of gWiz-GFP plasmid DNA with PEI at N:P of 0, 2, 4, 6, 8, 9, 10, 12, 14, 18, 27. Fluorescence was

measured as described above.

2.3.9 Transfection of Primary Hepatocytes in 384 Well Plates

Primary hepatocytes, extracted as described above, were plated manually by 8 channel pipetter as the BioTek MultiFlo peristaltic pump used for HepG2 cells caused too much damage to primary hepatocytes, in 45 µL of Wiliam's Essential Media (Gibco Life Technologies, Grand Island, NY, USA). Since primary hepatocytes quickly lost viability, transfections were performed immediately after cells were plated instead of 24 hr post plating.

Fluid handling was done with a Hamilton Microlab Star Liquid Handling System (Hamilton, Reno, NV, USA). The instrument was programmed to transfer fluid from 1 well of a 96 well plate to 12 wells of 1 row of a 384 well plate to deliver DNA or luciferin to wells. Contents of wells A, B, C... of column 1 of the 96 well plate were transferred to rows A, C, E... respectively of the 384 well plate, while column 2 of the 96 well plate was transferred to rows B, D, F... of the 384 well plate. This program could be used to make up to 16 experimental groups with up to 12 samples in each group. However, the last three wells in each row often showed less signal than the other wells, suggesting that material was not delivered as well (**Fig. 2-1**)

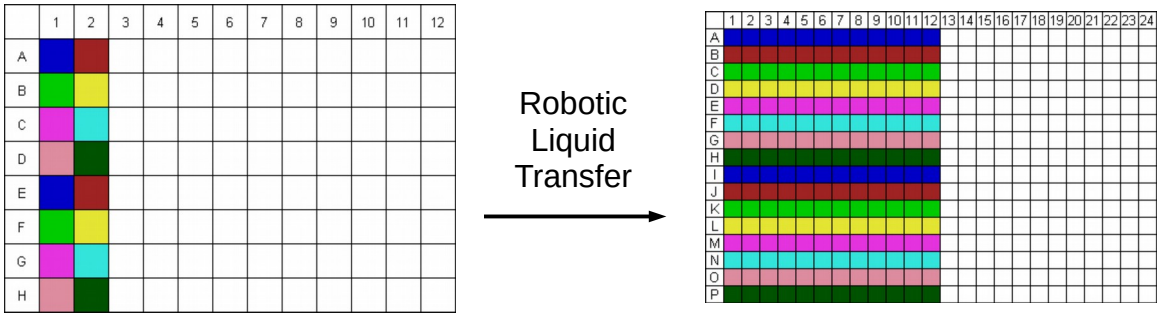

Figure 2-1: *Robotic Plating Diagram.* The Hamilton Microlab Star was programmed to transfer fluid from a 96 well plate to a 384 well plate. Wells are color coded to show what well in the 96 well plate is used for each well in the 384 well plate.

2.3.10 Effect of Collagen on Primary Hepatocyte Transfection

Rat Tail Collagen Type I (BD Biosciences, Franklin Lakes, NJ, USA) was diluted to 50 µg/mL in 20 mM acetic acid and 20 µL of solution was added to each well of alternating rows of a 384 well plate. Treated plates were incubated in cell culture hood for 2 hr, and rinsed three times with 50 µL PBS per well.

Primary hepatocytes were plated at 5000 cells per well in the collagen treated plates. At 24, 48, and 72 hr after plating, media was removed from some wells and cell viabilities were determined by hemocytometer with trypan blue staining.

Primary hepatocytes were plated in all wells at 5000 cells per well and transfected with 400 ng of gWiz-Luc PEI polyplexes at N:P of 0.5, 1.0, 2.0, 4.0, 7.0, 9.0, 11.0, and 13.0. At 24 hr post-transfection, bioluminescence was measured as described above.

2.3.11 Optimization of Primary Hepatocyte Cell Seeding Density

Primary hepatocytes were plated at 0, 15, 31, 62, 125, 250, 500, and 1000 cells per well in 384 well plates. Then, 400 ng of gWiz-Luc plasmid DNA PEI polyplex at N:P of 7 was added to each well of alternating rows, leaving other rows as untransfected controls. Bioluminescence

was measured at 24 hr post-transfection as described above.

2.3.12 Optimization of Primary Hepatocyte PEI N:P Ratio

Primary Hepatocytes were plated at 1000 cells per well in 384 well plates and transfected with 400 ng gWiz-Luc plasmid DNA PEI polyplexes at N:P of 0.5, 1, 2, 4, 7, 9, 11, and 13 in alternate rows. Bioluminescence was measured at 24 hr post-transfection as described above.

2.3.13 Primary Hepatocyte Bioluminescence Time Course

Primary Hepatocytes were plated at 250 cells per well in 384 well plates and transfected with 400 ng gWiz-Luc DNA PEI polyplexes at N:P of 7 in alternate rows. Bioluminescence of 1 row of transfected cells and 1 row of nontransfected cells was measured every 12 hr for 96 hr.

2.3.14 Optimization of Primary Hepatocyte DNA PEI Dose

Primary Hepatocytes were plated at 250 cells per well and transfected with 0, 50, 100, 150, 200, 300, 350, 400, 450, 500, 550, 600, 650, 700, or 750 ng of gWiz-Luc DNA PEI polyplexes at N:P of 7. Bioluminescence was measured at 24 hr post-transfection as described above.

2.3.15 Transfection of Primary Hepatocytes with Calcium Phosphate Nanoparticles

Calcium Phosphate, $CaPO_4$, DNA nanoparticles were produced with a procedure adapted from Olton et al[108]. Briefly, 13 µL of 0.5 M $CaCl_2$ was added to 117 µL of water containing 0.5 – 9.3 µg of gWiz-Luc plasmid DNA and allowed to equilibrate at room temperature for 15 min.

The DNA $CaCl_2$ solution was added to an equal volume, 130 µL, of 280 mM NaCl, 10 mM KCl, 12 mM dextrose, 50 mM HEPES, 1.25 mM Na_3PO_4, pH 7.5 at 13.4 µL per second using a syringe pump and vortexer to ensure rapid and consistent mixing.

Primary hepatocytes were plated at 250 cells per well in 384 well plates and $CaPO_4$ DNA nanoparticles were added with 0, 1, 5, 10, 20, 30, 40, 50, 100, 150, 200, 250, 300, 350, 400, 450, 500, 500, 600, 650, 700, or 750 ng DNA per well in volume of 5 µL. Bioluminescence was measured at 24 hr post-transfection as described above.

2.3.16 Effect of Excess DNA on $CaPO_4$ DNA Nanoparticle Transfection

$CaPO_4$ DNA nanoparticles were prepared as above, with 2.5 µg gWiz-Luc for approximately 50 ng of luciferase expressing DNA per well, and 0, 0.25, 0.5, or 2.5 µg of pSeap Control secreted alkaline phosphatase vector (Clontech, Mountain View, CA, USA) as a dummy plasmid. Primary hepatocytes were plated at 250 cells per well and transfected with these particles. Bioluminescence was measured at 24 hr post-transfection as described above.

2.3.17 Effect of PEGylated Polyacridine Peptide on $CaPO_4$ DNA Nanoparticle Transfection

$CaPO_4$ DNA nanoparticles were prepared as above with 2.5 µg gWiz-Luc plasmid DNA. After formation of particles, 0.0625, 0.125, 0.25, or 0.5 nmol of $(Acr\text{-}Lys_4)_3$-Acr-Lys-PEG_{5KDa}[184,185] was added to the particle suspension and incubated at room temperature for 15 minutes before addition to primary hepatocytes at 250 cells per well. Bioluminescence was measured at 24 hr post-transfection as described above.

2.3.18 siRNA Knockdown of Luciferase in Luciferase Expressing Primary Hepatocytes

Transgenic mice were bred to produce animals that constitutively expressed firefly luciferase in their livers. This was done by breeding B6.Cg-Tg(Alb-cre)21Mgn/J mice, which express Cre recombinase controlled by an albumin promoter, with FVB.129S6(B6)Gt(ROSA)26Sor<tm1(Luc)Kael>/J mice, which have a luciferase gene driven by the ROSA 26 sor locus. This produced a brown colored mouse, which was bred with albino C57BL/6 mouse (B6(Cg)-Tyr<c-2J>/J to produce albino mice with luciferase expression in the liver. All mice strains were obtained from Jackson Laboratories, Bar Harbor, ME, USA.

Primary hepatocytes were prepared as above from these transgenic mice. An anti-luciferase siRNA (Integrated DNA Technologies, Coralville, IA, USA) targeted against sequence GAUUAUGUCCGGUUAUGUA[240] with chemical modifications to prevent RNase degradation, was prepared with PEI at N:P of 9 with 0.022, 0.22, or 1.0 μg of RNA. RNA PEI polyplexes were delivered to hepatocytes and bioluminescence was measured as described above.

2.4 Results

2.4.1 Luciferase Calibration Curve

Luciferase was added to HepG2 cells and bioluminescence was measured to determine the relationship between amount of luciferase and bioluminescent signal with different amounts of luciferin in the presence of cells. In 384 well plates, background signal with no luciferase produced approximately 10^2 relative light units, RLU. Increasing the luciferase up to 300,000 pg per well produced a linear relationship across 7 orders of magnitude, and demonstrated that the detector was not saturated at 300,000 pg per well, which produced approximately $5x10^6$ RLU

(**Fig. 2-2A**). There was no significant difference between 10, 20, or 30 µL of ONE-Glo luciferin. Therfore, 10 µL was chosen as optimum amount of ONE-Glo for subsequent measurements in 384 well plates.

In 1536 well plates, luciferase was added at 0 to 20,000 pg per well with 1, 2, or 3 µL ONE-Glo. This still produced a linear relationship between pg of luciferase and RLU which covered 4 orders of magnitude (**Fig. 2-2B**). While there was no significant difference between 1, 2, or 3 µL of luciferin, the 1 µL results showed slightly higher standard deviations. Therefore, 2 µL ONE-Glo luciferin was chosen for subsequent measurements in 1536 well plates.

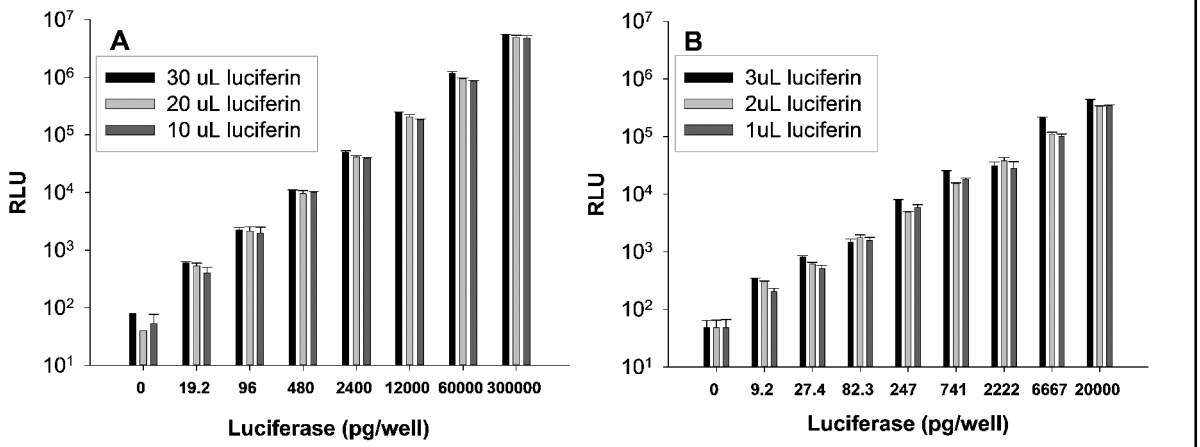

Figure 2-2: *Luciferase Standard Curve.* Purified luciferase enzyme was added to HepG2 cells on either 384 well plates in A or 1536 well plates in B. Both show good linearity and dynamic range.

2.4.2 Luciferase In Vitro Transfection of HepG2 Cells in 384 and 1536 Well Plates

HepG2 cells were transfected with gWiz-Luc luciferase expressing plasmid DNA using PEI as the transfection agent. In 384 well plates, bioluminescence was measured with 5, 10, 20, or 30 µL ONE-Glo luciferin. The 10, 20, and 30 µL samples all produced approximately 10^5 RLU, while the 5 µL samples produced approximately 10^4. All transfected wells showed significantly higher luminescence than non-transfected controls (**Fig. 2-3A**). Signal to

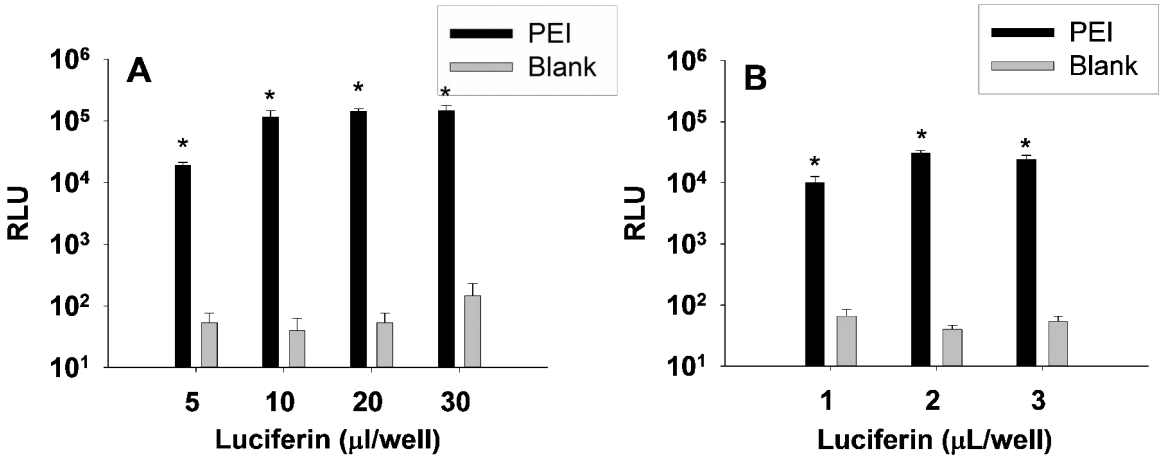

Figure 2-3: *Transfection of HepG2 Cells in 384 and 1536 Well Plates.* HepG2 cells were plated in 384 well plates in A or 1536 well plates in B and transfected with gWiz-Luc PEI polyplexes. Bioluminescence was measured with 5, 10, 20, or 30 µL ONE-Glo Luciferin in A or 1, 2, or 3 µL in B. Transfected cells show significantly higher signal than nontransfected controls. * = $p \leq 0.05$ relative to blank.

background between transfected and non-transfected wells was approximately 3000.

In 1536 well plates, bioluminescence was measured with 1, 2, or 3 µL of ONE-Glo luciferin. All three transfected groups produced approximately 10^4 RLU, significantly higher luminescence than non-transfected controls, however the 1µL samples produces a slightly lower signal than 2 or 3 µL (**Fig 2-3B**). Signal to background between transfected and non-transfected wells was approximately 455.

2.4.3 Optimization of Cell Seeding Number and DNA Dose

HepG2 cells were plated on 384 well plates at 2500 – 20,000 cells per well and transfected with 0 – 300 ng gWiz-Luc DNA PEI at N:P of 9. Non-transfected controls showed luminescence at background of 10^2 RLU. At 100 ng per well, cell seeding density had significant

effects on expression, with 2500 cells per well producing more luminescence than the higher density samples. However, as DNA PEI dose increased, the cell seeding density became less important and all produced approximately10^5 RLU (**Fig. 2-4A**). Cell seeding density of 5000 per well and DNA dose of 250 ng per well were chosen as optimum parameters for subsequent experiments in 384 well plates.

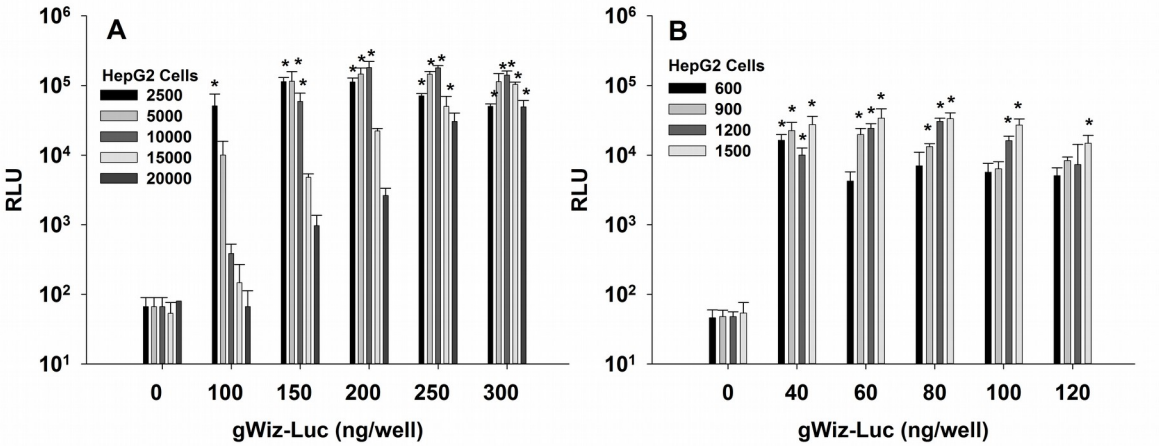

Figure 2-4: *Influence of Cell Plating Number and DNA Dose on Transfection.* HepG2 cells were plated in 384 well plates at 2500 – 20,000 cells per well and transfected with 0 – 300 ng gWiz-Luc PEI polyplexes in A, or 600 – 1500 cells per well were plated in 1536 well plates and transfected with 0 – 120 ng gWiz-Luc PEI polyplexes in B. In 384 well plates, optimal DNA dose was 250 ng, in 1536 plates, optimal DNA dose was chosen as 80 ng. * = $p \leq 0.05$ relative to 0 ng DNA dose.

On 1536 well plates, HepG2 cells were plated at 600-1500 cells per well and transfected with 0 – 120 ng gWiz-Luc PEI at N:P of 9. At 40 ng DNA PEI dose, all cell seeding densities produced approximately 10^4 RLU, significantly higher than background. As DNA dose increased the luminescence slightly decreased, especially on the lower cell seeding densities, such that at 120 ng DNA PEI, only the 1500 cell per well samples showed luminescence significantly higher than background (**Fig. 2-4B**). Cell seeding density of 1200 cells per well with DNA dose of 80 ng per well were chosen as optimum parameters for subsequent experiments in 1536 well plates.

2.4.4 Optimization of N:P Ratio and Bioluminescence Acquisition Time

HepG2 cells were plated in 384 well plates at 5000 cells per well and transfected with 250 ng of gWiz-Luc plasmid DNA with PEI at N:P ratios from 0 – 27. Bioluminescence was measured 5, 10, 25, and 60 min after addition of ONE-Glo luciferin. N:P ratios from 4 – 18 produced luminescence significantly higher than background, however N:P of 4 produced lower signal than other ratios (**Fig. 2-5A**). Luminescent signal was consistently, but not significantly, lower at later time points. N:P of 9 and a measurement time of 5 min were chosen as optimum parameters for 384 well plates.

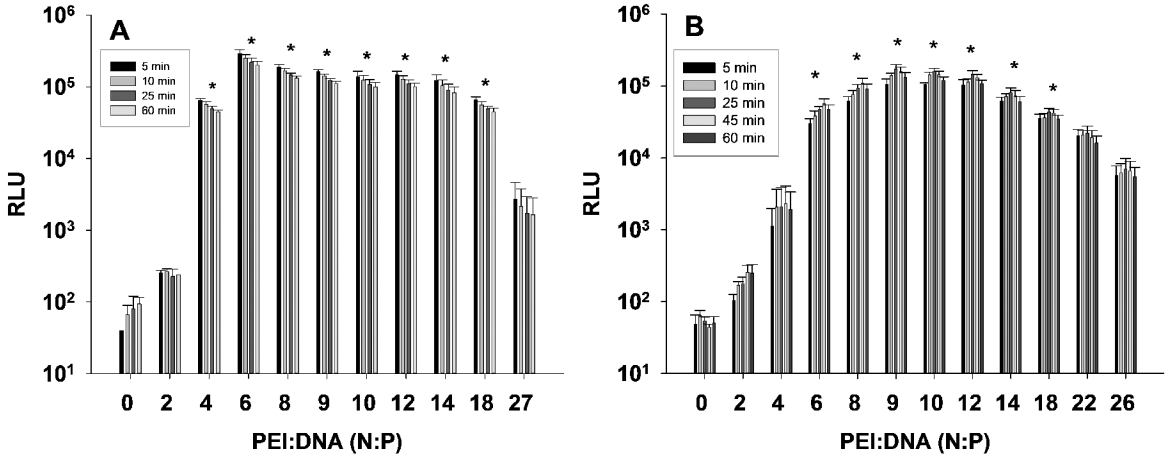

Figure 2-5: *Influence of Varying PEI to DNA Ratio and Bioluminescence Acquisition Time.* HepG2 cells were plated in 384 well plates at 5000 cells per well and transfected 250 ng gWiz-Luc PEI polyplex at N:P ratio of 0 – 27 in A, or plated in 1536 well plates at 1200 cells per well, transfected with 75 ng of gWiz-Luc PEI polyplex at N:P ratio of 0 – 26 in B. Bioluminescent acquisition time was varied from 5 – 60 min. * = $p \leq 0.05$ relative to 0 N:P ratio.

HepG2 cells were plated in 1536 well plates at 1200 cells per well and transfected with 75 ng gWiz-Luc plasmid DNA with PEI at N:P ratios from 0 – 26. Bioluminescence was measured at 5, 10, 25, 45, and 60 min after addition of ONE-Glo luciferin. N:P ratios from 6 – 18 produced luminescence significantly higher than background (**Fig. 2-5B**), with peak signal at

N:P of 9. Signal was slightly higher at 45 min than at other time points, but not significantly so. N:P of 9 and measurement time of 5 min were chosen as optimum parameters for 1536 well plates.

2.4.5 Whole Plate Transfections

HepG2 cells were plated in all wells of 384 well plates and transfected with 250 ng of gWiz-Luc PEI at N:P of 9. All transfected wells showed signal of approximately 10^5 RLU, with little variability from well to well, demonstrated by a Coefficient of Variance, CV, of 16% and Z' factor of 0.53 (**Fig. 2-6A**).

HepG2 cells plated in all wells of 1536 well plates and transfected with 80 ng gWiz-Luc PEI at N:P of 9 showed luminescence at approximately 10^4 RLU. Variation was slightly higher than in 384 well plates, with CV of 19% and Z' of 0.42. Wells around the edge of the plate showed more variability than wells in the interior (**Fig 2-6B**).

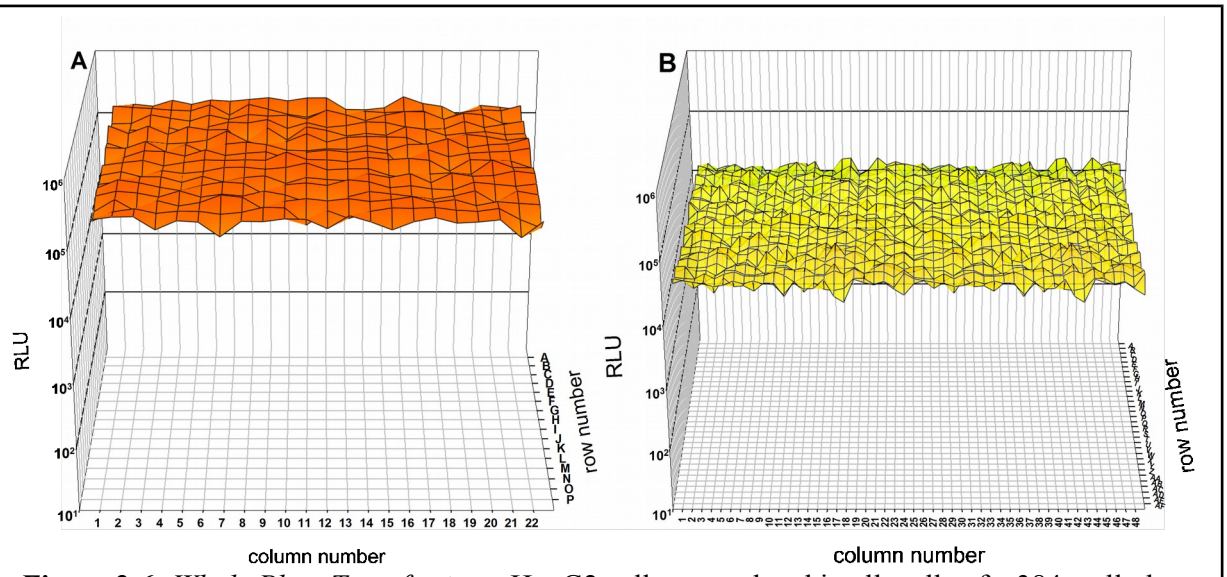

Figure 2-6: *Whole Plate Transfections.* HepG2 cells were plated in all wells of a 384 well plate in A or 1536 well plate in B and transfected according to optimized parameters.

2.4.6 Optimization of Other Cell Lines

Conditions for NIH 3T3 and CHO cells were optimized using similar procedures used for HepG2 and optimal conditions are outlined in **Table 2-1**.

Plate	384-Well Plate			1536-Well Plate		
Cell Type	**Cells/Well**	**DNA Dose ng/Well**	**S:B[a] Ratio**	**Cells/Well**	**DNA Dose ng/Well**	**S:B[a] Ratio**
HepG2	5000 – 15,000	150 – 300	2000	900 – 1200	40 – 100	400
HNIH 3T3	2500 – 5000	200 – 300	3800	400 – 900	60 – 120	750
CHO	2500 – 10,000	100 – 300	3200	600 – 1200	40 – 120	500
Volume[b]	25 µL			6 µL		
Polyplex	5 µL			2 µL		
ONE-Glo	10 µL			2 µL		

a: Signal to Background b. Volume of Media

Table 2-1: *Summary of Optimized Transfection Parameters for Cells on 384 and 1536-Well Plates.*

2.4.7 GFP Transfection

HepG2 cells were plated in 384 well plates at 10,000 cells per well and transfected with 250 ng Gwiz-GFP PEI at N:P of 0 – 27 and fluorescence was measured at 48 and 72 hr post-transfection. Signals were higher at 72 hr than at 48 hr, but with larger standard deviations. N:P ratios of 6 – 14 produced fluorescence above background, with N:P of 6 producing the highest signal (**Fig. 2-7A**). However, signal to background ratio was about 10 – 15.

HepG2 cells were plated in 1536 well plates at 1200 cells per well and transfected with 60 ng gWiz-GFP PEI at N:P of 0 – 27 and fluorescence was measured at 48 and 72 hr post-transfection. N:P from 6 – 12 produced signal significantly above background, with highest signal at N:P of 8 (**Fig. 2-7B**). Again, signal was higher at 72 hr, but standard deviations were also larger, and signal to background ratios still fell into the 10 – 15 range.

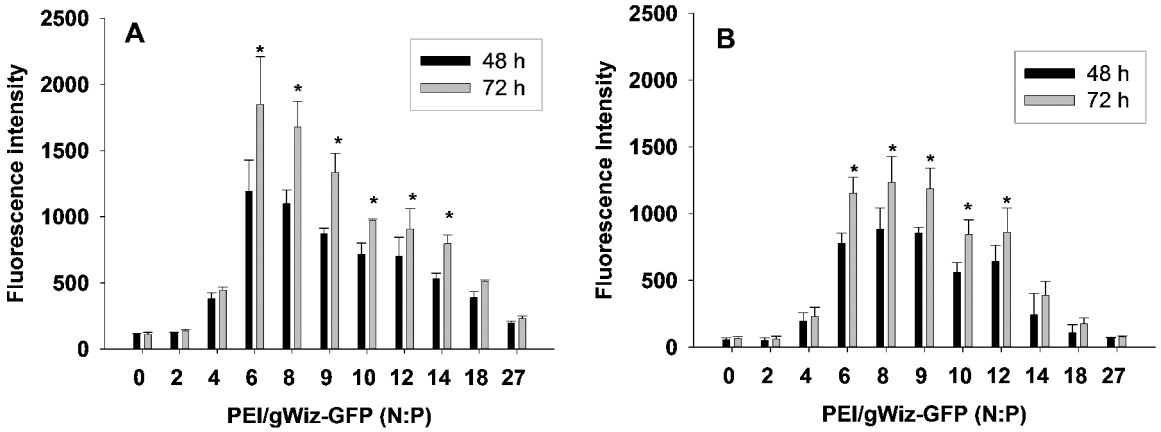

Figure 2-7: *Transfection of HepG2 Cells with GFP in 384 and 1536-Well plates.* HepG2 cells were plated it 10,000 cells per well in 384 well plates and transfected with 250 ng gWiz-GFP PEI polyplexes at N:P 0 – 27 in A or plated at 1500 cells per well in 1536 well plates and transfected with 60 ng gWiz-GFP PEI polyplexes at N:P 0 – 27 in B. Optimal N:P was 6 in 384 well plates and 6 – 8 in 384 well plates. * = $p \leq 0.05$ relative to 0 N:P.

2.4.8 Effect of Handling and Collagen Coating on Primary Hepatocyte Transfection

Primary hepatocytes were plated on 384 well plates at 5000 cells per well using either the BioTek Multiflow with the 5 µL or 1 µL cassette or manually with an 8-channel pipette. Viability was estimated 24 hr later using trypan blue exclusion on hemocytometer. The MutliFlo with 5 µL cassette produced viability of about 60%, while the cells passed through the 1 µL cassette were about 50% viable. The manually pipetted cells were about 80% viable.

Primary hepatocytes were plated on 384 well plates at 5000 cells per well with or without collagen coating. Cells were removed and viability was estimated at 24, 48, or 72 hr after plating. Viability was similar with or without collagen, with approximately 80% viable at 24 hr, 70% viable at 48 hr, and less than 40% viable at 72 hr.

Primary hepatocytes were plated at 5000 cells per well on 384 well plates in wells with or without collagen coating. Cells were transfected with 400 ng of gWiz-Luc plasmid DNA PEI at

N:P of 9 and bioluminescence was measured 24 hr post-transfection. N:P ratios of 4 and above produced luminescence of approximately 10^3 RLU whether collagen was present or not (**Fig. 2-8**).

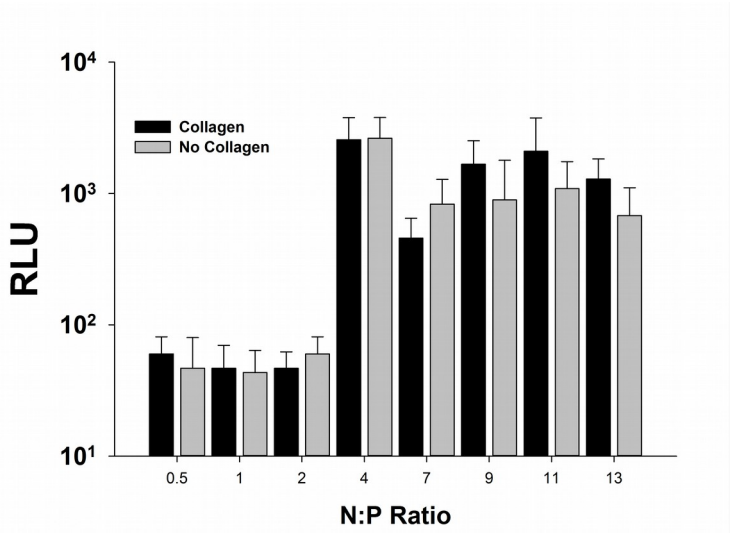

Figure 2-8: *Effect of Collagen Coating on Primary Hepatocyte Transfection.* Collagen coating has no significant effect.

2.4.9 Optimization of Primary Hepatocyte Cell Seeding Density

Primary hepatocytes were plated in 384 well plates at 0 – 1000 cells per well and transfected with 400 ng gWiz-Luc PEI at N:P of 7. All wells with cells and DNA produced luminescence of about 10^3 RLU, with 500 and 1000 cells per well being significantly higher than background (**Fig. 2-9A**). Interestingly, 15 – 250 cells per well produce about the same amount of luminescence. Therefore, 250 cells per well was chosen as optimum for primary hepatocyte cell seeding density.

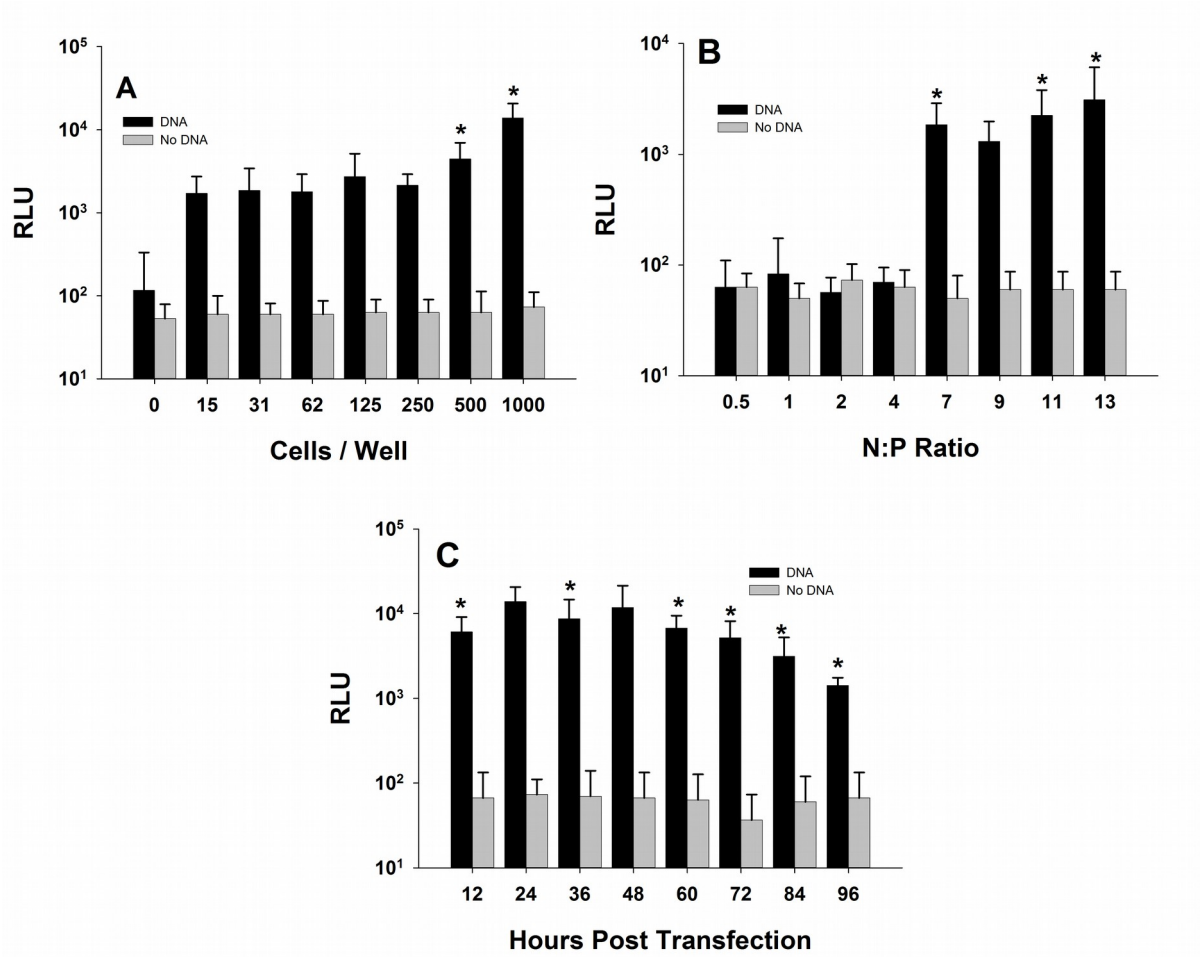

Figure 2-9: *Transfection of Primary Hepatocytes in 384-Well Plates.* Primary Hepatocytes were plated in 384 well plates at 0 – 1000 cells per well and transfected with 400 ng gWiz-Luc PEI polyplexes at N:P of 7 in A. Primary Hepatocytes were plated at 1000 cells per well and transfected with 400 ng gWiz-Luc PEI polyplex at N:P 0.5 – 13 in B. In C, 250 primary hepatocytes per well were plated and transfected with 400 ng gWiz-Luc PEI polyplexes at N:P of 7 and Luminescence was measured every 12 hr for 96 hr. Optimal cell seeding density was chosen to be 250 cells per well, with an optimal N:P of 7, and optimal measurement time of 24 hr. In A and B, * = significantly greater than nontransfected control, $p < 0.05$, in C * = significantly different from signal at 24 hr, $p < 0.05$.

2.4.10 Optimization of Primary Hepatocyte PEI N:P Ratio

Primary hepatocytes were plated in 384 well plates at 1000 cells per well and transfected with 400 ng of gWiz-Luc PEI at N:P of 0.5 – 13. N:P from 7 – 13 produced about 10^3 RLU, with

7, 11, and 13 being significantly higher than background (**Fig. 2-9B**). N:P of 7 was chosen as optimum for primary hepatocyte PEI transfections, as N:P higher than 7 could begin to show toxicity.

2.4.11 Primary Hepatocyte Luciferase Expression Timecourse

Primary hepatocytes were plated at 250 cells per well and transfected with 400 ng gWiz-Luc PEI at N:P of 7. At 12 hr intervals, a row of transfected cells and row of non-transfected cells were measured for bioluminescence. Luminescence was just below 10^4 RLU as early as 12 hr, and peaked at approximately 10^4 RLU from 24 – 48 hr, then gradually fell off to approximately 10^3 RLU at 96 hr (**Fig. 2-9C**). Signal at all time points except 48 hr were significantly below signal at 24 hr. Measurement at 24 hr was chosen as optimum, but signal was strong enough to measure even at 96 hr.

2.4.12 Optimization of Primary Hepatocyte DNA PEI Dose

Primary hepatocytes were plated at 250 cells per well in 384 well plates and transfected with 0 – 750 ng of gWiz-Luc PEI at N:P of 7. Signal plateaued at approximately 10^3 from 300 – 550 ng per well, which were all significantly higher than non-transfected cells (**Fig. 2-10A**). DNA dose of 400 ng per well was chosen as optimum for primary hepatocytes with PEI. When transfected under these optimal conditions, CV was 80% and Z' was -1.9.

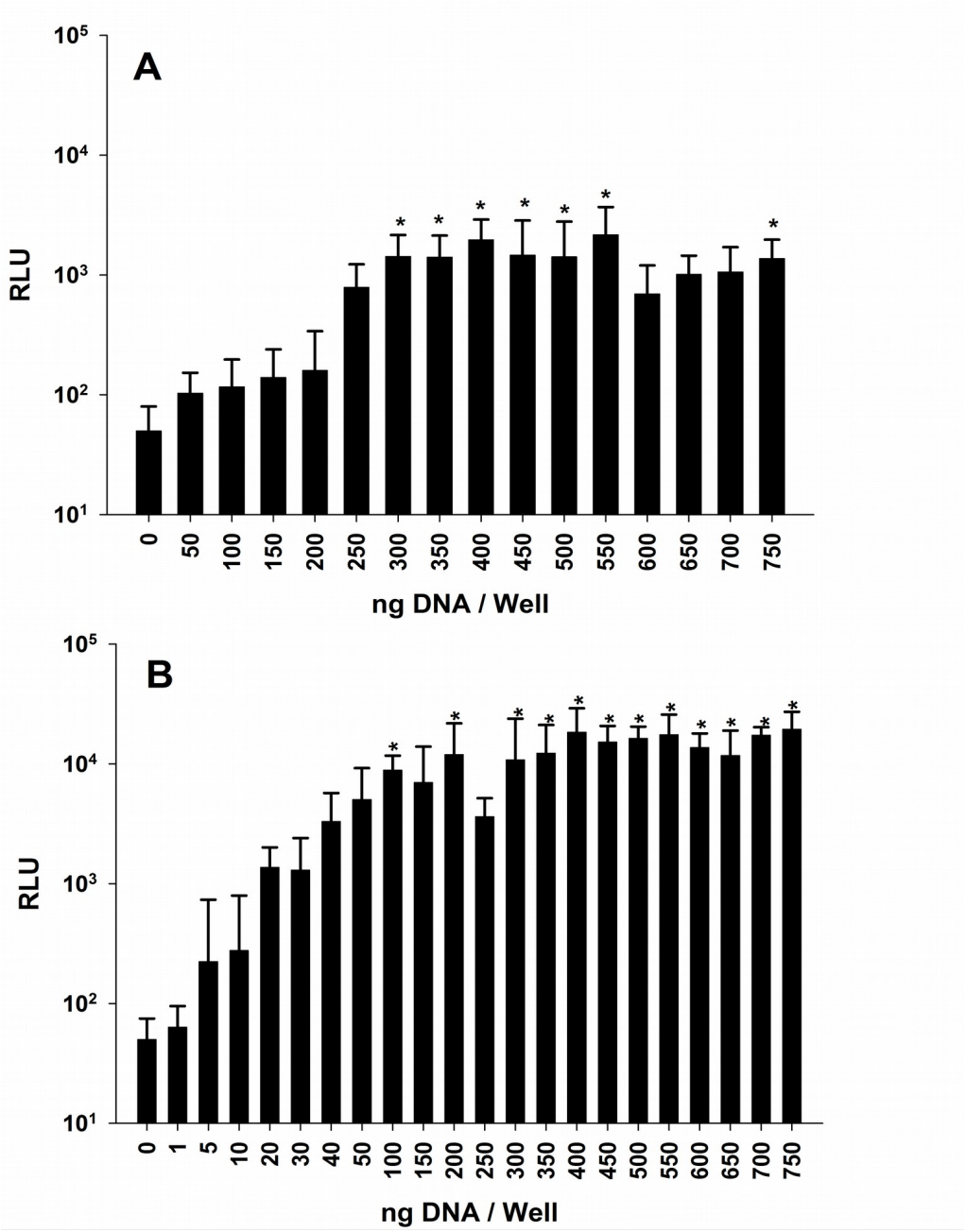

Figure 2-10: *PEI and $CaPO_4$ Transfection of Primary Hepatocytes.* Primary hepatocytes were plated at 250 cells per well and transfected with 0 – 750 ng gWiz-Luc PEI polyplex at N:P 7 in A or with 0 – 750 ng DNA $CaPO_4$ nanoparticles in B. With PEI, an optimal plateau is seen between 300 and 550 ng of DNA. With $CaPO_4$, all doses above 100 ng show the same high signal. * = significantly greater than 0 ng dose, $p < 0.05$.

2.4.13 Transfection of Primary Hepatocytes with Calcium Phosphate Nanoparticles

Primary hepatocytes were plated at 250 cells per well in 384 well plates. $CaPO_4$ DNA nanoparticles were prepared and dosed at 0 – 750 ng DNA per well. At doses of 100 ng per well and above, signal was approximately 10^4 RLU, an order of magnitude higher than average signal produced by PEI transfection (**Fig. 2-10B**). DNA dose of 250 ng per well was chosen as optimum for primary hepatocyte $CaPO_4$ DNA nanoparticle transfection. CV was 62% and Z' was -0.9.

2.4.14 Effect of Excess DNA on $CaPO_4$ DNA Nanoparticle Transfection

$CaPO_4$ DNA nanoparticles were produced with 2.5 μg gWiz-Luc plasmid DNA and 0.00, 0.25, 0.50, or 2.50 μg pSEAP plasmid to increase total DNA without changing amount of luciferase expressing DNA. Primary hepatocytes were plated in 384 well plates at 250 cells per well and transfected with the equivalent of 50 ng of gWiz-Luc $CaPO_4$ nanoparticles. Higher amounts of total DNA produced insignificantly higher luminescence (**Fig. 2-11**).

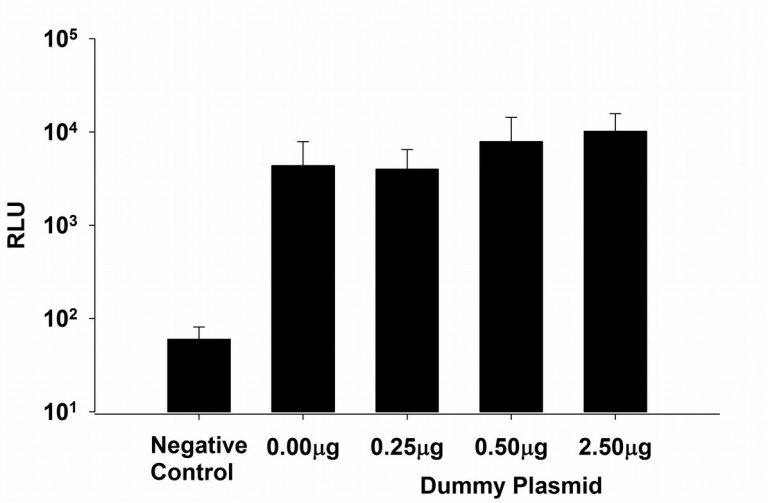

Figure 2-11: *Effect of Adding Dummy Plasmid when Producing $CaPO_4$ DNA Nanoparticles.* Additional DNA did not affect transfection.

2.4.15 Effect of PEGylated Polyacridine Peptide on $CaPO_4$ DNA Nanoparticle Transfection

$CaPO_4$ DNA nanoparticles were prepared with gWiz-Luc plasmid DNA and then treated with 0.000, 0.025, 0.050, 0.100, 0.200 nmol of PEGylated polyacridine peptide $(Acr\text{-}Lys_4)_3$-Acr-Lys-Cys-PEG_{5kDa} per µg of DNA. Primary hepatocytes were plated at 250 cells per well in 384 well plates and transfected with peptide treated nanoparticles. As amount of peptide increased, luminescence decreased, though the change was not statistically significant (**Fig. 2-12**).

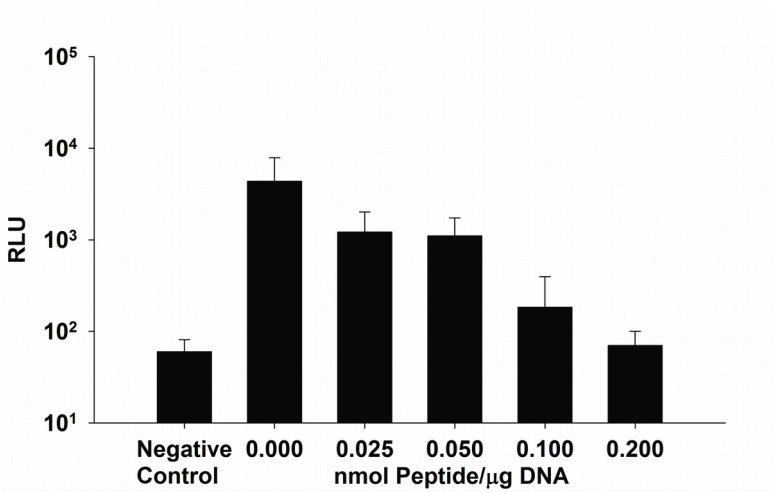

Figure 2-12: *Effect of Adding PEGylated Peptide to $CaPO_4$ DNA Nanoparticles.* Addition of PEG peptide inhibits transfection

2.4.16 siRNA Knockdown of Luciferase in Luciferase Expressing Primary Hepatocytes

Transgenic mice were bred to prepare albino animals that expressed luciferase in their livers. These animals were used to prepare primary hepatocytes, which were plated in 384 well plates at 250 cells per well. Cells were treated with 0, 0.022, 0.22, or 1.0 µg of anti-luciferase siRNA per well. All cells produced approximately 10^3 RLU (**Fig. 2-13**).

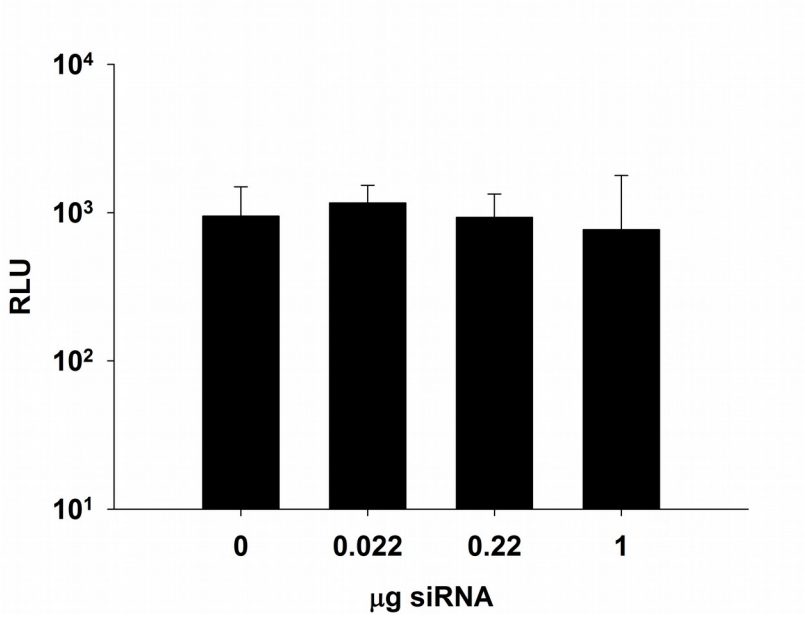

Figure 2-13: *Attempt to Knock Down Luciferase Expression in Primary Hepatocytes from Transgenic Mouse.* siRNA PEI polyplexes failed to reduce bioluminescence at 1 µg per well.

2.5 Discussion

The goal of this study was to find optimized parameters for the in vitro transfection of immortalized cell lines or primary hepatocytes in the miniature formats of 384 and 1536 well plates. By miniaturizing the assays, more experiments can be conducted with less material, and compromises were often made to reduce cost.

Luciferase assays were chosen due to the low background signal and high sensitivity offered by luminescence measurements. However, luciferase requires luciferin substrate, which is often expensive. In larger formats, such as 6 well plates, luciferase assays are usually performed by lysing the cells and manually scraping them out of the wells, then assaying the lysates in a luminometer. Promega ONE-Glo luciferin mixture simplifies this assay by combining the luciferin with the lysis buffer, so the mixture only needs to be added to the cells and measured in a plate reading luminometer. Promega recommends a 1:1 addition of ONE-Glo

to cell media, such as 30 µL ONE-Glo to 30 µL media. However, this study has demonstrated that in 384 well plates, a 1:3 ratio of ONE-Glo to media produces almost identical signal (**Fig. 2-2**), so 10 µL ONE-Glo can be added to 30 µL media, saving on reagent. This finding also applies to 1536 well plates, where 1, 2, or 3 µL ONE-Glo was added to 6 µL of media.

Similar results are obtained when purified recombinant luciferase is replaced with luciferase expressing transfected cells (**Fig. 2-3**). A preliminary transfection of HepG2 cells in 384 or 1536 well plates showed that in 384 well plates, 10, 20, and 30 µL of ONE-Glo added to 30 µL of media produced identical signal, while 5 µL ONE-Glo produced slightly less. In 1536 well plates, 1 µL produced slightly less luminescence than 2 or 3 µL. It should be noted that the 1536 well plate could not hold the entire volume of media and luciferin, 3 µL of media was removed prior to addition of ONE-Glo, adding an extra step to the procedure. Even the smallest ratio of ONE-Glo to media produced luminescence significantly higher than non-transfected controls, suggesting that less luciferin could be used to further save on materials if one was willing to sacrifice signal to background ratio. Therefore, 10 µL of ONE-Glo was chosen for 384 well plates and 2 µL was chosen for 1536 well plates.

Cell culture and transfection conditions were optimized, beginning with cell seeding density and DNA dose (**Fig. 2-4**). In 384 well plates, luminescence is strongly dependent on seeding density at low doses of DNA. At a 100 ng per well does of DNA-PEI, the lowest density of 2500 cells per well produced higher signal than the higher seeding densities. As DNA dose increased, the cell seeding density became less important, with all densities producing approximately 10^5 RLU, significantly higher than background. This relationship between cell seeding density and DNA dose may be explained by rate of cellular division[241]. At lower seeding

densities, HepG2 cells must divide several times to become confluent, where higher densities allow fewer divisions before the plate is filled. Because the nuclear envelope presents a significant barrier to plasmid DNA, cellular division is often necessary to get efficient gene transfer. If fewer cells divide over the course of transfection, fewer plasmids can enter nuclei and become expressed. However, at high doses of DNA PEI, the additional PEI may help overcome these barriers.

In 1536 well plates, the opposite pattern was observed. At low doses of DNA, all seeding densities showed equal luminescence at approximately 10^4 RLU. However, as DNA dose increases, the lower seeding densities lose signal. This may be explained by increasing amounts of PEI eventually showing toxicity and killing off cells that would have otherwise been transfected.

The ratio of PEI to DNA is another very important factor in transfection, and is commonly reported as Nitrogen:Phosphate, or N:P ratio[242]. At an N:P of 2, where DNA and PEI are present in approximately equal weights, DNA is fully bound by PEI through electrostatic interaction between the positively charged amines of PEI and negatively charged phosphates of the DNA backbone. As the amount of PEI increases beyond an N:P of 2, excess free PEI is believed to participate in the "proton sponge effect"[243,244], though the exact mechanism is debated[245]. When DNA PEI polyplexes are taken up by cells through endocytosis, the polyplex is trapped in an endosome, and must escape if the DNA is to be expressed. As the endosome matures, it become acidified, and its pH drops to as low as 5.5. PEI acts as a buffering agent, forcing the cell to pump additional protons into the endosome to achieve the same pH. With additional protons the endosome also receives additional chloride anions and osmotic pressure,

eventually bursting and releasing the polyplex. If there is not enough free PEI to act as a proton sponge, the polyplex cannot escape and there will be no transfection. However, PEI is toxic at high concentrations, so N:P ratio must be carefully controlled to ensure transfection without causing excessive damage to the cells. In 384 well plates, N:P in the range of 4 to 18 was able to transfect cells (**Fig. 2-5**), with 9 chosen as optimal because it was in the middle of the range. In 1536 well plates a range of 6 to 18 was also able to transfect cells, again N:P of 9 was chosen as optimal.

The time between adding ONE-Glo luciferin and measuring luminescence was also optimized (**Fig. 2-5**). In 384 well plates, 5 min was chosen because the signal was higher than at later time points, but not significantly so. Plates could be read as late as 60 min after addition of ONE-Glo with minimal loss of signal. In 1536 well plates, maximum signal was usually achieved at 45 min after addition of luciferin. This may be due to less efficient mixing in the smaller wells of the 1536 well plate. The 1536 well plates have more complicated timing than 384 well plates. The Janus automated workstation has a 384 pin head that can add luciferin to every well of a 384 well plate in one transfer, but a 1536 well plate needs 4 transfers to fill every well, requiring several minutes and creating well to well discrepancies in time between addition and measurement. When measuring the well plates, the Wallac Envision plate reader can read a 384 well plate in less than 1 min, while a 1536 well plate requires 15 min. It is probably best to begin measurement of 1536 well plates at 25 mins after addition of ONE-Glo, so that the 15 min needed to measure the plate happen before signal begins to fall after 45 min.

When whole plates were plated and transfected according to optimized parameters determined above, both showed fairly consistent signal across the plate (**Fig. 2-6**). The 1536 well

plate showed some variability around the edges of the plate, most likely due to evaporation from the outer wells. Most 1536 well plates come with a trench around the edge of the plate where additional media is added to help reduce evaporation, but it doesn't entirely prevent it. In 384 well plates, the signal to background ratio was 2000, CV was 16%, and Z' score, used to assess the quality of an assay for high throughput screening[246], was 0.53, which is above the 0.5 threshold for an acceptable assay. The 1536 well plate had a signal to background ratio of 400, CV of 19%, and Z' of 0.42, which is below the threshold for high throughput screening, but only uses about one-fourth of the DNA and cells required for a 384 well plate experiment.

Optimized parameters for NIH 3T3 and CHO cells were also determined, results are shown in **Table 2-1**. Optimal parameters are similar to those determined for HepG2 cells. However, differences in DNA plasmid, transfection agent, cell type, plate type, liquid handling equipment, and instrumentation require that parameters be optimized for each research project.

Green fluorescence protein, GFP, transfection was also explored for miniaturized transfection. GFP has the advantages of not requiring additional reagents for measurement and cells don't need to be lysed before measurement, allowing multiple measurements over time. GFP transfection has also been utilized in flow cytometry and fluorescence microscopy assays[207,218,222,223,226,231]. In 384 well plates HepG2 cells were transfected with gWiz-GFP at several N:P ratios, with N:P of 6 producing the highest signal at 48 and 72 hr post-transfection (**Fig. 2-7**). In 1536 well plates, peak signal was produced at N:P of 6 – 9. However, signal to background ratio in both 384 and 1536 well plates was only 10 – 15, much less than the ratio of 2000 for luciferase in 384 well plates or 400 in 1536 well plates. Developing a high throughput screening assay based on GFP transfection might save on reagents, but greatly reduced sensitivity may

complicate the results.

While mammalian cell lines are commonly used in in vitro studies, they are often derived from cancerous tissues, and many years of cell culture conditions can lead to altered gene expression, so that these cells may not accurately reflect cells in healthy tissue inside an animal. Extracting primary cells directly from animals can help improve the reliability of the results. However, the number of cells that can be obtained from most tissue preparations is limited.

Previous studies on primary hepatocytes have transfected the cells with calcium phosphate nanoparticles[231,232] and commercially available cationic lipids[233–235]. Cells were plated in 6 or 96 well plates at 10^5 to 10^6 cells per well. If primary hepatocytes can be plated and transfected in 384 well plates, more experimental samples can be obtained from each tissue preparation, reducing batch to batch variation and the number of animals needed.

Primary hepatocytes were obtained from mice by collagenase perfusion of the liver. High viability is critical to proper transfection. Viability was determined by trypan blue exclusion assay with hemocytometer. The minimum acceptable viability immediately after extraction was 85%, below which no luminescence was detectable after transfection. Primary hepatocytes are larger than HepG2 cells, and more fragile. Successful extraction of primary hepatocytes requires practice. It was determined that the peristaltic pump used to plate HepG2 cells into 384 well plates caused too much damage to the cells, and reduced viablity by as much as 50%. Manual plating with an 8 channel pipette was chosen. While plating the cells, the cell suspension must be gently shaken to prevent sedimentation. Because viability is so important, transfections were carried out immediately after plating instead of waiting 24 hr after plating as was done with HepG2 cells.

Several protocols recommend plating primary hepatocytes on collagen coated plates[239]. However, collagen coated plates cost more than non-coated plates and have limited shelf lives. To determine if collagen coating affected cell viability or luminescence, 384 well plates were prepared with alternating rows of collagen coated and non-coated wells. Primary cells were plated in all wells and media was recovered with gentle washing at 24, 48, and 72 hr after plating and viability was determined. Collagen made no difference in viability, which was approximately 80% at 24 hr, 70% at 48 hr, and less than 40% at 72 hr. When primary cells were transfected with gWiz-Luc PEI at different N:P ratios (**Fig. 2-8**), there was no significant difference between collagen coated and non-coated wells. Therefore, non-coated plates were chosen to simplify the procedure.

Optimal conditions for primary hepatocyte transfections were done by plating 0 – 1000 primary hepatocytes and transfecting with 400 ng of gWiz-Luc PEI at N:P of 7 (**Fig. 2-9A**). As few as 15 cells per well produced signal 10 fold higher than background, while 1000 cells per well produced luminescence 100 fold higher than background. Therefore, 250 cells per well was chosen as a compromise between signal and cost.

N:P ratios were tested in the range of 0.5 – 13 (**Fig. 2-9B**). N:P ratios of 7 or more produced luminescence of approximately 10^3 RLU. Therefore, 7 was chosen as the optimum to avoid toxicity from high PEI concentration.

Primary hepatocyte luminescence was measured every 12 hr for 96 hr (**Fig. 2-9C**). Signal peaked at approximately 10^4 RLU at 24 hr and stayed there until 48 hr before decaying to approximately 10^3 RLU at 96 hr. This gives a wide window for measurements, but viability must be taken into account. Batches of cells with lower initial viability may have reduced peak signal

and may only produce that signal for a shorter time.

Optimal DNA dose for primary hepatocyte PEI transfection was determined by dosing cells with 0 – 750 ng DNA per well at N:P of 7 (**Fig. 2-10A**). A plateau of higher signal at approximately 10^3 RLU was observed from 300 – 550 ng DNA per well. Therefore, 400 ng per well was chosen as optimum for PEI transfections because it was in the middle of this range. Doses higher than this range probably caused toxicity due to higher amounts of PEI.

Calcium phosphate DNA nanoparticles have been used been used to transfect cells in several previous studies, with a calcium to phosphate ratio of 200 giving high transfection efficiency[108]. Calcium phosphate is relatively simple to produce by mixing a solution of $CaCl_2$ with a buffered solution of Na_2PO_4, forming an insoluble hydroxyapatite ($Ca_{10}(PO_4)_6(OH)_2$) precipitation. If DNA is included and mixing is carefully controlled, plasmids can be entrapped in the particles. This protects them against nuclease degradation and allows uptake into cells. Similar to how PEI mediates the proton sponge effect, $CaPO_4$ can break open endosomes after acidification. At lower pH, the $CaPO_4$ nanoparticles dissolve, increasing the osmotic pressure.

$CaPO_4$ DNA nanoparticles were prepared and delivered to cells at DNA doses of 0 – 750 ng per well (**Fig. 2-10B**). Signal increased to approximately 10^4 RLU from 0 – 100 ng per well and stayed at that level at all higher doses. This signal was 10 fold higher than that achieved with PEI transfection, and because signal did not decrease with increased dose, toxicity is probably not an issue. DNA dose of 250 ng per well was chosen as optimum.

When primary hepatocytes were transfected with PEI at optimum conditions, signal to background ratio was approximately 10, CV was 80% and Z' was -1.9. When transfected with $CaPO_4$, signal to background was approximately 100, CV was 62% and Z' was -0.9. While these

values may be insufficient for high throughput screening, they can be most likely be improved by using more cells per well. The assay was optimized to reduce cost and get more experiments from each animal sacrificed. Previous studies using 6 well plates at 10^6 cells per well required 6 million cells per plate. At 250 cells per well, 6 million cells can fill 60 384 well plates.

An attempt to improve $CaPO_4$ DNA nanoparticle formation was done by forming particles with extra DNA. A secreted alkaline phosphatase vector was chosen as the excess DNA because it would increase total DNA without changing the amount of luciferase expressing DNA. $CaPO_4$ DNA nanoparticles were formed with 10:1, 5:1, and 1:1 ratios of luciferase plasmid to excess plasmid and used to transfect primary hepatocytes (**Fig. 2-11**). The excess DNA made no significant difference in luminescence.

PEGylated polyacridine peptides have been used to deliver DNA to mouse livers in vivo through hydrodynamic stimulation[183–185], and have been shown to protect the DNA in the bloodstream for up to 12 hr[247]. To test if these same peptides had an effect on $CaPO_4$ transfection, $CaPO_4$DNA nanoparticles were formed and then treated with 0.025, 0.05, 0.100, or 0.200 nmol of peptide per μg of DNA. When transfected with these particles, luminescence decreased as amount of peptide increased (**Fig. 2-12**). This may be due to peptides binding to surface exposed DNA and coating the particles with PEG groups. The PEG might interfere particle binding to cell surfaces and prevent uptake.

In an attempt to perform siRNA knockdown of luciferase expression, primary hepatocytes were taken from transgenic mice bred to express luciferase in their livers. An anti-luciferase siRNA[240] was used to form PEI polyplexes at N:P of 7 and was delivered to cells at 0.022, 0.22, and 1.0 μg per well (**Fig. 2-13**). However, there was no significant loss of

luminescence. All cells did show a signal of approximately 10^3 RLU, consistent with PEI transfection of wild type primary hepatocytes. If conditions for siRNA knockdown in primary hepatocytes in 384 well plates are found, this system could be used to study cells from transgenic animals.

In conclusion, miniaturized assays for transfection of mammalian cell lines and primary cells have the potential to be used to discover new transfection agents or other research. By using the smaller formats of the 384 and 1536 well plate, more data points can be obtained with fewer cells and less DNA. When using primary cells, where the number of cells are limited due to the need for extraction from tissue, the extra data points are very important. Primary hepatocyte transfection is improved by using less toxic transfection agents such as calcium phosphate instead of PEI. Signal to background ratios, coefficient of variation, and Z' factors are poor, but can probably be improved by increasing the number of cells per well at the cost of having fewer data points from each batch of cells. The information presented in this study can most likely be applied to other studies of primary cells, such as siRNA mediated knockdown. Primary cells should correlate more closely with the in vivo environment and produce more reliable data than use of cultured cancer cell lines.

3 The Uptake Mechanism of PEGylated DNA Polyplexes by the Liver Influences Gene Expression

In collaboration with Sanjib Khargharia, Nicholas Baumhover, and Jason Duskey

This research is also presented in Gene Therapy, 21 1021 – 1028 (2014) and Baumhover, at al, "Simple PEGylated Polylysine Peptides Mediate Potent Stimulated Gene Expression in Liver," in progress.

3.1 Abstract

Delivery of DNA for gene therapy relies on being able to protect DNA against nuclease degradation and increase its circulatory lifetime. PEGylated Polyacridine Peptides have been developed to bind DNA through electrostatic binding and intercalation and form PEGylated polyplexes. In this study, polyplex uptake by the liver was found to follow two distinct mechanisms. A rapid uptake dominated at low doses of polyplex, with 60% percent of the dose being taken up within 5 min and decaying with half-life of approximately 2 hr. At high doses, rapid uptake was saturated and a delayed uptake dominated, with percent of dose in liver climbing to 40% over 1 hr, followed by decay with half-life of approximately 15 hr. Additionally, large excesses of PEGylated Polyacridine peptide could saturate rapid uptake and extend the circulation time for low doses of DNA polyplex, most likely through the formation of peptide albumin nanoparticles. Inhibition of rapid uptake not only increased the circulation time for DNA polyplex, but extended the time the DNA could be hydrodynamically stimulated from 4 hr to 12 hr. Simple PEGylated polylysine compounds, which were not capable of protecting DNA at low doses, were shown to protect DNA in the bloodstream for up to 1 hr when dosed with a large

excess of peptide. The inhibition of rapid uptake at high doses of polyplex or large excesses of PEGylated peptide is consistent with saturation of scavenger receptors on Kupffer cells or sinusoidal endothelial cells of the liver. The delayed uptake of DNA polyplexes, when rapid uptake is inhibited, is consistent with accumulation of polyplexes in the Space of Disse, where they are protected against metabolism. Inhibition of scavenger receptor mediated rapid uptake should allow nanoparticles to circulate for much longer and improve nanoparticle-based therapies.

3.2 Introduction

The nonviral delivery of DNA for gene therapy faces several challenges, including protecting DNA against nuclease degradation, capture by nonparenchymal cells of the liver, targeting to specific tissues, crossing cellular membranes, and entering nuclei. A common method to protect DNA against nuclease degradation is by mixing it with a cationic polymer to form a polyplex[206,248]. While this works well for in vitro transfection, cationic DNA polyplexes often fail in vivo. Cationic DNA polyplexes can form aggregates with serum proteins and become lodged in the capillaries of the lung, leading to embolism and toxicity[249]. The addition of polyethyleneglycol can prevent aggregation and lung embolism[250], but results in significant first pass metabolism in the liver[249–258], with approximately 60% of the dose being captured.

PEGylated polyacridine peptides have been developed for binding DNA through electrostatic interactions between positively charged amines and negatively charged phosphates and intercalation into the DNA double helix. These peptides have been shown to form stable polyplexes with DNA, and protect that DNA in the bloodstream, increasing its pharmacokinetic half-life, and allowing it to be hydrodynamically stimulated at time points out to 4 hr[183–185].

However, despite the advantages PEGylated polyacridine peptides have over other cationic polymers, these polyplexes are still subject to uptake by the liver. It was not clear how transfection from hydrodynamic stimulation could be equal to direct hydrodynamic injection when polyplexes had time to circulate throughout the animal.

To better study these mechanisms, mice were dosed with radiolabeled ^{125}I-DNA PEGylated polyacridine peptide polyplexes at doses from 1 – 100 μg. Two distinct uptake mechanism were revealed, with low doses being dominated by a saturable rapid uptake into the liver followed by decay with half-life of approximately 2 hr. At high doses, an unsaturable delayed uptake into the liver dominated, followed by decay with half-life of approximately 15 hr. Higher doses also allowed hydrodynamic stimulation time to be extended from 4 hr to 12 hr.

Simple PEGylated polylysine peptides of the form PEG-Cys-Trp-Lys_N with N = 13 – 18 had been previously shown to form DNA polyplexes[259], but were not able to protect DNA in vivo[260]. However, similar polylysines with longer PEG, 30kDa vs. 5kDa, and up to 30 more lysines, were produced and tested. With large excesses of PEG-peptide, 1 μg doses of DNA could be protected in the bloodstream, and could be hydrodynamically stimulated at time points up to 1 hr. While this was much less than what excess polyacridine peptide could achieve, low doses of polylysine peptides could not protect DNA for 5 min. Both acridine and nonacridine peptides were studied in the presence of albumin, and were discovered to produce nanoparticles of 22 – 60 nm across.

The rapid and delayed uptake exhibited by PEG-peptide DNA polyplexes is similar to the uptake observed with liposomes, plasmid DNA, and viruses[46,261,262]. These compounds are caught by anionic scavenger receptors on Kupffer cells and liver sinusoidal endothelial cells[263–267].

When liposome dose was escalated, they were found to pass through the sinusoidal fenestrae and access the Space of Disse, where they could come into direct contact with hepatocytes[268]. Liposome biodistribution was also heavily influenced by serum protein binding[269]. Rapid liver uptake of plasmid DNA could be saturated with high doses, but delayed uptake was not observable due to metabolism in the bloodstream[46,47,270–273]. Several types of viruses also demonstrate rapid uptake by scavenger receptors at low doses. As doses were increased, viral transfection was directed towards hepatocytes and tumors[262,274–277]. Polyinosinic acid, a known scavenger receptor inhibitor, can be used to inhibit uptake of viruses by scavenger receptors and increase gene transfer efficiency in the liver or tumors[262,275–281]. Polyinosinic acid was able to reduce rapid uptake of PEGylated polyacridine peptide DNA polyplexes.

The similarities between PEGylated peptide DNA polyplex uptake and the uptake of liposomes, naked plasmid DNA, and viruses suggest that PEGylated peptide DNA polyplexes are also taken up by scavenger receptors on Kupffer cells and sinusoidal endothelial cells. Inhibition of scavenger receptors can allow the polyplexes to pass through liver fenestrae and reside in the Space of Disse. This also suggests a mechanism for delayed hydrodynamic stimulation, where polyplexes accumulate in the Space of Disse and are forced into hepatocytes by high pressure fluid from the hydrodynamic injection of normal saline.

3.3 Materials and Methods

3.3.1 Peptide Synthesis and Characterization

The compounds 9-Phenoxyacridine and Fmoc-Lysine(Acridine)-OH were prepared as previously described[196,197,282]. Briefly, 12 g phenol and 0.72 g NaOH were mixed and heated to

100 °C. Then, 2.8 g of 9-chloroacridine was added and stirred vigorously for 1.5 hr. The reaction was quenched with 100 mL of 2 M NaOH , and the reaction mixture was allowed to sit at room temperature overnight. A yellow precipitate was collected by filtration and washed with water and vacuum dried.

Fmoc-Lysine(Acridine)-OH was prepared by mixing 2.18 g of Fmoc-Lysine-OH in 6.78 g liquid phenol with 3 g 9-phenoxyacridine. Reaction mixture was kept under an argon atmosphere and heated to 60 °C for 4 hr. Then, 80 mL of diethyl ether was added with vigorous stirring to produce a yellow precipitate, which was collected by filtration and washed with diethyl ether. Product was allowed to dry under vacuum overnight.

$(Acr\text{-}Lys_4)_3$-Acr-Lys-Cys[184,185] and polylysine peptides (Cys-Trp-Lys_N, N = 13 – 18) were produced by solid phase peptide synthesis on 30 µmol scale using an APEX 396 synthesizer (Advanced ChemTech, Louisville, KY, USA) with standard Fmoc chemistry, with double couplings for each residue while activating with HBTU/HOBt using 5 fold excess of amino acid over resin. The N-terminus of truncated byproducts was acetylated was N-capped with 10 $^{v}/_{v}$% acetic anhydride:diisopropylethylamine. Peptides were removed from resin and side chains were deprotected using 95:2:3 mixture TFA:ethanedithiol:water for 2 hr followed by precipitation in cold ethyl ether for 45 min. Precipitated peptides were centrifuged for 10 min at 5000xg at 4 °C. Supernatant was removed and discarded.

Peptides were resuspended in 0.1 $^{v}/_{v}$% TFA and purified by RP-HPLC by injecting 2 µmol onto a Vydac C18 semi-preparative 2x25 cm column (Grace Davison Discovery Sciences, Deerfield, IL, USA) at 10 ml/min with 0.1 $^{v}/_{v}$% TFA with an acetonitrile gradient of 10 – 20 $^{v}/_{v}$% over 30 min while measuring absorbance at 280 nm. The major peaks from multiple runs were

collected, pooled, and concentrated by rotary evaporation, then lyophilized and stored at -20 C.

Peptides were resuspended in 0.1 $^{v}/_{v}$% TFA and quantified by absorbance. $(Acr\text{-}Lys_4)_3$-Acr-Lys-Cys was quantified using acridine absorbance at 409 nm, ε_{409nm} = 9266 $M^{-1}cm^{-1}$, and Cys-Trp-Lys_N was quantified using tryptophan absorbace at 280 nm, ε_{280nm} = 5600 $M^{-1}cm^{-1}$ on a Beckman DU 640 UV-Vis spectrophotometer (Beckman Coulter, Brea, CA, USA). Peptides were analyzed by LC-MS by injecting 2 nmol onto Vydac C18 analytical 0.47x25 cm column at 0.7 mL/min with 0.1 $^{v}/_{v}$% TFA with an acetonitrile of 5 – 35 $^{v}/_{v}$% over 30 min while acquiring electrospray ionization mass spectrometry in the positive mode on an Agilent 1100 series LC-MS system (Agilent Technology, Santa Clara, CA, USA).

The Cys residues on the peptides were PEGylated by reacting 2 µmol peptide with 2.4 µmol mPEG-maleimide in 4 mL of 100 mM ammonium acetate buffer at pH 7 for 2 hr at room temperature. $(Acr\text{-}Lys_4)_3$-Acr-Lys-Cys was PEGylated with 5 kDa PEG, while Cys-Trp-Lys_N peptides were PEGylated with 30 kDa PEG. PEGylated peptides were purified by semi-preparative RP-HPLC eluted at 10 mL/min with 0.1 $^{v}/_{v}$% TFA with 20 – 50 $^{v}/_{v}$% acetonitrile gradient over 30 min. The major peaks from multiple runs were collected and lyophilized as above. The TFA counter ion was replaced with an acetate counter ion by two freeze drying cycles with 1 $^{v}/_{v}$% acetic acid. PEG-peptides were reconstituted in water and quantified by UV-Vis spectrophotometry as above. Molecular mass of PEG-peptides was determined by ^{1}H-NMR analysis on a Varian 600 MHz spectrometer with 250 nmol peptide in 500 µL D_2O (99.96%) with acetone as internal standard. Mass was determined by integration ratio of PEG to peptide as previously reported[259].

3.3.2 DNA Preparation

pGL3 control vector (Promega, Madison, WI, USA), a 5.3 kb plasmid with firefly luciferase gene controlled by an SV40 promoter, and pSEAP control vector(Clontech, Mountain View, CA, USA), a 4.2 kb plasmid with secreted alkaline phosphatase controlled by an SV40 promoter, were grown in DH5α E. coli and purified by Qiagen Gigaprep kit (Qiagen, Germantown, MD, USA). Purified plasmid DNA was quantified on a NanoDrop Lite Spectrophotometer (Thermo Fisher Scientific, Pittsburgh, PA, USA).

3.3.3 Particle Size and Zeta Potential of PEG-Peptide Polyplexes

$(Acr\text{-}Lys_4)_3$-Acr-Lys-PEG_{5kDa} DNA polyplexes were formed by mixing 48 µg pGL3 plasmid DNA in 48 µL 5 mM HEPES at pH 7.5 with 38.4 nmol $(Acr\text{-}Lys_4)_3$-Lys-Cys-PEG_{5kDa} in 48 µL 5 mM HEPES pH 7.5. The polyplex mixture was diluted to 1.6mL with 5mM HEPES pH 7.5.

PEG_{30kDa}-Cys-Trp-Lys_N DNA polyplexes were formed by mixing 48 µg pGL3 plasmid DNA in 48 µL 5 mM HEPES at pH 7.5 with 48 nmol PEG_{30kDa}-Cys-Trp-Lys_N in 48 µL 5 mM HEPES pH 7.5. The polyplex mixture was diluted to 1.6 mL with 5 mM HEPES pH 7.5.

Particle size was measured by quasi-elastic light scattering, QELS, at a scatter angle of 90° on a Brookhaven Zetaplus particle sizer (Brookhaven Instruments Corporation, Holtzville, NY, USA). Intensity averaged multimodal distribution analysis was used to determine mean particle size, followed by zeta potential analysis as the mean of 10 measurements.

Particle size and zeta potential of DNA PEG-peptide polyplexes were also determined in solutions of bovine serum albumin, BSA, in 5 mM HEPES pH 7.5 at concentrations from 0 – 5

mg/mL of protein. Additionally, mixtures of 80 nmol PEG-peptide in 1.6 mL 5 mg/mL BSA 5 mM HEPES pH 7.5 were analyzed for particle size and zeta potential after 30 min incubation at room temperature.

3.3.4 Radioiodination of Plasmid DNA

pGL3 plasmid DNA was radioiodinated as previously described[283]. Briefly, 20 µg DNA was dissolved in 20 µL 0.1 M ammonium acetate pH 5. In a separate vial, 10 µL of 250 µM KI , 10 µL 30 mM Thallium Chloride, and 100 µCi of $Na^{125}I$ in 0.1 M NaOH were mixed. DNA was transferred to the iodination vial and heated at 60 °C for 45 min. The vial was then cooled, and 5 µL of 0.1 M sodium sulfite and 20 µL 1 M ammonium acetate pH 7.0 were added to quench the reaction. Reaction vial was then heated to 60 °C for 60 min to remove any unstable iodine adducts from DNA.

Iodinated DNA was then purified by anion exchange chromatography on a Qiagen Tip-100 column. Unbound iodine was washed out, and iodinated DNA was eluted. DNA was further purified by isopropanol and ethanol precipitations. Iodinated DNA was dissolved in TE buffer and quantified by absorbance at 260 nm, and specific activity was determined by gamma counting.

Iodinated DNA quality was examined by thin layer chromatography in 1:1 acetone:ethyl acetate mobile phase to assess amount of free iodine. Iodinated DNA was also mixed with 2 µL loading buffer and loaded into a 1% agarose gel with Tris-Borate EDTA buffer and electrophoresed at 70 V for 60 min[284]. The gel was dried on a zeta probe membrane and autoradiographed on a Phosphor Imager (Molecular Devices, Sunnyvale, CA, USA) to assess if

DNA was intact.

3.3.5 Pharmacokinetic Analysis of PEGylated DNA Polyplexes

Radioiodinated PEG-peptide polyplexes were formed with ^{125}I-pGL3 and $(Acr\text{-}Lys_4)_3$-Acr-Lys-Cys-PEG_{5kDa} at 0.8nmol peptide per μg DNA in HEPES Buffered Mannitol, HBM, 5 mM HEPES, 0.27 M mannitol, pH 7.4. Triplicate mice were tail vein dosed with 1, 3, 5, 10, 50, or 100 μg of radioiodinated polyplex in 100 μL HBM. Blood samples were taken by drawing10 μL of blood from the tail vein every hour from 5 min to 8 hr, and immediately frozen. Blood samples were directly gamma counted to determine amount of radiation in the blood at each time point.

Blood samples were treated with 500 μL of 0.5 mg/mL proteinase K in 100 mM NaCl, 1% SDS, 50 mM Tris-HCl, pH 8 for 12 hr at 37 °C as previously described[260]. DNA was extracted with 500 μL of 24:25:1 phenol:chloroform:isoamyl alcohol to remove PEG-peptide, proteins, and other hydrophobic components. The aqueous layer was transferred to a clean vial and DNA was precipitated with 1 mL absolute ethanol and centrifuged at 13,000xg for 10 min[183]. Supernatant was removed and DNA pellet was dried dissolved in 5 mM HEPES pH 7.4 and electrophoresed and imaged as above.

3.3.6 Biodistribution Analysis of PEGylated DNA Polyplexes

Radioiodinated polyplexes were formed with 0.6 μCi ^{125}I-pGL3 DNA, pSEAP DNA, and $(Acr\text{-}Lys_4)_3$-Acr-Lys-Cys-PEG_{5kDa} at 0.8 nmol peptide per μg DNA. Polyplexes were dosed by tail vein injection to triplicate mice at doses of 1, 3, 5, 10, 50, or 100 μg of DNA. At times from 5

min to 8 hr, mice were anesthetized with an intraperitoneal injection of 100 mg/kg ketamine and 10 mg/kg xylazine and euthanized by cervical dislocation. Mice were dissected and the liver, lungs, spleen, stomach, kidney, heart, small intestine, and large intestine were collected, rinsed with normal saline, and gamma counted to determine the amount of radiation in each organ.

Radioiodinated polyplexes were formed with 0.6 μCi ^{125}I-pGL3 and 0.8, 10, 20, 40, 60, or 80 nmol of $(Acr\text{-}Lys_4)_3$-Acr-Lys-Cys-PEG_{5kDa} peptide in 100 μL HBM and delivered to triplicate mice by tail vein injection. At 5 min post-injection, mice were anesthetized, euthanized, dissected, and had their major organs harvested and gamma counted as above.

Radioiodinated polyplexes were formed with 0.6 μCi of ^{125}I-pGL3 and 0, 5, 10, 20, 40, or 80 nmol of PEG_{30kDa}-Cys-Trp-Lys_N peptide in 100 μL HBM and dosed in triplicate mice by tail vein injection. At 5 min post-injection, mice were anesthetized, euthanized, dissected, and had their major organs harvested and gamma counted as above.

Polyinosinic acid was prepared by dissolving 200 μg in 100 μL HBM, and then delivered to triplicate mice by tail vein injection. At 5 min post-injection, mice were dosed with 1 μg 0.6 μCi ^{125}I-pGL3 $(Acr\text{-}Lys_4)_3$-Acr-Lys-Cys-PEG_{5kDa} polyplex. At 5 min after polyplex dose, mice were anesthetized, euthanized, dissected, and had their major organs harvested and gamma counted as above.

3.3.7 Recovery of Rapid-Uptake Capacity

DNA polyplexes were prepared with 50 μg pSEAP DNA and 40 nmol $(Acr\text{-}Lys_4)_3$-Acr-Lys-PEG_{5kDa} in 100 μL HBM. Triplicate mice were tail vein dosed with these polyplexes, or with 40 or 80 nmol of $(Acr\text{-}Lys_4)_3$-Acr-Lys-Cys-PEG_{5kDa} without DNA in 100 μL HBM to inhibit rapid

uptake. Mice were dosed with 1 µg of ^{125}I-pGL3 $(Acr\text{-}Lys_4)_3$-Acr-Lys-Cys-PEG_{5kDa} at 5 min, 2, 4, or 8 hr after the initial injection. At 5 min after injection of iodinated DNA, mice were anesthetized, euthanized and dissected as above. Livers were harvested and gamma counted.

3.3.8 Delayed Hydrodynamic Stimulation

pGL3 DNA polyplexes were prepared at 1, 50, or 100 µg with $(Acr\text{-}Lys_4)_3$-Acr-Lys-Cys-PEG_{5kDa} at 0.8 nmol peptide per µg DNA in 100 µL HBM. Alternatively, 1 µg of pGL3 DNA was prepared with 40 or 80 nmol of $(Acr\text{-}Lys_4)_3$-Acr-Lys-Cys-PEG_{5kDa} in 100 µL HBM. These formulations were delivered to triplicate mice by tail vein injection. At 1, 2, 3, 4, 5, 7, 9, 12, 15, and 18 Hr post-injection, mice were given hydrodynamic-stimulatory injections of normal saline at 0.9 $^{v}/_{wt}$% of mouse body weight, administered over 5 seconds. At 24 hr after HD-stimulation injection, mice were anesthetized by 3% isofluorane and intraperitoneally injected with 80 µL of 30 µg/µL D-Luciferin (Gold Biotechnology, St. Louis, MO, USA) in PBS.

At 5 min after luciferin injection, mice were imaged for bioluminescence in an IVIS Imaging 200 Series (Xenogen, Hopkins, MA, USA). Bioluminescent imaging was performed in a light-tight chamber with temperature-controlled stage, while mice were administered 3% isofluorane. Images were acquired with medium binning, at 24.6 cm field of view, and 10 second exposure time. Bioluminescent imaging data is reported as photons/sec/cm^2/steradian in a 2.86 cm diameter region of interest placed over the liver. Data was converted to pmol luciferase in the liver by a previously reported standard curve[186]. Results were analyzed for statistical significance at $p \leq 0.05$ by Dunnet T3 test using SPSS 21 ANOVA software (IBM SPSS Statistics, IBM, Armonk, NY, USA).

Alternatively, 1 μg of pGL3 DNA was prepared with 80 nmol of PEG_{30kDa}-Cys-Trp-Lys_N where N = 15, 20, or 25 in 100 μL HBM and delivered to triplicate mice by tail vein injection. At 1 hr post-injection, mice were given hydrodynamic stimulatory injections of normal saline and imaged as described above. Additionally, 1 μg of pGL3 plasmid DNA was prepared with 10, 40, or 80 nmol of PEG_{30kDa}-Cys-Trp-Lys_{25} in 100 μL HBM and delivered to triplicate mice by tail vein injection, followed by hydrodynamic stimulation at 1 hr and bioluminescent imaging as described above.

3.3.9 Imaging of Polyplexes in the Liver

pGL3 DNA was covalently labeled with Mirus Bio Label IT Tracker Cy5 kit (Mirus Bio, Madison, WI, USA) according to manufacturer's instructions. Cy5 polyplexes were formed with 50 μg of Cy5-pGL3 DNA prepared with 40 nmol $(Acr\text{-}Lys_4)_3$-Acr-Lys-Cys-PEG_{5kDa} in 100 μL HBM and tail vein injected into a mouse. An equivalent dose of unlabeled pGL3 polyplex was prepared and dosed as negative control. At 1 hr post-injection, mice were anesthetized and euthanized as above. Livers were removed, cut into small portions, and fixed with formaldehyde for 24 hr. Liver tissues were frozen, cryosectioned at 10 μm slices, fixed in cold acetone, and stained with either DAPI or biotinylated ulex agglutinin and Alexa 488 conjugated streptavidin (Life Technologies, Grand Island, NY, USA). Images were acquired on a Zeiss LSM 710 confocal microscope (Zeiss, Jena, Germany) using a 63x1.4 numerical aperture objective lens with excitation at 488 nm and emission at 637 nm.

3.4 Results

3.4.1 PEG-Peptide Synthesis

A series of PEG-Polylysine peptides were snytheszied and purified. Cys-Trp-Lys_N peptides with N = 10, 15, 20, 25, or 30 lysines were synthesized by solid phase peptide synthesis. Peptides were purified by RP-HPLC with yields of 19 – 33%. LC-ESI-MS determined that peptide masses were close to expected masses (**Table 3-1**).

PEGylation was performed with maleimide-PEG_{30kDa} with yields of 75 – 88%. ^{1}H-NMR analysis was used to determine average molecular mass by comparing integration of PEG protons at 3.62 ppm to lysine ε CH_2 protons at 2.92 ppm[259].

Polylysine Peptide[a]	% Yield	Mass (Calc / Obs)		
$(Acr\text{-}Lys_4)_3$-Acr-Lys-Cys	20.0	3008.9 / 3008.8		
Cys-Trp-Lys_{10}	33.4	1589.1 / 1589.0		
Cys-Trp-Lys_{15}	32.2	2229.9 / 2230.2		
Cys-Trp-Lys_{20}	28.8	2870.8 / 2870.6		
Cys-Trp-Lys_{25}	19.2	3511.7 / 3511.2		
Cys-Trp-Lys_{30}	18.9	4152.5 / 4152.3		
PEG Peptide[b]	**% Yield**	**Mass (Calc / Obs)**	**IC_{50}**	**R^2**
$(Acr\text{-}Lys_4)_3$-Acr-Lys-Cys-PEG_{5kDa}	77.0	8909 / 8697	14.86	0.99
PEG_{30kDa}-CWK_{10}	80.2	31589 / 31717	20.2	0.991
PEG_{30kDa}-CWK_{15}	88.5	32230 / 32839	10.8	0.999
PEG_{30kDa}-CWK_{20}	79.7	32871 / 33320	5.5	0.999
PEG_{30kDa}-CWK_{25}	74.7	33512 / 34957	2.1	0.999
PEG_{30kDa}-CWK_{30}	86.5	34152 / 36655	2.1	0.999

[a]Determined by ESI Mass Spectrometry
[b]Determined by ^{1}H-NMR Spectroscopy

Table 3-1: *PEG-Peptide Yield and IC_{50} data.*

3.4.2. Particle Size and Zeta Potential Analysis of PEG-Peptide Polyplexes

$(Acr\text{-}Lys_4)_3$-Acr-Lys-Cys-PEG_{5kDa} DNA polyplexes were formed at 0.8 nmol PEG-peptide per μg DNA. This peptide to DNA ratio has been shown to saturate DNA with acridinylated peptides, forming stable polyplexes[184]. Particle size was found to be 170 nm diameter by multi-modal intensity dynamic light scattering, multi-modal volume analysis showed a diameter of 91 nm, while multi-modal number analysis showed a diameter of 62 nm. Multi-modal intensity analysis was chosen as the measurement method. Polyplexes prepared at 100 μg DNA in 100 μL retained their 172 nm diameter, due to PEGylation preventing aggregation. Zeta potential of $(Acr\text{-}Lys_4)_3$-Acr-Lys-Cys-PEG_{5kDa} DNA polyplexes was determined to be +15 mV in 5 mM HEPES.

PEG_{30kDa}-Cys-Trp-Lys_N DNA polyplexes were formed at 1.0 nmol PEG-peptide per μg DNA. As lysine chain length increase from 10 – 30 residues, particle diameter decreased from 200 – 150 nm (**Fig. 3-1A**). Zeta potential analysis showed that the 10 lysine peptide produced a +3 mV charge, while the 15 lysine peptide produced a +9 mV charge, and 20, 25, and 30 lysines produced +15 mV charges (**Fig. 3-1D**).

Polyplex particle size and zeta potential were also determined in solutions of bovine serum albumin to better mimic physiological conditions. $(Acr\text{-}Lys_4)_3$-Acr-Lys-Cys-PEG_{5kDa} DNA polyplex particle size was not affected by addition of BSA, but zeta potential changed from +15 mV to -3 mV as BSA was titrated from 0 – 5 mg/mL (**Fig. 3-1C**). The 5 mg/mL BSA had negligible effect on PEG_{30kDa}-Cys-Trp-Lys_N DNA polyplex particle size (**Fig. 3-1B**), however, zeta potential was changed to +6 mV for 10, 15, 20, and 25 lysines, while the 30 lysine peptide polyplex had a charge of approximately +10 mV (**Fig 3-1E**).

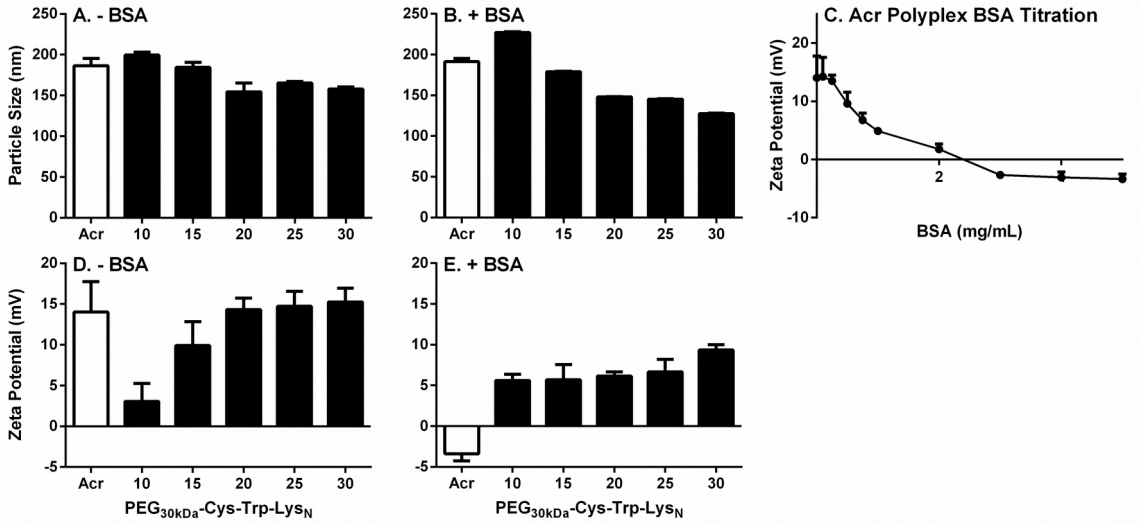

Figure 3-1: *Particle Size and Zeta Potential of Acridine and nonacridine Peptides with or without BSA.* Without BSA, both acridine and nonacridine peptides produce particles of 150 – 200 nm, in A. With BSA, particle sizes changed, with shorter lysine peptides producing larger particles and longer peptides producing smaller particles in B. When the zeta potential for acridine peptide polyplexes was measured with BSA, charge changed from +15 mV to -3 mV in C. Zeta potential of nonacridine polyplexes without BSA in D show that longer peptides have higher charges, up to 15mV. When measured with BSA in E, zeta potentials are reduced.

When 80 nmol of PEG-peptide were dissolved in 5 mg/mL BSA and tested for particle size, $(Acr\text{-}Lys_4)_3$-Acr-Lys-Cys-PEG_{5kDa} was shown to form particles with diameter of approximately 22 nm, while 5 mg/mL BSA without peptide failed to show significant particles (**Fig. 3-2A**). PEG_{30kDa}-Cys-Trp-Lys_N peptides showed particles with diameter of 60 nm for 10 lysine peptides to 43 nm for 30 lysine peptides (**Fig. 3-2B**). The size difference between acridine and nonacridine peptides is most likely explained by the difference in PEG lengths, 5 and 30 kDa, respectively.

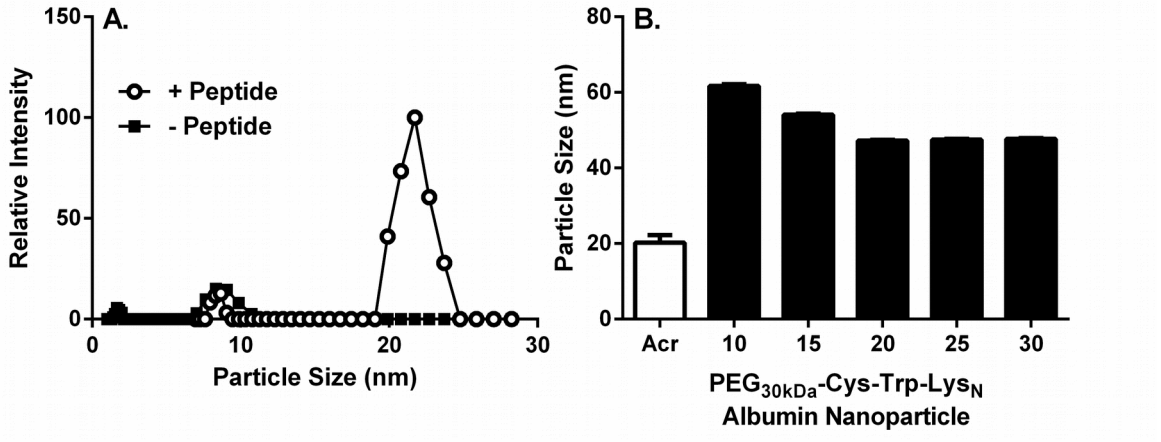

Figure 3-2: *PEG-Peptide Albumin Nanoparticle size.* Particle size distribution of of 5 mg/mL BSA with or without 80 nmol $(Acr\text{-}Lys_4)_3$-Acr-Lys-Cys-PEG_{5kDa} is shown in A. In B, particle size of PEG-peptide albumin nanoparticles is shown for nonacridine peptides.

3.4.3 Pharmacokinetics Analysis of PEG-Peptide Polyplexes

$(Acr\text{-}Lys_4)_3$-Acr-Lys-Cys-PEG_{5kDa} DNA polyplex doses were prepared at 1, 3, 5, 10, 50, and 100 µg pGL3 DNA with 0.6 µCi ^{125}I-pGL3 tracer and 0.8 nmol peptide per µg DNA. Polyplexes were delivered to mice by tail vein injection and blood samples were collected at time points from 5 min to 8 hr.

Gamma counting of blood samples produced pharmacokinetic profiles with dose-dependent changes (**Fig. 3-3A**). Polyplex doses from 1 – 10 µg showed an increase of ^{125}I-pGL3 concentration in blood to a C_{max} at times from 1 – 5 hr followed by loss of ^{125}I-pGL3 in blood. The time of C_{max} increased as polyplex dose increased, with 1 µg polyplex dose C_{max} occuring at 1 hr post-injection, 3 µg at 2 hr, 5 µg at 3 hr, and 10 µg at 5 hr. The 50 and 100 µg polyplex doses gave a reversed trend, with loss of ^{125}I-pGL3 over 4 hr (**Fig. 3-3B**).

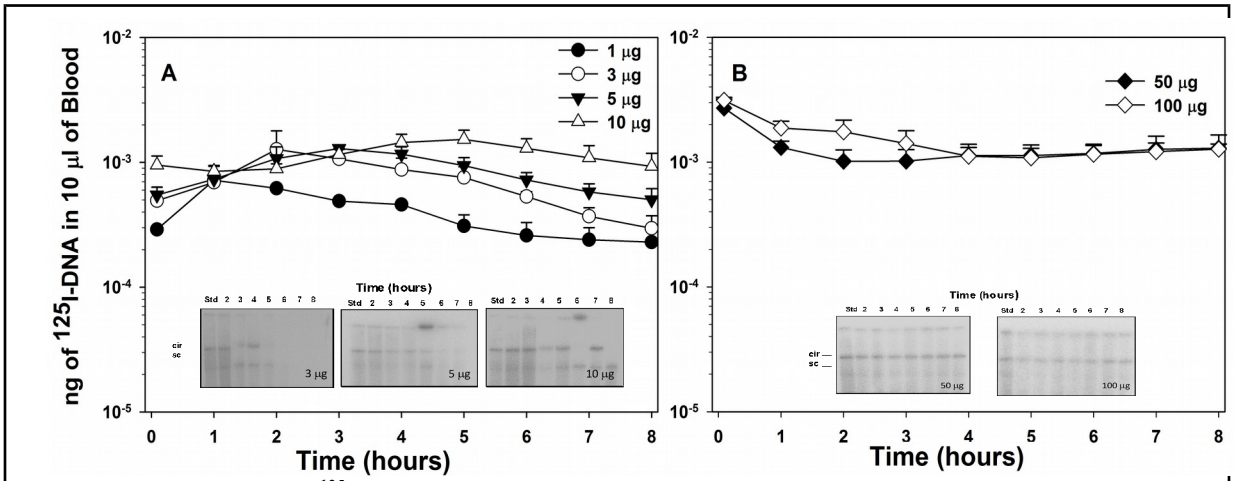

Figure 3-3: *Amount of ^{125}I-DNA in blood.* Radiation in blood was measured after dosing 1, 3, 5, or 10 µg in A, or 50 or 100 µg in B, of $(Acr\text{-}Lys_4)_3$-Acr-Lys-Cys-PEG_{5kDa} polyplex. Insets show agarose gel autoradiograms showing intact plasmid DNA at times up 8 hr.

Electrophoresis of extracted ^{125}I-pGL3 DNA showed that increased amounts of polyplex led to greater stability (**Fig. 3-3A Inset**). The 3 µg dose shows intact circular ^{125}I-pGL3 bands for up to 4 hr. Circular DNA bands were obtained as late as 7 hr for the 10 µg dose, and 8 hr for 50 and 100 µg polyplex doses (**Fig. 3-3B Inset**).

3.4.4 Biodistribution Analysis of PEG-Peptide Polyplexes

Mice were dosed with $(Acr\text{-}Lys_4)_3$-Acr-Lys-Cys-PEG_{5kDa} DNA polyplexes at 1, 3, 5, 10, 50, and 100 µg with a 0.6 µCi ^{125}I-pGL3 tracer. Major organs were harvested at time points from 5 min to 8 hr and gamma counted. The liver was the major site of bioaccumulation at all doses of polyplex, with <5% in lung and <8% in spleen (**Fig. 3-4A**). At 1 – 5 µg doses, the percent of dose in stomach peaked at 16% at 2 hr post-injection, likely due to metabolism of ^{125}I-pGL3 in the liver and excretion into the duodenum through the bile. Since the duodenum is close to the stomach it might be accidentally included with the stomach instead of the small intestine during

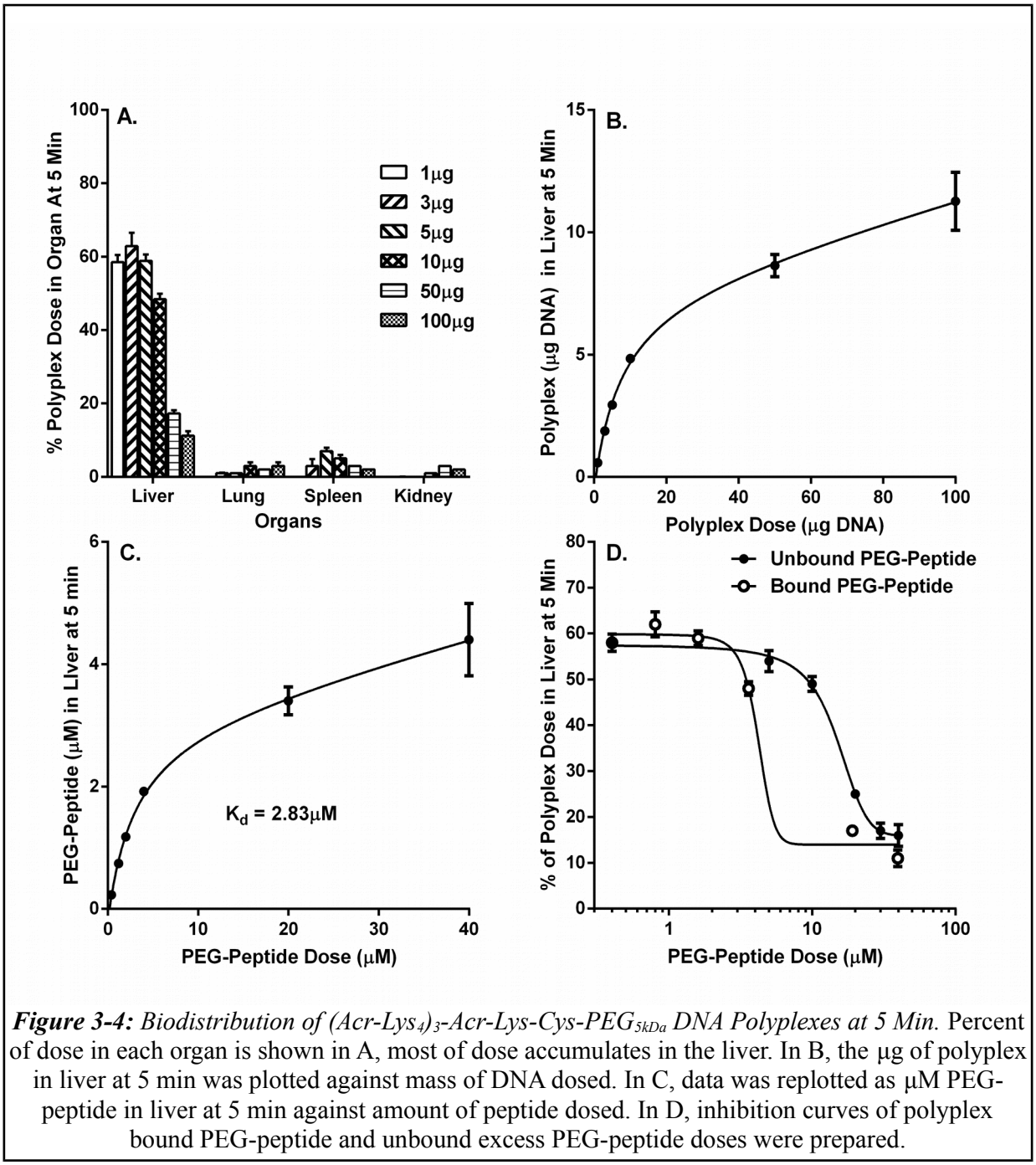

Figure 3-4: *Biodistribution of (Acr-Lys$_4$)$_3$-Acr-Lys-Cys-PEG$_{5kDa}$ DNA Polyplexes at 5 Min.* Percent of dose in each organ is shown in A, most of dose accumulates in the liver. In B, the μg of polyplex in liver at 5 min was plotted against mass of DNA dosed. In C, data was replotted as μM PEG-peptide in liver at 5 min against amount of peptide dosed. In D, inhibition curves of polyplex bound PEG-peptide and unbound excess PEG-peptide doses were prepared.

dissection.

As polyplex dose increased, the percent of dose accumulated in the liver at 5 min post-injection decreased. The 1 – 5 μg doses produced ~60% of dose in the liver at 5 min, while the 10 μg dose produced 50% of dose in the liver, the 50 μg dose produced 18% of dose in liver, and 100 μg dose produced 11% of dose in liver at 5 min (**Fig. 3-4A**).

These results were replotted in terms of μg DNA dosed vs μg DNA in liver at 5 min, creating a saturation curve (**Fig. 3-4B**). This saturation appeared to result from binding to a receptor, and was further analyzed by assuming the 20 g mice had 2 mL of blood and that PEG-peptide remained bound to the DNA throughout the 5 min biodistribution time. Data was plotted as μM PEG-peptide dosed vs μM PEG-peptide in liver at 5 min. This curve was fitted by non-linear least squares regression using Graphpad Prism 6 (Graphpad Software, La Jolla, CA, USA). The best fit curve modeled binding to a single receptor site with apparent k_d of 2.84 μM of PEG-peptide with 3.31 μM of receptor in the liver with $r^2 = 0.98$ (**Fig. 3-4E**). Results were also plotted in terms of μM PEG-peptide dosed vs % of PEG-peptide taken up by liver at 5 min to obtain a half-maximal inhibitory concentration of 8 μM for polyplex bound PEG-peptide (**Fig. 3-4D**).

Based on these findings, it was hypothesized that rapid uptake of a 1 μg dose of DNA could be inhibited by co-dosing large amounts of PEG-peptide, far above the normal 0.8 nmol peptide per μg DNA. A 1 μg tracer dose of ^{125}I-pGL3 (0.6 μCi) was combined with 0.8, 10, 20, 40, 60, or 80 nmol $(Acr\text{-}Lys_4)_3$-Acr-Lys-Cys-PEG_{5kDa} and delivered to mice by tail vein injection. The percent of dose in the liver at 5 min was determined as before. As the PEG-peptide dose increased, the percent of dose in the liver decreased from 60% to 16%. The data was plotted as μM of PEG-peptide vs percent of dose in liver at 5 min, producing an inhibition curve with a half

maximal inhibitory concentration of 14.86±0.02 μM, twice that determined for polyplex-bound PEG-peptides, 6.82±0.06 μg (**Fig. 3-4D**).

This suggests that scavenger receptors could be responsible for the rapid uptake of polyplexes by the liver. A 200 μg dose of polyinosinic acid, a known scavenger receptor inhibitor, was able to inhibit the rapid uptake of a 1 μg 0.6 μCi dose of ^{125}I-pGL3 PEG-peptide polyplex to 21±3.2% at 5 min, significantly less than the no polyinosinic acid control, 58±1.9%, $p < 0.001$.

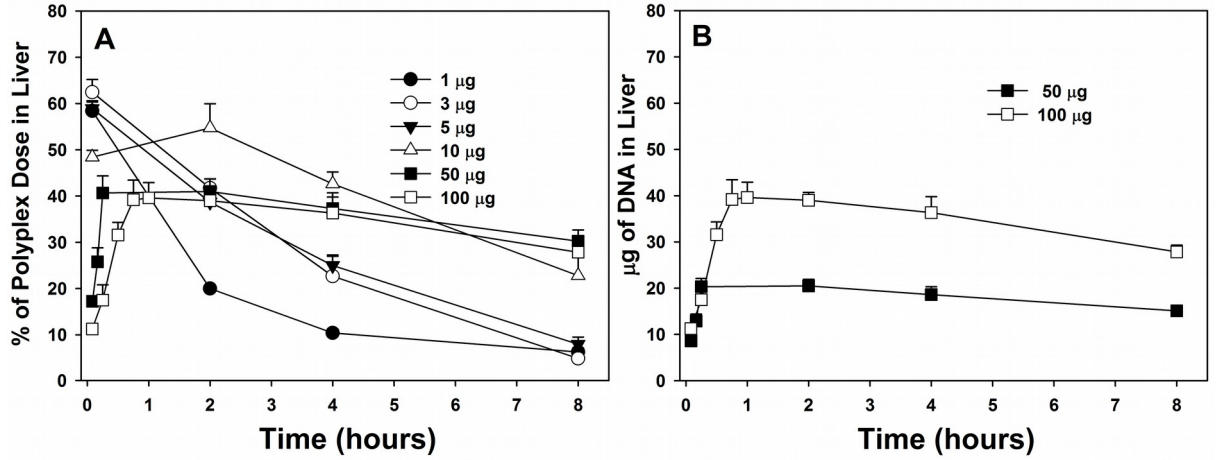

Figure 3-5: *PEG-Peptide Polyplex Biodistribution to the liver over 0 – 8 hr.* In A, Percent of dose in liver after dosing 1 – 100 μg of $(Acr\text{-}Lys_4)_3$-Acr-Lys-Cys-PEG_{5kDa} ^{125}I-pGL3 polyplex shows rapid uptake and decay at low doses, and delayed uptake and slow decay at high doses. In B, the 50 and 100 μg doses are replotted as μg polyplex in liver to show identical uptake rates of 0.5 μg/min.

The biodistribution data from later time points, 1 – 8 hr, was also analyzed. The 1 μg polyplex dose resulted in 60% of the dose accumulating in the liver at 5 min post-injection, but declined to <10% of dose at 4 – 8 hr, resulting in a metabolic elimination half-life of 2.1 hr (**Fig. 3-5A**). The 3 and 5 μg polyplex doses resulted in 60% of dose in the liver at 5 min post-injection, declining to 25% at 4 hr and 10% at 8 hr, with a metabolic half-life of 2.6 hr. The 10 μg polyplex

dose resulted in 50% of dose in the liver at 5 min, increasing to 55% at 2 hr, then declining to 30% at 8 hr, with metabolic half-life of 5.1 hr. The 50 and 100 μg polyplex doses resulted in 17% and 11% of dose in liver at 5 min, respectively. The 50 μg polyplex dose increased to 40% of dose in liver at 15 min, and 100 μg polyplex dose increased to 40% at 45 min, revealing a delayed-uptake behavior. Both 50 and 100 μg polyplex doses slowly declined from 40% with metabolic half-lives of 15 hr. Data for 50 and 100 μg polyplex doses was replotted in terms of time vs μg of polyplex in liver (**Fig. 3-5B**). Both doses showed a delayed-uptake rate of 0.5 μg/min.

Similar delayed uptake behavior was observed when a 0.6 μCi tracer dose of ^{125}I-pGL3 polyplex was dosed with 40 or 80 nmol of (Acr-Lys$_4$)$_3$-Acr-Lys-Cys-PEG$_{5kDa}$. Though the percent of dose in the liver climbs as high as 55% before declining (**Fig. 3-6**).

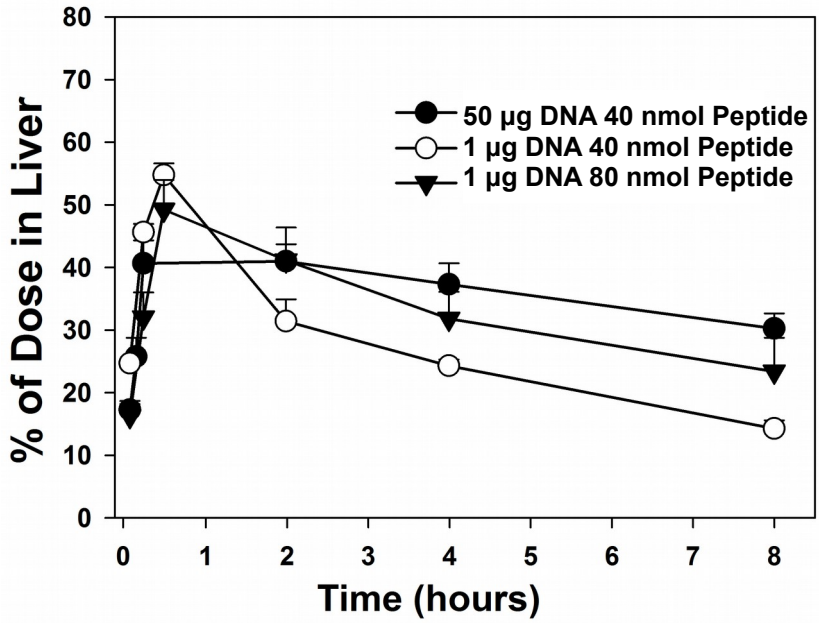

Figure 3-6: *Delayed Uptake Induced by Large Excess of PEG-Peptide.* A 0.6 μCi tracer dose of ^{125}I-pGL3 DNA mixed with 1 – 80 nmol (Acr-Lys$_4$)$_3$-Acr-Lys-Cys-PEG$_{5kDa}$ was delivered to mice, and livers were gamma counted at 0 – 8 hr, showing delayed uptake and slow decay. The 50 μg polyplex dose is included for comparison.

PEG_{30kDa}-Cys-Trp-Lys_N polyplexes were prepared with 1 μg (0.6 μCi) of ^{125}I-pGL3 DNA and 0, 5, 10, 20, 40, or 80 nmol of peptide and delivered to mice by tail vein injection. Organs were harvested at 5 min post-injection and gamma counted. Again, the liver was the major site of accumulation at 5 min, and the percent of dose in liver decreased as amount of PEG-peptide increased. Data was plotted in terms of μM PEG-peptide dosed, assuming blood volume of 2 mL, vs percent of dose in liver and fitted by non-linear least squares regression by GraphPad Prism 6 (**Fig. 3-7**). IC_{50} values were determined based on the fitted equations (**Table 3-1**). The 10 lysine peptide produced an IC_{50} of 20.1 μM, showing weak inhibition of rapid-uptake into the liver. The 15 lysine peptide was twice as potent, with IC_{50} of 10.8 μM and maximal inhibition at 20 μM PEG-peptide dose. The 20 lysine peptide showed greater potency, with IC_{50} of 5.5 μM. The 25 and 30 lysine peptides both showed an IC_{50} of 2.1 μM.

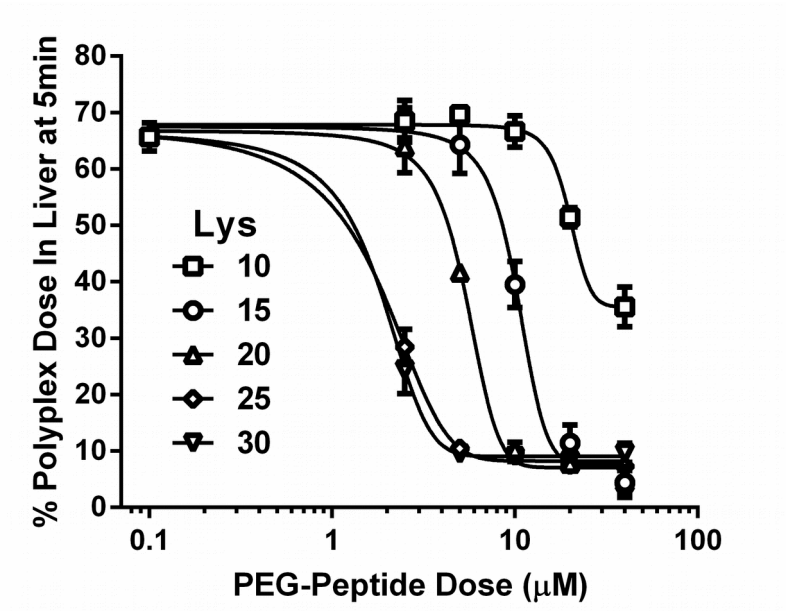

Figure 3-7: *Inhibition of Rapid Polyplex Uptake by Simple PEGylated Polylysine Peptides.* Plotting concentration of PEG-peptides dosed vs. percent of dose in the liver at 5 min shows that the peptides inhibit rapid uptake, and that IC_{50} decreases as lysine length increases, until the peptide is 25 or 30 lysines long, which are equally potent.

3.4.5 Recovery of Rapid-Uptake Capacity

Mice were dosed with 50 µg of $(Acr\text{-}Lys_4)_3$-Acr-Lys-Cys-PEG_{5kDa} pGL3 polyplex or 40 or 80 nmol of $(Acr\text{-}Lys_4)_3$-Acr-Lys-Cys-PEG_{5kDa} with no DNA to saturate the liver's rapid-uptake capacity. Then, 1 µg (0.6 µCi) ^{125}I-pGL3 $(Acr\text{-}Lys_4)_3$-Acr-Lys-Cys-PEG_{5kDa} polyplex was dosed at 5 min, 2, 4, or 8 hr after the initial injection, and the percent of radioactive dose in the liver was determined at 5 min after the second injection (**Fig. 3-8**). All three formulations showed loss of rapid-uptake capacity at 5 min, the 50 µg polyplex dose produced approximately 20% of dose in liver, the 40 nmol PEG-peptide dose produced approximately 25% of dose in liver, and the 80 nmol PEG-peptide dose produced approximately 12% of dose in liver at 5 min biodistribution time. All three formulations showed recovery of rapid-uptake capacity by 4 hr, where 50 – 60% of dose was captured by the liver at 5 min biodistribution time.

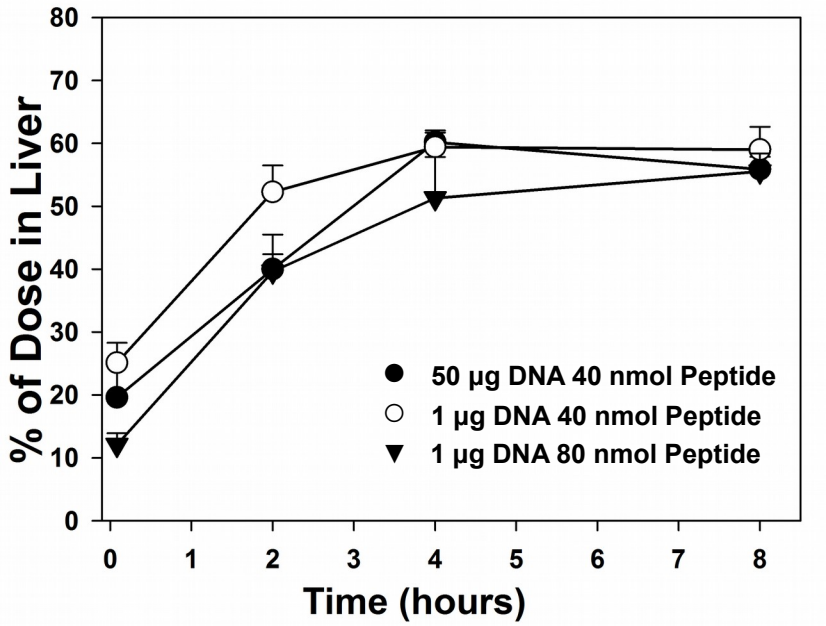

Figure 3-8: *Recovery of Rapid Uptake Capacity After Inhibition.* Mice were dosed with 50 µg of DNA $(Acr\text{-}Lys_4)_3$-Acr-Lys-Cys-PEG_{5kDa} polyplex or 40 or 80 nmol of $(Acr\text{-}Lys_4)_3$-Acr-Lys-Cys-PEG_{5kDa} peptide. At 0 – 8 hr post-injection, mice were dosed with 0.6 µCi tracer dose of ^{125}I-pGL3 polyplex and amount of dose in the liver was determined 5 min later. Rapid uptake capacity is restored by 4 hr.

3.4.6 Hydrodynamic Delayed Stimulation of PEG-Peptide Polyplexes

To determine if inhibiting the rapid uptake of PEG-peptide DNA polyplexes by the liver actually extended how long plasmid DNA remained transfection competent, a series of delayed hydrodynamic stimulation experiments were performed.

PEG-peptide polyplexes were prepared with 1 μg of pGL3 luciferase expressing plasmid DNA with 50 or 100 μg of pSEAP secreted alkaline phosphatase expressing plasmid DNA to increase total amount of DNA while keeping luciferase expressing DNA constant. These

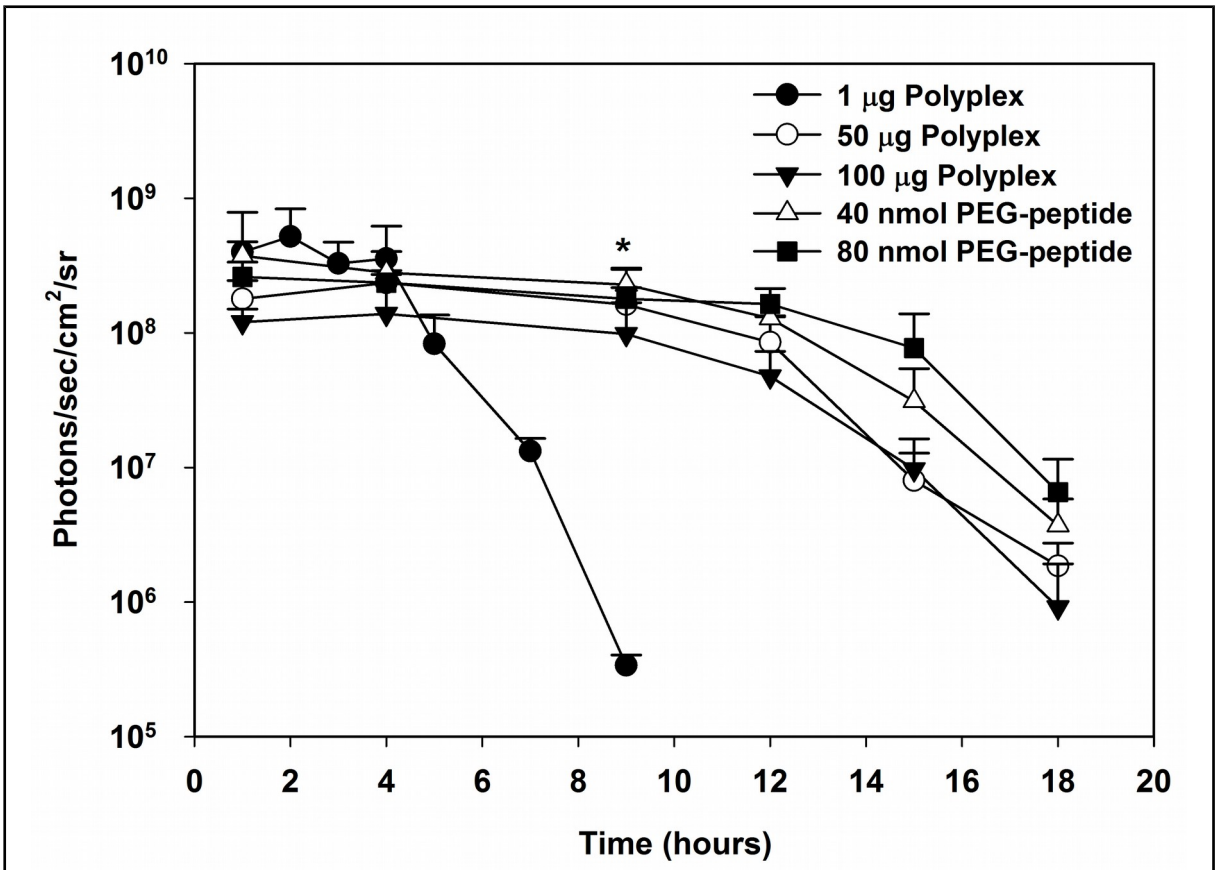

Figure 3-9: *Delayed Hydrodynamic Stimulation with Rapid-Uptake Inhibition.* pGL3 Plasmid DNA with either 50 or 100 μg of $(Acr\text{-}Lys_4)_3$-Acr-Lys-Cys-PEG_{5kDa} DNA polyplex or 40 or 80 nmol of excess $(Acr\text{-}Lys_4)_3$-Acr-Lys-Cys-PEG_{5kDa} peptide was hydrodynamically stimulated at time time points up to 18 hr. Delayed hydrodynamic stimulation of 1 μg pGL3 polyplex is shown as comparison (●). Under high doses of polyplex or excess peptide, luciferase expression at 9 hour stimulation time is significantly greater than 1 μg pGL3 polyplex at 9 hours, * = $p < 0.05$.

polyplexes were dosed by tail vein injection and followed by hydrodynamic stimulatory doses of normal saline at 1, 2, 3, 4, 5, 7, 8, 12, 15, or 18 hr, and imaged for bioluminescence at 24 hr after hydrodynamic stimulation.

Saturating rapid-uptake with large doses of PEG-peptide DNA polyplex extended the time for polyplexes to remain transfection competent in the liver from 4 hr at low doses to 12 hr at high doses (**Fig. 3-9**).

Similarly, 1 μg of pGL3 plasmid was dosed with 40 or 80 nmol of $(Acr\text{-}Lys_4)_3$-Acr-Lys-Cys-PEG_{5kDa} and followed by hydrodynamic stimulatory doses. These conditions also extended transfection competence time in the liver to 12 – 15 hr (**Fig. 3-9**).

Additionally, 1 μg of pGL3 plasmid DNA was combined with 80 nmol of PEG_{30kDa}-Cys-Trp-Lys_N with N = 15, 20, or 25 lysines. PEG-peptide polyplexes were delivered by tail vein injection and followed by hydrodynamic stimulatory injections of normal saline at 1 hr post-injection. The 15 lysine PEG-peptide polyplex produced approximately $1x10^7$ photons/sec/cm^2/steradian, one tenth of the signal produced by direct hydrodynamic injection of 1 μg pGL3 plasmid DNA (**Fig. 3-10A**). The 20 lysine PEG-peptide polyplex produced approximately $5x10^7$ photons/sec/cm^2/steradian, and the 25 lysine PEG-peptide polyplex produced approximately $2.5x10^8$ photons/sec/cm^2/steradian, demonstrating that 80 nmol of PEG_{30kDa}-Cys-Trp-Lys_{25} can protect a 1 μg dose of pGL3 DNA for up to 1 hr in the liver.

To establish a relationship between inhibition of rapid-uptake by PEG_{30kDa}-Cys-Trp-Lys_{25} and level of hydrodynamic stimulated gene expression, 1 μg of pGL3 DNA was prepared with 10, 40, or 80 nmol of the 25 lysine PEG-peptide. Mice were dosed with PEG-peptide polyplex and administered a saline hydrodynamic stimulatory injection at 1 hr post-injection. The 10 nmol

dose produced no detectable luciferase expression (**Fig. 3-10B**), while the 40 nmol dose produced approximately $1x10^7$ photons/sec/cm^2/steradian, and the 80 nmol dose produced approximately $2.5x10^8$ photons/sec/cm^2/steradian. This showed that more effective inhibition of rapid-uptake led to better expression after hydrodynamic stimulation.

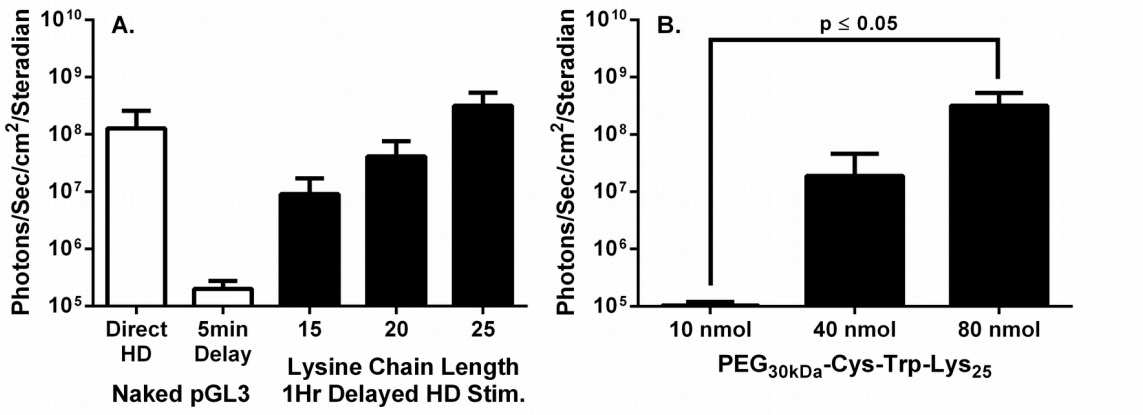

Figure 3-10: *Delayed Hydrodynamic Stimulation with Simple PEGylated Polylysine Peptides.* In A, 1 µg pGL3 DNA was dosed with 80 nmol of PEG_{30kDa}-Cys-Trp-Lys_N peptide, with N = 15, 20, or 25 lysines and hydrodynamically stimulated at 1 hr. The 25 lysine peptide restored full expression compared to direct hydrodynamic injection of pGL3 DNA. In B, the 25 lysine peptide was dosed at 10, 40, or 80 nmol with 1 µg pGL3 DNA. The 40 and 80 nmol peptide doses produced luciferase after 1 hr delayed hydrodynamic stimulation, but only the 80 nmol produced full level expression, significantly higher than background, $p \leq 0.05$.

3.4.7 Imaging of Polyplexes in the Liver

Cy5 polyplex was prepared with 50 µg Cy5 fluorescently labeled pGL3 plasmid DNA and 40 nmol $(Acr\text{-}Lys_4)_3$-Acr-Lys-PEG_{5kDa} in 100 µL HBM and delivered to mice by tail vein injection. Livers were removed and fixed at 1 hr post-injection and prepared for microscopic imaging. Fluorescent microscopy was used to locate the Cy5-DNA in the liver as red points (**Fig. 3-11**). Cy5-DNA is found outside the hepatocytes, and only in the experimental mouse. The

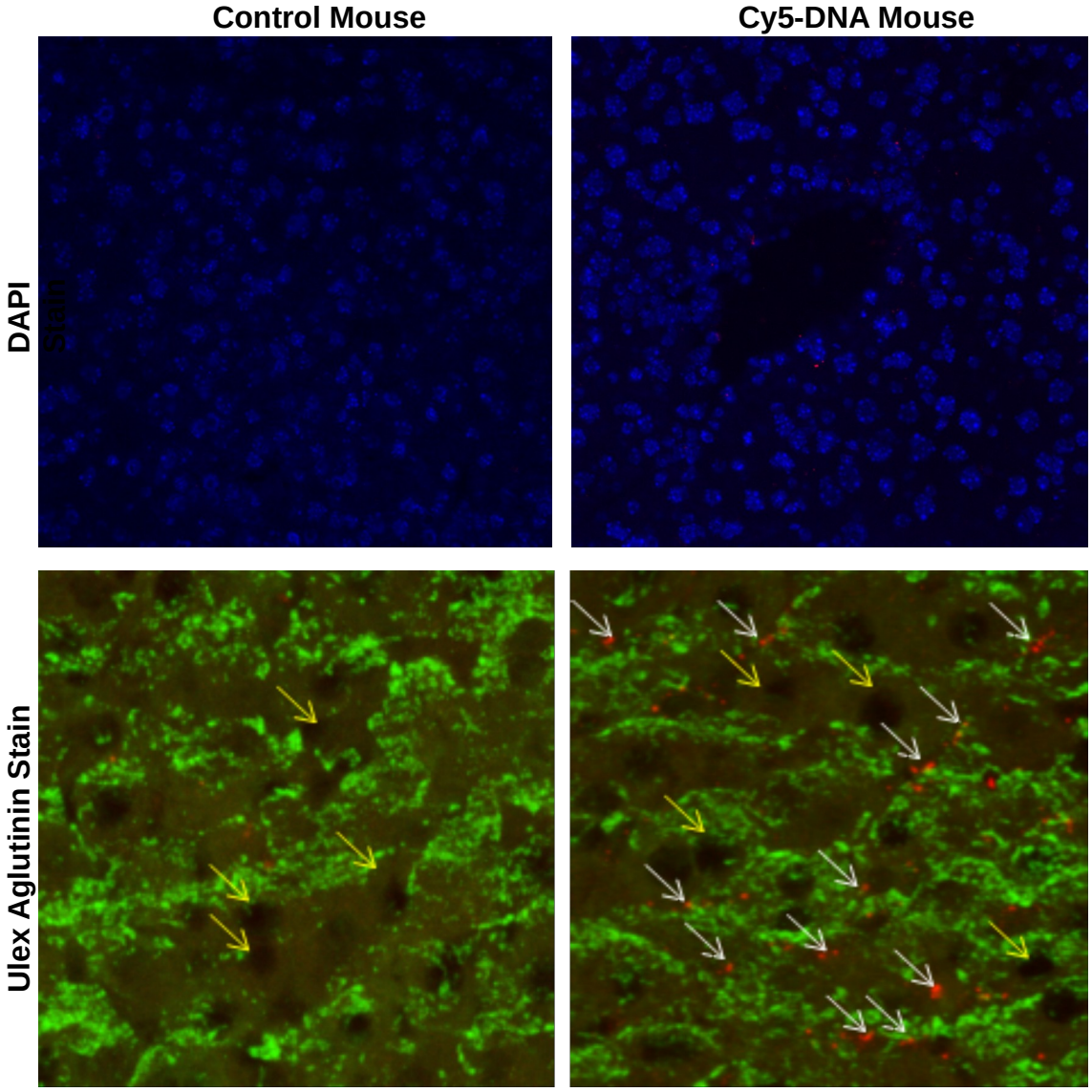

Figure 3-11: *Imaging of Cy5-DNA Polyplexes in the Liver.* Cy5 labeled pGL3 DNA was prepared with $(Acr\text{-}Lys_4)_3$-Acr-Lys-Cys-PEG_{5kDa} and delivered to mice. At 1 hr post-injection livers were removed and prepared for imaging. Cy5 polyplex is visible when tissue is stained with biotinylated ulex aglutinin and FITC-streptavidin. Polyplex does not appear to be inside cells, consistent with it being in the Space of Disse. Yellow arrows point to nuclei, white arrows point to Cy5 DNA.

control mouse received non-labeled DNA PEG-peptide polyplex and does not show red points.

3.5 Discussion

Previous studies have shown that delayed hydrodynamic stimulation is a useful technique for studying how DNA polyplex formulations can protect plasmid DNA in the bloodstream[183–185]. When DNA is properly protected, a delayed hydrodynamic stimulation can produce transgene expression at levels equal to direct hydrodynamic delivery of DNA at up to 4 hr after initial injection[184,185]. However, it was not clear how the expression level in the liver could be the same after DNA polyplexes had been allowed to circulate throughout the body for an extended period of time rather than immediately delivered to the liver as in direct hydrodynamic injection.

To examine the mechanism behind delayed hydrodynamic injection in more detail, PEG-peptide DNA polyplexes were characterized with or without 5 mg/mL BSA to better mimic physiological conditions. Actual blood has an albumin concentration closer to 50 mg/mL, however concentrations this high create artifacts during particle size and zeta potential measurements. $(Acr\text{-}Lys_4)_3$-Acr-Lys-Cys-PEG_{5kDa} DNA polyplexes had diameters of approximately 170 nm with zeta potential of +15 mV when measured without BSA. When BSA was added, particle size did not significantly change, but zeta potential did, changing from +15 mV to -3 mV at 5 mg/mL BSA (**Fig. 3-1E**). Simpler polylysine PEG-peptides were prepared to compare to the polyacridine PEG-peptides. The polylysine PEG_{30kDa}-Cys-Trp-Lys_N DNA polyplexes had diameters of 150 – 200 nm, with longer peptides making smaller particles, most likely due to higher charges and higher affinity for the DNA backbone. Similarly to $(Acr\text{-}Lys_4)_3$-Acr-Lys-Cys-PEG_{5kDa}, addition of BSA did not significantly alter particle size and reduced the zeta potential (**Fig. 3-1**). However, the polylysine peptide polyplex zeta potentials did not become negatively charged, but were reduced to approximately +6 mV.

The particle size and zeta potential of nanoparticles have important implications for pharmacokinetics and biodistribution. The fenestrated endothelia of the liver sinusoids have pores, known as fenestrae, that allow proteins and other small particles to cross the sinusoid wall and enter the Space of Disse. These fenestrae have a diameter of approximately 100 nm in humans and 140 nm in mice[7], but follow a distribution with some smaller or larger pores. The particle size measured by dynamic light scattering is also an average of a distribution of sizes. The 150 – 200 nm diameter PEG-peptide polyplexes used in this study are small enough that some population of particles most likely overlaps with some population of fenestrae, allowing the particles to pass through.

Zeta potential is important for circulatory stability and toxicity. Particles with strong positive charge can aggregate proteins in the bloodstream, forming large enough particles to obstruct narrow capillaries in the lung[249]. However, a negatively charged particle is subject to uptake by scavenger receptors on liver sinusoidal endothelial cells and Kupffer cells, which can quickly remove a population of particles from the bloodstream[47,58,260,268,270,272,274,285]. PEGylation is often used to mask the charges on particles and bring zeta potential close to neutral[249,259,260]. The fact that DNA PEG-peptide polyplexes show reduction of zeta potential in the presence of 5 mg/mL BSA implies that these particles may become even more negative in the blood where protein concentration is higher. Negatively charged particles would become candidates for scavenger receptor uptake.

Interestingly, PEG-peptides were demonstrated to form particles in the presence of 5 mg/mL BSA even without DNA (**Fig. 3-2**). These particles had small diameters, 22 – 60 nm, allowing them to easily pass through fenestrae. Polylysine peptide albumin particles showed

decreased diameter as lysine chain length increased, the additional lysines most likely increase affinity for albumin and create a more tightly packed particle. The $(Acr\text{-}Lys_4)_3$-Acr-Lys-Cys-PEG_{5kDa} peptide albumin particle shows a 22 nm diameter, even smaller than the 30 lysine polylysine peptide, the hydrophobic acridines may increase affinity for albumin, or the longer PEG on the polylysine peptides creates the larger diameter. PEGylation probably prevents the particles from forming larger aggregates.

When radioiodinated DNA was used to form $(Acr\text{-}Lys_4)_3$-Acr-Lys-Cys-PEG_{5kDa} polyplexes and injected into mice at increasing doses, the pharmacokinetic profile changed as dose increased (**Fig. 3-3**). At low doses of 1, 3, 5, and 10 μg, the amount of DNA in the blood increased to a maximum concentration at 1, 2, 3, and 10 hr post-injection, respectively. High doses of 50 or 100 μg produced profiles with maximum blood concentration at 5 min post-injection. By extracting plasmid DNA from the blood samples and analyzing by gel electrophoresis it was shown that higher doses of polyplexes lead to better protection of plasmid DNA in the blood, with intact circular DNA detectable at 8 hr post injection at the 50 and 100 μg doses.

Dissecting mice after administration of increased doses of $(Acr\text{-}Lys_4)_3$-Acr-Lys-Cys-PEG_{5kDa} PEG-peptide radioiodinated DNA polyplexes showed that the liver captured most of the dose at 5 min post-injection (**Fig. 3-4A**). As the amount of polyplex dosed increased, the percent of dose in the liver at 5 min decreased. When plotted in terms of μg of DNA polyplex in the liver, a saturation curve was revealed (**Fig. 3-4B**). By replotting the data in terms of μM of PEG-peptide, an inhibition curve was created, (**Fig. 3-4D**), with IC_{50} of approximately 8 μM. It was suspected that rapid uptake of polyplexes by the liver was mediated by scavenger receptors. As

the polyplex dose increased the scavenger receptors became saturated, allowing the remaining polyplex to avoid capture and continue circulation. This hypothesis was supported by data from polyinosinic acid administration. Polyinosinic acid is a known scavenger receptor inhibitor[274], and injection of 200 μg of PolyI was able to reduce the rapid uptake of ^{125}I-pGL3 polyplex from 60% to 20% of dose.

When biodistribution analysis was carried out over 8 hr, the percent of polyplex dose in the liver showed two distinct patterns (**Fig. 3-5A**). At low doses, the percent of dose in the liver at 5 min was approximately 60%, and declined with a half-life of approximately 2 hr. At high doses, the percent of dose in the liver at 5 min was low, 10 – 20%. The percent of dose in liver increased to approximately 40% within 1 hr before declining with half-life of approximately 15 hr. When plotted in terms of μg of polyplex rather than percent of dose, the 50 and 100 μg polyplex doses showed an uptake rate of approximately 0.5 μg/min (**Fig. 3-5B**). This identical rate is consistent with particles passing through fenestrated sinusoidal endothelium into the Space of Disse. Once in the Space of Disse, the particles are protected against scavenger receptor uptake. Because the percent of dose in the liver peaks at 40% and then decays slowly, the polyplex concentration in the Space of Disse most likely reaches a dynamic equilibrium, with particles entering and leaving through fenestrae at equal rates. Even though the delayed uptake is only observable at high doses of polyplex, low doses are probably subject to some delayed uptake as well. Even 1 μg polyplex doses can be hydrodynamically stimulated at time points up to 4 hr post-injection, even though the half-life of polyplex in the liver is only 2 hr.

Additionally, the delivery of 1 μg of DNA with excess amounts of peptide also showed delayed uptake into the liver followed by decay with long half-lives (**Fig. 3-6**). This is most

likely related to the formation of peptide albumin particles observed during particle sizing experiments (**Fig. 3-2**). nonacridine polylysine peptides were also able to produce albumin particles, and were also shown to inhibit rapid uptake of polyplex in the liver (**Fig. 3-7**), with longer peptides making smaller particles (**Fig. 3-2B**) and smaller IC_{50} (**Table 3-1**).

By administering a dose of 50 µg polyplex or 40 or 80 nmol of $(Acr\text{-}Lys_4)_3$-Acr-Lys-Cys-PEG_{5kDa} to inhibit rapid uptake, followed by injection of 1 µg of ^{125}I-pGL3 polyplex at 5 min – 8 hr post-injection, it was shown that rapid uptake could be inhibited for as long as 4 hr after injection of the inhibitory dose (**Fig. 3-8**). This shows that clearance of PEG-peptide polyplex or PEG-peptide albumin particles was slow compared to the delayed uptake of polyplexes by the liver, which occurs over a period of 1 hr.

Delayed hydrodynamic stimulation has been used to study how well different polyplex formulations protect DNA in the bloodstream over time[184,185]. Previous studies have shown that a 1 µg dose of pGL3 $(Acr\text{-}Lys_4)_3$-Acr-Lys-Cys-PEG_{5kDa} polyplex can be hydrodynamically stimulated as late as 4 hr post-injection while retaining a full level of expression. In this study, the technique was applied to demonstrate that inhibition of rapid uptake by scavenger receptors would protect the DNA polyplexes in the bloodstream for an extended period of time. Both high doses of DNA $(Acr\text{-}Lys_4)_3$-Acr-Lys-Cys-PEG_{5kDa} polyplex and 1 µg DNA with large excesses of $(Acr\text{-}Lys_4)_3$-Acr-Lys-Cys-PEG_{5kDa} were able to achieve full level expression at time points as late as 12 hr post-injection (**Fig. 3-9**), three times as long as without rapid uptake inhibition.

nonacridine polylysine PEG-peptides were not capable of protecting DNA in the bloodstream for more than 5 min when dosed at 1 µg of polyplex at 0.8 nmol PEG-peptide per µg DNA[260]. However, when PEG-peptide was escalated as high as 80 nmol, 1 µg polyplex doses

could be hydrodynamically stimulated at 1 hr post-injection (**Fig. 3-10**). Longer lysine chains, which have higher affinity for DNA, show better signal, with a 25 lysine peptide showing full level expression at 1 hr stimulation time. The amount of peptide was also shown to be important, with 80 nmol of PEG-peptide producing full level expression. However, hydrodynamic stimulation of PEGylated polylysine DNA polyplexes at 2 hr produced no detectable signal (Data not shown). This demonstrates that simple peptides with much lower affinity for DNA than their acridine containing counterparts can be made to protect DNA in the bloodstream for 1 hr when dosed at levels high enough to inhibit rapid uptake by the liver. However their weaker affinity still results in much shorter stimulation times than those achieved by acridine containing peptides.

This shows that protecting DNA polyplexes in circulation is complex. Peptides must protect DNA against degradation by nucleases, which requires tight binding. Peptides must also inhibit scavenger receptors to prevent the rapid uptake of polyplexes by Kupffer cells and sinusoidal endothelial cells, which requires large doses. While simple polylysine peptides are easier to synthesize than the acridine peptides, they do not have the affinity required to protect DNA for longer periods of time.

DNA was labeled with Cy5 fluorophore and used to prepare $(Acr\text{-}Lys_4)_3$-Acr-Lys-Cys-PEG_{5kDa} polyplexes, which were dosed to mice at 50 μg doses. When the livers were removed and sectioned and imaged by microscopy, red points were visible in the Cy5-DNA experimental mouse but not in the control mouse under both DAPI and ulex agglutinin staining (**Fig. 3-11**). The red Cy5-DNA was not seen inside hepatocytes, which is consistent with the hypothesis that particles accumulate in the Space of Disse. However, the Space of Disse is approximately 1 μm

wide[286], near the limit of resolution for optical microscopy, and the polyplexes are less than 200 nm wide, so standard optical microscopy techniques cannot precisely determine the location of polyplexes in the liver.

Nonviral delivery of DNA to specific tissues requires that DNA must circulate through the bloodstream for enough time to find their targets while remaining intact. Two major mechanisms that quickly remove intact DNA from the bloodstream are degradation by nucleases[260] and uptake by scavenger receptors[46]. Polyacridine peptides have been shown to protect DNA against degradation in the bloodstream[184,185], but were not previously known to inhibit scavenger receptor mediated uptake. This study has shown that high doses of PEG-peptide, either as bound DNA polyplex or unbound free peptide with 1 μg DNA, can inhibit the rapid uptake of DNA by scavenger receptors. This not only improves the circulation time of DNA, but extends the time at which DNA can be hydrodynamically stimulated to achieve high level protein expression. Additionally, rapid uptake inhibition can be achieved using simple polylysine peptides, suggesting that scavenger receptor inhibition may be accomplished through easily produced substances. These results should help stabilize DNA in the bloodstream, and may be applicable to delivery of other nanoparticle scale compounds, including liposomes or viruses. Longer circulation times and better DNA stability should help develop vehicles that deliver DNA without hydrodynamic injection, allowing nonviral delivery to better compete with viral gene delivery.

4 PEGylated Polyacridine Peptide Enhances mRNA Expression in Vivo

In collaboration with Jacob A. Poliskey, Elizabeth Mullins, and Nicholas Baumhover

This research is also presented in Crowley, et al, "Efficient Expression of mRNA PEG-Peptide Polyplexes in Liver," in progress.

4.1 Abstract

Non-viral delivery of mRNA has gained much interest in recent years, due to mRNA's potential to transiently produce protein in cells without the need for nuclear entry, which inhibits nonviral DNA delivery. This transient expression could be useful for genome-editing techniques such as CRISPR/Cas or TALEN endonucleases, or to express toxic proteins to treat cancer. However, mRNA is much less stable than DNA, and is highly susceptible to nuclease digestion. Preventing this digestion is critical to effective non-viral delivery of mRNA. This study applies PEGylated Polyacridine Peptides, previously shown to stabilize DNA in vivo, to mRNA. Peptides with and without acridine showed similar affinity for mRNA and similar ability to protect against RNase challenge. However, only the acridinylated peptide was capable of enhancing protein expression in vivo when mRNA peptide polyplex was delivered to mice by hydrodynamic tail vein injection. Polyplex with 1 μg of luciferase mRNA and PEGylated acridinylated peptide produced bioluminescent signal 10 fold higher than luciferase expressing plasmid DNA at 24 hr post-injection. Additionally, the acridinylated peptide was able to protect mRNA against degradation in an in vitro serum incubation followed by hydrodynamic delivery. PEGylated polyacridine peptides show the potential to protect mRNA against degradation in vivo, and may be helpful in the eventual nonviral delivery of mRNA without hydrodynamic

dosing. Additionally, tailed mRNA was shown to bind to Oligo(dT), Oligo(rU), and Poly(rU) in an attempt to improve peptide binding and better protect mRNA in vivo. Oligo(dT) was shown to eliminate bioluminescence after hydrodynamic dosing of mRNA. Oligo(rU) and Poly(rU) did not interfere with bioluminescence after direct hydrodynamic injection, but were not able to produce bioluminescence after delayed hydrodynamic stimulation. Finally, polyadenosine tailing of mRNA was attempted with the ATP analogs 1-Thio-ATP or 2'-Fluoro-2'-dATP. These analogs were shown to be ineffective substrates for polyadenosine tailing of mRNA.

4.2 Introduction

While most gene therapy research has focused on delivering DNA to treat disease, recent innovations in RNA synthesis and genome editing have generated interest in delivery of messenger RNA, mRNA. mRNA has advantages over DNA for certain applications, including no need for nuclear entry, no chance for random insertion into the genome, and the transient expression of potentially cytotoxic proteins[287]. However, mRNA delivery is hampered by ubiquitous RNase enzymes and immune responses[288].

The earliest report of mRNA delivery comes from 1990[289], where naked luciferase mRNA was injected into mouse muscle and produced detectable levels of luciferin. Since then, much of the mRNA delivery research has focused on mRNA vaccines[290–292], and takes advantage of mRNA's immunogenic properties to act as a "self-adjuvant"[293]. However, these immunogenic responses could hinder non-vaccine applications of mRNA, resulting in reduced protein expression.

mRNA has been delivered in vivo with cationic lipids and cationic polymers. When

injected intravenously, the RNA is often expressed the spleen[294–297]. mRNA has also been delivered in vivo using a lipid calcium phosphate nanoparticle[298]. mRNA is condensed with protamine and trapped in a calcium phosphate core coated with a lipid bilayer. PEGylated lipids are added to the outer surface of the bilayer to "stealth" the particle against serum proteins and aggregation. These particles accumulate in tumors, most likely due to the enhanced permeability and retention, or EPR, effect.

Another method to deliver RNA in vivo is hydrodynamic tail vein injection[170,171]. RNA is dissolved in a large volume of saline, normally equal to 8 – 10% of a mouse's mass, such that a 20 g mouse will get 1.8 mL of saline. The RNA saline solution is injected into the animal's tail vein in 5 - 7 seconds. The high pressure forces the RNA into the hepatocytes where it can be expressed. Hydrodynamic dosing has been used to deliver DNA[172,173], RNA[174], proteins[299], viruses[177], nanoparticles[176], and even whole cells[178] to mouse liver. The liver is the primary target of hydrodynamic delivery due to its unique architecture of fenestrated sinusoidal endothelium. The 100 – 140 nm fenestrae allow fluid and particles direct access to the hepatocytes[8], and allows the liver to swell up during the hydrodynamic injection and accommodate the large volume of saline with minimal injury[179,300,301].

The first report of hydrodynamic delivery of mRNA to mice was McCaffrey et al., 2002[175], and required injection of 50 μg of luciferase expressing mRNA with 30 μg competitor RNA and 400 units of RNase inhibitor to protect the luciferase mRNA from RNases. The mice produced detectable luciferase expression in their livers at 3 hr post injection.

Many advances in mRNA technology have occurred to improve both the stability and efficiency of mRNA. One technique is the addition of β-globin untranslated regions, UTRs. Most

mRNAs have half-lives on the order of minutes to hours in the cytoplasm, however, α-globin and β-globin mRNA have half-lives between 16 and 48 hours[302]. The enhanced stability is caused by structural elements in the 3' UTR, however α-globin and β-globin 3' UTRs stabilize mRNA through different mechanisms. α-globin 3' UTR is vulnerable to ribosomal read through. If the ribosome reads as few as 4 codons past the stop codon, the protective structures of the 3' UTR are unfolded and the mRNA is destabilized and produces less than 1% normal α-globin protein levels. Stop codon mutations are responsible for α-thalassemia constant spring, the most common non-deletional thalassemia[303]. When preparing a gene for in vitro transcription, β-globin UTRs are often spliced 5' and 3' of the gene to help stabilize the mRNA in the cytoplasm[287,296,297].

Nucleotide substitution can also improve mRNA's transfection quality. It has been shown that substitution of uridine with pseudouridine and cytidine with 5-methyl-cytidine during in vitro transcription, as well as HPLC purification of in vitro transcribed mRNA can improve mRNA translation and reduce immune response[294–296,304].

Cationic peptides have been used to protect plasmid DNA in vivo. PEGylated polyacridine peptides have been shown to protect plasmid DNA in the bloodstream of mice for up to 12 hr[183–185,197,247]. A 1 μg dose of plasmid remains fully transfection competent after hydrodynamic stimulation, where DNA polyplex is i.v. dosed in a small volume followed by a hydrodynamic injection of normal saline after some delay. Hydrodynamic stimulation is a useful technique to determine how well a formulation protects DNA in the bloodstream[183]. PEGylated polyacridine peptides enhance DNA circulatory half-lives by inhibition of nuclease degradation and inhibition of uptake by liver fenestrated endothelial cells and Kupffer cells[247]. nonacridine PEGylated polylysine peptides are also capable of protecting DNA during circulation when

delivered in large doses[305].

Given that polyacridine peptides bind to, and protect, double stranded DNA, it was hypothesized they could bind to, and protect, mRNA. Even though mRNA is single stranded, RNAs often adopt complex secondary structures and form double helices (**Fig. 4-1**). These helices could allow the acridines to intercalate and enhance peptide binding over nonacridine polylysine peptides. Experience with PEGylated polyacridine peptides with DNA suggests that higher affinity leads to greater stability in the bloodstream[184]. These peptides may confer similar stability to mRNA.

It was also hypothesized that PEGylated polyacridine peptide binding could be improved with the addition of uridine or thymine polymers to bind to the 3' PolyA tail and increase the amount of double stranded RNA available for peptide to bind to.

Additionally, the use of nucleotide analogs to stabilize RNA against RNase activity has been demonstrated with RNA aptamers[306]. Modifications to the RNA backbone, either with phosphorothioate groups instead of phosphates, or replacing the 2' hydroxyl with a fluoride group prevents degradation in vivo[307]. It was hypothesized that the 3' polyadenosine tail could be synthesized with ATP analogs to incorporate these modifications and protect it against degradation.

In this study, luciferase mRNA was produced through in vitro transcription and was tested with PEGylated peptides. These peptides were shown to bind to mRNA and provide protection against RNase activity in vitro. Hydrodynamic injection was used to deliver mRNA to mouse liver, and it was shown that polyacridine peptides enhanced luciferase expression. It was also shown that PolyA tailed mRNA could be bound to Oligo(dT), Oligo(rU), and Poly(rU).

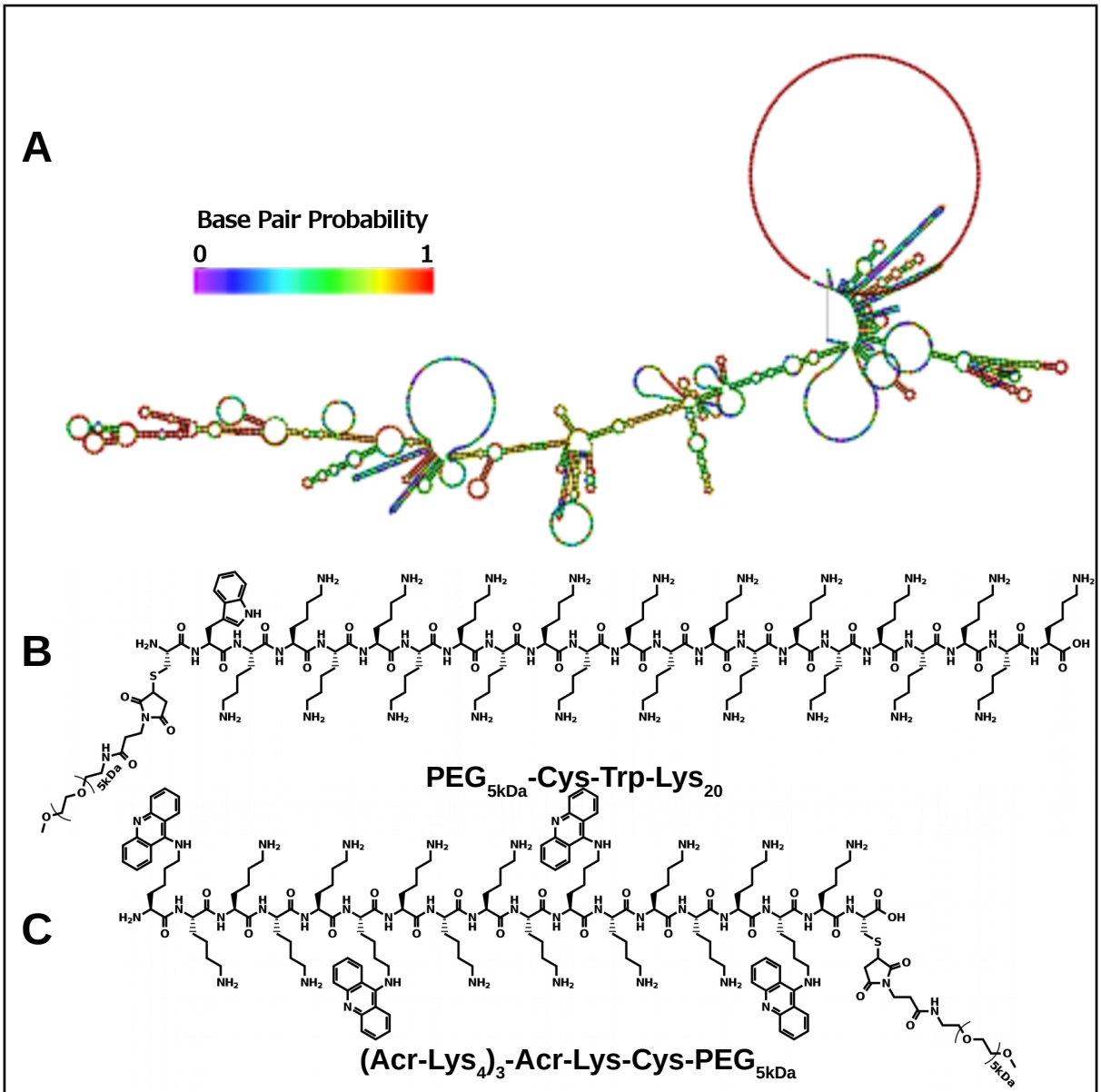

Figure 4-1: *Structures of Luc-UTR mRNA, nonacridine and acridine PEG-peptides.* The predicted secondary structure of Luc-UTR mRNA is shown in A, with many double helices. In B, the nonacridine PEGylated polylysine peptide PEG_{5kDa}-Cys-trp-Lys_{20} is shown, and in C, the acridine containing $(Acr\text{-}Lys_4)_3$-Acr-Lys-Cys-PEG_{5kDa} is shown.

Oligo(dT) binding prevented mRNA from functioning after hydrodynamic delivery, while Oligo(rU) and Poly(rU) did not affect bioluminescence. Polyadenosine tailing was attemped with 1-Thio-ATP and 2'-Fluoro-2'-dATP, but was not successful.

4.3 Materials and Methods

4.3.1 DNA Preparation

pGL3 control vector (Promega, Madison, WI, USA), a 5.3kb plasmid with firefly luciferase gene controlled by an SV40 promoter, was grown in DH5α E. coli and purified by Qiagen Gigaprep kit (Qiagen, Germantown, MD, USA). Purified plasmid DNA was quantified on a NanoDrop Lite Spectrophotometer (Thermo Fisher Scientific, Pittsburgh, PA, USA).

4.3.2 mRNA Synthesis

An initial attempt to produce luciferase mRNA was made by cutting the Luciferase gene from gWiz-Luc plasmid DNA (Aldevron, Fargo, ND, USA) using the NotI and BamHI cut sites and inserting into the pcDNA3.1(-) vector (Life Technologies, Grand Island, NY, USA) at those same cut sites, downstream from the T7 promoter.

Improved template DNA for in vitro transcription was prepared by synthesizing the firefly luciferase gene with 5' and 3' untranslated regions, UTRs, from human β globin with codon optimization for expression in mice (GenScript, Piscataway, NJ, USA). This synthesized gene was named Luc-UTR. Luc-UTR was inserted into the pcDNA3.1(-) vector between the XbaI and BamHI sites, downstream from the T7 promoter site. Luc-UTR pcDNA3.1(-) was grown in DH5α E. coli and isolated with a Qiagen Miniprep kit (Qiagen, Germantown, MD, USA).

Purified Luc-UTR pcDNA3.1(-) plasmid was linearized with HindIII-HF (New England Biolabs, Ipswich, MA, USA) at 37 °C for 60 min. Residual RNase A from the miniprep was removed by digestion with 1.2 U proteinase K (Thermo Fisher Scientific, Pittsburgh, PA, USA)

in 0.5% SDS (Research Products International, Mt. Prospect, IL, USA). Linearized template DNA was purified by phenol:chloroform:isoamyl alcohol extraction and isopropanol precipitation. Precipitated DNA was resuspended in RNase Free H_2O and quantified on a NanoDrop Lite Spectrophotometer.

Pre-mRNA was produced by in vitro transcription using the Ambion MEGAscript T7 Kit (Life Technologies, Grand Island, NY, USA) according to manufacturer's instructions. Briefly, 1 µg linearized template Luc-UTR pcDNA3.1(-) DNA was added to 7.5 mM ATP, GTP, CTP, UTP with 10X reaction buffer and T7 RNA Polymerase in total volume of 20 µL. The mixture was incubated at 37 °C for 4 hr. After transcription, 2 units of TURBO Dnase in 1 µL was added to the reaction mixture and incubated at 37 °C for another 15 min. The reaction was stopped by addition of 115 µL RNase free water and 15 µL 5 M ammonium acetate 100 mM EDTA. Pre-mRNA was purified by phenol:chloroform:isoamyl alcohol extraction and isopropanol precipitation. Purified pre-mRNA was quantified on NanoDrop Lite Spectrophotometer.

The 3' PolyA tail was added to the pre-mRNA using the Ambion PolyA Tailing Kit (Life Technologies, Grand Island, NY, USA) adapted from manufacturer's instructions. Briefly, pre-mRNA was mixed with 1 mM ATP, 50 mM Tris-HCl, 250 mM NaCl, 10 mM $MgCl_2$, pH 7.9, and 8 units E. coli polyadenosine polymerase in total volume of 100 µL. Reaction mixture was incubated at 37 °C for 1 hr. Then, 35 µL RNase free H_2O and 15 µL ammonium acetate stop solution were added. Tailed mRNA was purified by phenol:chloroform:isoamyl alcohol extraction and isopropanol precipitation. Purified pre-mRNA was quantified on NanoDrop Lite Spectrophotometer.

The 5' cap was added to tailed mRNA using the Vaccinia Capping System and mRNA Cap 2'O-methyltransferase (New England Biolabs, Ipswich, MA, USA) according to manufacturer's instructions. Briefly, 10 µg of RNA was heated to 65 °C for 5 min, then chilled on ice for 5 min. RNA was then mixed with 0.5 mM GTP, 0.2 mM SAM, 10 units Vaccinia Capping Enzyme, and 50 units mRNA cap 2'O-methyltransferase in total volume of 20 µL. The reaction mixture can be scaled according to the mass of mRNA. The mixture was incubated at 37 °C for 1 hr. Capped, tailed, mRNA was then purified by phenol:chloroform:isoamyl alcohol extraction and isopropanol precipitation. Purified mRNA was quantified on NanoDrop Lite Spectrophotometer. RNA was stored in -70 °C freezer.

Additionally, batches of mRNA were synthesized as above, but UTP and CTP were substituted with pseuodouridine triphosphate (Ψ) and/or 5-methylcytidine triphosphate (5meC) (Trilink Biotechnologies, San Diego, CA, USA).

4.3.3 Gel Electrophoresis

mRNA was examined for size and integrity by agarose native gel electrophoresis. A 1% gel was produced by dissolving 0.5 g agarose (Research Products International, Mt. Prospect, IL, USA) with 50 mL 0.5X Lithium Boric Acid Electrophoresis Buffer (Faster Better Media, Baltimore, MD, USA) and 2 µL 50 µg/mL ethidium bromide (Bio-Rad Laboratories, Hercules, CA, USA). Because RNA secondary structure can create multiple bands on non-denaturing gels, RNA samples were heated to 65 °C for 5 min and were chilled on ice for 5 min to obtain a single band on gel. RNA was prepared at 1 µg for each lane with 5X LB Loading Medium (Faster Better Media, Baltimore, MD, USA) and loaded into the gel. Electrophoresis was carried out at

145 V for 30 min using a Bio-Rad PowerPac 200 (Bio-Rad Laboratories, Hercules, CA, USA). Gels were imaged using a UVP BioSpectrum Imaging System and VisionWorks®LS software (UVP, Upland California).

4.3.4 Oligo(dT) Binding Assay

Oligo$(dT)_{25}$ cellulose beads (New England Biolabs, Ipswich, MA, USA) at 83.3 µg/µL were measured as 10 µL aliquots in PCR tubes, spun down, and storage buffer was removed. Beads were washed twice with 20 µL of Oligo(dT) loading buffer, 0.5 M NaCl, 20 mM Tris-HCl, 1.0 mM EDTA, pH 7.5. RNA samples at 1 µg each were diluted to 10 µL with Oligo(dT) loading buffer, heated to 65 °C for 5 min and chilled on ice for 5 min. RNA samples were then mixed with Oligo$(dT)_{25}$ cellulose beads for 5 min at room temperature. RNA-Bead mixtures were spun down, 5X LB Loading Medium was added, and supernatents were loaded into 1% agarose gels alongside untreated RNA controls. Electrophoresis and imaging were performed as described above.

4.3.5 Thermal Melt Assay

Solutions were prepared with 1 µg mRNA in 1xSSC buffer, 150 mM NaCl, 15 mM sodium citrate, pH 7.4 with total volume of 90 µL in PCR tubes. Thiazole orange was prepared by dissolving 5 mg in 1000 µL methanol, followed by 1000 fold dilution in 1xSSC buffer, 10 µL of which was added to the mRNA solutions. Samples were placed in a BioRad Icycler thermal cycler with MyIQ Single Color Real Time PCR Dectection System (BioRad Laboratories, Hercules, CA, USA) and held at 25 °C for 5 min, then heated to 85 °C over 10 min, with

fluorescence measured every 10 seconds. Melting point was determined by calculating the negative first order derivative of the fluorescence vs temperature plot.

4.3.6 Synthesis of PEG-Peptides

$(Acr\text{-}Lys_4)_3$-Acr-Lys-Cys and Cys-Trp-Lys_{20} were prepared as previously described[184,185,305], by solid phase peptide synthesis using an Apex 396 Synthesizer (Advanced ChemTech, Louisville, KY, USA), using standard FMOC procedures. PEGylation of the Cys residues was performed by reacting 1 μmol of peptide with 1.1 μmol of PEG_{5kDa}-maleimide in 4 ml of 100 mM HEPES buffer pH 7 for 12 hr. PEGylated peptides were then purified by semi-preparative scale RP-HPLC.

4.3.7 Formulation and Characterization of RNA PEG-Peptide Polyplexes

RNA polyplexes were formed by mixing equal volumes of mRNA and PEG-Peptide at 0.8 nmol peptide per 1 μg of RNA.

Thiazole Orange displacement was used to show peptide-RNA binding. mRNA was dissolved at 40 μg in 4 mL 1 mM sodium Citrate pH 6.4 with 40 μL 0.5 mg/mL thiazole orange in methanol. Solutions of $(Acr\text{-}Lys_4)_3$-Acr-Lys-PEG_{5kDa} were prepared in triplicate at 0, 125, 250, 625, and 1250 pmol of peptide in 1 mM sodium citrate pH 6.4 at total volume of 250 μL. RNA thiazole orange solution was added to each peptide solution in equal volumes (250 μL each) and allowed to incubate at room temperature for 20 min. Fluorescence intensity of each sample was then measured with λ_{ex} = 484 nm and λ_{em} = 535 nm using a Perkin Elmer LS50B

fluorometer (Perkin Elmer, Waltham, MA, USA).

A band shift assay was performed by making polyplexes with 1 μg mRNA and PEG-Peptide at 0.00, 0.01, 0.05, 0.10, 0.30, 0.70, or 1.00 nmol peptide per μg RNA. RNA polyplexes were loaded onto 1% agarose gels and electrophoresis and imaging were performed as above.

Particle size and zeta potential were determined by dynamic light scattering with a Brookhaven Zetaplus (Brookhaven Instruments, Holtsville, NY, USA) using 2 mL of RNA polyplex at 30 μg/mL in 5 mM HEPES pH 7.5.

4.3.8 RNase Protection Assay

Polyplexes were prepared with 2 μg of Tailed Luc-UTR mRNA and 1.6 nmol of either $(Acr\text{-}Lys_4)_3$-Acr-Lys-Cys-PEG_{5kDa} or PEG_{5kDa}-Cys-Trp-Lys_{20}. mRNA polyplexes were incubated with 0, 3, 10, 30, 100, 300, 1000, or 3000 ng/ml of RNase A (Thermo Fisher Scientific, Pittsburgh, PA, USA) in total volume of 20 μl of 5 mM HEPES buffer, pH 7.4 for 10 min at 37 °C. Proteinase K was diluted to 0.5 mg/mL in 500 μL 100 mM NaCl, 50 mM Tris, and 1% SDS, pH 8.0 and added to the samples, which were incubated at 37 °C for 30 min to destroy the RNase. RNA was extracted with 500 μL phenol:chloroform:isoamyl alcohol followed by ethanol precipitation. Pelleted RNA was dried and resuspended in 10 μl of 5 mM HEPES buffer. RNA was electrophoresed and imaged as described above.

4.3.9 Hydrodynamic Dosing of RNA

RNA polyplexes were prepared with 5 μg of mRNA and 4 nmol of PEG-Peptide as described above. Triplicate ICR male mice were weighed, and average mass was used to

calculate volume necessary for hydrodynamic dosing, at 0.09 mL per gram of animal mass. RNA polyplexes were dissolved in enough normal saline for 5 hydrodynamic doses. Triplicate mice were restrained and hydrodynamically dosed with 1 μg of RNA polyplex by tail vein injection in 5 – 7 seconds. Doses of pGL3 luciferase expressing plasmid DNA at 1 μg were used as a positive control.

4.3.10 Delayed Hydrodynamic Stimulation

Delayed hydrodynamic stimulation is performed in a similar manner to standard hydrodynamic injection. However, delayed hydrodynamic stimulation delivers mRNA polyplex in a small volume, 100 μL, of HEPES buffered mannitol, HBM (5 mM HEPES, 270 mM mannitol, pH 7.4). The polyplexes are allowed to circulate through the bloodstream for some time, after which a hydrodynamic bolus dose of normal saline with no additional RNA is injected into the tail vein. Bioluminescent imaging is performed 24 hr after hydrodynamic injection as described below.

4.3.11 Bioluminescent Imaging

At 24 hr after hydrodynamic dosing of RNA polyplexes, mice were anesthetized with 2.5% isofluorane gas and intraperitoneally dosed with 80 μL of 30 μg/μL D-Luciferin (Gold Biotechnology, St. Louis, MO, USA) in phosphate buffered saline. At 5 min post injection, mice were imaged for bioluminescence in an IVIS Imaging 200 Series (Xenogen, Hopkins, MA, USA), with 2.5% isofluorane gas, medium binning, 24.6 cm field of view, and 10 second acquisition time.

4.3.12 Serum Incubation Assay

Three mice were anesthetized with intraperitoneal injection of 100 mg/kg ketamine and 10 mg/kg xylazine, their blood was collected through cardiac puncture. The pooled mouse blood was allowed to clot at room temperature for 15 min. Clotted blood was centrifuged at 5000 RPM at 4 °C for 10 min. Serum was removed and split into 100 µL aliquots and stored at -70 °C.

RNA polyplexes were prepared with 5 µg of mRNA and 4 nmol of PEG-Peptide as described above in total volume of 5 µL. Polyplexes were diluted with 15 µL of mouse serum and allowed to incubate at room temperature for 30 min. The polyplex serum mixture was diluted with normal saline and used for hydrodynamic dosing as described above.

4.3.13 Expression Time Course

Luc-UTR mRNA polyplexes were prepared with $(Acr\text{-}Lys_3)_4$-Acr-Lys-Cys-PEG_{5kDa} at 0.8nmol peptide per µg mRNA. Triplicate mice were hydrodynamically injected with 1 µg doses of polyplex and imaged at 4, 24, 36, 48, 60, 72, 84, and 96 hr to determine how expression changed over time.

4.3.14 Oligo(dT) and Oligo(rU) Binding

Polythymine DNA oligos at 16, 20, 24, 28, and 32 bases long and a 32 base long polyuridine RNA oligo (Integrated DNA Technologies, Coralville, IA, USA) were mixed with capped and tailed Luc-UTR mRNA at 10 “Tail Equivalents”, assuming 200 nt long PolyA tails. These mixtures were delivered to mice by hydrodynamic tail vein injection.

To determine approximately how many copies of Oligo(rU) were needed to bind one copy of tailed mRNA, Oligo(rU) was mixed with tailed Luc-UTR mRNA at 0, 0.8, 1.7, 4.2, 8.4, 12.6, 16.8, 83.6, 166.8, 419.2, 836.2, and 1674.6 to 1 ratios of Oligo(rU) to mRNA in Oligo(dT) binding buffer as described above. Oligo(rU)-mRNA mixtures were then used with the Oligo(dT) cellulose bead binding assay as above.

PolyA tail length was estimated by assuming that Oligo(dT) cellulose beads could only bind tailed mRNA if at least 25 consecutive adenines were available for binding. Since the Oligo(rU) is 32 bases long, 32 uridines + 25 adenines is 57 bases, and 32 uridines divided by 57 bases is 56%. So complete inhibition of Oligo(dT) bead binding should occur when the Oligo(rU) occupies at least 56% of the tail. PolyA tail length was estimated by multiplying the Oligo(rU):mRNA ratio by 32 uridines, then dividing by 56%.

Oligo(rU) binding to tailed mRNA was also examined by thermal melt assay. Tailed and untailed mRNA solutions were prepared at 10 µg RNA with 100 µL 5 µg/mL thiazole orange in total volume of 900 µL 1xSSC buffer. RNA solutions were aliquotted into 90 µL portions in PCR tubes. Oligo(rU) solutions were prepared in 1xSSC buffer at total volume of 30 µL and 10 µL of each solution was added to mRNA solutions such that ratio of Oligo(rU) to mRNA was 0, 0.8, 1.7, 4.2, 8.4, 12.6, 16.8 to 1. Solutions were placed in the thermal cycler and melt curves were performed as described above.

4.3.15 Poly(rU) and Poly(rA) Binding

Poly(rU), Poly(rA), and Poly(rU)·Poly(rA) duplex (Sigma Aldrich, St. Louis, MO, USA) were dissolved in 1xSSC at approximately 1 mg/mL and stored at -70 °C.

Poly(rU)·Poly(rA) duplex was dissolved at 0.0, 0.2, 0.4, 0.6, 0.8 and 1.0 µg in 90 µL of 1xSSC buffer with 10 µL of 1000 fold diluted thiazole orange for a total volume of 100 µL in PCR tubes. Samples were placed in the thermal cycler and melting curves were obtained as above.

Poly(rU)·Poly(rA) duplex was dissolved at 1.0 or 50.0 µg in 90 µL of 1xSSC buffer with 10 µL of 1000 fold diluted thiazole orange as above. Samples were melted multiple times to study affect of repeated heating and cooling on fluorescence. Additionally, a "reverse" melt curve was obtained by heating RNA solutions to 85 °C for 5 min followed by cooling to 25 °C over 60 cycles, at 10 seconds per cycle.

Tailed Luc-UTR mRNA at 1.0 µg was mixed with 0.0 – 1.0 µg of Poly(rU) or Poly(rU)·Poly(rA) duplex in 25 µL of 1xSSC and loaded into 1% non-denaturing agarose gels and electrophoresed as above. Additionally, 1.0 µg tailed or untailed Luc-UTR mRNA was mixed with 1.0 µg of Poly(rU), 1.0 µg Poly(rU) plus 1.0 µg Poly(rA), or 2.0 µg Poly(rU)·Poly(rA) duplex in 30 µL 1xSSC and electrophoresed as above.

Tailed or untailed Luc-UTR at 1.0 µg was mixed with 1.0 µg Poly(rU) and/or 1.0 µg Poly(rA) in 90 µL 1xSSC with 10 µL of 1000 fold diluted thiazole orange. Samples were placed in the thermal cycler and melting curves were obtained as above. Additionally, 10 µg of tailed or untailed Luc-UTR mRNA was dissolved in 1xSSC buffer with 100 µL of 1000 fold diluted thiazole orange for a total volume of 900 µL and divided into 90 µL aliquots in PCR tubes. Poly(rU) was dissolved at 0 – 1.0 µg/µL in 30 µL 1xSSC and 10 µL of each was added to each mRNA tube to obtain 0.0, 0.5, 1.0, 2.5, 5.0, 7.5, and 10.0 µg Poly(rU). Samples were placed in the thermal cycler and melt curves were obtained as above.

Poly(rU), Poly(rU) plus Poly(rA), or Poly(rU)·Poly(rA) duplex at 1.0 μg was dissolved in 25 μL 1xSSC with 0.00. 0.01, 0.05, 0.10, 0.25, 0.50, 0.75, 1.00 nmol of $(Acr\text{-}Lys_4)_3$-Acr-Lys-Cys-PEG_{5kDa}. Samples were loaded into 1% non-denaturing agarose gels and electrophoresed as above.

Particle sizing was performed by mixing 48 μg Poly(rU)·Poly(rA) duplex in 0.8 mL 5 mM HEPES pH 7.4 and 38.4 nmol $(Acr\text{-}Lys_4)_3$-Acr-Lys-Cys-PEG_{5kDa} was dissolved in 0.8 mL 5 mM HEPES pH 7.4. Solutions were combined to produce RNA PEG-peptide polyplexes at 0.8 nmol peptide per μg RNA. Particle size and zeta potential measurements were carried out as above.

Hydrodynamic dosing of mRNA Poly(rU)·Poly(rA) mixtures were carried out by mixing 1.0 μg tailed Luc-UTR mRNA with 1.0 μg Poly(rU) or 2.0 μg Poly(rU)·Poly(rA) duplex and $(Acr\text{-}Lys_4)_3$-Acr-Lys-Cys-PEG_{5kDa} at 0.8 nmol peptide per μg RNA. Samples were delivered to mice by either direct hydrodynamic injection or delayed hydrodynamic stimulation at 5 min post-injection. Additionally, 1.0 μg tailed Luc-UTR mRNA was mixed with 50 μg Poly(rU)·Poly(rA) duplex and $(Acr\text{-}Lys_4)_3$-Acr-Lys-PEG_{5kDa} at 0.8 nmol per μg RNA and delivered to mice by either direct hydrodynamic injection or delayed hydrodynamic stimulation at 5 min post-injection. Bioluminescence imaging was carried out 24 hr later as described above.

4.3.16 PolyA Tailing with ATP Analogs

Pre-mRNA was prepared through in vitro transcription as above. However, tailing was carried out using the ATP analogs 1-Thio-ATP or 2'-Fluoro-2'-dATP (Trilink Biotechnologies,

San Diego, CA, USA). Several reaction conditions were tested including variations of reaction time, reaction temperature, ATP analog concentration, manganese ion concentration, addition of spermidine, admixtures with ATP, or use of yeast polyadenosine polymerase. Presence or absence of PolyA tail was determined by band shift assay or Oligo(dT) cellulose bead binding assay with gel electrophoresis. Tailed mRNA was capped as above and delivered to mice through hydrodynamic tail vein injection.

"Standard" reaction conditions are as above, but with 1 mM of either 1-Thio-ATP or 2'-Fluoro-2'-dATP.

Reaction time was varied by setting up 5 reactions with standard conditions and incubating at 37 °C. Every hour a reaction was removed from the thermal cycler and placed on dry ice to stop the reaction. After all samples had been frozen, they were thawed and purified by phenol:chloroform:isoamyl extraction and isopropanol precipitation as described above.

Reaction temperature was varied by setting up reactions with standard conditions and incubating at 37 °C. Temperature was increased from 37 °C to 60 °C over 60 min.

ATP analog concentration was varied by setting up reactions with either 0.5 mM or 10 mM ATP analog, representing one half or 10 times the standard concentration.

Effect of manganese ion concentration was tested by setting up reactions with 100 μM, 500 μM, 1000 μM, 1500 μM, 2000 μM, or 2500 μM of $MnCl_2$.

Effect of spermidine addition was tested by setting up reactions with 1 mM spermidine (Sigma Aldrich, St. Louis, MO, USA).

ATP admixtures were set up using either 10:1 or 1:1 ratios of ATP analog:ATP, maintaing total "ATP" concentration at 1 mM.

Yeast Polyadenosine Polymerase was tested by setting up reactions with 53.3 units of yeast polyadenosine polymerase (Affymetrix USB Products, Cleveland, OH, USA) instead of E. coli polyadenosine polymerase. Because the unit definitions provided by the different manufacturers were different, 53.3 units of yeast enzyme were used to match the enzyme activity (8 units) of E. coli polymerase.

4.4 Results

4.4.1 mRNA Synthesis

Capped and tailed Luc-UTR mRNA was produced by in vitro transcription and quantified by absorbance at 260 nm. Typical yields for a 20 µL reaction were approximately 200 µg of pre-mRNA. After tailing and capping, final yield was 100 – 150 µg, with significant batch to batch variation. Pre-mRNA typically had a 260/280 ratio of approximately 2.0, tailed mRNA would have a 260/280 ratio between 2.0 and 2.4, though this was most likely due to carryover of free ATP from the tailing reaction, as capped mRNA usually had a lower 260/280 ratio, approximately 2.0, implying loss of free ATP after the final purification. Gel electrophoresis showed that the mRNA formed good bands with minimal smear, implying little to no degradation by RNase. Gels often produced two bands, most likely due to mRNA secondary structures with different migration rates. Single bands could be produced by heat denaturing the mRNA and chilling it on ice. This also made RNA ladders unreliable, as the nondenatured RNA could not be trusted to run according to size. However, tailed mRNA could be distinguished from nontailed mRNA by band shift.

4.4.2 mRNA Polyplex Characterization

The thiazole orange displacement assay showed that (Acr-Lys_4)$_3$-Acr-Lys-PEG_{5kDa} caused significant loss of fluorescence at 50 pmol peptide per μg of RNA, and near total loss of fluorescence at 250 pmol per μg (**Fig. 4-2**). Both are well below the 800 pmol per μg used to formulate RNA polyplexes, implying that the mRNA is saturated with peptide.

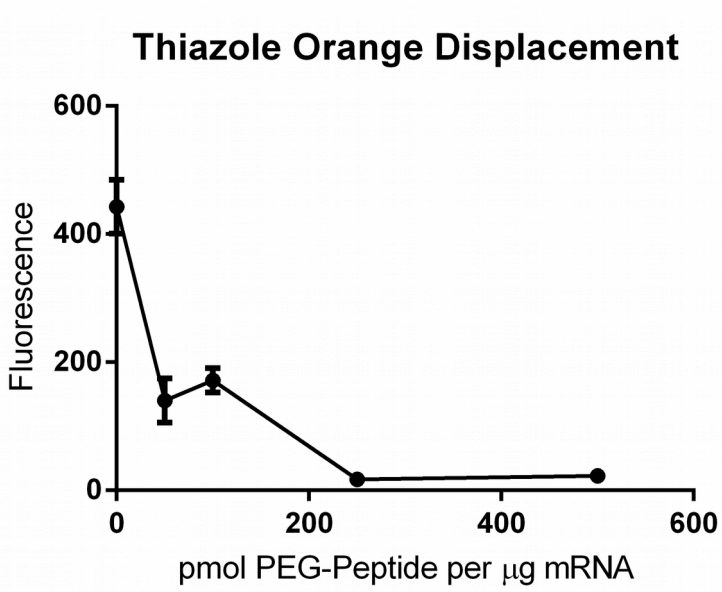

Figure 4-2: *Thiazole Orange displacement assay with Luc-UTR mRNA and (Acr-Lys_4)$_3$-Acr-Lys-Cys-PEG_{5kDa}.* mRNA is saturated by 250 pmol of peptide per μg mRNA.

Band shift assays using (Acr-Lys_4)$_3$-Lys-Cys-PEG_{5kDa} and PEG_{5kDa}-Cys-Trp-Lys_{20} RNA polyplexes demonstrated that both peptides bound to the mRNA and formed polyplexes that inhibited migration. Both peptides completely inhibited migration at 0.10 nmol peptide per μg RNA (**Fig. 4-3**). At 0.7 and 1.0 nmol/μg, (Acr-Lys_4)$_3$-Lys-Cys-PEG_{5kDa} formed polyplexes that ran up the gel, opposite from naked mRNA. This showed that the polyplexes were stable enough to not dissociate under electrophoresis conditions.

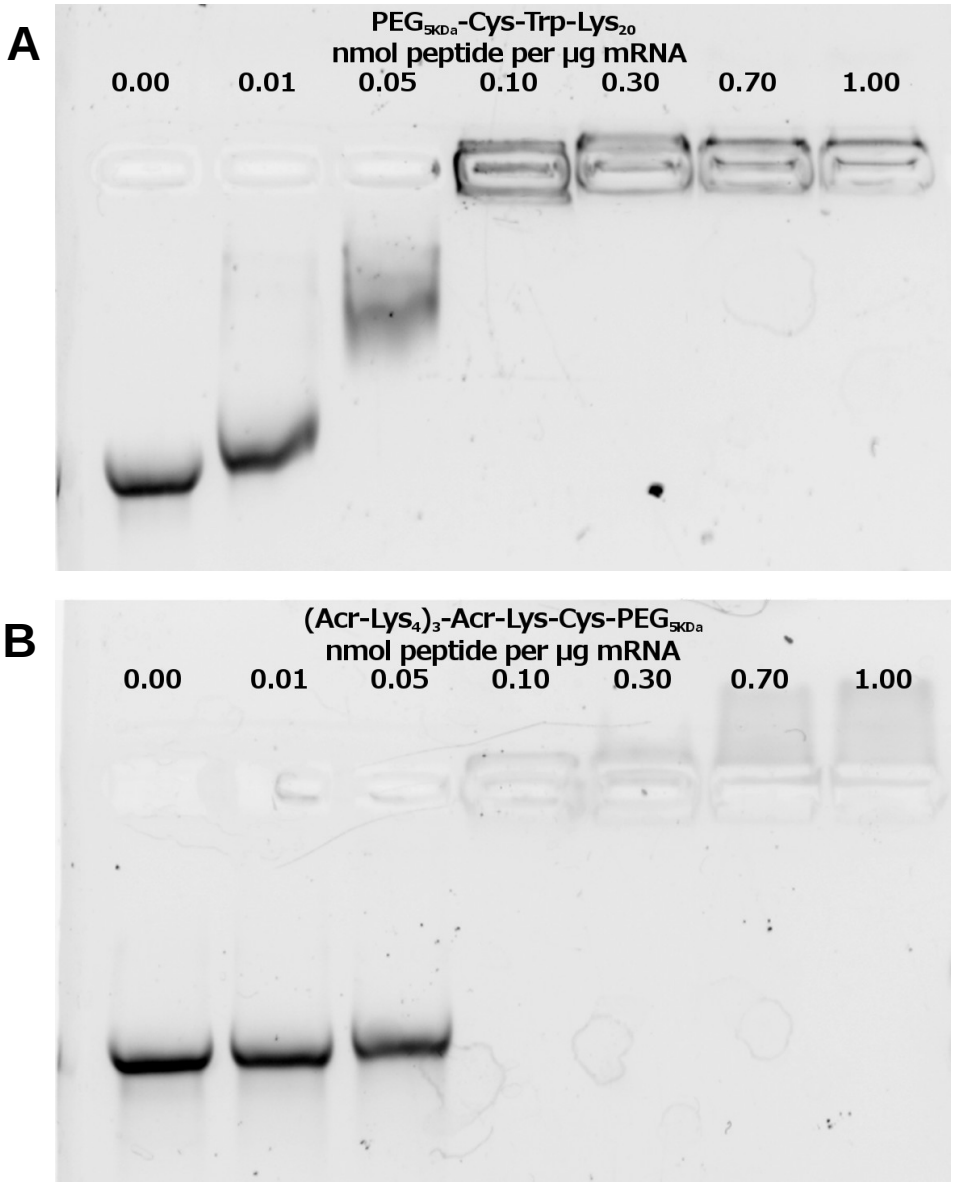

Figure 4-3: *Band shift assays demonstrate mRNA binding to PEG_{5kDa}-Cys-Trp-Lys_{20} and $(Acr\text{-}Lys_4)_3$-Acr-Lys-Cys-PEG_{5kDa}.* mRNA migration is inhibited by 0.10 nmol of nonacridine peptide in A, or acridine peptide in B.

Dynamic light scattering data showed that RNA polyplexes with $(Acr\text{-}Lys_4)_3$-Acr-Lys-Cys-PEG_{5kDa} formed particles with diameter of 104 nm and zeta potential of +15 mV. When pGL3 plasmid DNA is used, the same peptide forms particles with diameter of 170 nm, and

+15mV zeta potential[177]. This is consistent with the shorter length of mRNA vs plasmid DNA (1.6 kb vs 5.3 kb).

4.4.3 RNase Protection Assays

mRNA was complexed with PEG_{5kDa}-Cys-Trp-Lys_{20} or $(Acr\text{-}Lys_4)_3$-Acr-Lys-Cys-PEG_{5kDa} and incuabated with 0 – 3000 ng/mL RNase A for 10 min, then RNase was digested with proteinase K and RNA was purified by phenol:chloroform:isoamyl alcohol extraction and ethanol precipitation. Purified RNA was electrophoresed on 1% non-denaturing agarose gel. When PEG_{5kDa}-Cys-Trp-Lys_{20} was used, RNA remained intact at 30 ng/mL RNase A, but showed degradation at 100 ng/mL. When $(Acr\text{-}Lys_4)_3$-Acr-Lys-Cys-PEG_{5kDa} was used, RNA also showed some degradation at 100 ng/mL, but appeared less degraded than with the nonacridine peptide (**Fig. 4-4**).

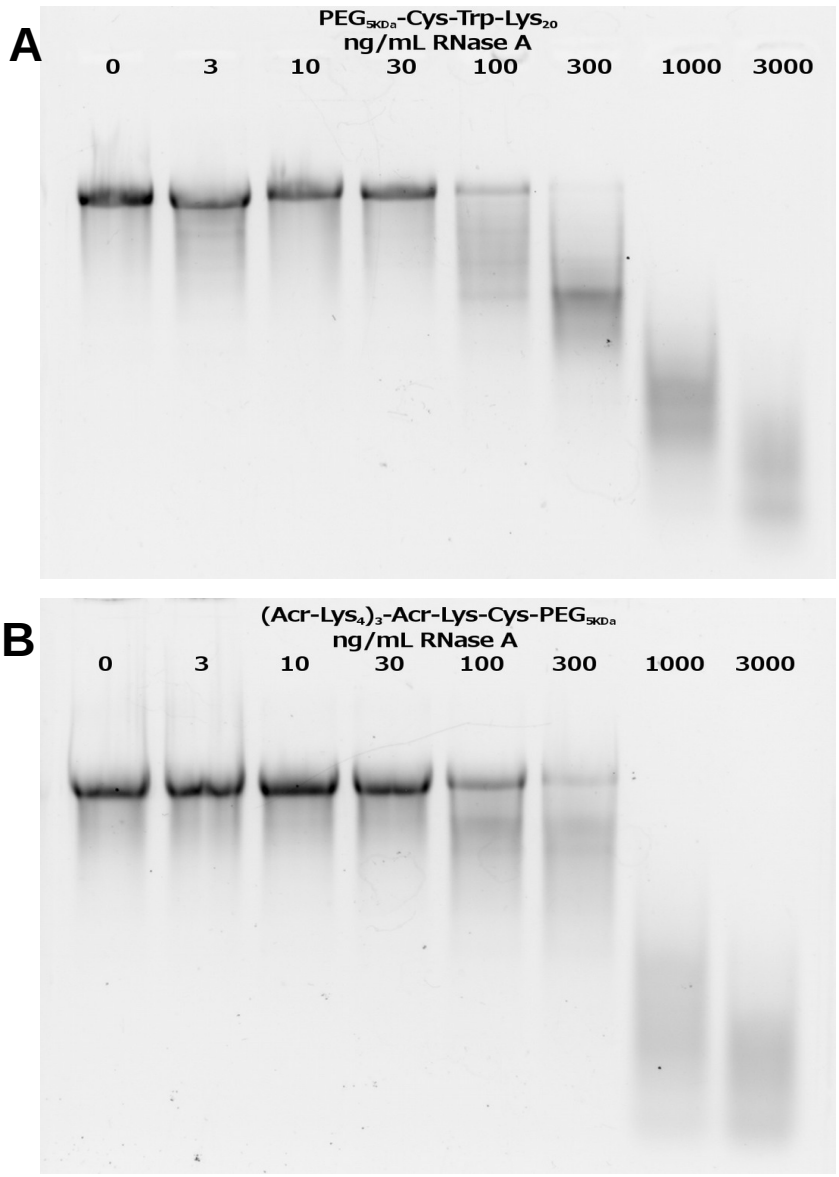

Figure 4-4: *mRNA is protected from RNase by PEG-peptides.* mRNA is protected from up to 30 ng/mL of RNase A by nonacridine peptide in A, or acridine peptide in B.

4.4.4 Hydrodynamic Dosing and Bioluminescence

The initial attempt to produce luciferase mRNA was able to produce mRNA that was used in hydrodynamic injection. However, in order to detect any luminescence, 20 μg of mRNA had to be injected rather than 1 μg, and bioluminescent imaging had to be performed at 4 hr post-injection rather than 24 hr post-injection. Mice produced approximately 1.0×10^6 photons/sec/cm^2/steradian, **(Fig. 4-5)** which was above background, but very poor, especially considering the amount of material needed.

Luc-UTR mRNA at 1 μg was hydrodynamically dosed into mice and bioluminescence was measured 24 hr post-injection. mRNA without peptide produced a bioluminescent signal of

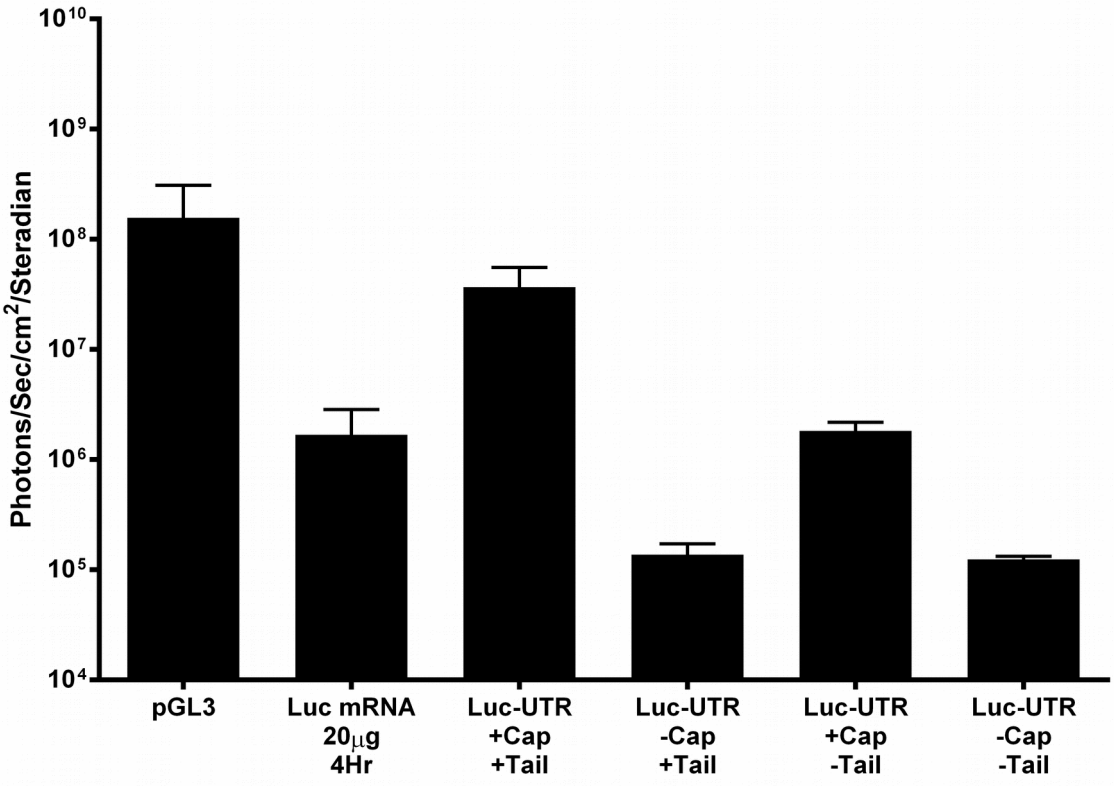

Figure 4-5: *Direct Hydrodynamic Dosing of mRNA.* Luc-UTR mRNA at 1 μg is comparable to an equal mass of pGL3 plasmid DNA and better than the original Luciferase mRNA tested at 20 μg. Luc-UTR mRNA requires a 5' cap to express luciferase, and the 3' PolyA tail improves expression.

$3.7x10^7$ photons/sec/cm^2/steradian. The pGL3 plasmid DNA control produces $1.0 – 5.0 x10^8$ photons/sec/cm^2/steradian, so when equal masses of naked mRNA and DNA are used, the DNA produces higher luciferase expression. This is not unexpected, as each DNA plasmid can produce several mRNA transcripts. Direct hydrodynamic dosing of capped, untailed Luc-UTR mRNA produces approximately $1.8x10^6$ photons/sec/cm^2/steradian. Hydrodynamic dosing of tailed mRNA without the 5' cap, or uncapped, untailed, mRNA produces no detectable bioluminescent signal (**Fig. 4-5**).

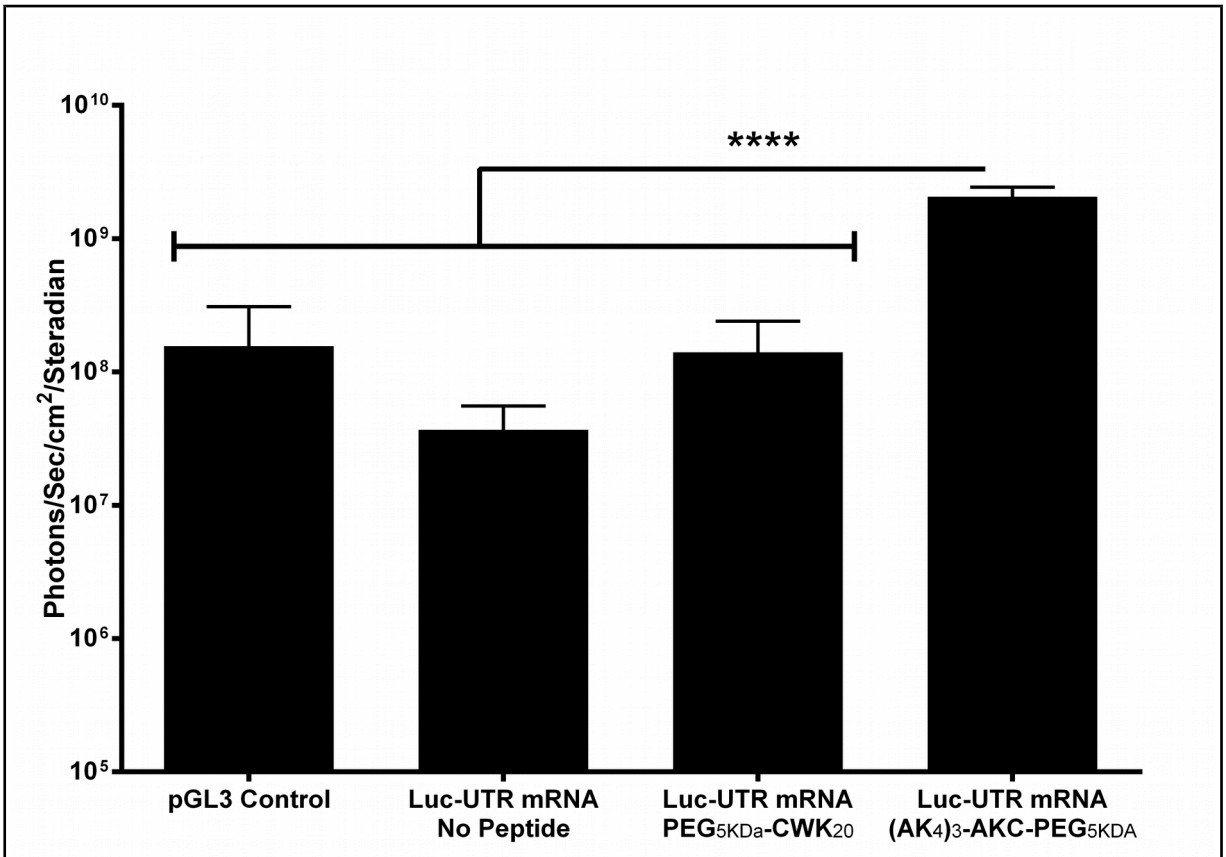

Figure 4-6: *Hydrodynamic Dosing of Luc-UTR mRNA PEG-Peptide Polyplexes.* $(Acr\text{-}Lys_4)_3$-Acr-Lys-Cys-PEG_{5kDa} mRNA polyplexes produce significantly higher bioluminescence than pGL3 plasmid DNA or PEG_{5kDa}-Cys-Trp-Lys_{20} mRNA polyplex. **** = $p < 0.0001$.

However, when mRNA is bound to $(Acr\text{-}Lys_4)_3$-Acr-Lys-PEG_{5kDa} to form RNA polyplexes, hydrodynamic dosing produced $1.4x10^9$ photons/sec/cm^2/steradian, significantly higher than unbound mRNA, but not significantly different from pGL3 DNA. When PEG_{5kDa}-Cys-Trp-Lys_{20} is used, signal is not significantly different from unbound mRNA (**Fig. 4-6**).

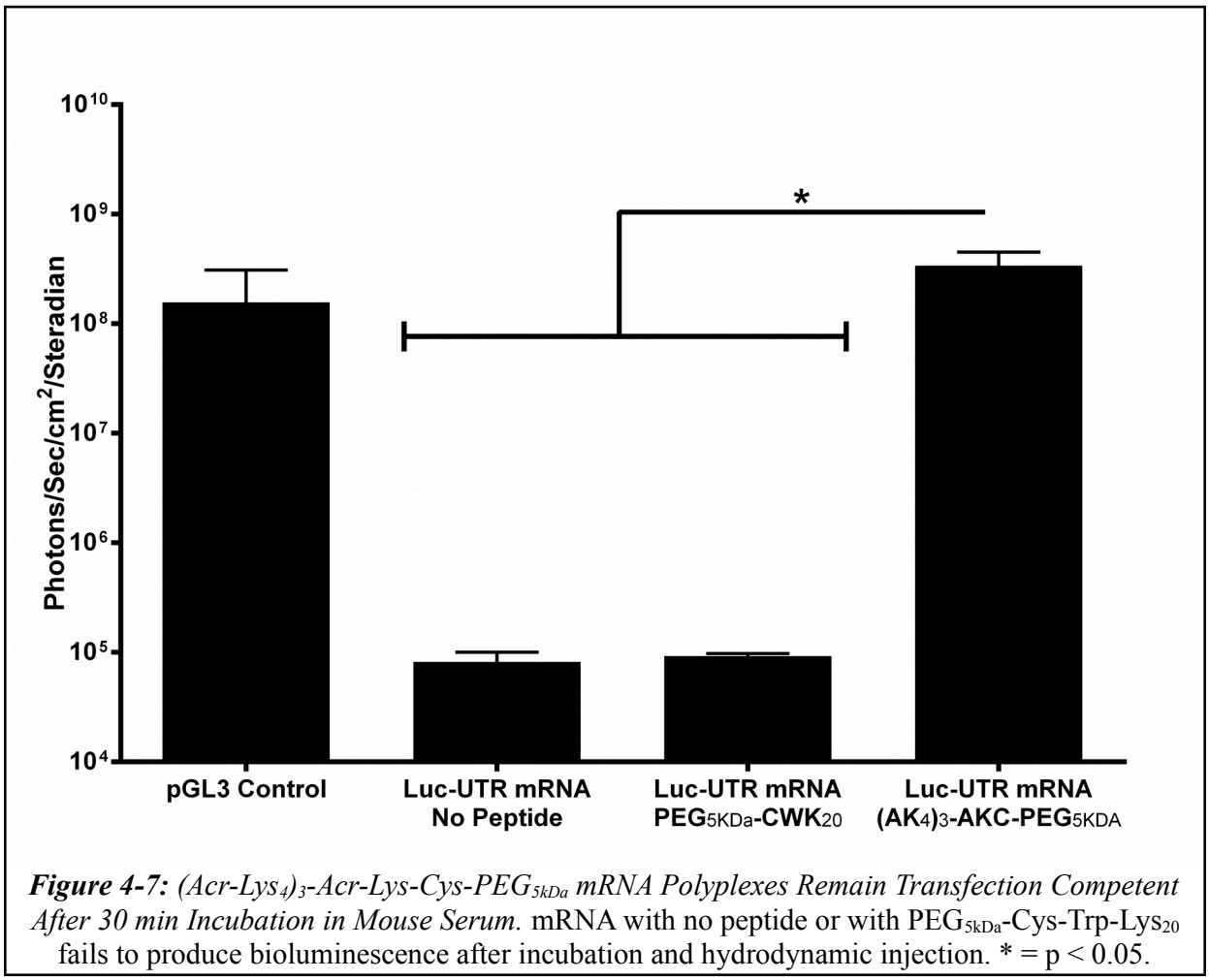

Figure 4-7: *$(Acr\text{-}Lys_4)_3$-Acr-Lys-Cys-PEG_{5kDa} mRNA Polyplexes Remain Transfection Competent After 30 min Incubation in Mouse Serum.* mRNA with no peptide or with PEG_{5kDa}-Cys-Trp-Lys_{20} fails to produce bioluminescence after incubation and hydrodynamic injection. * = $p < 0.05$.

4.4.5 Serum Protection Assay

Luc-UTR mRNA incubated in mouse serum for 30 min was not capable of producing bioluminescence after hydrodynamic dosing into mice. mRNA PEG_{5kDa}-Cys-Trp-Lys_{20} polyplex

was also not able to produce bioluminescence after incubation. However, mRNA $(Acr\text{-}Lys_4)_3$-Acr-Lys-Cys-PEG_{5kDa} polyplex was still able to produce $1x10^8$ photons/sec/cm^2/steradian after incubation and hydrodynamic delivery, indicating that acridines are necessary for at least partial protection against serum RNases (**Fig. 4-7**).

4.4.6 Expression Time Course

Bioluminescent signal at 4 hr post injection was already over $1x10^9$ photons/sec/cm^2/steradian, and remained there at 24 hr. Both images had some pixels that saturated the detector, so actual signal may be higher at either of these time points.

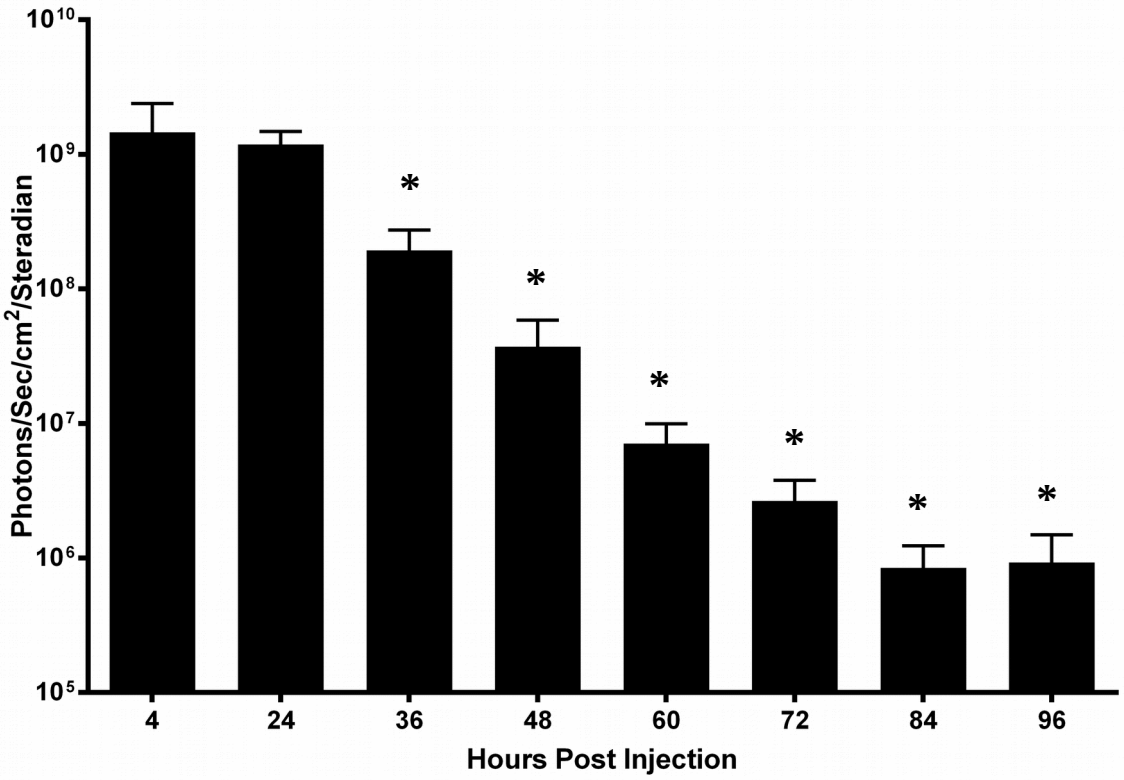

Figure 4-8: *$(Acr\text{-}Lys_4)_3$-Acr-Lys-Cys-PEG_{5kDa} Luc-UTR mRNA Polyplexes Produce Detectable Levels of Bioluminescence for at Least 72 hr Post-Injection*. * = $p \leq 0.05$ relative to 4 hr time.

Bioluminescent signal decreased after 24 hr, and was at background by 84 hr (**Fig 4-8**).

4.4.7 Oligo(dT) and Oligo(rU) Binding

Luc-UTR mRNA bound to Oligo(dT) at 16 or 32 bases long and hydrodynamically injected had 2 orders of magnitude less bioluminescence than nonbound mRNA (**Fig. 4-9A**). When bound to 32 base long Oligo(rU), bioluminescence was not significantly different from unbound control after direct hydrodynamic injection. However, when a 5 min delayed hydrodynamic stimulation was performed, there was no expression (**Fig. 4-9B**).

Luc-UTR mRNA was bound to several ratios of Oligo(rU) and assayed for binding with Oligo(dT) cellulose beads. Bead binding appeared to be completely inhibited by Oligo(rU) to mRNA ratios of 4.2:1 and above, partially inhibited by 0.84:1 and 1.67:1 ratios (**Fig. 4-9C,D**). With total inhibition occurring between 4.2:1 and 8.4:1 ratios, PolyA tail length was estimated at 200 – 500 adenines, consistent with the PolyA tailing kit manufacturer's claim for PolyA tail length.

Tailed and untailed Luc-UTR mRNA was bound to several ratios of Oligo(rU) and assayed by thermal melt curves with thiazole orange from 25 °C to 85 °C. Tailed mRNA showed strong fluorescence at 25 °C with 8.4, 12.6, and 16.8 to 1 ratios of Oligo(rU) to mRNA, similar to the results from gel electrophoresis(**Fig. 4-9E,F**). Melting point was determined to be approximately 48 °C for the 8.4 to 1 ratio, and approximately 50 °C for the 12.6 and 16.8 to 1 ratios. Untailed mRNA did not show increased fluorescence with any ratio of Oligo(rU) (**Fig. 4-9G,H**).

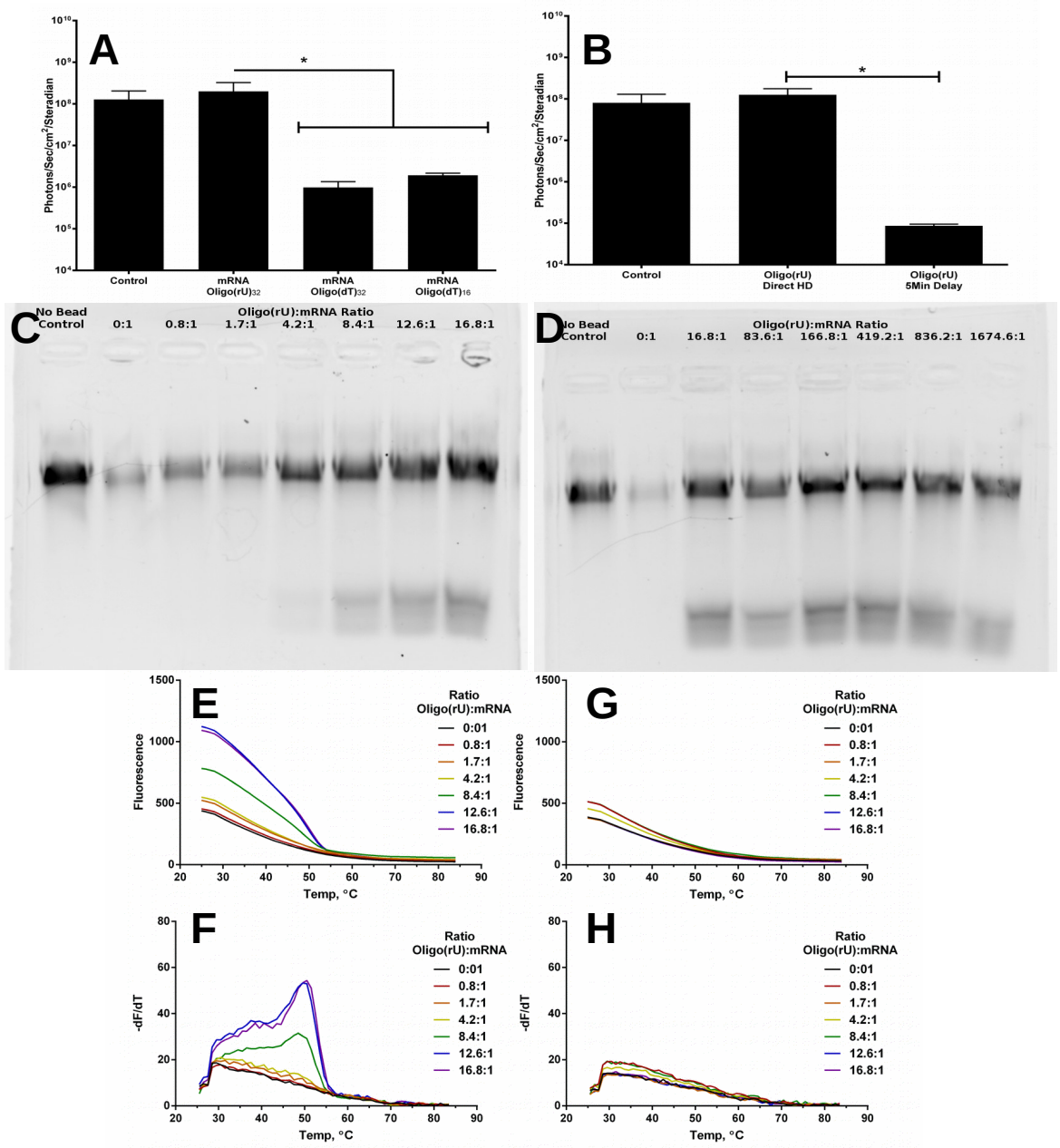

Figure 4-9: *mRNA with Oligo(rU) or Oligo(dT) Binding.* **A:** Oligo(rU) bound mRNA PEG-polyplex is still transfection competent, however Oligo(dT) bound mRNA polyplex produces very little bioluminescence with either 16 or 32 thymines. **B:** Though Oligo(rU) bound mRNA polyplex produces bioluminescence after direct hydrodynamic injection, it fails after delayed hydrodynamic stimulation. **C, D:** Oligo(rU) binds to tailed mRNA and prevents mRNA binding to Oligo(dT) cellulose beads at as little as 4.2 copies of Oligo(rU) per mRNA. **E, F:** Tailed mRNA binds Oligo(rU) and shows fluorescene in thiazole orange melt curve assay, mRNA Oligo(rU) complex melts at approximately 50 ºC. **G, H:** Untailed mRNA fails to bind Oligo(rU).

4.4.8 Poly(rU) and Poly(rA) Binding

Poly(rU)·Poly(rA) duplex at 0.0 – 1.0 μg was mixed with thiazole orange and melted in the thermal cycler. As amount of RNA increased, fluorescence increased, such that 1.0 μg of RNA produced approximately 1000 relative light units. As temperature increased, fluorescence decreased, then steeply fell off at 60 – 65 °C. The negative first derivative of the fluorescence was plotted to determine the inflection point of the melt curve and assign a melting point to the RNA. All amounts of RNA had melting points at approximately 65 °C (**Fig. 4-10A**).

Poly(rU)·Poly(rA) duplex was dissolved at 1.0 μg or 50 μg in 100 μL with thiazole orange and melted multiple times in the thermal cycler. When 1.0 μg of RNA was melted the first time, fluorescence at 25 °C was approximately 400 relative light units, while subsequent melt curves showed approximately 600 relative light units (**Fig. 4-10C,D**). When RNA was heated to 85 °C then cooled to 25 °C, a very similar curve was obtained, but the melting point was approximately 60 °C, less than the 65 °C melting point when temperature is increased from 25 °C to 85 °C (**Fig. 4-10C,D**). At 50 μg, RNA behaved similarly to 1.0 μg, however when RNA was cooled from 85 °C to 25 °C, fluorescence became much stronger, almost twice as high as initial fluorescence when heating from 25 °C to 85 °C (**Fig. 4-10E,F**).

Tailed Luc-UTR mRNA at 1.0 μg was mixed with 0.00 – 1.00 μg of Poly(rU) or Poly(rU)·Poly(rA) duplex and analyzed by gel electrophoresis. Poly(rU) by itself is not visible on agarose gel because ethidium bromide cannot intercalate. However, as amount of Poly(rU) increased, the mRNA bands in the gel became less intense and a smear became visible at 0.25 μg of Poly(rU). With Poly(rU)·Poly(rA) duplex, mRNA bands also became less intense as the RNA

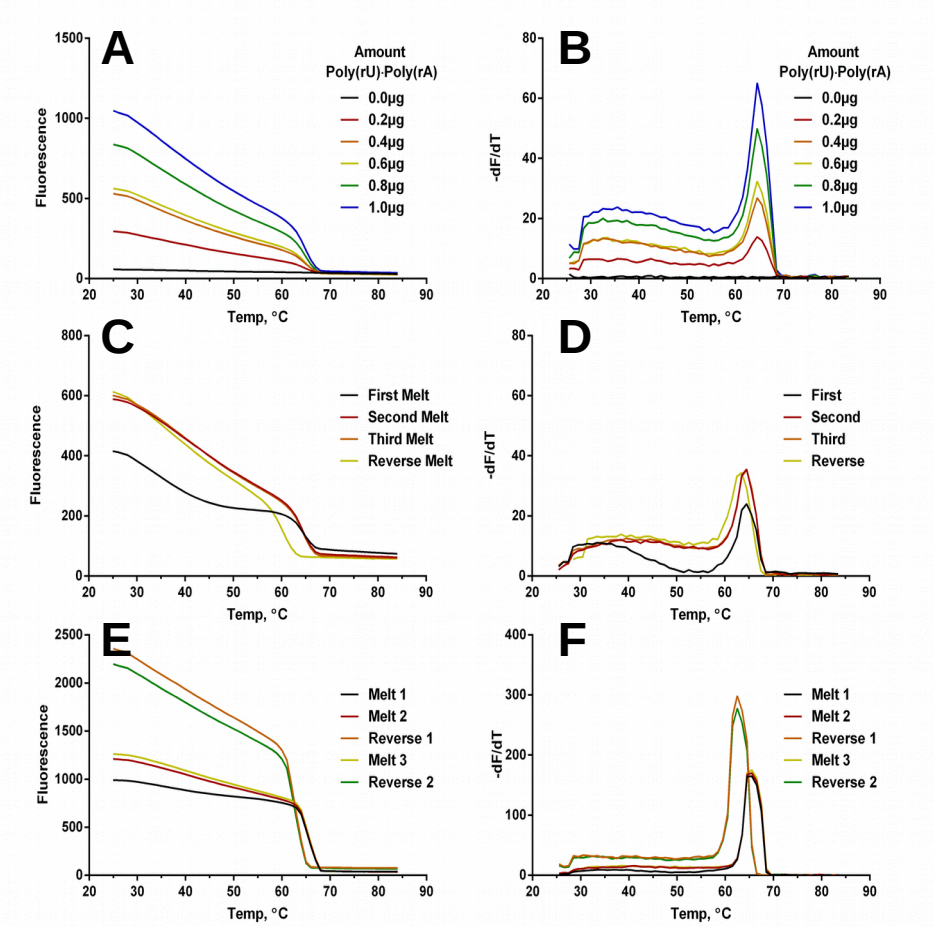

Figure 4-10: *Melting Properties of Poly(rU)·Poly(rA) Duplex.* **A, B:** Increasing amount of RNA increases fluorescence. Poly(rU) Poly(rA) melts at 65 °C. **C, D:** Melting RNA a second time increases fluorescent intensity. Subsequent melting does not change fluorescence. Cooling RNA instead of heating it produces a similar melt curve, but melting point appears slightly lower. **E, F:** Melting 50 µg of RNA shows that melting behavior does not change much at high concentrations of RNA. However, cooling the RNA produces much higher fluorescent intensities.

polymer increased. A smear became visible at 0.05 µg of duplex, and drastically changed appearance at 0.50 µg of duplex, becoming very dark at the bottom of the smear and the mRNA bands are no longer visible (**Fig. 4-11A,B**).

Tailed or untailed Luc-UTR at 1.0 µg was mixed with 1.0 µg of Poly(rU), 1.0 µg Poly(rU) and 1.0 µg of Poly(rA), or 2.0 µg of Poly(rU)·Poly(rA) duplex and electrophoresed.

With Poly(rU), untailed mRNA appears to be almost identical to untailed mRNA by itself.

However, the tailed mRNA with Poly(rU) shows smearing and a slight band shift compared to tailed mRNA by itself. With the mixture of Poly(rU) and Poly(rA) or the premade Poly(rU)·Poly(rA) duplex, neither the tailed or untailed mRNA bands were visible. All lanes showed a dark smear, however lanes with tailed mRNA showed a taller smear, reaching further up the gel (**Fig. 4-11C**).

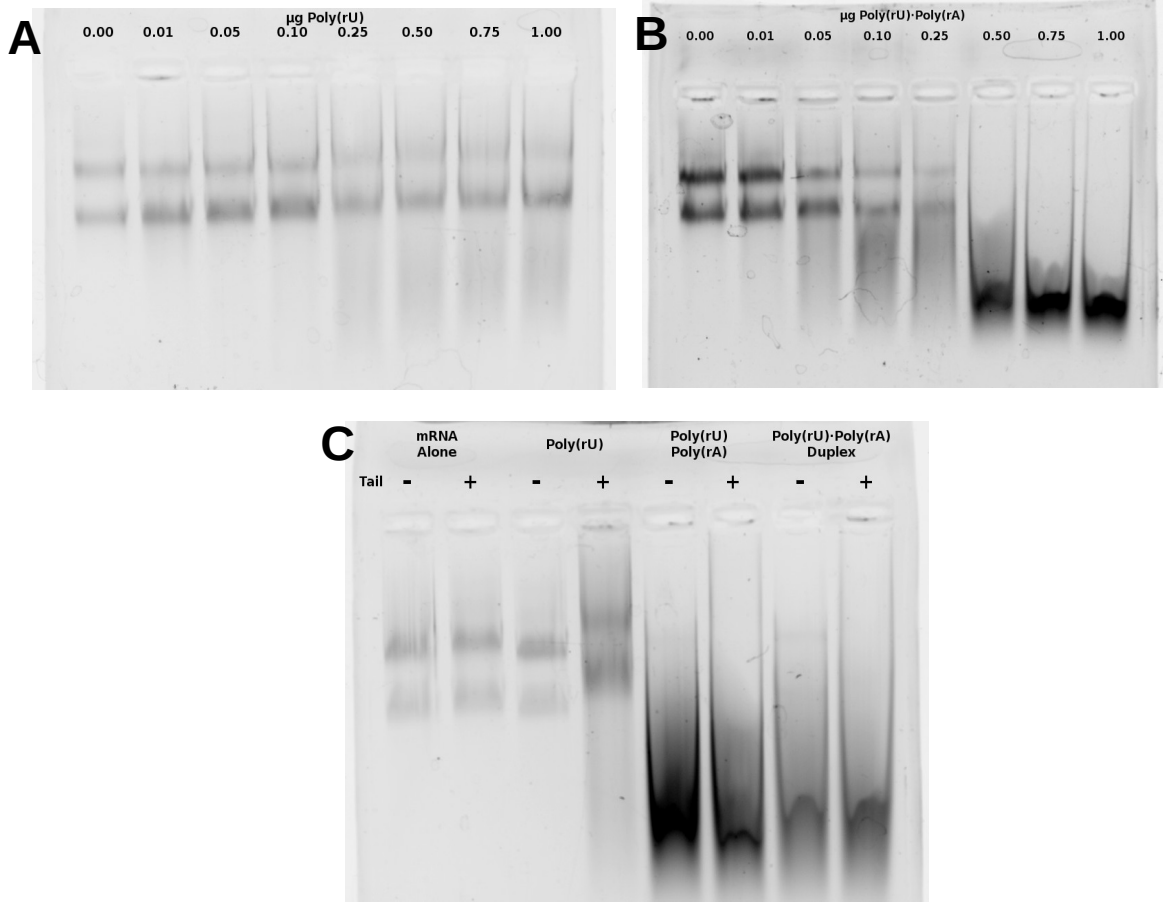

Figure 4-11: *mRNA Binding to Poly(rU) and Poly(rU)·Poly(rA) Duplex.* **A:** Tailed mRNA was mixed with 0 – 1 µg of Poly(rU). Smear at 0.25 µg and above suggests binding. **B:** Tailed mRNA was mixed with Poly(rU)·Poly(rA) duplex. Smearing changes and mRNA bands disappear at 0.5 µg and above. **C:** Tailed or untailed mRNA was mixed with Poly(rU) or Poly(rU)·Poly(rA) duplex. tailed mRNA shows smearing with poly(rU) or a taller smear with duplexes.

Tailed or untailed mRNA at 1.0 µg was mixed with 1.0 µg of Poly(rU) or Poly(rA), or Poly(rU) and Poly(rA) were mixed at 1.0 µg each with thiazole orange and subjected to melt curve analysis. Before mixing, both tailed and untailed mRNA showed almost identical melt curves with no clear melting point. Poly(rU) by itself showed almost no fluorescence at any temperature (**Fig. 4-12A,B**). Interestingly, Poly(rA) showed fluorescence at 25 °C just as intense as the mRNA fluorescence, but fluorescence was quickly lost as temperature increased, with melting point at approximately 30 °C (Fig. **4-12C,D**).

When mRNA was mixed with Poly(rU), tailed mRNA showed much higher fluorescence than either RNA alone. Tailed mRNA by itself had fluorescence at 25 °C of 400 relative light units, while the tailed mRNA Poly(rU) mixture had approximately 1300 relative light units, and melted at approximately 64 °C. Untailed mRNA had nearly identical melt curves with or without Poly(rU) (**Fig. 4-12A,B**). When mRNA was mixed with Poly(rA), tailed mRNA with Poly(rA) showed a slight increase in fluorescence, from 400 to 550 relative light units. Untailed mRNA showed no change in fluorescence (**Fig. 4-12C,D**).

When Poly(rU) and Poly(rA) were mixed, fluorescence at 25 °C was approximately 1200 relative light units with melting point at approximately 65 °C. Interestingly, fluorescence showed a slight increase just below the melting point (**Fig. 4-12E,F**).

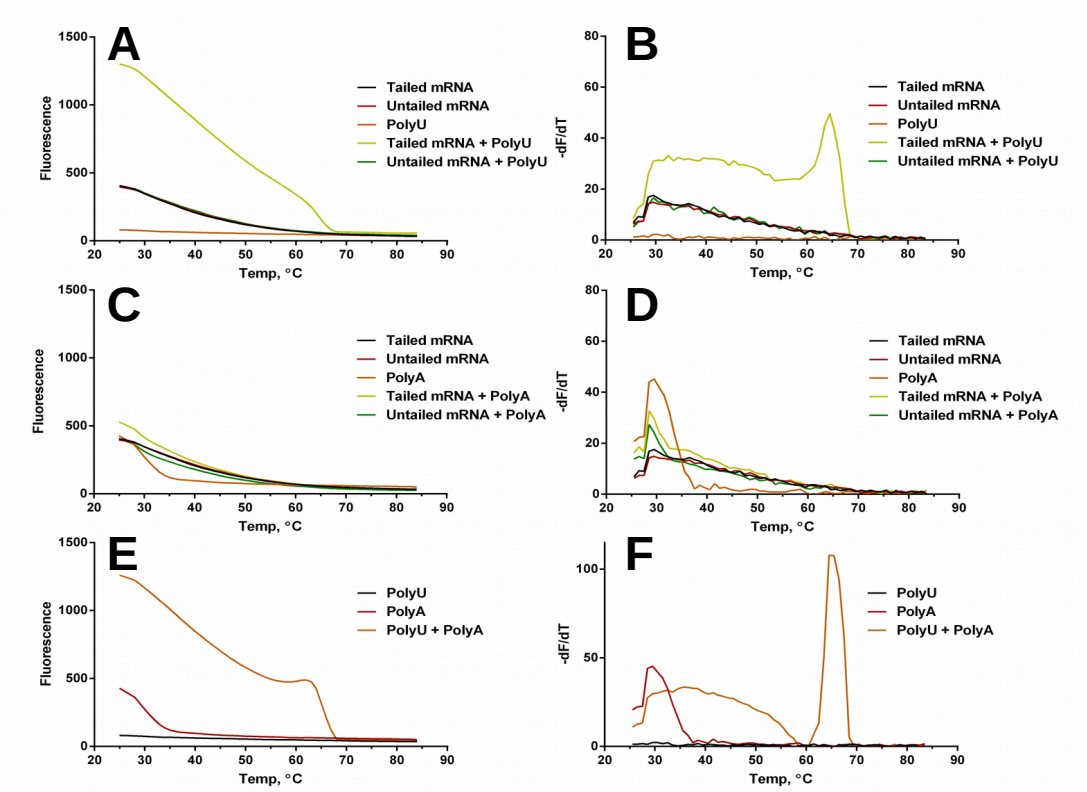

Figure 4-12: *Melt Curves of mRNA, Poly(rU), Poly(rA) Mixtures.* **A, B:** Tailed or untailed mRNA with Poly(rU). Only tailed mRNA shows binding, melts at 64 °C. **C, D:** Tailed or untailed mRNA with Poly(rA). Neither mRNA binds, but Poly(rA) shows some fluorescence on its own at 25 °C. **E, F:** Poly(rU) mixed with Poly(rA) shows binding with melting point at 65 °C.

Tailed or untailed Luc-UTR mRNA was mixed with 0.0 – 10.0 µg of Poly(rU) and subjected to melt curve analysis. Tailed mRNA with Poly(rU) showed fluorescence from approximately 800 – 1000 relative light units, while untailed mRNA with Poly(rU) showed fluorescence at approximately 300 – 400 relative light units, similar to tailed mRNA without Poly(rU). The melting points of the tailed mRNA Poly(rU) mixtures were approximately 65 °C (**Fig. 4-13**).

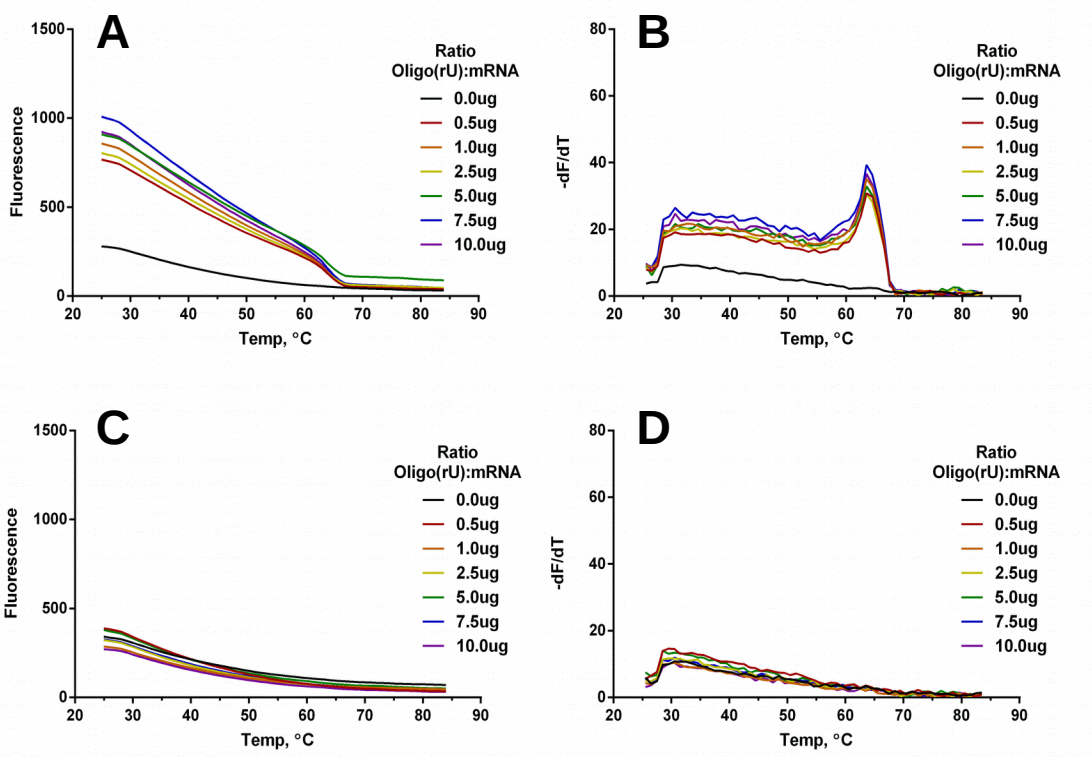

Figure 4-13: *Tailed and Untailed mRNA was Mixed with 0 – 10 µg Poly(rU) and Melted.* **A, B:** Tailed mRNA showed strong fluorescence with 0.5 µg of Poly(rU) and above, melted at 65 °C. **C, D:** Untailed mRNA showed no binding with any amount of Poly(rU).

Poly(rU), Poly(rU) plus Poly(rA), and premade Poly(rU)·Poly(rA) duplexes at 1.0 µg were mixed with 0.00 – 1.00 nmol of $(Acr\text{-}Lys_4)_3$-Acr-Lys-Cys-PEG_{5kDa} and analyzed by gel electrophoresis. Poly(rU) is not visible by itself, but some smearing is visible at 0.30, 0.70. and 1.00 nmol of peptide, these smears are moving up the gel, similar to high concentrations of peptide with mRNA. Both mixtures of Poly(rU) and Poly(rA) duplex showed smears at 0.00 and 0.01 nmol of peptide, but smears at 0.01 nmol of peptide did not migrate as far. No smears are visible at 0.05 or 0.10 nmol of peptide, and smears moving up the gel are visible at 0.30 nmol of peptide and above (**Fig. 4-14**).

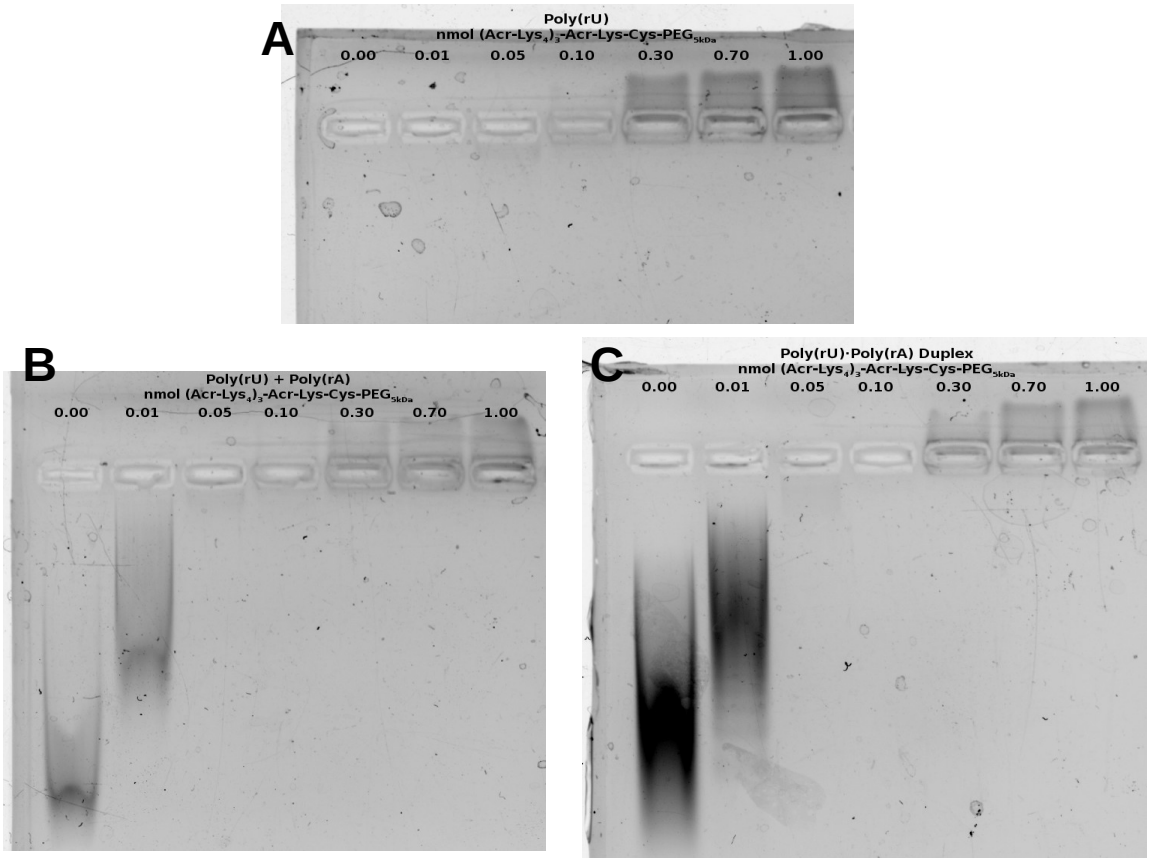

Figure 4-14: *RNA Homopolymer Peptide Binding.* Poly(rU) (**A**), a mixture of Poly(rU) and Poly(rA) (**B**), and Poly(rU)·Poly(rA) duplex (**C**) were mixed with 0 – 1 nmol of $(Acr\text{-}Lys_0)_3$-Acr-Lys-Cys-PEG_{5kDa} and electrophoresed. Poly(rU)·Poly(rA) mixtures show complete inhibition of migration at 0.05 nmol peptide, while Poly(rU) remains invisible.

Particle size and zeta potential of Poly(rU)·Poly(rA) duplex with $(Acr\text{-}Lys_4)_3$-Acr-Lys-Cys-PEG_{5kDa} at 0.8 nmol peptide per µg RNA were obtained by dynamic light scattering. Particles were obtained with diameter of approximately 114 nm and zeta potential at +7 mV, consistent with observations of mRNA.

Tailed Luc-UTR mRNA was mixed with Poly(rU) or Poly(rU)·Poly(rA) duplex at 1.0 µg each, and polyplexed with $(Acr\text{-}Lys_4)_3$-Acr-Lys-Cys-PEG_{5kDa} at 0.8 nmol peptide per µg RNA.

RNA polyplexes were delivered to mice by hydrodynamic tail vein injection. When polyplexes were delivered by direct hydrodynamic dosing, all samples produced 10^9 photons/sec/cm^2/steradian, equal to mRNA control (**Fig. 4-15A**). However, when RNA polyplexes were delivered by small volume injection followed by hydrodynamic stimulation at 5 min, no luminescence was detected (**Fig. 4-15A**).

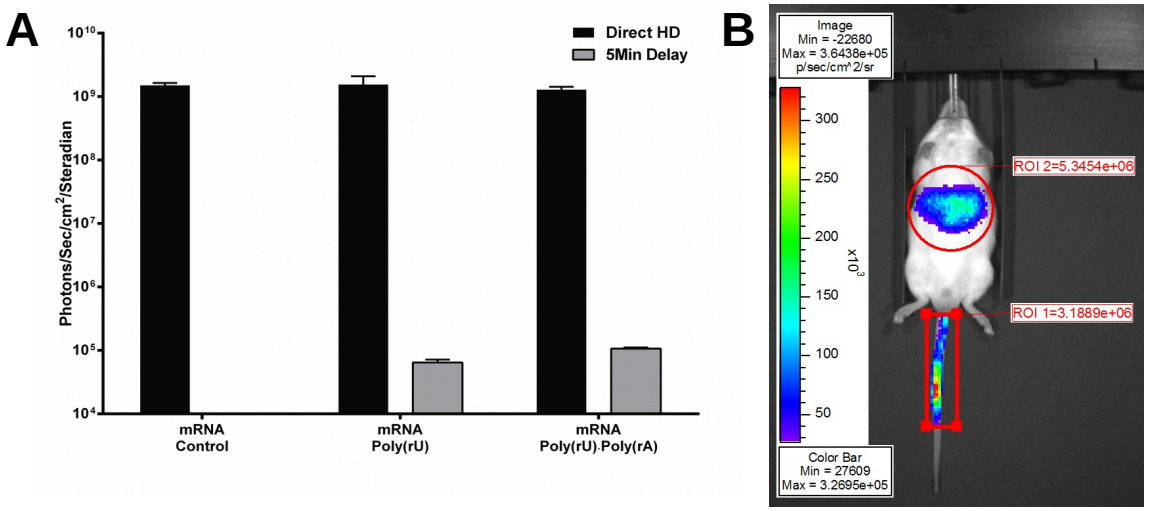

Figure 4-15: *Hydrodynamic Injection of mRNA Poly(rU)·Poly(rA) Polyplexes.* **A:** Direct Hydrodynamic injection of 1 µg Luc-UTR mRNA with 1 µg of Poly(rU)·Poly(rA) produced expression equal to mRNA polyplex control. Delayed hydrodynamic stimulation at 5 min failed to produce bioluminescence. **B:** Direct or delayed hydrodynamic injection of 1 µg mRNA with 50 µg Poly(rU)·Poly(rA) was lethal to all but 1 mouse. Surviving mouse received a lower dose, and produces lower bioluminescence, with significant luminescence in the tail.

When 1.0 µg mRNA was mixed with 50 µg of Poly(rU)·Poly(rA) duplex and (Acr-$Lys_4)_3$-Acr-Lys-Cys-PEG_{5kDa} and delivered to 8 mice by either direct hydrodynamic injection or delayed hydrodynamic stimulation, all but 1 mouse died less than 24 hr post-injection. The surviving animal only received 80% of the hydrodynamic injection due to a slipped needle, and probably only received approximately 40 µg of Poly(rU)·Poly(rA) duplex. This mouse produced

approximately $5x10^6$ photons/sec/cm^2/steradian in the liver, and approximately $3x10^6$ photons/sec/cm^2/steradian in the tail (**Fig. 4-15B**).

4.4.9 Tailing with ATP Analogs

An early attempt at tailing with 1-Thio-ATP and 2'-Fluoro-2'-dATP produced mRNA that was able to produce bioluminescence equal to ATP tailed mRNA, and was still able to produce luminescence after delayed hydrodynamic stimulation with delay times of 5, 30, and 60 min. However, attempts to replicate this result were unsuccessful.

Reaction time was varied from 1 to 5 hr using either ATP or 2'-Fluoro-2'-dATP. Tailed mRNAs were tested with the oligo(dT) bead binding assay. ATP tailed mRNA did not show noticable band shift, but did show band loss at all time points, with smearing becoming more apparent at longer time points(**Fig. 4-16A**). The 2'-Fluoro-2'-dATP tailed mRNA did not show band shift or band loss on gel (**Fig. 4-16B**). mRNAs were capped and tested for activity with hydrodynamic dosing. ATP tailed mRNA showed loss of bioluminescence over time, with the 3, 4, and 5 hr reactions having significantly less signal than the 1 hr reaction ($P < 0.05$) (**Fig. 4-16C**). The 2'-Fluoro-2'-dATP mRNA tailed for 1 hr showed poor signal, with later time points having lower signal (not significantly different from 1 hr time point) (**Fig. 4-16D**).

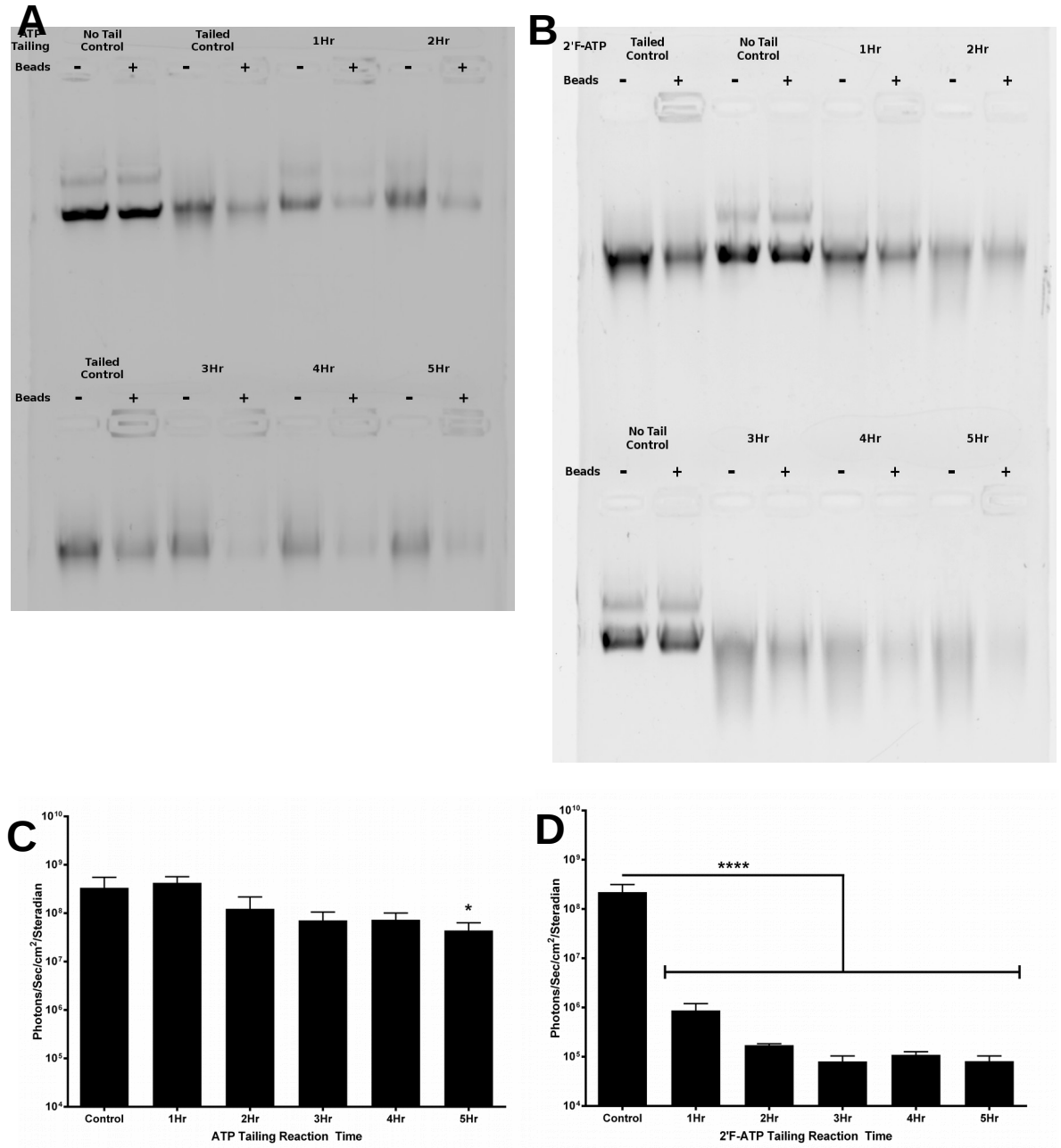

Figure 4-16: *Affect of Longer Reaction Times on PolyA Tailing.* **A:** Tailing with ATP was able to produce tailed mRNA as expected. As reaction time increased, band intensity slightly decreased. **B:** Tailing with 2'-Fluoro-2'-dATP failed to produce tailed mRNA at any time, bands became smeared as reaction time increased. **C:** ATP tailed mRNA showed decreased luciferase expression as tailing reaction time increases, with 5 hr reaction producing significantly less luminescence than mRNA polyplex control, * = $p < 0.05$. **D:** 2'-Fluoro-2'-dATP tailed mRNA produced very little luminescence at 1 hr reaction time, and was background at all other reaction times. **** = $p < 0.0001$.

Reaction temperature was tested with a temperature ramp from 37 °C to 60 °C over 1 hr. Neither 1-Thio-ATP, or 2'-Fluoro-2'-dATP showed band shift, though ATP tailed mRNA was shifted relative to the ATP analogs, it was not shifted relative to a non-tailed control (**Fig. 4-17**).

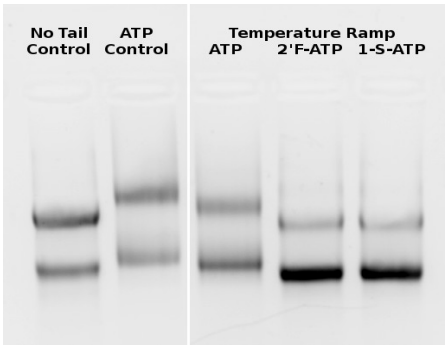

Figure 4-17: *Effect of Increasing Temperature During Tailing Reaction.* Temperature was increased from 37 ºC to 60 ºC over 1 hr. The ATP reaction still shows some band shift, while 2'-fluoro-2'-dATP and 1-thio-ATP show no evidence of tailing.

ATP and 2'-Fluoro-2'-dATP concentration was varied at 0.5 mM, 1.0 mM and 10 mM. The 10 mM ATP tailed mRNA showed very high 260/280 ratio, 4.24, most likely due to carryover through the purification. This overestimated the true mRNA concentration, so that less mRNA was actually used on gels. The 10 mM ATP tailed mRNA showed band shift, but not more than 1.0 mM ATP tailed mRNA control (**Fig. 4-18A**). Both the 1.0 mM ATP control and 10.0 mM ATP mRNA showed band loss on oligo(dT) bead binding assay (**Fig. 4-18B**). However, the 10 mM or 0.5 mM 2'-Fluoro-2'-dATP and 1-Thio-ATP did not show band shift or band loss (**Fig. 4-18**).

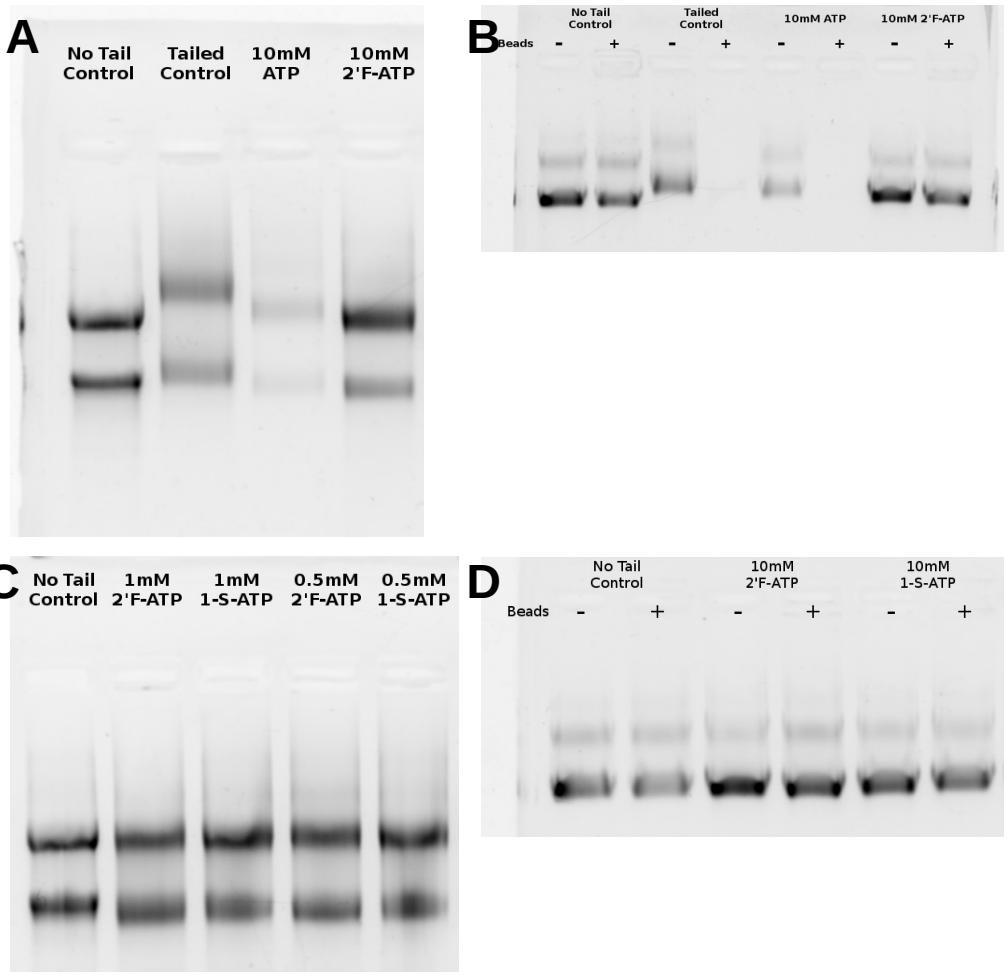

Figure 4-18: *Effect of Changing Concentration on Tailing Reaction.* **A:** Increasing substrate concentration 10 fold shows that 10 mM ATP still forms tailed mRNA, but band shift is reduced. 10 mM 2'-Fluoro-2'-dATP shows no band shift. **B:** mRNA tailed with 10 mM ATP still shows band loss on Oligo(dT) bead binding assay, while 2'-Fluoro-2'-dATP tailed mRNA shows no band loss. **C, D:** Reducing substrate concentration to 0.5 mM also fails to produce evidence of tailing by either band shift or band loss for 2'-Fluoro-2'-dATP or 1-Thio-ATP.

Manganese ion concentration was tested because many polyadenosine polymerase buffer recipes call for small amounts of manganese. When 1-Thio-ATP was tested with 0 µM, 500 µM, 1000 µM, 1500 µM, 2000 µM, 2500 µM $MnCl_2$, band shift was not seen on a formaldehyde denaturing gel (**Fig. 4-19A**). When 1-Thio-ATP and 2'-Fluoro-2'dATP were tested at 100 µM

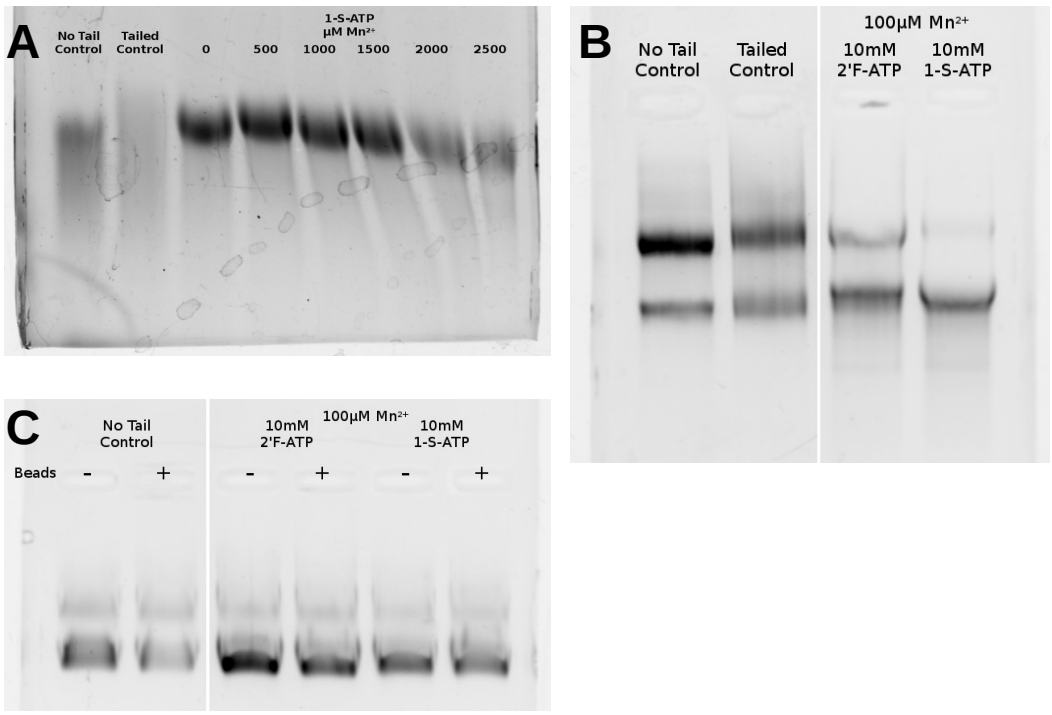

Figure 4-19: *Effect of Manganese on Tailing Reaction.* **A:** Formadehyde denaturing gel of mRNA tailed with 1-Thio-ATP with 0 – 2500 μM Mn^{2+}, no band shift. **B:** mRNA tailed with 10 mM 2'-Fluoro-2'-dATP in 100 μM Mn^{2+}, no band shift. **C:** Oligo(dT) bead binding assay of mRNA tailed with 10 mM 2'-Fluoro-2'-dATP or 1-Thio-ATP in 100 μM Mn^{2+}, no band loss.

$MnCl_2$, no band shift or band loss was seen on gel (**Fig. 4-19B,C**).

ATP, 1-Thio-ATP, and 2'-Fluoro-2'-dATP tailing was tested with the addition of 1 mM spermidine. ATP tailed mRNA showed band shift similar to no spermidine control (**Fig. 4-20A**), 1-Thio-ATP and 2'-Fluoro-2'-ATP showed no band shift (**Fig. 4-20B**).

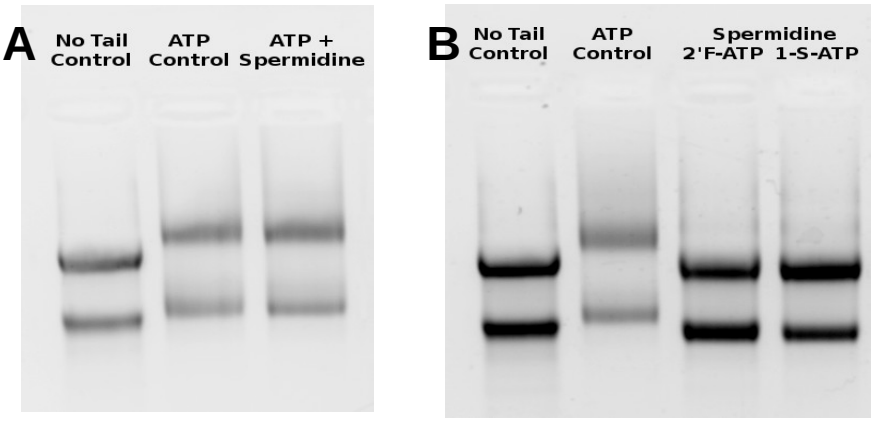

Figure 4-20: *Effect of Spermidine on Tailing Reaction.* **A:** Spermidine does not show any affect on mRNA tailing with ATP. **B:** Tailing with 2'-Fluoro-2'-dATP or 1-Thio-ATP and 1 mM spermidine does not produce a band shift.

Admixtures of ATP and either 1-Thio-ATP or 2'-Fluoro-2'-dATP were tested because the successful initial tailing attempt may have had leftover ATP from the in vitro transcription step. This leftover ATP may have helped the ATP analogs become incorporated into the polyA tail. Admixtures at 10:1 and 1:1 ratios of ATP analog:ATP were tested, with total concentration held constant at 1 mM. The 10:1 ratios with 1-Thio-ATP and 2'-Fluoro-2'-dATP showed no visible band shift (**Fig. 4-21A**). The 1:1 ratios showed band shift (**Fig. 4-21B**). Both nucleotides at 1:1 and 2'-Fluoro-2'-dATP at 10:1 ratios showed band loss on oligo(dT) bead binding assay (**Fig. 4-21C**). These mRNAs were capped and tested in hydrodynamic dosing experiments. All but the 1-Thio-ATP 10:1 ratio showed luciferase expression with direct hydrodynamic injection(**Fig. 4-21D**), however none showed activity after hydrodynamic stimulation with 5 min delay .

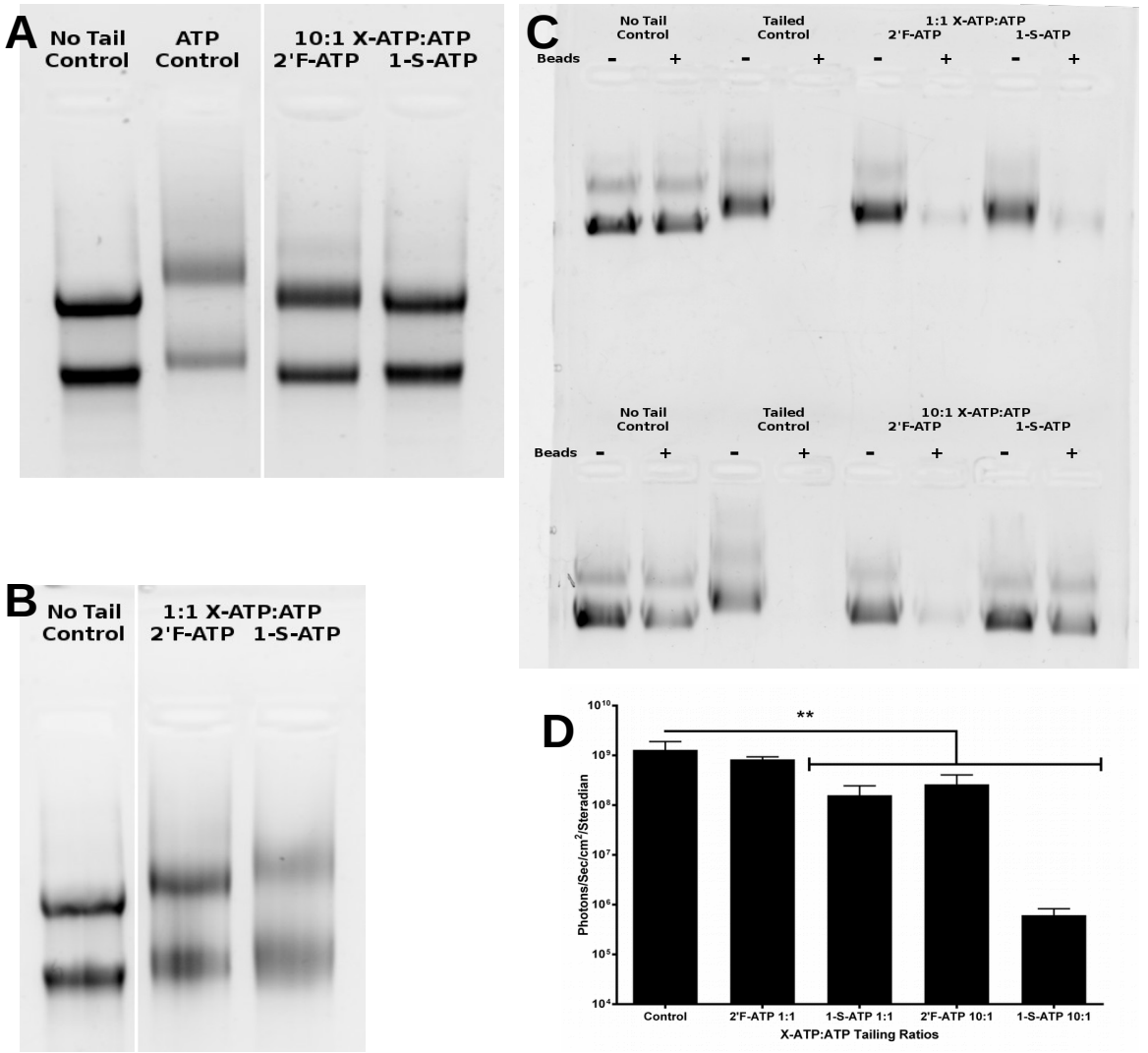

Figure 4-21: *Tailing mRNA with Mixtures of ATP and ATP Analogs.* **A:** mRNA tailed with 10:1 ratios of 2'-Fluoro-2'-dATP or 1-Thio-ATP to ATP does not show visible band shift. **B:** mRNA tailed with 1:1 ratios of 2'-Fluoro-2'-dATP or 1-Thio-ATP does show a band shift. **C:** All tailed mRNA except 10:1 1-Thio-ATP:ATP show band loss on oligo(dT) bead binding assay. **D:** All tailed mRNAs except 10:1 1-Thio-ATP:ATP show luminescence, but signal is less than mRNA polyplex control, ** = $p < 0.01$.

Yeast polyadenosine polymerase was tested to see if an equivalent enzyme from a different species would have a more favorable substrate specificity. mRNA tailed with ATP, 1-Thio-ATP, or 2'-Fluoro-2'-dATP showed no band shift or band loss (**Fig. 4-22**).

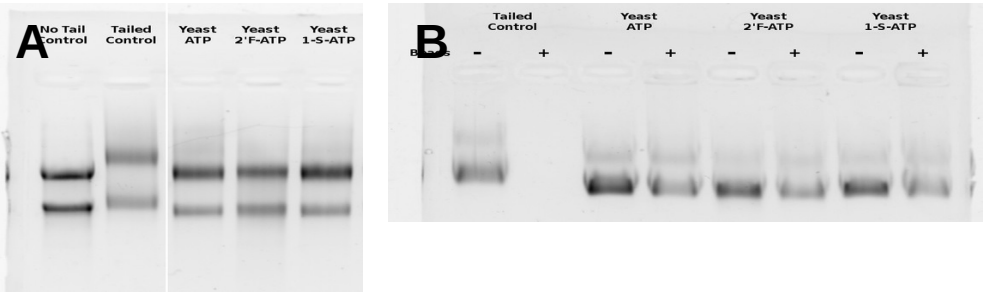

Figure 4-22: *mRNA Tailing with Yeast Polyadenosine Polymerase.* Yeast PAP fails to produce band shift in A, or band loss in B with any ATP substrate.

4.5 Discussion

Thiazole orange displacement (**Fig. 4-2**) and Gel electrophoresis band shift assays (**Fig. 4-3**) demonstrated that $(Acr\text{-}Lys_4)_3$-Acr-Lys-Cys-PEG_{5kDa} and PEG_{5kDa}-Cys-Trp-Lys_{20} would bind to in vitro transcribed mRNA. These peptides have been previously shown to bind to DNA, and that the polyacridinylated peptide could protect DNA in the bloodstream of mice for up to 12 hr[308]. However, plasmid DNA has different structural properties than mRNA. Most obviously, plasmid DNA is circular, and entirely double stranded, allowing for efficient intercalation of acridines at any position. mRNA is linear and single stranded, however, mRNA can adopt very complex secondary structures with significant amounts of RNA forming double helices (**Fig. 4-1**). Furthermore, DNA double helices typically form a B helix, whereas RNA double helices prefer the A helix[309]. These differences in amount of double strandedness and shape of helix could affect how well polyacridine peptides bind.

Dynamic light scattering particle size and zeta potential measurements show that mRNA polyplexes formed with PEGylated polyacridine peptide form particles with mean diameter of

104 nm and zeta potential of +15 mV. The 104 nm diameter is smaller than the 170 nm diameter measured for pGL3 plasmid DNA with the same peptide[308], but zeta potential is the same for both. The RNA polyplexes should be small enough to pass through the fenestrae of mouse liver sinusoids, which have an average diameter of 140 nm. Human liver sinusoids have fenestrae with smaller average diameter, approximately 100 nm[7], however the fenestrae diameter in all species follows a distribution, so some human fenestrae would be large enough for a 104 nm particle to pass through.

PEGylated polyacridine DNA polyplexes have been demonstrated to bind to serum albumin, and that this binding changes the zeta potential from positive to slightly negative[308]. Negatively charged particles are candidates for scavenger receptor uptake on liver sinusoidal endothelial cells and Kupffer cells. This charge reversal can turn DNA polyplexes into scavenger receptor ligands resulting in rapid clearance from the bloodstream. Though this was not studied, RNA polyplexes would likely have similar behavior.

To determine if the PEGylated peptides could protect mRNA against RNase, RNA peptide polyplexes were subjected to RNase A incubations at increasing concentrations of RNase, and analyzed by gel electrophoresis (**Fig. 4-4**). Both peptides could protect RNA at 30 ng/mL of RNase A, but degradation began at some point between 30 and 100 ng/mL. The acridinylated $(Acr\text{-}Lys_4)_3$-Acr-Lys-Cys-PEG_{5kDa} peptide may show less degradation at 100ng/mL than the non-acridinylated peptide. This would be consistent with the acridine moieties producing higher affinity and better protection.

Hydrodynamic tail vein injection of mRNA was able to produce high levels of luciferase expression, comparable to the hydrodynamic delivery of pGL3 plasmid DNA (**Fig. 4-5**). When

mRNA was injected without peptide, bioluminescence was lower than that for plasmid DNA at 24 hr post injection. This is not unexpected, as each DNA plasmid can produce several copies of mRNA that can each produce several copies of protein. However, DNA must enter the nucleus to transcribe RNA, whereas mRNA only needs to reach the cytoplasm. Most likely, during hydrodynamic injection, a higher proportion of the mRNA dose reaches the cytoplasm than DNA dose reaches the nuclei. Dosing capped mRNA without 3' PolyA tail produces a small amount of bioluminescence. The 5' cap may be sufficient to recruit ribosomes and translate some luciferase, however untailed mRNA has a short half life[310]. Alternatively, hydrodynamic injection may force some mRNA into the nucleus, where it may recruit PolyA tailing enzymes and become tailed.

Importantly, Luc-UTR mRNA was able to produce much stronger bioluminescence at lower doses and for longer times than the initial attempt at luciferase mRNA. This is most likely due to improvements made during the synthesis of the Luc-UTR gene, including codon optimization and addition of untranslated regions. These changes would increase the rate of protein translation and mRNA cytoplasmic half-life, resulting in greater amounts of protein. The original luciferase mRNA was able to produce bioluminescence comparable to the first reported hydrodynamic injection of mRNA in McCaffrey et al[175].

When mRNA was bound to a PEGylated peptide without acridines, PEG_{5kDa}-Cys-Trp-Lys_{20}, bioluminescence was not significantly different from mRNA without peptide. mRNA bound to a polyacridine peptide gave significantly more bioluminescence than mRNA without peptide (**Fig. 4-6**). Since polyacridine peptides can bind mRNA through a combination of electrostatic and intercalative interactions, it should bind mRNA with higher affinity than a nonacridine peptide, which relies on electrostatic interactions alone. In the bloodstream or

cytoplasm of an animal, nonacridine peptides may be stripped off the RNA and bind to cell membranes, proteins, and other molecules. This could expose the RNA to nucleases, resulting in degradation and loss of bioluminescence.

To examine the RNase protection more closely, RNA polyplex was incubated in mouse serum for 30 min, then hydrodynamically injected into mice (**Fig. 4-7**). mRNA polyplex with polyacridine peptide was transfection competent after 30 min of serum incubation, demonstrating that $(Acr\text{-}Lys_4)_3$-Acr-Lys-Cys-PEG_{5kDa} could protect mRNA in serum. However, mRNA with either no peptide or the nonacridine PEG_{5kDa}-Cys-Trp-Lys_{20} peptide was not transfection competent. The additional binding affinity provided by the acridines is most likely responsible for the greater protection in serum.

The expression time course reveals that protein expression begins very quickly, with maximum bioluminescent signal appearing as soon as 4 hr post injection (**Fig. 4-8**). Signal remained high for 24 hr and gradually fell from 24 hr to 84 hr. Bioluminescence remained above background for 72 hr. This duration is comparable to expression from pGL3 plasmid DNA.

To test if PEGylated Polyacridine Peptide could protect mRNA in the bloodstream like it can protect plasmid DNA, delayed hydrodynamic stimulation was performed with mRNA polyplex at a 5 min delay. However, no bioluminescence was detected. The discrepancy between the serum incubation and delayed stimulation experiments might be related to incubation conditions. Serum incubation was done in total volume of 20 μL at room temperature. In this low volume, simplified model, peptide could bind at equilibrium, and any peptide that dissociates from the mRNA could rebind. However, in the bloodstream, any peptide that dissociates is likely to find something else to bind to and will not rebind to the mRNA. Additionally, the 3'

polyadenosine tail is a large section of single stranded mRNA that does not form double helices because there is no sufficiently long polyuridine tract to bind to. This means that polyacridine peptides will not bind to the polyadenosine tail with much affinity. In the bloodstream, the peptide might rapidly dissociate, exposing the tail to degradation. Once the 3' tail is removed, the mRNA cannot be used for translation. Therefore, two strategies were selected for protecting the 3' PolyA tail against degradation.

The first strategy used polythymine DNA oligos, Oligo(dT), or polyuridine RNA oligos, Oligo(rU) to bind to the PolyA tail, forming double stranded DNA:RNA or RNA:RNA helices. These helices should have higher affinity for polyacridine peptide and could be better protected. However, binding mRNA with Oligo(dT) at either 16 or 32 bases long caused the bioluminesence after hydrodynamic dosing to decrease by two orders of magnitude (**Fig. 4-9**). Binding mRNA to Oligo(rU) at 32 bases did not affect bioluminescence after direct hydrodynamic dosing, but was not able to protect the RNA in the bloodstream for 5 min either. Oligo(rU) was shown to bind to tailed mRNA by inhibition of Oligo(dT) cellulose bead binding and thermal melt curve analysis, while not binding to untailed mRNA. The amount of Oligo(rU) needed to full bind tailed mRNA closely matched between both assays.

The loss of bioluminescent signal after Oligo(dT) binding is interesting, and may be caused by RNAse H activity. RNAse H is a ribonuclease that recognizes RNA:DNA double helices and hydrolyzes the RNA strand. This enzyme is normally involved in DNA replication, where it removes the RNA primers from the lagging strand of the replication fork[311–313]. In this case, RNAse H may be degrading the PolyA tail and leaving the mRNA unable to translate protein.

Because oligo(rU) was so short, only 32 bases with a predicted melt point of about 42 °C, longer RNA polymers were chosen for testing. Poly(rU) and Poly(rA) are heterogenous polymers produced by Polynucleotide Phosphorylase[314,315]. The Poly(rU)·Poly(rA) duplex has been shown to be more resistant toward RNase than single stranded RNAs[316–318]. Additionally, with its greater double strandedness, it was hypothesized that the duplex could bind the polyacridine peptide with higher affinity than mRNA. Poly(rU)·Poly(rA) was shown to have greater fluorescence with thiazole orange than tailed or untailed mRNA, which demonstrates the greater double strandedness. Additionally, the melting points of Poly(rU)·Poly(rA) or Poly(rU) tailed mRNA complexes were approximately 65 °C (**Fig. 4-10**), higher than the melting point for tailed mRNA with Oligo(rU), 48 °C, or for mRNA alone, which shows no clear melting point (**Fig. 4-9**). mRNA by itself may not show a clear melting point due to its complex secondary structures, which would melt at different temperatures.

When a sample of RNA was melted more than once, the later melt curves often showed greater fluorescent intensity than the first melt curve (**Fig. 4-10**), suggesting that heating the RNA to denature it and allowing it to cool slowly could produce a more stable secondary structure with greater affinity for thiazole orange. This effect was greater when 50 μg Poly(rU)·Poly(rA) was cooled from 85 °C to 25 °C, where fluorescence at 25 °C was twice as high than when the same RNA was heated from 25 °C to 85 °C.

When 1.0 μg of tailed mRNA was combined with 0.00 – 1.00 μg Poly(rU) or Poly(rU)·Poly(rA) duplex and electrophoresed, both gels showed smears at higher amounts of RNA (**Fig. 4-11**). The poly(rU) gel shows some loss of mRNA band intensity and slight band shift as Poly(rU) amount increases, with smearing visible at 0.25 μg or more of Poly(rU). The

Poly(rU)·Poly(rA) duplex gel shows even greater loss of mRNA band intensity and smearing at as low as 0.05 μg of duplex RNA. At 0.50 μg or more of duplex, mRNA bands were not visible at all and only a smear with very intense lower region could be seen. Because the Poly(rU) and Poly(rA) polymers are heterogenous, smearing is expected. The mRNA bands might lose intensity as the mRNA binds to Poly(rU) polymers of different sizes and becomes spread out.

Tailed and untailed mRNA at 1.0 μg was mixed with Poly(rU) by itself or a hand made mixture of Poly(rU) and Poly(rA) or premade Poly(rU)·Poly(rA) duplex and analyzed by gel electrophoresis (**Fig. 4-11**). Because untailed mRNA with Poly(rU) looks like untailed mRNA alone, untailed mRNA was probably not binding to Poly(rU). When either mixture of Poly(rU)·Poly(rA) was used, dark smears were visible with either tailed or untailed mRNA. None of these lanes had any visible mRNA bands, but lanes with tailed mRNA had taller smears than lanes with untailed mRNA.

Agarose gel electrophoresis was not producing clear results with heterogenous RNA polymers, therefore thermal melt curve analysis was used to study binding of mRNA and Poly(rU) (**Fig. 4-12**). When tailed mRNA was combined with Poly(rU), fluorescent intensity increased approximately three fold, while untailed mRNA showed no change in fluorescence when combined with Poly(rU). The tailed mRNA Poly(rU) mixture had a melting point of approximately 65 °C, similar to the Poly(rU)·Poly(rA) duplex melt curves. Tailed and untailed mRNA combined with Poly(rA) did not show much change in fluorescence intensity, implying lack of interaction between mRNA and Poly(rA). Poly(rA) alone showed some fluorescence at 25 °C that quickly disappeared as temperature increased, suggesting that the Poly(rA) is adopting some structure that binds thiazole orange. Previous studies have shown the formation of a

parallel double helix formed by two molecules of Poly(rA) under certain buffer condtions[319–321], but these conditions were not used in this current study. When Poly(rU) and Poly(rA) were mixed and melted, the melting point was 65 °C, similar to the commercially available premade duplex. Because fluorescence of Poly(rU) with either tailed mRNA or Poly(rA) was high at 25 °C before RNA was melted, the RNA was most likely able to base pair without heating under these buffer conditions. However, since fluorescence increased after the first melt, heating is probably necessary to get more complete base pairing.

When tailed or untailed mRNA was combined with 0 – 10 μg of Poly(rU), fluorescence appeared to reach maximum with tailed mRNA at as low as 0.5 μg of Poly(rU) (**Fig. 4-13**). Untailed mRNA did not show any major change in fluorescence at any amount of Poly(rU), again demonstrating that untailed mRNA does not interact with Poly(rU).

Poly(rU), Poly(rU) with Poly(rA), or Poly(rU)·Poly(rA) duplex at 1 μg was mixed with $(Acr\text{-}Lys_4)_3$-Acr-Lys-Cys-PEG_{5kDa} and analyzed by gel electrophoresis (**Fig. 4-14**). This showed that Poly(rU) or Poly(rU)·Poly(rA) duplexes were capable of binding the polyacridine peptide, and that this binding inhibited migration through the gel. Partial inhibition was achieved at 0.01 nmol of peptide with total inhibition at 0.05 nmol of peptide and above. mRNA did not show total migration inhibition until 0.10 nmol of peptide, suggesting that Poly(rU)·Poly(rA) duplex had higher affinity for polyacridine peptide than mRNA, consistent with its greater double strandedness. Particle size and zeta potential measurements showed that Poly(rU)·Poly(rA) duplex could form peptide polyplexes with $(Acr\text{-}Lys_4)_3$-Acr-Lys-Cys-PEG_{5kDa} with diameter of approximately 114 nm and zeta potential of +7 mV, similar to particles obtained with mRNA.

In an attempt to protect mRNA in vivo, 1.0 μg doses of tailed Luc-UTR mRNA was prepared with 1.0 μg Poly(rU) or 2.0 μg of Poly(rU)·Poly(rA) duplex and $(Acr\text{-}Lys_4)_3$-Acr-Lys-Cys-PEG_{5kDa} and hydrodynamically delivered to mice (**Fig. 4-15**). It was hypothesized that the duplexed RNA would form polyplexes that trapped mRNA and had higher affinity for polyacridine peptide. While direct hydrodynamic injection produced bioluminescence equal to mRNA polyplex control, delayed hydrodynamic stimulation at 5 min produced no detectable signal. In an attempt to inhibit scavenger receptor uptake and improve polyplex circulation time[308], 1.0 μg of Luc-UTR mRNA was mixed with 50 μg of Poly(rU)·Poly(rA) duplex and delivered by hydrodynamic injection. Unfortunately, only one of the eight mice dosed with this formulation survived to 24 hr post-injection. The surviving mouse only received a partial hydrodynamic dose, and only received about 40 μg of Poly(rU)·Poly(rA). This animal produced $5x10^6$ photons/sec/cm^2/steradian in the liver, much less than mRNA polyplex control. It is not known if this reduced signal is due to toxicity from Poly(rU)·Poly(rA) or lower pressures because it did not receive the entire hydrodynamic dose. This mouse also showed significant luminescence in its tail, not usually seen with hydrodynamic dosing of mRNA.

While Poly(rU)·Poly(rA) is known to have immunogenic properties[322–324], acute toxicity was not expected. A 50 μg dose of Poly(rU)·Poly(rA) in a 27 g mouse is approximately 1.8 mg/kg, close to doses used in human clinical trials with no adverse affects[325–327]. One potential source of toxicity may be activation of 2'-5'-oligoadenylate synthetase and RNase L[295,328,329], which cleaves single stranded RNA, including some sites on ribosomes, during viral infections. This prevents translation of viral proteins, but can kill cells if kept active for too long.

The second strategy for tail protection was based on synthesizing the PolyA tail from ATP analogs designed to confer nuclease resistance. ATP analogs 1-Thio-ATP and 2'-Fluoro-2'-dATP were chosen because phosphorothioate and 2'-Fluoro modifications are used to create stabilized RNA for siRNA and RNA aptamer applications[306,307]. However, those RNA sequences are much shorter than a messenger RNA, and are usually chemically synthesized, allowing for easy addition of the nucleotide analogs. Even aptamers that are too long for chemical synthesis can be produced through in vitro transcription with a mutant T7 RNA polymerase that incorporates nucleotide analogs with modifications at the 2' position[307].

An early attempt at tailing mRNA with these ATP analogs was able to produce mRNA that not only produced good expression with direct hydrodynamic dosing, but could also produce bioluminescence after 5, 30, and 60 min delays between small volume mRNA dose and hydrodynamic stimulatory injection. However, attempts to replicate this result were difficult. Polyadenosine polymerase is specific for ATP, when made to accept other nucleotides, tails are usually very short, often just a single nucleotide long[330–333]. Though 1-Thio-ATP and 2'-Fluoro-2'-dATP are more similar to ATP, they are expected to be less efficient substrates.

To encourage tailing, reactions were carried out under several different conditions. ATP and 2'-Fluoro-2'-dATP were used in reactions incubated at 37 °C for 1, 2, 3, 4, or 5 hr (**Fig. 4-16**). ATP was able to produce polyA tails that bound oligo(dT) cellulose beads at all time points, but 2'-Fluoro-2'-dATP was not able to produce detectable PolyA tails. When these mRNAs were capped and delivered to mice by hydrodynamic dosing, the mRNA tailed with ATP for longer reaction times showed loss of expression, and 2'-Fluoro-2'-dATP showed no expression, because there was no significant tailing. The loss of expression after longer reaction times was

interesting, but it is not clear whether the RNA was being slowly degraded or if tail length was too long.

The effect of a temperature ramp on 3' tailing was tested for ATP, 1-Thio-ATP, and 2'-Fluoro-2'-dATP (**Fig. 4-17**). Increasing the temperature from 37 °C to 60 °C over 1 hr or the use of spermidine were reported to improve 3' end labeling using ATP analogs and yeast polyadenosine polymerase in previous literature[334], but did not improve tailing in this study (**Fig. 4-20 and 4-22**). The temperature ramp not only did not improve tailing with ATP analogs, but did not produce detectable tails with ATP, the increased temperature most likely denatured the polyadenosine polymerase before significant tailing had time to occur.

Increasing the substrate concentration ten fold also failed to produce detectable tails with 1-Thio-ATP and 2'-Fluoro-2'-dATP (**Fig. 4-18**). When ATP was increased, mRNA was still tailed, but tails did not appear longer than when tailing was performed using the standard concentration of substrate. Previous reports suggested that substrate inhibition of polyadenosine polymerase was possible under certain circumstances[335], so 1-Thio-ATP and 2'-Fluoro-2'-dATP were used in reactions at half the standard substrate concentration, but no detectable tailing was produced.

Manganese is often added to polyadenosine polymerase reactions because it has been shown to improve the activity of the enzyme, however, at high enough concentration manganese has also been shown to inhibit tailing[332–335]. The Ambion PolyA tailing kit used in this study suggests adding $MnCl_2$ so that the reaction mixture contains 2.5 mM Mn^{2+}, however literature suggests that Mn^{2+} as low as 100 μM may be too high[335]. Because of this, most tailing reactions were carried out without the manganese, but to test if manganese could promote reaction with ATP analogs, reactions were performed with different concentrations of Mn^{2+}. However, no

detectable tailing was seen with either analog (**Fig. 4-19**).

Admixtures of ATP and ATP analogs were tested to determine if tails could be produced with some mixture of the two nucleotides (**Fig. 4-21**). Incomplete purification may have allowed some ATP to be carried over from the in vitro transcription step to the tailing step, creating an inadvertent admixture. 1:1 and 10:1 ratios of 1-Thio-ATP or 2'-Fluoro-2'-dATP to ATP were tested. The 1:1 ratios showed clear band shift compared to nontailed RNA, and the 10:1 ratios showed very small band shift. Oligo(dT) bead binding showed that all but 10:1 1-Thio-ATP sample bound to the beads. Direct hydrodynamic dosing showed that all but 10:1 1-Thio-ATP sample could produce luciferase, demonstrating that tailing was necessary for expression. None of the samples showed bioluminescence after hydrodynamic stimulation with 5 min delay, indicating that the mRNA was not stable in the bloodstream.

One explanation for why the original results could not be replicated may be the template DNA. During the in vitro transcription step for the successful batch of RNA, the DNAse digestion step was accidentally skipped. Since the linear DNA template contained a powerful CMV promoter upstream of the luciferase gene, even a small amount of DNA could have caused significant luciferase expression.

This study has demonstrated that in vitro transcribed mRNA with natural nucleotides can produce protein levels in vivo that are competitive with plasmid DNA when delivered through hydrodynamic injection. PEGylated polyacridine peptides used to protect DNA in vivo were shown to protect mRNA from RNase activity in vitro, and could enhance luciferase expression by approximately 15 fold, and kept signal above background for 72 hr. These findings show that mRNA has the potential to replace DNA in some gene delivery applications. mRNA delivery

may be further enhanced through the use of modified nucleotides such as pseudouridine and/or 5-methylcytidine, which have been shown to improve protein expression and reduce immune response[294–298]. mRNA stability may be improved with different peptides with higher affinity for mRNA. While hydrodynamic injection may not be applicable to human healthcare, it remains a useful research tool. With the improvements to mRNA hydrodynamic delivery demonstrated in this study, in vivo mRNA transfection may become useful for expression of genome editing nucleases or transposases in conjunction with plasmid DNA.

5 Phospholipase A2 and Nuclear Entry

In collaboration with Jianfeng Jin

5.1 Abstract

Nonviral DNA delivery requires the DNA to enter the nucleus of cells before it can be transcribed and translated to treat disease. However, nuclear entry remains a significant barrier to efficient DNA delivery. Several viruses have been found with phospholipase A2 activity in their capsid proteins, and if this activity is removed, they are no longer able to efficiently infect cells. It was hypothesized that phospholipase A2 activity may play a role in delivering the viral DNA into the nucleus. This study chemically modified bee venom phospholipase A2 in an attempt to prepare it for nonviral DNA delivery. The enzyme was labeled with DNA binding polyacridine peptides, nuclear localizing peptides, biotin, and hepatocyte targeting oligosaccharides. However, chemical modification often damaged enzyme activity and phospholipase often harmed gene transfection rather than improve it. Phospholipase mutants with free thiols were also produced in bacterial expression systems and attempts were made to chemically modify them. However, these mutant proteins were not easily modified, most likely due to addition of glutathione or other reducing agents to their free thiols.

5.2 Introduction

Gene therapy, viral or nonviral, requires that the DNA cargo be carried across cellular membranes such as the plasma membrane, endosomal membrane, or nuclear envelope. Viruses

have developed methods to cross these membranes through billions of years of evolution. Nonviral systems are still challenged by these membranes. Endosomal escape and nuclear entry are important barriers to efficient nonviral gene delivery systems[73,100,336,337]. Escaping the endosome has been addressed by using fusogenic peptides such melittin[191,197], or by exploiting the proton sponge effect using cationic polymers such as PEI[101].

Crossing the nuclear envelope is still challenging. In rapidly dividing cells, the nuclear envelope is disassembled and rebuilt every time the cell divides, creating an opportunity for DNA polyplexes in the cytoplasm to enter the nucleus. However, non-dividing quiescent cells do not divide often enough to take advantage of this. The nuclear envelope is a double layered membrane contiguous with the endoplasmic reticulum. It is perforated with many nuclear pore complexes which allow small molecules to pass through by diffusion and large molecules, such as proteins and RNAs, to pass through by active transport[147,148].

Nuclear pore complexes can dilate to allow larger particles through, but only to about 39nm[50], not large enough for most nonviral DNA delivery particles to pass through. This diameter is not large enough for most viruses to pass through either. Viruses have mechanisms for delivering their DNA into the nucleus, and it may be possible to borrow these mechanisms for nonviral nuclear entry.

One possible mechanism may be phospholipase A2, PLA2 (EC 3.1.1.4), activity found in the VP1 coat protein of parvoviruses[338–341]. The coat protein contains a PLA2 domain that is normally inactive, but when the virus enters the endosome, the domain is activated as the endosome becomes acidified. The PLA2 domain is pushed through to the surface of the capsid, where it can access the endosomal membrane and hydrolyze phospholipids. This destabilizes the

membrane, tearing the endosome open and allowing the virus to escape into the cytoplasm. If this PLA2 activity is lost due to mutation, the virus is far less efficient at infecting cells. It was hypothesized that this PLA2 activity may also be involved in nuclear entry, and that PLA2 activity could be incorporated into a nonviral DNA delivery system to assist with nuclear entry (**Fig. 5-1A**).

The phospholipases A2 are a broad class of enzymes found in almost all organisms[342–344]. They hydrolyze phospholipid esters at the 2-acyl position and produce a fatty acid and lysophospholipid[345] (**Fig. 5-1B**). PLA2 is involved in several cellular signaling pathways, such as inflammation[346] and apoptosis[347]. PLA2 is also found in the venom of many venomous animals such as bees[348–350], wasps[351], spiders[352,353], scorpions[354], centipedes[355], snakes[356], gila monsters[357], cuttlefish[358], sea anemones[359], cone snails[360], and others, creating an interesting example of convergent evolution[361]. These PLA2s often have neurotoxic and hemorrhagic activity, although some venom PLA2s are toxic while having no catalytic activity, acting as ligands for receptors on neurons[362–364]. Several enzyme activity assays have been developed for phospholipase A2[365–372], ranging from simple spectrophotometric assays to FRET and radiation based assays.

Bee venom PLA2 is a well characterized protein and member of the Group III PLA2 family[364,373–376]. The enzyme is produced as a 167 amino acid 19kDa protein. The first 18 amino acids are a pre-peptide involved in properly secreting the protein during synthesis. The next 15 amino acids are a pro-peptide that keeps the enzyme inactive until it is cleaved by a protease. The mature protein is 134 amino acids long and 15.2kDa. The mature protein has 12 lysines and 10 cysteines, which form 5 disulfide bonds, and the active site can be inactivated by mutating a histidine to glutamine. The enzyme is glycosylated, but the glycosylation is highly

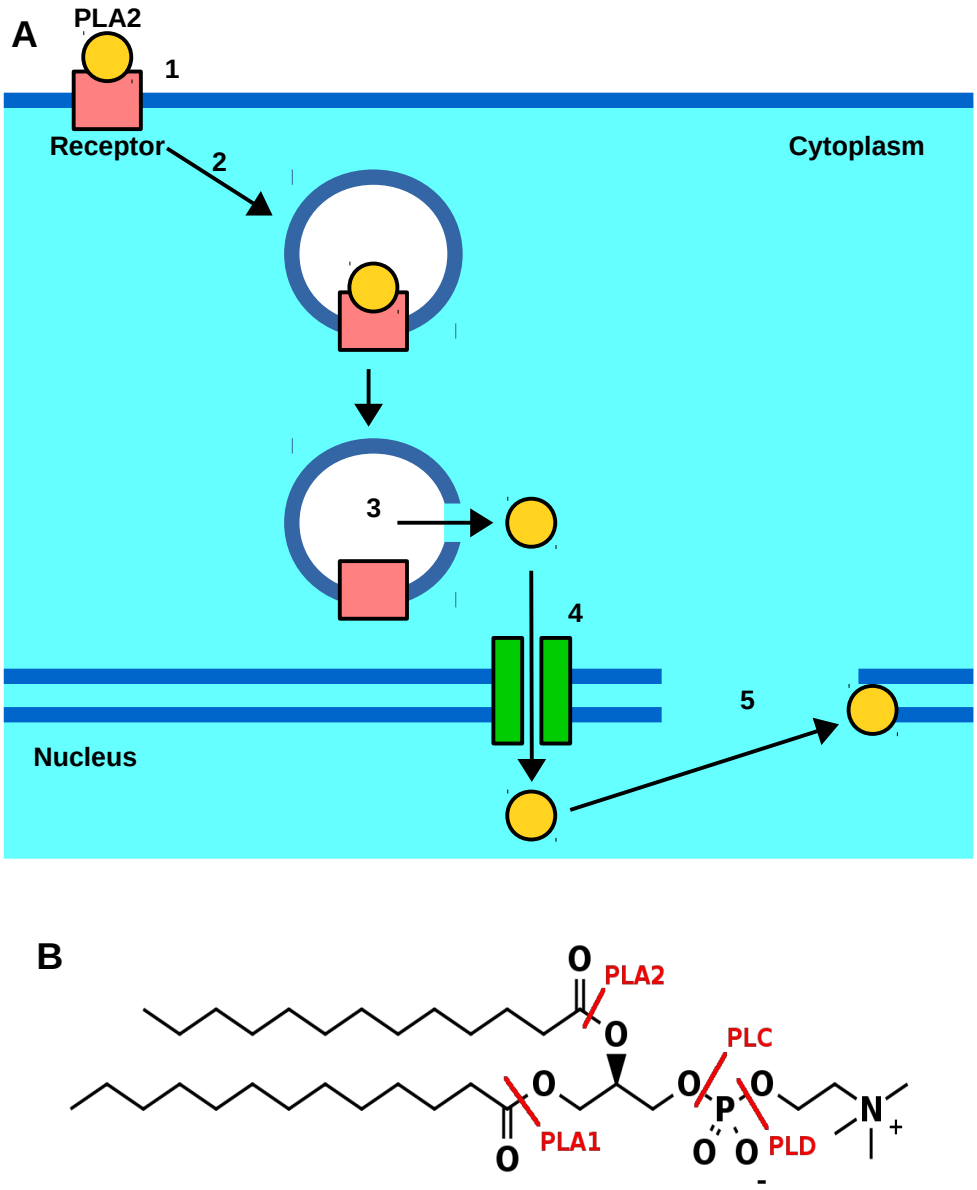

Figure 5-1: *PLA2 for Nuclear Entry.* PLA2 is hypothesized to help DNA polyplexes enter the nucleus in A. First a modified PLA2 binds to a target receptor, 1, and is internalized through endocytosis, 2. Then the PLA2 disrupts the endosomal membrane and escapes into the cytoplasm, 3. Once in the cytoplasm, PLA2 enters the nucleus, 4, where it attacks the nuclear envelope, creating holes for DNA polyplexes to pass through, 5. In panel B, a model phosphatidylcholine is shown with the sites were the different phospholipase enzymes hydrolyze the molecule.

heterogeneous. PLA2 acts synergistically with another bee venom component, the fusogenic peptide melittin, to lyse membranes[377]. The enzyme is also a common allergen in bee sting allergy[378]. The mature enzyme is also commercially available from honeybee venom gland extracts.

Some venom phospholipases, such as bee venom PLA2, have also been expressed in recombinant expression systems such as bacteria and insect cells[379–383]. In bacteria, the PLA2 proteins are typically packaged in inclusion bodies and must be unfolded and refolded. This makes production more complicated and reduces yield. Expression in insect cells was able to produce properly folded, mature, active enzymes with glycosylation. Several mammalian phospholipase enzymes have also been produced in recombinant expression systems[363,384–392].

Bee venom PLA2 has been utilized in some nonviral DNA delivery studies. One study attached PLA2 to an atomic force microscopy probe and touched the enzyme to the surface of cells. The enzyme was able to create holes in the cellular membrane up to 10 μm across. Plasmid DNA was then delivered through these holes by AFM probe[393]. Another study covalently linked bee venom PLA2 to PEI and used it to transfect cells in vitro. PEI with PLA2 was less toxic than PEI without PLA2, and was able to produce higher levels of transgene expression at high N:P ratios[394]. PLA2 was delivered to cells in vitro with DNA in cationic cycloamylose nanogels, and showed higher transgene expression than nanogel and DNA alone[395].

This study attempted to modify bee venom PLA2 through bioconjugate chemistry techniques. Wild type commercially available enzyme was modified using reagents that reacted with primary amines, such as NHS esters and 2-Iminothiolane. Recombinant PLA2 was also made in an attempt to add free thiols in known locations, so that the enzyme could be site

specifically labeled with thiol reactive reagents[396,397].

5.3 Materials and Methods

5.3.1 PLA2 Activity Assays

Bee Venom Phospholipase A2 (Sigma Aldrich, St. Louis, MO, USA) was dissolved in phosphate buffered saline to obtain an enzyme concentration of 10 µg/µL.

PLA2 enzyme activity was measured according to a previously described colorimetric assay[366]. Briefly, 124 mg of bromothymol blue was dissolved in 100 mL of 2 mM HEPES, 10 mM $CaCl_2$, pH 7.5 and stored at 4 °C. Phosphatidylcholine (Sigma Aldrich, St. Louis, MO, USA) was dissolved at 160 mg/mL in methanol and stored at -20 °C. Immediately before performing the assays, 500 µL of phosphatidylcholine was added to 10 mL of bromothymol blue buffer and 10 µL Triton X-100 and vigorously mixed by vortexing. Buffer was adjusted to pH of 7.5 with 5 M NaOH and turned dark green. Buffer was sterile filtered with 0.2 µm syringe filter. The assay was performed by adding 500 µL of filtered dye buffer to a cuvette, then 1 µg of PLA2 was added to the buffer. The cuvette was covered with parafilm, quickly mixed by inversion, and placed in a Beckman DU640 UV-Visible spectrophotometer (Beckman Coulter, Brea, CA, USA). Absorption at 640 nm was measured every 10 sec for 180 sec. As PLA2 hydrolyzed phosphatidylcholine to lysophospholipid and fatty acids, the pH decreased and the buffer changed from green to yellow and absorbance at 640 nm was lost. Data were analyzed by comparing the initial velocity of the absorption plots to a PLA2 standard.

An alternative colorimetric assay was performed using the sPLA2 Assay Kit (Cayman Chemical Company, Ann Arbor, MI, USA). The provided assay buffer was diluted 10 fold to

obtain a concentration of 25 mM Tris-HCl, 10 mM $CaCl_2$, 100 mM KCl, 0.3 mM Triton X-100, pH 7.5. Dithionitrobenzoate, DTNB, was dissolved in 1 mL H_2O to obtain 10 mM DTNB, 400 mM Tris-HCl, pH 8.0 and kept on ice in the dark. Diheptanoyl Thio-phosphatidylcholine, diheptanoyl Thio-PC, was dissolved in 12 mL of assay buffer to obtain a final concentration of 1.66 mM. Bee venom PLA2 was provided at 100 µg/mL as a positive control, and diluted 100 fold with assay buffer. The assay was set up in 96 well plates, with 2 wells as non-enzymatic controls with 10 µL DTNB solution and 15 µL of assay buffer. Positive control wells were set up with 10 µL DTNB, 10 µL Bee Venom PLA2 standard, and 5 µL assay buffer. Sample wells were prepared with 10 µL DTNB, 10 µL of PLA2 sample, and 5 µL of assay buffer. Reactions were initiated by adding 200 µL of diheptanoyl Thio-PC substrate solution to each well as quickly as possible. The plate was mixed by shaking and absorbance at 405 nm was measured every 15 sec for 300 sec on a Biotek EL808 plate reading spectrophotometer (BioTek Instruments, Winooski, VT, USA). As PLA2 hydrolyzed the diheptanoyl Thio-PC substrate, the free thiols reacted with DTNB to produce 5-thio-2-nitrobenzoate, which is yellow, with $\varepsilon_{405} = 12.8\ mM^{-1}cm^{-1}$. PLA2 activity in µmol/min/mL was determined using the equation:

$$Activity = \frac{\Delta A_{405}/min}{10.0\,mM^{-1}} \times \frac{0.225\,mL}{0.01\,mL} \times Dilution$$

5.3.2 SDS-PAGE Gel Electrophoresis

SDS-PAGE gels were set up with 15% resolving gel made with 4.5 mL 40% 37.5:1 Acrylamide:Bis-Acrylamide (BioRad Laboratories, Hercules, CA, USA), 3 mL 1.5 mM Tris-HCl pH 8.8, 4.26 mL ddH_2O, 120 µL 10 $^{w}/_{v}$% Sodium Dodecyl Sulfate, 5 µL TEMED, and 120 µL 10 $^{w}/_{v}$% Ammonum Persulfate. A 4% stacking gel was made with 800 µL 40% 37.5:1

Acrylamide:Bis-Acrylamide, 2 mL 0.5 M Tris-HCl pH 6.8, 5 mL ddH_2O, 80 µL 10 $^{w}/_{v}$% SDS, 16 µL TEMED, 80 µL 10 $^{w}/_{v}$% Ammonium Persulfate. Gels were cast in BioRad mini PROTEAN glass plates (BioRad Laboratories, Hercules, CA, USA) at 1.5 mm thick.

Electrophoresis running buffer was prepared at 10X concentration with 30 g Tris base, 145 g glycine, and 10 g SDS in 1 L ddH_2O. Gel staining buffer was prepared with 1 g coomassie brilliant blue, 400 mL 95% ethanol, 100 mL glacial acetic acid, and brought to 1 L with ddH_2O. Destaining buffer was prepared with 400 mL 95% ethanol, 100 mL glacial acetic acid, and brought to 1 L with ddH_2O.

Protein sample loading buffer was prepared at 6X concentration with 6 mL glycerol, 3 mL 0.5 M Tris-HCl pH 6.8, 1 g SDS, 600 µL β-Mercaptoethanol, and 5 mg bromophenol blue and divided into 1 mL aliquots and stored at -20 °C. When protein samples had disfulfide bonds that needed to be preserved, protein sample loading buffer was prepared without β-Mercaptoethanol. Protein samples were prepared with 5 µg of protein and protein sample loading buffer with ddH_2O to bring loading buffer to 1X concentration in PCR tubes. Samples were denatured by heating to 95 °C for 5 min. Samples were loaded into the gel and electrophoresed at 200 V, until the dye front reached the seal near the bottom of the glass plates. Gels were stained and destained and imaged using a UVP Biospectrum gel imaging system (UVP, Upland, CA, USA).

5.3.3 Agarose Gel Electrophoresis

DNA complexes were analyzed by agarose gel electrophoresis by pouring a 0.8% agarose gel with TBE buffer and ethidium bromide. DNA complexes were prepared at 1 µg amounts and

mixed with 5X DNA loading buffer. Samples were loaded into the gel and electrophoresed at 100 V for 45 min. Gels were imaged on the UVP Biospectrum imaging system.

5.3.4 LC-MS Analysis

LC-MS analysis of compounds was performed using 1 nmol of compound in 100 µL ddH_2O on a Vydac C18 analytical 0.47x25 cm column at 0.7 mL/min with 0.1 $^{v}/_{v}$% TFA with an acetonitrile gradient of 15-30 $^{v}/_{v}$% over 30 min, while acquiring electrospray ionization mass spectrometry in positive mode on an Agilent 1100 Series LC-MS system (Agilent Technology, Santa Clara, CA, USA).

5.3.5 BCA Assay

Protein concentrations in cell lysates were measured by BCA assay (Pierce Thermo Fisher Scientific, Rockford, IL, USA). A standard curve was obtained by diluting 2 µg/µL bovine serum albumin in a 2 fold serial dilution from 2 µg/µL – 16 ng/µL in 20 µL volumes with lysis buffer in triplicate in a 96 well plate, with a 0 µg/µL blank control. Cell lysate samples at 20 µL were added to other wells in the 96 well plate. BCA assay reagents A and B were mixed in a 50:1 ratio at a volume equal to 200 µL times the number of wells. The assay was performed by adding 160 µL of mixed BCA reagent to each well, incubating the plate at 37 °C for 20 min, then measuring absorption at 562 nm on the BioTek EL808 plate reading spectrophotometer. Luciferase activity was reported in terms of RLU per µg of protein.

5.3.6 Hydrodynamic Delivery

pGL3 plasmid DNA was prepared as either plasmid alone or in combination with peptides and/or proteins at a dose of 1 μg plasmid per mouse. DNA dose was diluted in normal saline at a volume equal to 0.09% of the animal's mass. DNA dose was delivered to mice by hydrodynamic tail vein injection in 5 sec.

At 24 Hr post injection, mice were anesthetized by 3% isolfluorane and intraperitoneally injected with 80 μL of 30 μg/μL D-Luciferin (Gold Biotechnology, St. Louis, MO, USA) in PBS. At 5 min after luciferin injection, mice were imaged for bioluminescence in an IVIS Imaging 200 Series (Xenogen, Hopkins, MA, USA). Bioluminescent imaging was performed in a light-tight chamber with temperature controlled stage, while mice were administered 3% isofluorane. Images were acquired with medium binning, at 24.6 cm field of view, and 10 sec exposure time. Bioluminescent imaging data is reported as photons/sec/cm^2/steradian in a 2.86 cm diameter region of interest placed over the liver.

Alternatively, DNA doses were prepared in HBM and delivered by tail vein injection in a volume of 100 μL. At some time after injection, mice were given an injection of normal saline of volume equal to 0.09% of the mouse's mass in 5 sec. Mice were imaged for bioluminescence as described above.

5.3.7 Synthesis of PLA2-Cys-(Acr-Lys)$_6$

N-(γ-Maleimidobutyrloxy)succinimide ester, GMBS, (Pierce Thermo Fisher Scientific, Rockford, IL, USA) was dissolved at 1 mg in 250 μL DMF. Bee venom PLA2 was derivatized by taking 20 μg of PLA2 from a 10 μg/μL stock solution, then 30 nmol GMBS was added to

create a 2 fold molar excess over lysines in PLA2, or 20 fold excess over PLA2 itself. Then, 50 mM $NaHCO_3$ at pH 8 was added to bring the volume to 20 µL in a 0.5 mL microcentrifuge vial. Reaction mixture was incubated at room temperature for 30 min. Reaction mixture was diluted with 480 µL 10 mM ammonium acetate pH 7.5 and transferred to 0.5 mL Amicon Ultra 10 kDa MWCO spin filters (EMD Millipore, Bellerica, MA, USA) and centrifuged at 14,000 RPM for 10 min. Concentrated sample was diluted with 480 µL 50 mM $NaHCO_3$ and spun again. Changing buffer to ammonium acetate helps to eliminate any residual GMBS and adjusts the pH for better compatibility with the pH indicator based PLA2 activity assay.

Concentrated sample was collected and transferred to a 0.5 mL microcentrifuge vial. $(Acr\text{-}Lys)_6$-Cys peptide[183] (**Fig. 5-2**) was added in 0 – 3 fold excess over PLA2 and incubated at room temperature for 30 min. Reaction mixture was spin filtered as above to remove excess peptide. PLA2-Cys-$(Acr\text{-}Lys)_6$ was analyzed by SDS-PAGE electrophoresis and PLA2 activity assays as above.

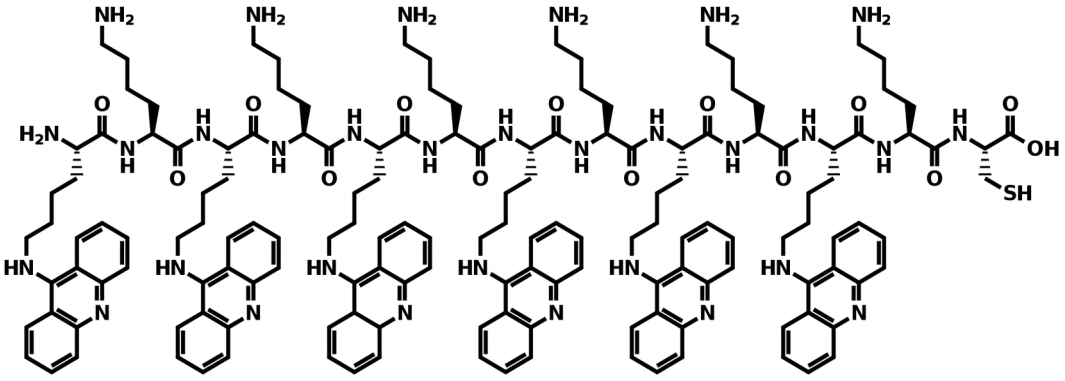

Figure 5-2: *$(Acr\text{-}Lys)_6$-Cys Peptide.* This peptide has 6 acridines for intercalating into DNA. It was developed prior to the $(Acr\text{-}Lys_4)_3$-Acr-Lys-Cys peptide and does not protect DNA in the bloodstream as effectively.

5.3.8 Synthesis of PLA2-Avidin-$(Acr\text{-}Lys)_6$ Complexes

PLA2 was biotinylated by mixing 20 µg PLA2 with with sulfosuccinimidyl-6-(biotinamido) hexanoate, NHS-Biotin, (Pierce Thermo Fisher, Rockford, IL, USA) at 10 fold excess over PLA2 in 50 mM $NaHCO_3$ in total volume of 20 µL. Reaction mixture was incubated at room temperature for 30 min and spin filtered as above to remove excess biotin and change buffer to ammonium acetate.

$(Acr\text{-}Lys)_6$-Cys peptide was biotinylated by mixing 5 nmol of peptide with Maleimide-PEG_2-Biotin (Pierce Thermo Fisher, Rockford, IL, USA) in 5 fold excess over peptide in 10 mM ammonium acetate in total volume of 20 µL. Reaction mixture was incubated at room temperature for 30 min.

PLA2-biotin and $(Acr\text{-}Lys)_6$-Cys-Biotin were complexed with Avidin through a templated synthesis on DNA. pGL3 plasmid DNA at 1 µg was mixed with 0.1 nmol $(Acr\text{-}Lys)_6$-Biotin in ddH_2O. Avidin (Pierce Thermo Fischer, Rockford, IL, USA) was added in 4 fold excess over $(Acr\text{-}Lys)_6$-Biotin to prevent aggregation. PLA2-biotin was added in 4 fold excess over Avidin. Complexes were analyzed by agarose gel electrophoresis.

5.3.9 Reaction of PLA2 with 2-Iminothiolane

PLA2 was reacted with 2-iminothiolane (Pierce Thermo Fisher, Rockford, IL, USA), also known as Traut's Reagent, to add thiol groups to the lysines on the enzyme. PLA2 at 20 µg was mixed with a 10 fold excess of 2-iminothiolane in 50 mM $NaHCO_3$ pH 8. Reaction was incubated at room temperature for 30 min and spin filtered as above to remove excess 2-iminothiolane. PLA2-Iminothiolane was analyzed by SDS-PAGE gel and PLA2 activity assay as

above.

5.3.10 Synthesis of NLS-Thiopyridine Peptide

The SV40 Nuclear Localizing Sequence, NLS, peptide[146] CPKKKRKVG was previously synthesized by solid phase peptide synthesis and provided by Nicholas Baumhover. The peptide was prepared for conjugation with PLA2-Iminothiolane by creating the thiopyridine derivative, NLS-TP. Dithiopdipyridine reaction buffer was prepared by mixing a 10:3 solution of 2 M acetic acid:isopropanol. Dithiodipyridine, DTDP, (Pierce Thermo Fisher, Rockford, IL, USA) was dissolved in methanol at approximately 40 nmol/μL. NLS peptide at 500 nmol was reacted with 10 fold excess of DTDP in total volume of 1300 μL DTDP reaction buffer at room temperature for 30 min. Reaction was quenched by diluting the mixture 2:1 with 0.1% TFA. Reaction mixture was split into 100 nmol portions and purified by semi-preparative scale HPLC with 0.1% TFA with an acetonitrile gradient of 0% – 20% over 40 min with flow rate of 5 mL/min. The major peaks were collected and pooled, volume was reduced to approximately 2 mL by rotary evaporation. Solution was frozen on dried ice and placed on the freeze drier overnight. Dried peptide was dissolved in 1.0% acetic acid to exchange the TFA counter ion with acetate. Solution was frozen and freeze dried again and peptide was dissolved in ddH_2O. NLS-TP was analyzed by LC-MS as above.

5.3.11 Synthesis of PLA2-NLS

PLA2-NLS was synthesized with with either NLS-TP or a previously produced NLS-Maleimide peptide provided by Nicholas Baumhover. PLA2-Iminothiolane produced as above

was reacted with 15 µg of enzyme and 20 fold excess of either peptide in 50 mM $NaHCO_3$ at 90 µL total volume at room temperature for 7 hr. Reaction mixtures were spin filtered as above to remove excess peptide. PLA2-NLS derivatives were analyzed with PLA2 activity assay and SDS-PAGE electrophoresis as above.

5.3.12 Synthesis of PLA2-Tri with I-Tri

I-Tri, a triantennary oligosaccharide prepared from bovine fetuin protein and derivatized with a tyrosine to add absorption at 280nm and an iodoacetamide group to allow reaction with thiol groups, was previously prepared[189]. PLA2-Iminothiolane was reacted with 0 – 25 fold excess of I-Tri in 50 mM $NaHCO_3$ for 6 hr. Reaction mixtures were spin filtered as above and analyzed by SDS-PAGE gel electrophoresis and PLA2 enzyme activity assay.

Additionally, PLA2-Iminothiolane was prepared with 5 – 50 fold excess of 2-iminothiolane and reacted with 5 fold excess of I-Tri and analyzed as above. A reaction time course was studied by producing PLA2-Iminothiolane with 15 fold excess of 2-iminothiolane and 10 fold excess of I-Tri at reaction times from 30 min to 24 hr and analyzed as above. Effect of pH on the reaction was studied by reacting PLA2-Iminothiolane with 5 fold excess of I-Tri in 50 mM $NaHCO_3$ at pH 7.0 – 9.5 and analyzed as above.

5.3.13 Synthesis of Tri-Thiopyridine

Triantennary oligosaccharide, with tyrosine to provide a primary amine, was previously produced[189]. Tri at 1.5 µmol was reacted with 150 µmol of 2-iminothiolane in 3.5 mL 100 mM $NaHCO_3$ for 3 hr at room temperature. Tri-Iminothiolane was purified by size exclusion

chromatography on G-10 column with 0.1% TFA as mobile phase. Tri-iminothiolane peak was collected at approximately 25 min in a 500 mL round bottom flask and dried to about 2 mL by rotovap. Solution was frozen on dry ice and placed on the freeze drier overnight.

Tri-Iminothiolane was derivativized with DTDP by dissolving the freeze dried 1.5 µmol Tri-iminothiolane with 100 fold excess of DTDP. The 150 µmol DTDP was dissolved in as little methanol as possible and added to 5 mL of 10:3 2 M acetic acid:isopropanol. The Tri-Iminothiolane was added to the reaction mixture and incubated at room temperature overnight while shaking. Tri-thiopyridine, Tri-TP, was purified by size exclusion chromatography on G-10 column as above. The peak was collected and freeze dried, product was dissolved in 3 mL 0.1% TFA and analyzed by HPLC.

5.3.14 Synthesis of PLA2-Tri wth Tri-Thiopyridine

PLA2-Iminothiolane was produced as above with 10 – 50 fold excess of 2-iminothiolane. PLA2-Iminothiolane was reacted with 5 – 20 fold excess of Tri-TP in 50 mM $NaHCO_3$ for 2 hr. Samples were spin filtered as above to remove excess Tri-TP. PLA2-Tri was analyzed by SDS-PAGE electrophoresis and PLA2 enzyme activity assay as above.

5.3.15 Affinity Chromotography with Lectin Column

PLA2-Tri was produced on a 50 µg scale with 10 fold excess of 2-iminothiolane and 5 fold excess of Tri-TP as above. A lectin affinity chromatography column was obtained with Erythrina cristagalli immobilized lectin (EY Laboratories Inc., San Mateo, CA, USA). This lectin has affinity for the terminal galactose residues on the triantennary oligosaccharide. Wash buffer

was prepared with 50 mM Tris, 150 mM NaCl, 10 mM $CaCl_2$, pH 7.5. Elution buffer was made by adding enough lactose to wash buffer to obtain 100 mM lactose. Column was prepared and equilibrated with 500 µL of wash buffer. PLA2 samples were added to column at 50 µg amounts and washed with 300 µL aliquots of wash buffer. Fractions were collected in 0.5 mL microcentrifuge vials in 500 µL aliquots for a total of 10 fractions. PLA2-Tri was eluted in the same manner with elution buffer, collecting another 10 fractions. Fractions were analyzed by PLA2 activity assay as above. Fractions were concentrated by pooling all elution fractions and concentrating on 10 kDa MWCO spin filters as above. Concentrated samples were analyzed by SDS-PAGE electrophoresis as above.

5.3.16 PLA2 Gene Construction

Several forms of bee venom phospholipase A2 gene were produced by synthesizing the complete Bee Venom PLA2 gene with codon optimization for expression in E. coli with a C-terminal NLS sequence PKKKRKVG (GeneArt Life Technologies, Grand Island, NY, USA) and then manipulating the gene with site-directed mutagenesis and PCR. The original gene with leader peptides and NLS intact was referred to as BV-NLS. Bee venom PLA2 with no signal peptide, propeptide, or NLS was produced by using PCR to amplify the desired portion of the gene while inserting a new start codon, and was referred to as BVM, or Bee Venom Mature. Bee venom PLA2 without the leader sequences, but with NLS was also produced by PCR amplification and referred to as BVM-NLS. An active site mutant was produced by site-directed mutagenesis of BVM-NLS to convert the histidine at position 67 to a glutamine and referred to as H67Q[375]. Two additional mutants were produced by changing the cysteine at either position 37

or 113 to alanine to break disulfide bonds and leave free thiols, and were referred to as C37A or C113A. All genes were inserted into into the PET28 plasmid (Novagen EMD Millipore, Bellerica, MA, USA).

Additionally, 2 human phospholipase A2 genes were synthesized. Human Group III PLA2 contains 3 domains, the N terminal domain, middle domain, and C terminal domain. The middle domain has similar sequence and structure to bee venom PLA2[398]. The middle domain of human Group III PLA2 was cloned into the PET28 plasmid. Human Group X PLA2 was also synthesized with an N terminal NLS sequence and cloned into PET28.

5.3.17 PLA2 Expression in Bacteria

PLA2 genes in PET28 plasmid were inserted into BL21 E. coli cells and grown overnight on agar plates at 37 °C. Colonies were picked and grown overnight in 5 mL of Terrific Broth, then transferred to 500 mL cultures and incubated at 37 °C while shaking at 250 RPM for 7 hr. Cells were induced by addition of 0.5 mL of 0.5 M IPTG, shaking speed was reduced to 180 RPM and cells were incubated another 16 hr. Cells were split into 50 mL Falcon tubes and spun down at 4000 RPM for 30 min and pellets were suspended in 4 mL 50 mM Tris pH 8.0 with 4 µL Triton X-100, 8 µL protease inhibitor cocktail (Roche Diagnostics, Mannheim, Germany), 16 µL 0.5 M EDTA, and 300 µL 10 mg/mL lysozyme. Mixtures were incubated at 37 °C while shaking at 180 RPM for 30 min, then frozen on dry ice. Mixtures were thawed and 400 µL of 1 M $MgCl_2$ and 4 µL DNase were added, and mixtures were incubated at 37 °C while shaking at 180 RPM for 30 min. Mixtures were spun at 11,000 RPM for 10 min and supernatent was removed.

Pellets were suspended in 20 mL detergent solution, 200 mM NaCl, 1% deoxycholic acid, 1% Triton X-100. Mixtures were centrifuged again at 11,000 RPM for 10 min, supernatent was removed and pellets were suspended in 20 mL 1%Triton X-100, 1 mM EDTA, and centrifuged again at 11,000 RPM for 10 min. Supernatents were removed and pellets were suspended again in 20 mL 1% Triton X-100, 1 mM EDTA and centrifuged again. Supernatents were removed and pellets were suspended in 8 mL 100 mM Tris, 6 M Guanidine HCl, 100 mM DTT, pH 8.3 to unfold the PLA2 trapped in inclusion bodies. Mixtures were incubated overnight at 4 °C. Mixtures were centrifuged at 11,000 RPM for 10 min, supernatents were recovered and pH was adjusted to 4, then dialyzed against 1 L of 4 M guanidine HCl, 20 mM acetic acid for 4 hr at 4 °C. Dialysis buffer was replaced with fresh 4 M guanidine HCl, 20 mM acetic acid and dialyzed another 4 hr at 4 °C. Dialysis buffer was replaced again and dialyzed at 4 °C overnight. Dialysis buffer was changed to a refolding buffer, 1 M Tris-HCl, 10 mM $CaCl_2$, 1 mM EDTA, 5 mM glutathione, 1 mM glutathione disulfide, pH 8.3 and protein sample was dialyzed at 4 °C for 24 hr. Protein solution was recovered and centrifuged at 20,000 RPM for 20 min.

The supernatent was taken and buffer was replaced with 50 mM Tris-HCl, 10 mM $CaCl_2$, pH 7.0 using a PD-10 column (GE Healthcare, Buckinghamshire, UK). Fractions collected from the PD-10 column were tested for PLA2 activity and active fractions were processed by FPLC on an AKTApurifier FPLC with 5 mL HiTrap SP cation exchange column (GE Healthcare, Buckinghamshire, UK) with a flow rate of 5 mL/min with 50 mM Tris-HCl 10 mM $CaCl_2$, pH 7.0, with NaCl gradient of 0 – 1 M over 20 min. Absorbance at 280 nm was monitored and fractions were collected and pooled. Pooled fractions were concentrated with an Amicon ultrafiltration unit with YM-3 membrane under nitrogen gas. Refolded protein was analyzed by

SDS-PAGE electrophoresis and PLA2 activity assays.

5.3.18 Chemical Modification of Mutant PLA2

PLA2 C37A or C113A at 5 μg was reacted with 0 – 5 fold excess of I-Tri in 100mM $NaHCO_3$ for 24 hr at room temperature. Additionally, the reaction was run at pH 7, 8, 9, or 10. Protein samples were analyzed by SDS-PAGE electrophoresis as above.

To test if the proteins had free thiol available for labeling, wild type PLA2, C37A, or C113A were reacted with stoichiometric amounts of TCEP at room temperature for 30 min to help reduce disulfides in 100 mM Tris pH 7.0. Samples were spin filtered in 3 kDa spin filters to remove excess TCEP. A 20 fold excess of PEG_{5kDa}-maleimide was added to the reduced protein samples and allowed to react at room temperature for 24 hr, then analyzed by SDS-PAGE electrophoresis.

5.4 Results

5.4.1 Synthesis of PLA2-Cys-$(Acr\text{-}Lys)_6$

Bee venom PLA2 was conjugated to $(Acr\text{-}Lys)_6$-Cys peptide using the heterobifunctional linker GMBS. Initial attempts at the reaction showed that PLA2 could be multiply labeled with $(Acr\text{-}Lys)_6$ and visualized on SDS-PAGE gel (**Fig. 5-3A**). However, not all free $(Acr\text{-}Lys)_6$-Cys was removed from the labeled PLA2, demonstrated by presence of free $(Acr\text{-}Lys)_6$-Cys peptide on SDS-PAGE gel (**Fig. 5-3B**). Additionally, the reaction with GMBS and peptide greatly reduced PLA2 activity (**Fig. 5-3D**). The PLA2 labeling reaction was reoptimized to use a 10 fold excess of GMBS to help preserve activity (**Fig. 5-3C**). These reaction conditions still allowed

labeling with (Acr-Lys)$_6$-Cys, but with less evidence of multiple labeling (**Fig. 3E**), however, enzyme activity was still harmed (**Fig. 5-3F**). Interestingly, enzyme activity was improved after

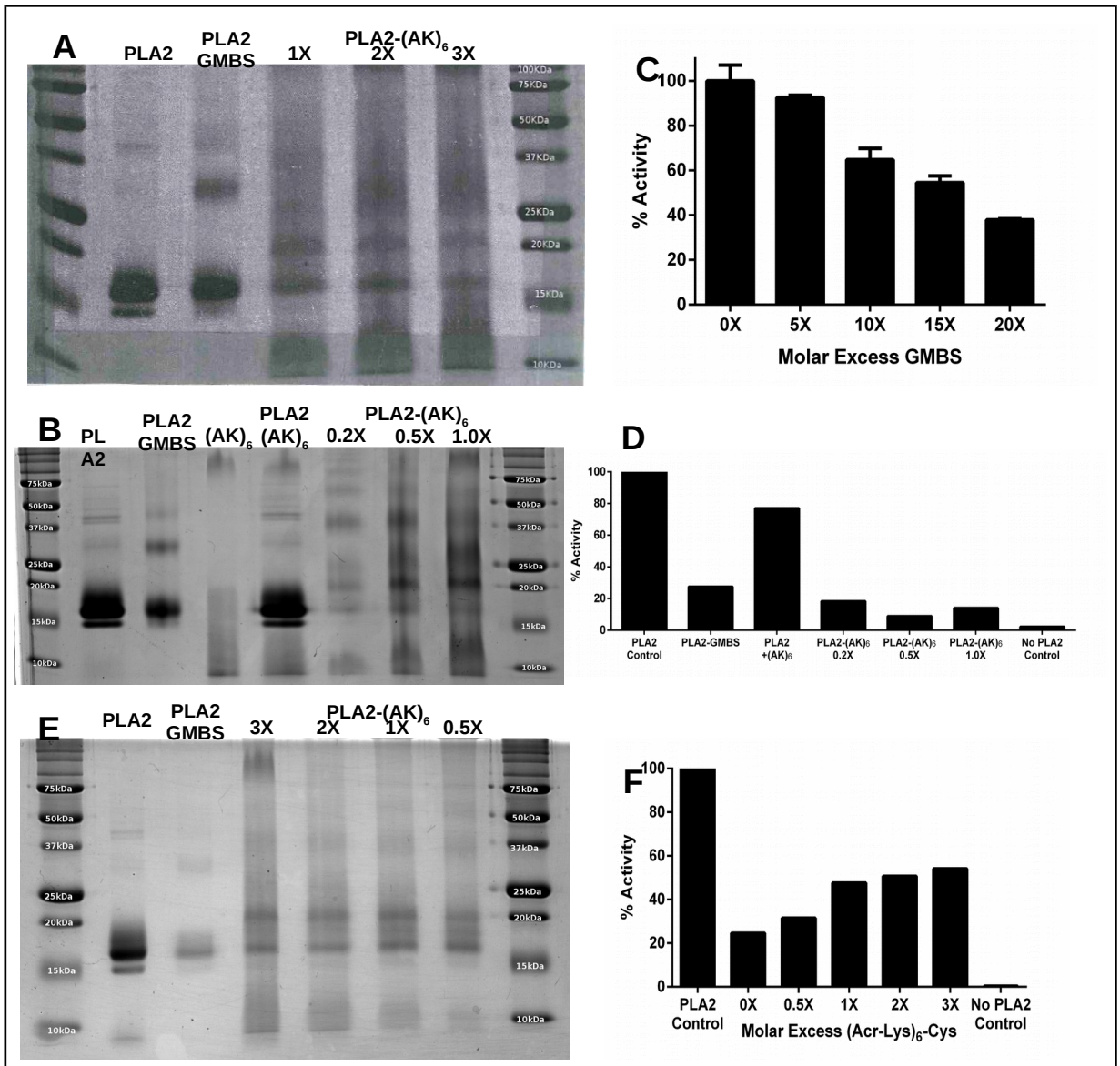

Figure 5-3: *SDS-PAGE and Enzyme Activity Analysis of PLA2-(Acr-Lys)$_6$.* PLA2 can be conjugated with (Acr-Lys)$_6$-Cys peptide using GMBS, and multiple additions of peptide can be seen as laddering as in panel A. However, GMBS treatment can also lead to PLA2 aggregation as seen in A and B, which reduces enzyme activity as seen in C. In panel B, a free (Acr-Lys)$_6$-Cys control lane is included to show that not all of the peptide becomes bound to PLA2-GMBS. PLA2-(Acr-Lys)$_6$ loses enzyme activity as shown in D. The amount of leftover free peptide can be reduced if less peptide is used, shown in E, however using less peptide leads to a greater loss of PLA2 activity, in F.

reaction with $(Acr\text{-}Lys)_6$-Cys.

5.4.2 Synthesis of PLA2-Avidin-$(Acr\text{-}Lys)_6$ Complexes

PLA2 was biotinylated with 0 – 10 fold excess of NHS-Biotin. Enzyme activity was not severely harmed at any amount of biotin (**Fig. 5-4A**). When PLA2-biotin was combined with 0 – 1 molar equivalents of Avidin, using more Avidin greatly reduced enzyme activity (**Fig. 5-4B**), indicating that PLA2 had been successfully biotinylated. Incubation of PLA2-Biotin Avidin complexes with a 100 or 200 fold excess of free biotin for up to 4 hr restored PLA2 activity (**Fig. 5-4C**), indicating that even the strong Avidin-biotin complex could be overcome with a large excess of free biotin.

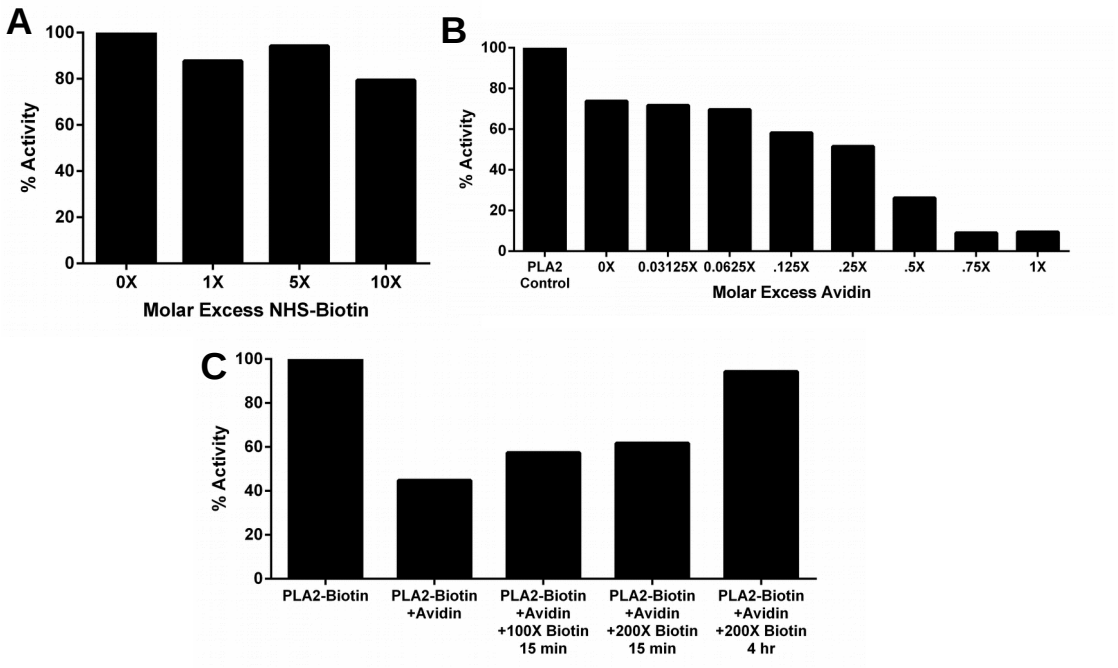

Figure 5-4: *Enzyme Activity of PLA2-Biotin.* In panel A, PLA2 was reacted with 0 - 10 fold excess of NHS-Biotin, and showed little loss of activity. When PLA2-Biotin is combined with Avidin in B, enzyme activity is lost as the amount of Avidin approaches the amount of PLA2. When PLA2-Avidin complexes are incubated in large excesses of free biotin for up to 4 hr in C, PLA2 activity is restored, indicating that PLA2-Biotin is released from Avidin.

(Acr-Lys)$_6$-Cys was reacted with a maleimide-PEG$_2$-biotin and analyzed by LC-MS. The total ion chromatograph, absorbance at 280 nm, and fluorescence at 409 nm all showed 3 peaks (**Fig. 5-5**). The third peak with retention time of approximately 22 min showed a mass of 3247.4, almost identical to the expected mass of 3248.1. However, peak 2 was 15.45 mass units heavier than expected, and peak 1 was 31.3 mass units heavier than expected. This is most likely explained by addition of 1 or 2 oxygen atoms to the sulfur atom of biotin. This biotin-sulfoxide results from a reaction of biotin with oxygen gas in the presence of UV light and reduces affinity for Avidin[399].

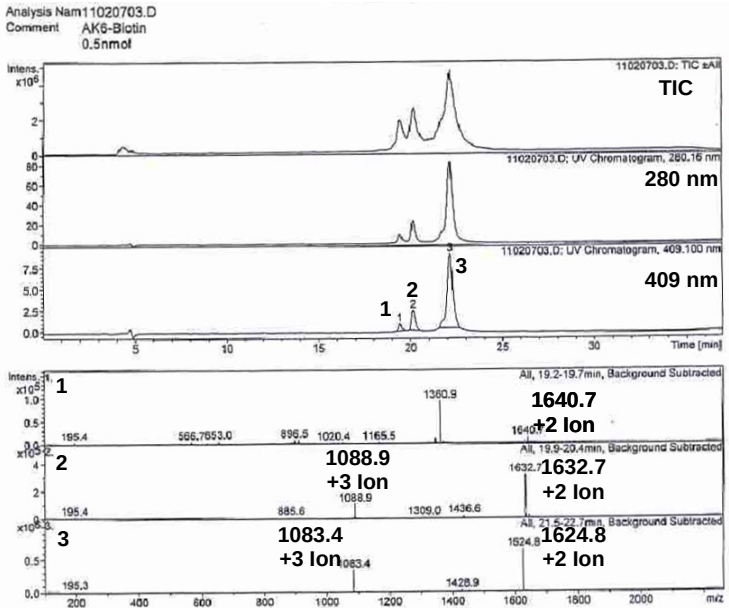

Figure 5-5: *LC-MS Analysis of (Acr-Lys)$_6$-Biotin.* (Acr-Lys)$_6$-Cys was reacted with a maleimide-Biotin. LC-MS shows correct mass at 3247.4, but also shows masses corresponding to biotin sulfoxide with 1 or 2 additional oxygen atoms.

Biotinylated PLA2 and (Acr-Lys)$_6$-Cys were combined with Avidin in the presence of plasmid DNA in an attempt to use the DNA as a template to build complexes. When components were combined in a 1:1:1 ratio, visible flocculates were formed, most likely as 1 Avidin bound

$(Acr\text{-}Lys)_6$ peptides on different plasmids. To prevent flocculation, the amount of Avidin was increased to 4 fold excess over $(Acr\text{-}Lys)_6$-Cys-Biotin and PLA2-Biotin was increased to 4 fold excess over Avidin. However, when agarose gel electrophoresis was used to perform band shift assays on DNA $(Acr\text{-}Lys)_6$-Biotin Avidin PLA2-Biotin complexes, the addition of PLA2-biotin allowed DNA to migrate through the gel. Complexes with biotinylated peptide and Avidin show no migration of DNA (**Fig. 5-6A**). This suggests that PLA2-biotin was displacing the $(Acr\text{-}Lys)_6$-Biotin from Avidin, releasing the DNA from the complex.

To help reduce this displacement, PLA2 was biotinylated with less NHS-Biotin, 1 – 10 fold excess rather than 10 fold excess. When these complexes were electrophoresed, the 3:1 and 1:1 biotin:PLA2 samples showed no DNA migration (**Fig. 5-6B**). DNA with different combinations of $(Acr\text{-}Lys)_6$-Biotin, Avidin, and PLA2-Biotin was electrophoresed to demonstrate what components were needed to inhibit DNA migration (**Fig. 5-6C**). When both peptide and Avidin were used, DNA migration was inhibited and most DNA remained in the well. The addition of PLA2-Biotin did not change this. When DNA was combined with $(Acr\text{-}Lys)_6$-Biotin and PLA2-Biotin, but no Avidin, DNA was able to migrate and did not remain in the well. However, when DNA was mixed with Avidin, either with or without PLA2-Biotin, some DNA remained in the well, suggesting that Avidin itself binds DNA, most likely through electrostatic binding.

Hydrodynamic dosing of 1 μg pGL3 plasmid DNA peptide polyplex with a mixture of 95% $(Acr\text{-}Lys)_6$-Cys-PEG_{5kDa} and 5% $(Acr\text{-}Lys)_6$-Biotin into mice showed 5 fold less bioluminescence than DNA with 100% of $(Acr\text{-}Lys)_6$-Cys-PEG_{5kDa} (**Fig. 5-6D**). When Avidin was added, bioluminescence was 100 fold less than the 100% $(Acr\text{-}Lys)_6$-Cys-PEG_{5kDa} control.

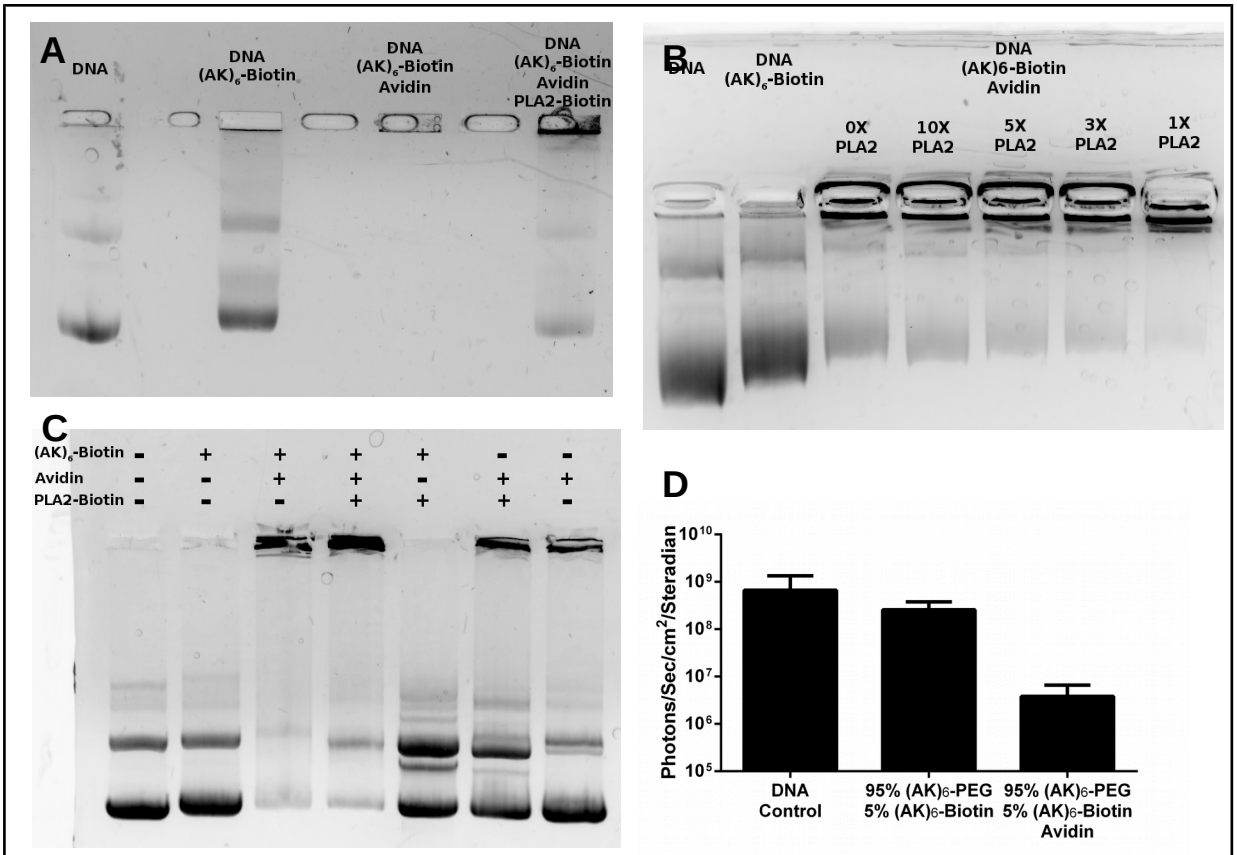

Figure 5-6: *PLA2-Avidin-(Acr-Lys)$_6$ Complexes Bind to DNA.* The band shift assay in A shows a slight band shift when DNA is bound to (Acr-Lys)$_6$-Biotin, and that migration is stopped when also bound to Avidin, however some migration is restored upon additon of PLA2-Biotin. In B, the amount of PLA2-Biotin was varied, and more PLA2-Biotin seemed to show more DNA released from Avidin. In panel C, DNA was tested with or without different components of the complex, and Avidin was able to inhibit some DNA migration by itself, trapping the DNA in the well. Mice were hydrodynamically dosed with these complexes in D, and the Avidin complex shows a loss of signal.

5.4.3 Hydrodynamic Dosing of pGL3 DNA and PLA2

Mice were hydrodynamically injected with 1 μg doses of pGL3 DNA and 0 – 50 μg of unmodified bee venom PLA2. As the dose of PLA2 increased, the bioluminescence decreased (**Fig. 5-7**). When mice were dosed with 15 or 50 μg of PLA2, they died. The mice that received 50 μg doses died within 15 min of injection, while those who received 15 μg doses died within 1 hr.

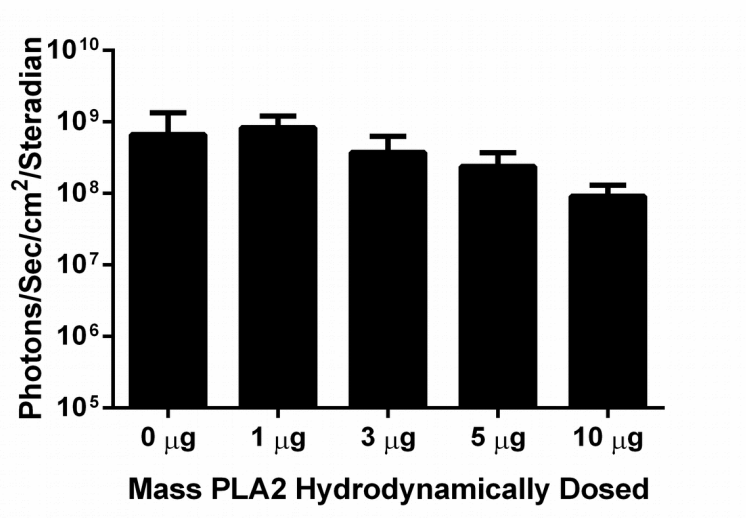

Figure 5-7: *Hydrodynamic Co-Dosing of DNA and PLA2.* Different amounts of bee venom PLA2 were mixed with 1 μg doses of pGL3 plasmid DNA and hydrodynamically injected into mice. As the amount of PLA2 used increased, the bioluminescent signal decreased. Mice that received more than 10 μg of PLA2 died.

5.4.4. Synthesis of PLA2-Iminothiolane

Bee venom PLA2 was reacted with 0 – 10 fold excess of 2-Iminothiolane and tested for activity. Even a 10 fold excess of 2-Iminothiolane did not harm PLA2 activity (**Fig. 5-8**).

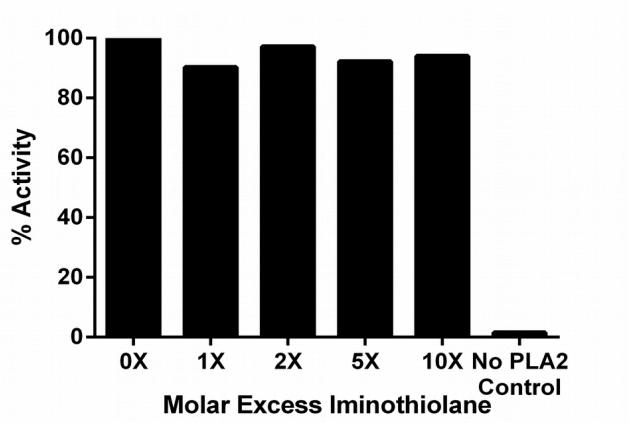

Figure 5-8: *Synthesis of PLA2-Iminothiolane.* Bee venom PLA2 was reacted with a 0 – 10 fold excess of 2-Iminothiolane. PLA2 activity was not harmed.

5.4.5 Synthesis of NLS-Thiopyridine Peptide

A thiopyridine derivative of the SV40 NLS peptide CPKKKRKVG was produced by reacting the NLS peptide with DTDP. LC-MS analysis showed that modified peptide had a mass of 1209.592 mass units, very close to the 1209.531 mass units predicted for the molecule (**Fig. 5-9A**).

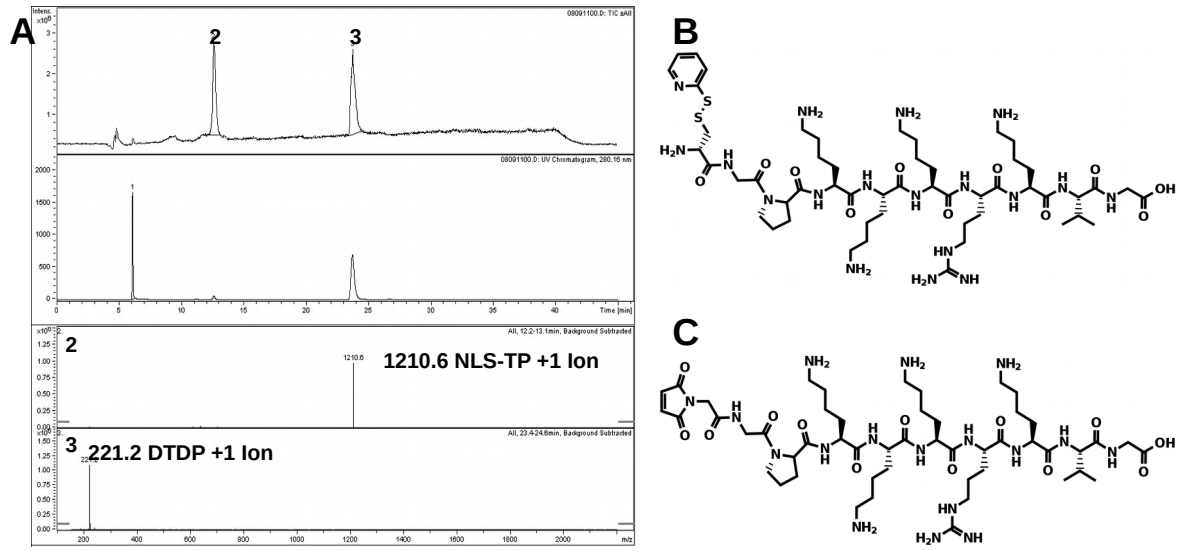

Figure 5-9: *LC-MS Analysis of NLS-Thiopyridine.* The SV40 NLS-Cys peptide was reacted with DTDP to produce NLS-TP and verified by LC-MS with mass of 1209.592 in panel A. The structure of NLS-TP is shown in panel B, while the NLS-Maleimide peptide that was also used is shown in C.

5.4.6 Synthesis of PLA2-NLS

PLA2-Iminothiolane was conjugated with either NLS-Thiopyridine (**Fig. 5-9B**) or NLS-Maleimide (**Fig. 5-9C**) in a 1, 3, or 5 fold excess. PLA2-NLS enzyme activity was not severely affected (**Fig. 5-10A**). SDS-PAGE analysis of PLA2-NLS showed that PLA2-NLS produced with NLS-Thiopyridine formed high mass aggregrates that failed to migrate through the gel. PLA2-NLS produced with NLS-maleimide formed proteins that did migrate, with laddering suggesting smaller aggregates or 2 or 3 PLA2 molecules (**Fig. 5-10B**). PLA2-NLS was treated with TCEP to reduce disulfide bonds and again analyzed by SDS-PAGE. This restored some of

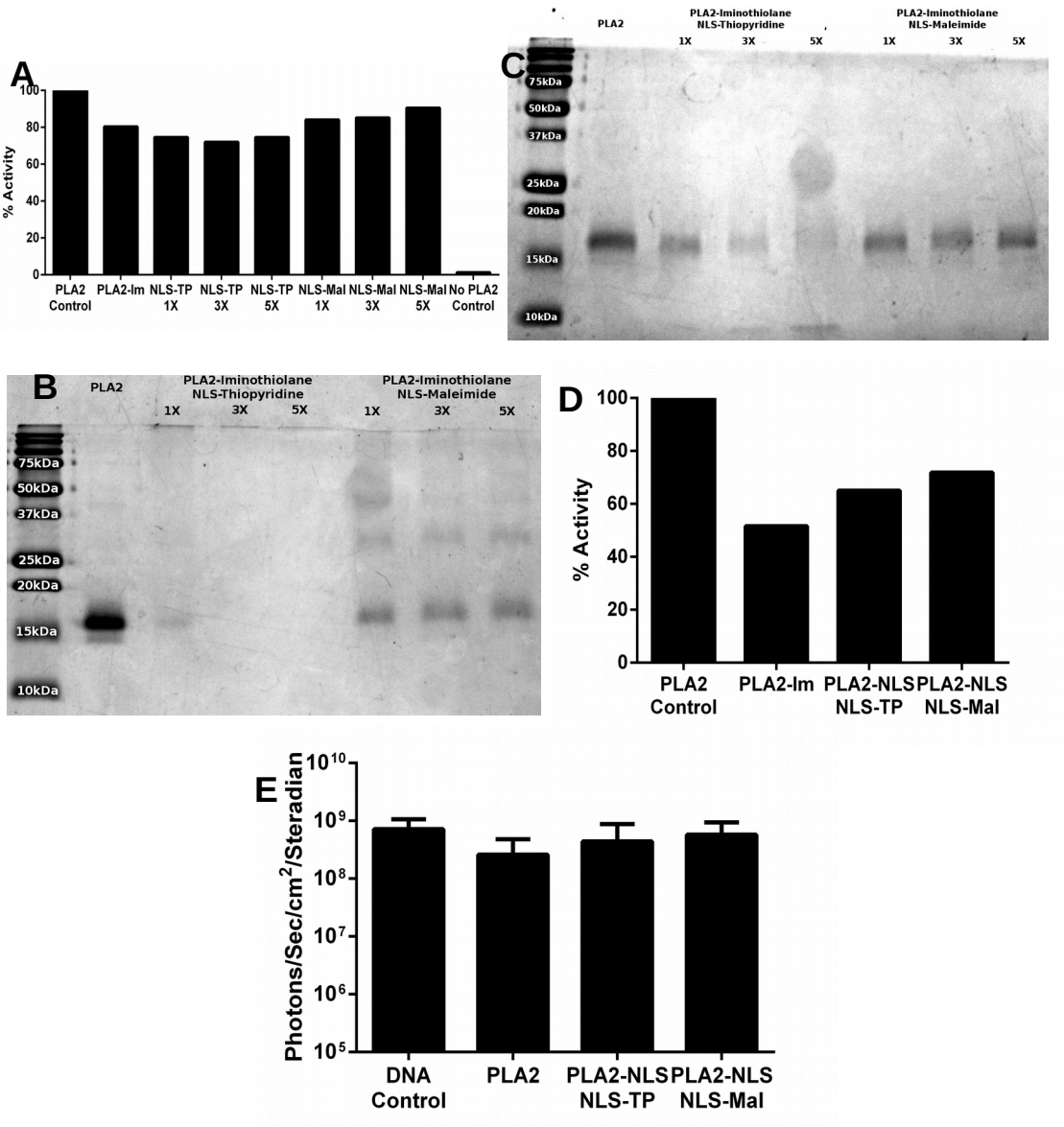

Figure 5-10: *Synthesis of PLA2-NLS.* PLA2-Iminothiolane was reacted with 1, 3, or 5 fold excess of either NLS-TP or NLS-Maleimide. Panel A shows that loss of enzyme activity was minimal. SDS-PAGE showed that use of NLS-TP produced a PLA2-NLS that did not migrate through the gel, and PLA2 dimers and trimers are visible in NLS-Maleimide lanes in B. When PLA2-NLS was treated with TCEP to reduce disulfide bonds in C, PLA2 migration was restored in the NLS-TP lanes and PLA2 aggregates disappeared from the NLS-Maleimide lanes. When PLA2-Iminothiolane was allowed to incubate for an extended amount of time, significant loss of activity was seen in D. However, addition of NLS provided some protection. When PLA2-NLS at 1 µg was co-dosed with pGL3 DNA by hydrodynamic injection in E, PLA2-NLS did not seem to reduce bioluminescent signal by as much as PLA2, but differences are not significantly different from DNA alone.

the protein's ability to migrate and eliminated laddering (**Fig. 5-10C**). These gels show PLA2-Iminothiolane forms disulfide linked aggregates that can be broken up by reducing agents. When PLA2-Iminothiolane was allowed to incubate for 7 hr, PLA2 activity was reduced by about half, while PLA2-NLS with either NLS peptide lost less activity (**Fig. 5-10D**), suggesting that addition of peptide protected the PLA2 against aggregation.

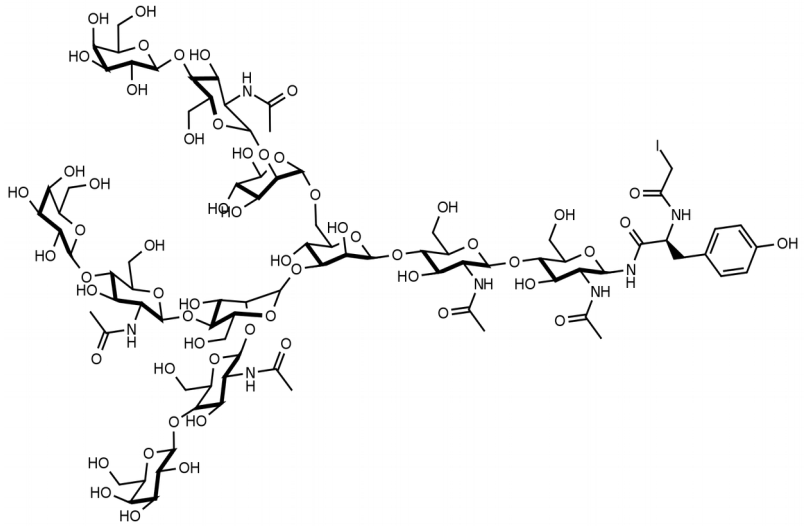

Figure 5-11: *Structure of I-Tri.* The triantennary oligosaccharide from bovine fetuin has high affinity for the ASGPR, and can be used to target molecules to hepatocytes. I-Tri has been modifed with a tyrosine to provide absorbance at 280 nm and an iodoacetamide group to react with thiols.

5.4.7 Synthesis of PLA2-Tri with I-Tri

PLA2-Iminothiolane was conjugated with the iodoacetamide derivative of Triantennary oligosaccharide (**Fig. 5-11**), I-Tri, in 5 – 25 fold excess. SDS-PAGE analysis shows that larger excesses of I-Tri produces laddering, showing singly and doubly modified PLA2 (**Fig. 5-12A**). PLA2 enzyme activity was greatly harmed when a 0, 5, or 10 fold excess of I-Tri was used, but not when 15, 20, or 25 fold excess of I-Tri was used (**Fig. 5-12B**), suggesting that Tri modifications protect PLA2 activity.

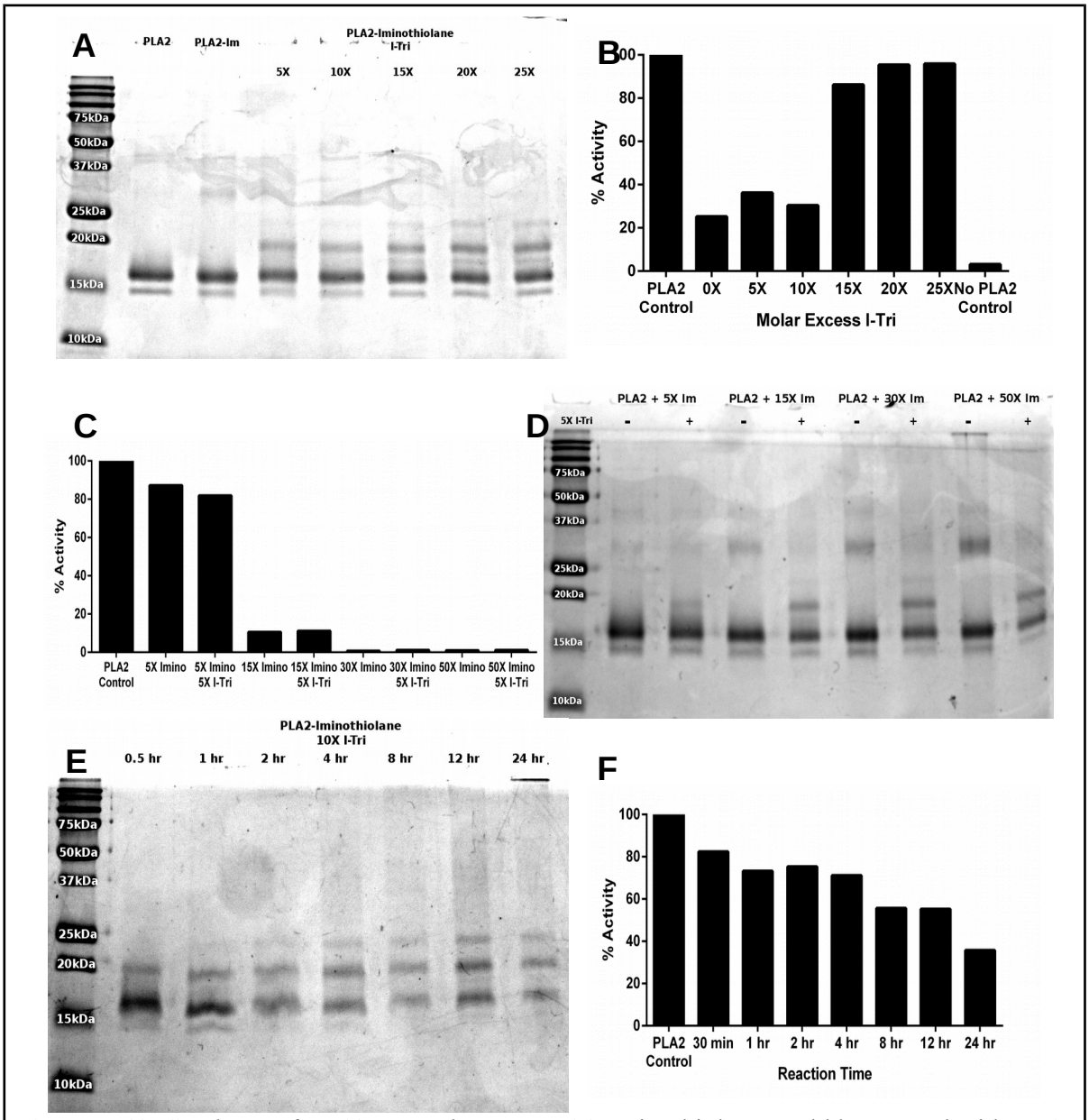

Figure 5-12: *Synthesis of PLA2-Tri with I-Tri.* PLA2-Iminothiolane could be reacted with 5 - 25 fold excesses of I-Tri to produce PLA2-Tri with 1 or 2 oligosaccharides, as seen in A. However, when less than a 15 fold excess of I-Tri was used, PLA2 activity was greatly reduced, as seen in B. To encourage complete labeling of PLA2, the amount of 2-Iminothiolane was increased to as much as 50 fold excess, then reacted with 5 fold excess of I-Tri. However, 15 fold or more excess of 2-Iminothiolane eliminates PLA2 activity, as seen in C. SDS-PAGE in D shows that unmodified PLA2 was still present, with PLA2 dimers present in lanes without I-Tri. A reaction time course is shown in E, and demonstrates that unmodified PLA2 was still present after 24 hr of reaction, and that enzyme activity decreased as reaction time increased, as shown in F.

However, even at 25 fold excess of I-Tri, significant amounts of unmodified PLA2 remained. To try and get a complete reaction, the amount of 2-Iminothiolane used was increased to 15, 30, and 50 fold excess over PLA2, then reacted with a 5 fold excess of I-Tri. PLA2 activity was greatly reduced when reacted with 15 fold excess of 2-Iminothiolane, and completely eliminated with 30 or 50 fold excesses (**Fig. 5-12C**). Addition of I-Tri did not change enzyme activity. When analyzed by SDS-PAGE gel, 15, 30, and 50 fold excesses of 2-Iminothiolane showed higher mass bands of PLA2 dimers, while samples with I-Tri showed a band indicating singly labeled PLA2-Tri. All lanes showed significant amounts of unmodified PLA2 (**Fig. 5-12D**).

To drive the reaction toward completion, PLA2 was reacted with a 15 fold excess of 2-Iminothiolane and 10 fold excess of I-Tri over a 24 hr period. Samples were taken at several time points and analyzed by SDS-PAGE and PLA2 activity assays. SDS-PAGE showed that singly labeled PLA2-Tri appeared as early as 30 min, and doubly labeled PLA2-Tri appeared by 12 hr, but unmodified PLA2 remained at 24 hr (**Fig. 5-12E**). As reaction time went on, PLA2 activity decreased (**Fig. 5-12F**).

5.4.8 Synthesis of PLA2-Tri with Tri-Thiopyridine

The thiopyridine derivative of the triantennary oligosaccharide (**Fig. 5-13A**) was produced by reacting the free amine on the tyrosine residue of Tri with 2-Iminothiolane, then reacting the free thiol produced by 2-Iminothiolane with DTDP.

PLA2-Iminothiolane was produced with 20 or 50 fold excess of 2-Iminothiolane, then a 20 fold excess of Tri-Thiopyridine. PLA2 enzyme activity almost completely lost when PLA2-

iminothiolane was not reacted with Tri-Thiopyridine, but was better protected when Tri-Thiopyridine was added (**Fig. 5-13B**). SDS-PAGE analysis showed that PLA2-Iminothiolane totally disappeared from the gel. PLA2-Tri prepared with a 20 fold excess of 2-Iminothiolane showed several bands, suggesting that many Triantennary groups had been added. PLA2-Tri produced with a 50 fold excess of 2-Iminothiolane showed bands representing singly and doubly labeled PLA2-Tri (**Fig. 5-13C**).

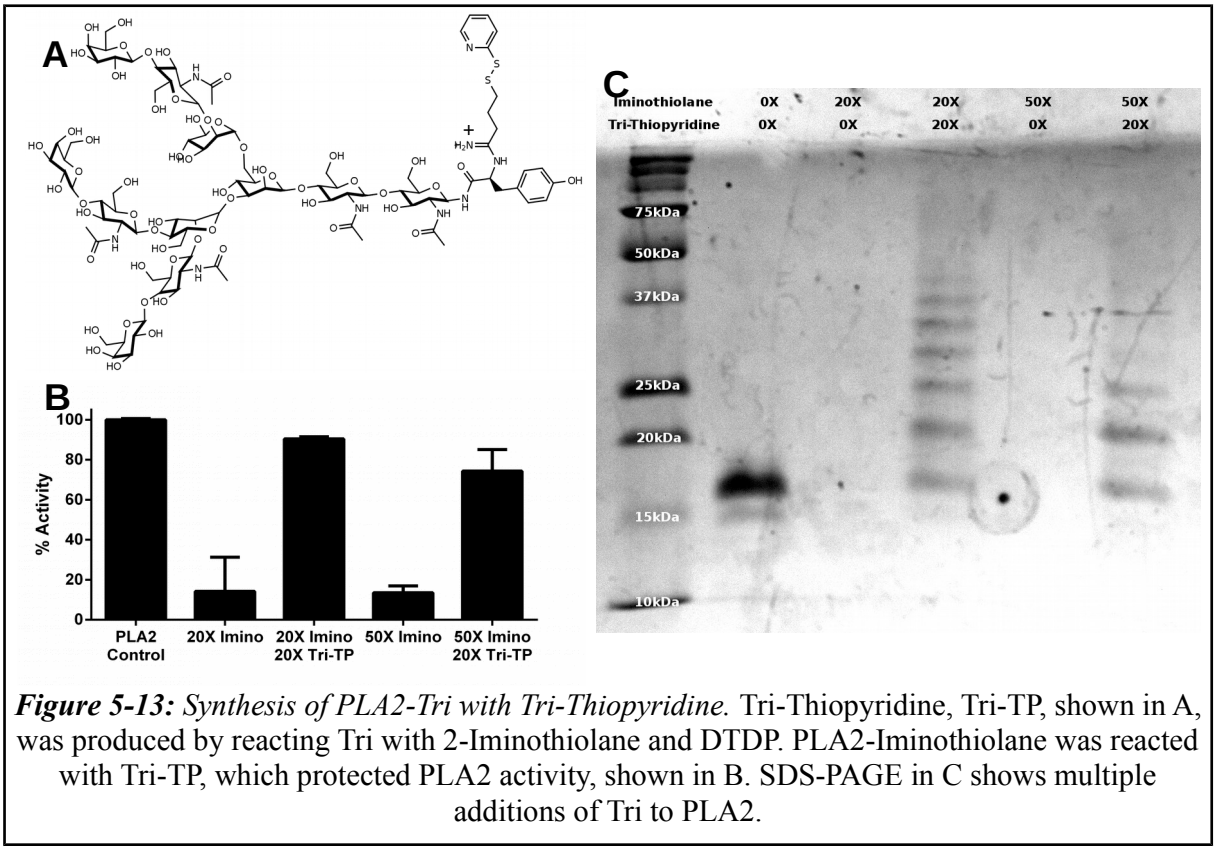

Figure 5-13: *Synthesis of PLA2-Tri with Tri-Thiopyridine.* Tri-Thiopyridine, Tri-TP, shown in A, was produced by reacting Tri with 2-Iminothiolane and DTDP. PLA2-Iminothiolane was reacted with Tri-TP, which protected PLA2 activity, shown in B. SDS-PAGE in C shows multiple additions of Tri to PLA2.

5.4.9 Purification of PLA2-Tri by Lectin Column

PLA2 and PLA2-Tri produced with Tri-Thiopyridine were run through an Erythrina cristagalli immobilized lectin column[400–402], fractions were collected and analyzed for PLA2 enzyme activity by plotting the negative rate of change in absorbance. Fractions 1 – 10 used a

wash buffer to remove unbound protein, while fractions 11 – 20 used a lactose containing elution buffer to remove bound proteins. PLA2 produced activity in fractions 4 – 12, while PLA2-Tri produce activity in 2 broad peaks, fractions 4 – 11 and then 13 – 18 (**Fig. 5-14A**). This shows that PLA2-Tri can be bound by the lectin and separated from unmodified PLA2. When the number of wash fractions and elution fractions were increased to 15 each instead of 10, better separation between the modified and unmodified PLA2 was obtained (**Fig. 5-14B**). When the fractions from the 2 peaks are pooled and concentrated and analyzed by SDS-PAGE, the PLA2-Tri lane shows no unmodified PLA2 (**Fig. 5-14C**), however, the PLA2-Iminothiolane lane

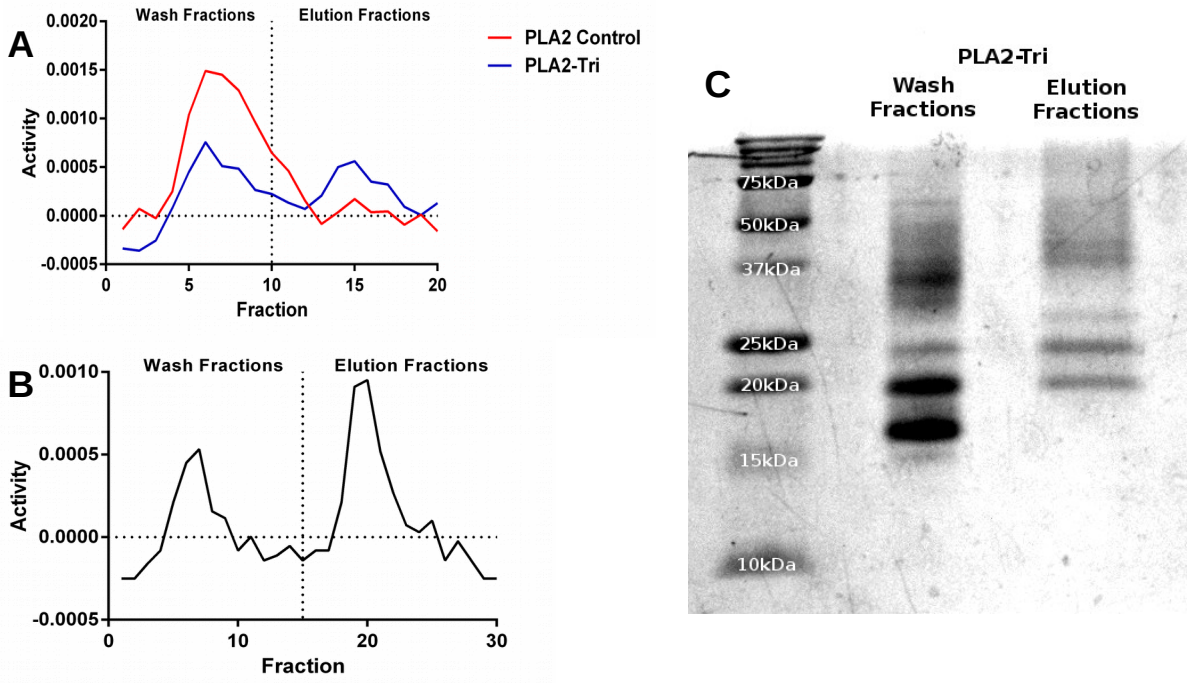

Figure 5-14: *Purification of PLA2-Tri by Lectin Column.* An Erythrina cristigalli immobilized lectin column was used to remove PLA2-Tri from unmodified PLA2, using 10 wash fractions and 10 elution fractions. PLA2 activity in each fraction was measured to produce A. When the number of fractions was increased to 15 each, the resolution between modified and unmodified PLA2 improved in B. When fractions were pooled and concentrated and run on SDS-PAGE in C, unmodified PLA2 was removed from PLA2-Tri. However, some PLA2-Tri was still present in the PLA2 lane, suggesting either column overloading or column failure.

shows what is probably PLA2-Tri contamination. The lectin column eventually failed to separate modified and unmodified PLA2-Tri, this gel probably showed the early stages of column failure.

5.4.10 PLA2 Expression in Bacteria

The bee venom and human PLA2 genes were successfully modified and cloned into PET28 plasmids for bacterial expression, and confirmed by sequencing.

Results from a representative PLA2 purification and refolding are shown. PLA2 C37A was expressed in E. coli, inclusion bodies were recovered and unfolded. Proteins were refolded and initially purified by FPLC (**Fig. 5-15A**). Fractions were collected and pooled into 4 groups, fractions 7 – 10, fractions 11 – 16, fraction 17, and fraction 18. Pooled fractions were analyzed by SDS-PAGE (**Fig. 5-15B**), with bands at about 15kDa appearing in the fractions 11 – 16 and fraction 17 lanes. The fraction 11- 16 sample and fraction 17 samples were separately run on FPLC to further purify the samples. The fraction 11 – 16 sample produced 2 broad peaks, with the second peak having PLA2 enzyme activity (**Fig. 5-15C**). The fraction 17 sample produced 2 broad peaks, with the first peak having PLA2 enzyme activity (**Fig. 5-15C**). Collected fractions were analyzed by SDS-PAGE (**Fig. 5-15D**), with 15kDa bands appearing in the flowthrough in both samples, all peaks of the fraction 11 – 16 sample, and the first 2 peaks of the fraction 17 sample. Protein concentration and specific activity were measured for each fraction, and peak concentration was obtained in fractions 19 – 26 of fraction 17, with 17.5 mg/mL of total protein. (**Fig. 5-15E**). However, peak specific activity was found in fractions 9 – 18 of fraction 17, at 53.8 Units/mg.

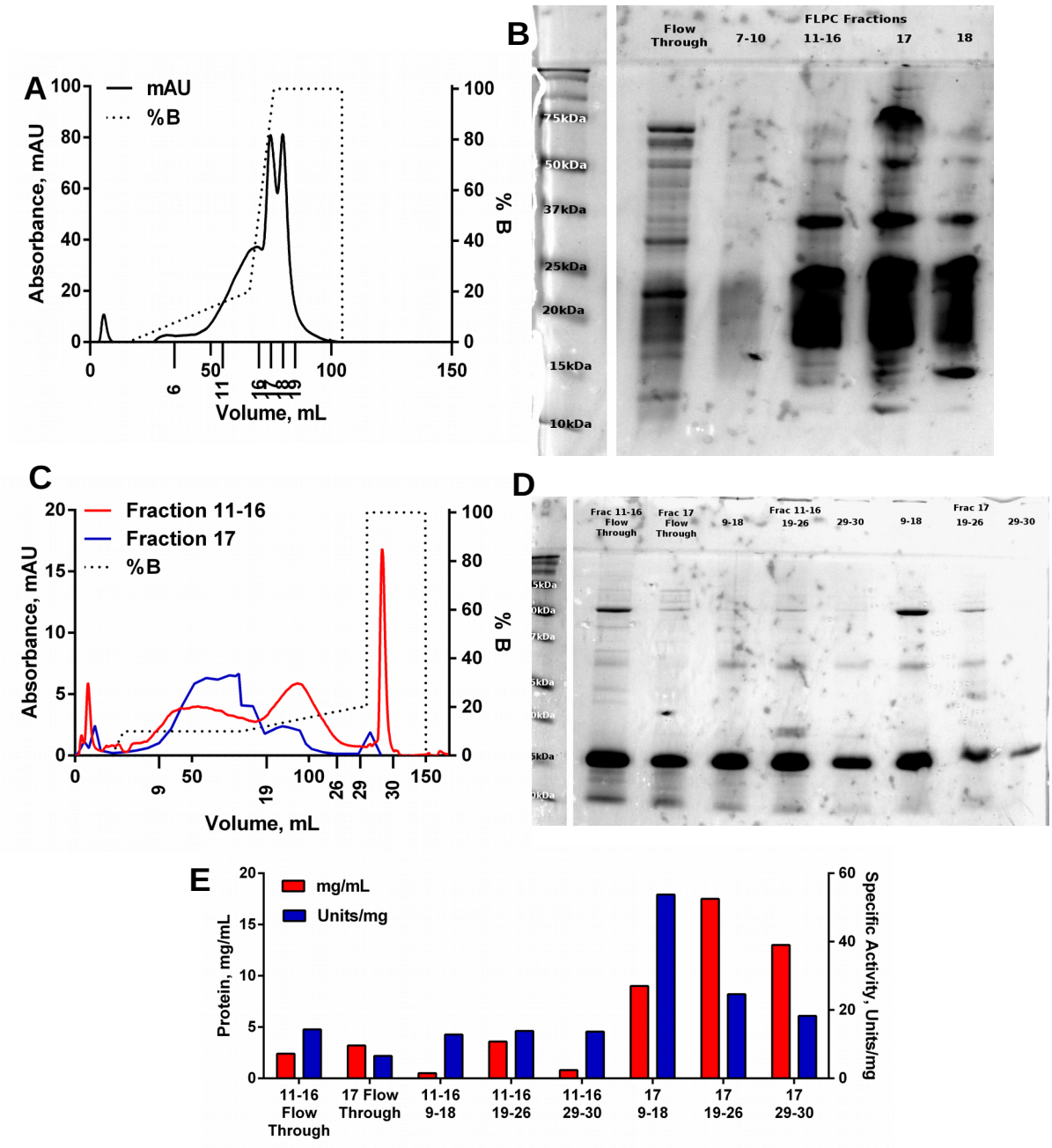

Figure 5-15: *Recombinant Expression of PLA2 in E. coli.* PLA2 C37A was expressed in BL21 E. coli, unfolded, and refolded. Refolded protein solution was purified by ion exchange chromatography in A, and fractions 11 - 16 and 17 were taken because of the protein band they showed on SDS-PAGE in B. Fractions 11-16 and 17 were purified by another round of ion exchange chromatography in C, where peaks 9 - 18, 19 - 26, and 29 - 30 were collected from both. All fractions and the flowthrough samples showed proteins at 15 kDa on SDS-PAGE in D, consistent with PLA2 C37A. Fractions were analyzed for protein concentration and specific activity in E, with fractions 9 - 18 of fraction 17 showing the highest specific activity

5.4.11 Chemical Modification of Mutant PLA2

Bee venom PLA2 C113A was treated with I-Tri in 0 – 5 fold excess for 24 hr and analyzed by SDS-PAGE. Higher mass bands were visible in the 4 and 5 fold excess samples (**Fig. 5-16A**), indicating that some PLA2 had been singly labeled with Tri. However, these bands were very faint, demonstrating the reaction did not work well. PLA2 C113A (**Fig. 5-16B**) and C37A (**Fig. 5-16C**) were also treated with a 3 fold excess of I-Tri for 24 hr in 100mM Tris at pH of 7, 8, 9, or 10. No higher mass band was visible in any lanes, again indicating the reaction did not work. PLA2 C113A was treated with a 20 fold excess of PEG_{5kDa}-Maleimide for 24 hr in 100

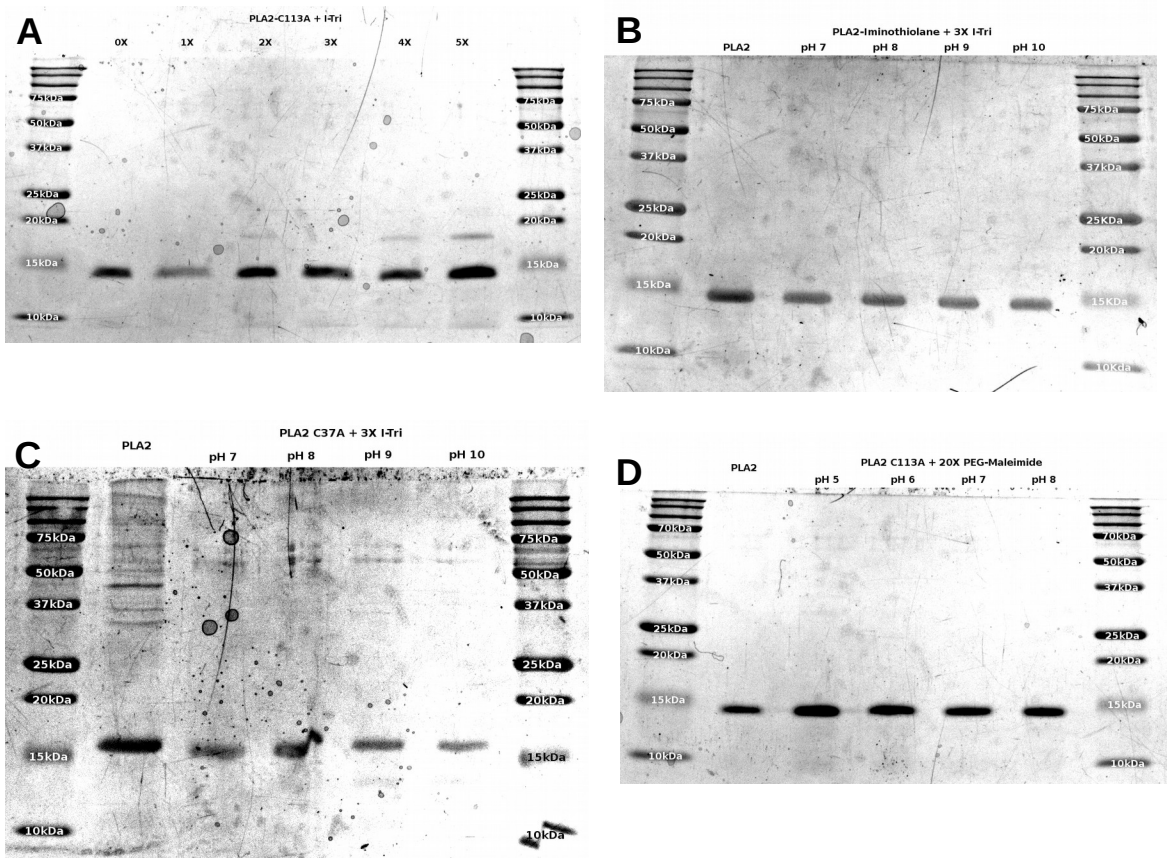

Figure 5-16: *Chemical Modification of PLA2 C37A or C113A.* Purified PLA2 C113A was reacted with I-Tri, and showed some labeling at 4 or 5 fold excess of I-Tri in A, but not much. When PLA2 C113 in panel B, or C37A in panel C, were reacted with I-Tri at pH 7 - 10, no labeled bands were seen. No labeled bands were seen when PLA2 C113A was reacted with a 20 fold excess of PEG-Maleimide in panel D.

mM Tris at pH 5, 6, 7, and 8. Again, no higher mass bands were visible in any lane (**Fig. 5-16D**).

Wild type bee venom PLA2, PLA2 C37A, and PLA2 C113A were treated with an excess of TCEP for 30 min to reduce disulfide bonds. PLA2 samples were then treated with 20 fold excesses of PEG_{5kDa}-Maleimide for 24 hr and analyzed by SDS-PAGE. The wild type PLA2 with PEG shows a faint band at 15 kDa, another faint band at approximately 25 kDa, and dark band at approximately 32kDa (**Fig. 5-17A**). This shows that wild type PLA2 could be almost entirely double labeled with PEG_{5kDa}-Maleimide. However, the PLA2 C37A and PLA2 C113A lanes show no protein bands at all. Wild type PLA2 and PLA2 C113A were treated with or without TCEP and with or without PEG_{5kDa}-maleimide at 42 °C for 24 hr and analyzed by SDS-PAGE. All PLA2 samples with PEG showed very faint higher mass bands (**Fig. 5-17B**). It is not clear why the wild type PLA2 failed to react with PEG_{5kDa}-Maleimide this time, but heating the reaction to 42 °C did not make the reaction work much better with PLA2 C113A.

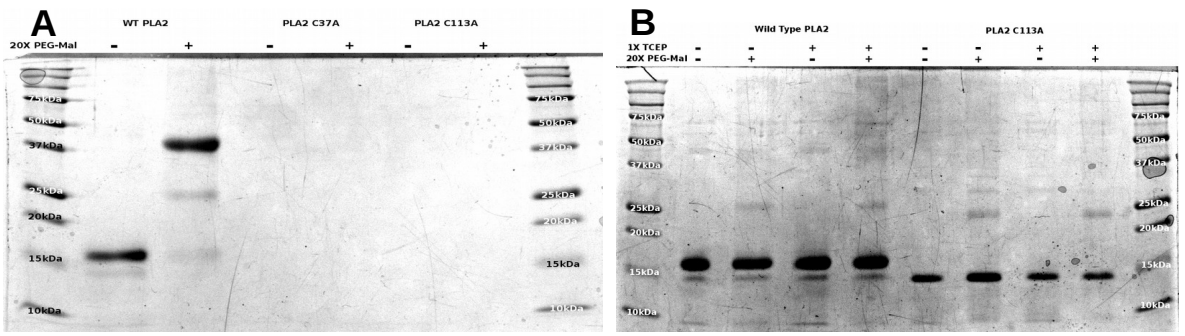

Figure 5-17: *Reaction of TCEP Treated PLA2 with PEG-Maleimide.* In panel A, wild type PLA2, PLA2 C37A, and PLA2 C113A were treated with TCEP and then reacted with PEG-Maleimide. Wild Type PLA2 shows two labeled bands, indicating that disulfides were reduced and the free thiols could react with the maleimide. However, no bands are seen in the C37A or C113A lanes. The experiment was repeated in B with wild type PLA2 and PLA2 C113A while heating at 42 °C. In this experiment, faint labeled bands are present in all samples with PEG-Maleimide, but reactions did not work well.

PLA2 C37A was analyzed by LC-MS. A peak with retention time of 15 min and mass of 16,620.5 g/mol was obtained (**Fig. 5-18A**), while a mass of 16,346.6 g/mol was expected. Some LC-MS runs showed a small peak in the Total Ion Chromatogram at 28 min. The 16,620.5 g/mol mass might be explained by the addition of glutathione to the free thiol on the protein.

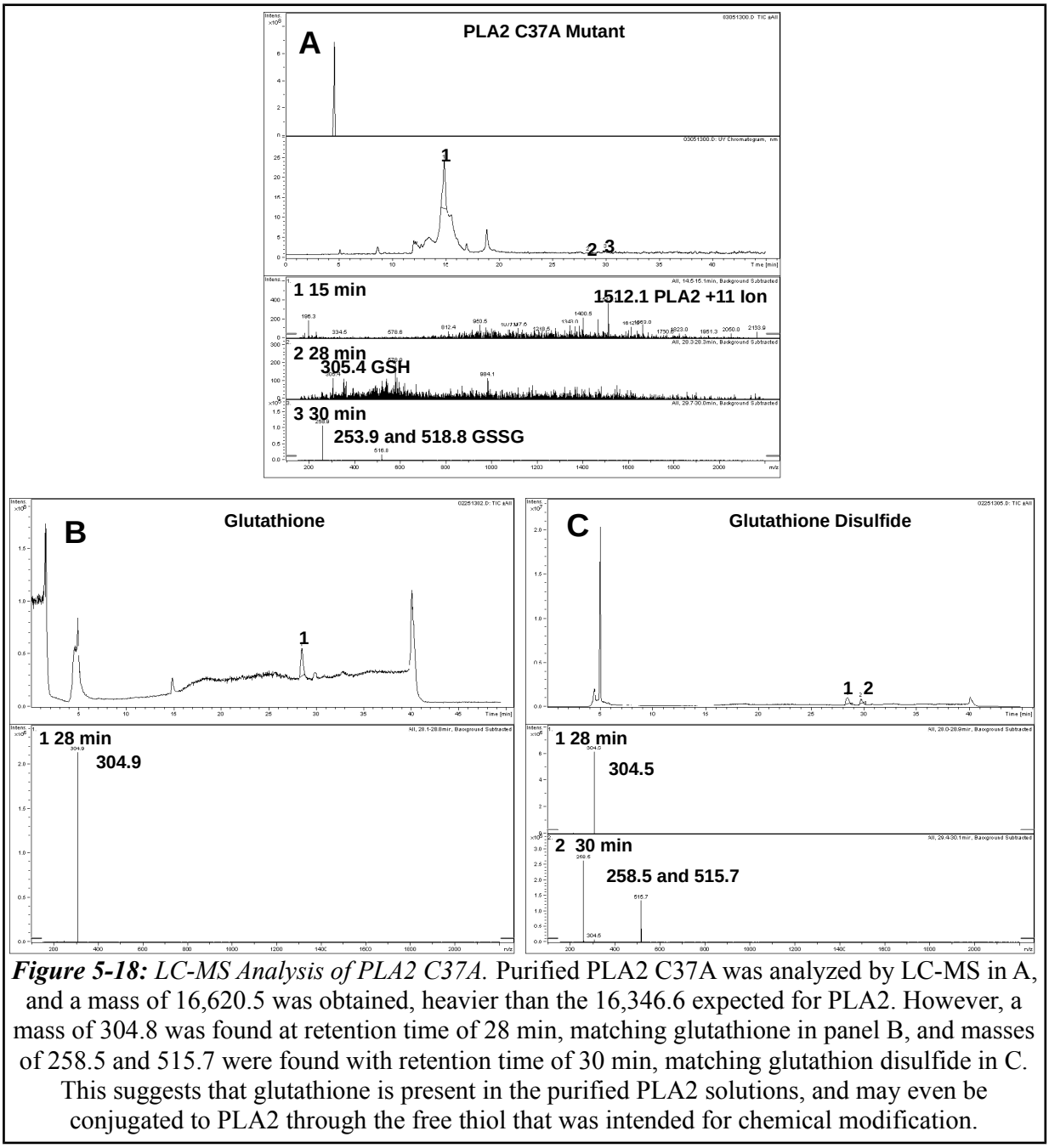

Figure 5-18: *LC-MS Analysis of PLA2 C37A.* Purified PLA2 C37A was analyzed by LC-MS in A, and a mass of 16,620.5 was obtained, heavier than the 16,346.6 expected for PLA2. However, a mass of 304.8 was found at retention time of 28 min, matching glutathione in panel B, and masses of 258.5 and 515.7 were found with retention time of 30 min, matching glutathion disulfide in C. This suggests that glutathione is present in the purified PLA2 solutions, and may even be conjugated to PLA2 through the free thiol that was intended for chemical modification.

Glutathione was analyzed by LC-MS (**Fig. 5-18B**), and produced a small peak in the Total Ion Chromatogram at 28 min with a mass of 304.8 g/mol, close to the 307.32 expected for glutathione. Glutathione disulfide was also analyzed by LC-MS and produced a peak in the Total Ion Chromatogram at 30 min with mass peaks at 258.5 and 515.7 (**Fig. 5-18C**). When the 16,346.6 g/mol of PLA2 C37A is added to the 307.32 g/mol of glutathione, a mass of 16,653.9 g/mol is obtained, about 33.4 g/mol heavier than the 16,620.5 g/mol observed for PLA2 C37A. Unfortunately, obtaining a clean LC-MS of any PLA2 sample proved too difficult to get more precise results. The PLA2 C37A LC-MS also showed a low intensity mass peak of 305.4 mass units with retention time of about 28 min and mass peaks of 258.9 and 516.8 mass units with retention time of 30 min. This indicates that a small amount of free glutathione and a larger amount of oxidized glutathione disulfide may have been present in the purified protein samples, and could have interfered with any attempts to label free thiols on PLA2.

5.5 Discussion

Phospholipases play an important role in several biochemical processes, including cellular signalling, inflammation, and apoptosis[342–344,346,347]. Additionally, several species have utilized phospholipases in their venoms[348–361]. Phospholipase A2 activity is also important for viruses to infect their host cells[338–341]. In the laboratory, PLA2 has been able to create large holes in cellular membranes[393]. These features make PLA2 an interesting target for delivery of large particles to cells. Particles that are too large or too charged to pass through cellular membranes need assistance to enter cells or escape endosomes, and PLA2's ability to create holes in membranes may allow particles such as DNA polyplexes into the cytoplasm. If PLA2 can be

directed to the nuclear envelope, it might be able to help polyplexes enter the nucleus and become expressed.

However, the original hypothesis that PLA2 would help DNA polyplexes enter the nucleus was based on the adeno associated virus requiring PLA2 activity to infect cells[338], was later refuted by research that demonstrated that virus mutants without PLA2 activity were still able to enter the nucleus when microinjected into cells[403]. This shows that PLA2 is involved in endosomal escape, but another mechanism is responsible for the virus delivering its DNA cargo to the nucleus.

Bee venom PLA2 was an attractive choice for the PLA2 used in this study. Bee venom PLA2 is relatively small, approximately 15 kDa, with 5 disulfide bonds to increase stability, and 12 lysines available for chemical modification[348]. Importantly, bee venom PLA2 extracted from honey bee venom glands is commercially available and relatively inexpensive.

Bee venom PLA2 has been used in previous studies in attempts to improve nonviral delivery of DNA to cells in vitro[393–395]. Our initial attempts to prepare PLA2 for DNA delivery involved attaching the polyacridine peptide (Acr-Lys)$_6$-Cys to the lysines of PLA2 through the heterobifunctional crosslinker GMBS (**Fig. 5-3**). This was done to try and produce a version of PLA2 that could bind DNA and still digest cellular membranes. PLA2 could be labeled with multiple peptides, but the reaction was never able to go to completion, and enzyme activity was lost. Excess free (Acr-Lys)$_6$-Cys was also very difficult to remove, which would have interfered with binding to DNA. Due to loss of activity and purification problems, this project was halted in favor of other PLA2 labeling strategies. However, an interesting phenomenon was observed where PLA2 labeled with (Acr-Lys)$_6$-Cys retained more activity than PLA2 labeled with GMBS

alone. This may have been because GMBS replaces a hydrophilic lysine with a hydrophobic maleimide, while the $(Acr\text{-}Lys)_6$-Cys peptide adds several additional lysines to restore solubility.

A PLA2-Avidin-$(Acr\text{-}Lys)_6$ complex was designed using biotinylated PLA2 and $(Acr\text{-}Lys)_6$-Cys. PLA2 was biotinylated with an NHS-Biotin compound, which did not seem to harm activity (**Fig. 5-4**). When this PLA2-Biotin was bound to Avidin, enzyme activity was lost. When very small amounts of Avidin were used, little activity was lost. When Avidin was added in a 1:1 ratio to PLA2, almost all activity was lost. This is likely due to the formation of crosslinked PLA2-Avidin aggregates. When aggregates were incubated with a large excess of free biotin, PLA2 activity was restored, demonstrating that Avidin binding could be reversed.

The $(Acr\text{-}Lys)_6$-Cys peptide was biotinylated with a Maleimide-PEG_2-Biotin compound. LC-MS showed that the biotinylation was successful (**Fig. 5-5**), but that approximately 20% of the biotin had been oxidized to form biotin sulfoxide[399], which has reduced affinity for Avidin.

DNA, $(Acr\text{-}Lys)_6$-Biotin, Avidin, and PLA2-Biotin were mixed and analyzed on agarose gel electrophoresis (**Fig. 5-6**). When mixed in equal molar amounts, visible flocculation occurred, suggesting that Avidin was crosslinking plasmids and creating large aggregates. To prevent aggregation, the amount of Avidin was increased to 4 fold excess over peptide and PLA2-Biotin was increased to 4 fold excess over Avidin. DNA migration could be inhibited by addition of $(Acr\text{-}Lys)_6$-Biotin and Avidin, however, addition of PLA2-Biotin restored some DNA migration. This is most likely due to PLA2-Biotin displacing some $(Acr\text{-}Lys)_6$-Biotin from Avidin, freeing the DNA from the complex. When PLA2 biotinylation was changed to use less biotin, this displacement was no longer seen. Interestingly, DNA migration could be partially inhibited by addition of Avidin alone, suggesting that Avidin could bind DNA on its own, most

likely through electrostatic interaction.

The DNA-$(Acr\text{-}Lys)_6$-Avidin complex was hydrodynamically dosed into mice to see how it affected in vivo transfection (**Fig. 5-6**). Unfortunately, bioluminescent signal from the Avidin complexes was much smaller than DNA $(Acr\text{-}Lys)_6$-Cys-PEG_{5kDa} controls. The large amount of protein attached to the DNA could have adversely affected the biodistribution and pharmacokinetic profiles, even in direct hydrodynamic injection. Even replacing 5% of $(Acr\text{-}Lys)_6$-Cys-PEG_{5kDa} with $(Acr\text{-}Lys)_6$-Cys-Biotin reduced bioluminescent signal after hydrodynamic dosing.

A simpler hydrodynamic dosing experiment was designed by dosing mice with 1 μg of pGL3 plasmid DNA and 0 – 50 μg of unmodified bee venom PLA2 (**Fig. 5-7**). As the amount of PLA2 increased, the bioluminescent signal decreased. At doses above 10 μg, mice quickly died. The loss of signal was most likely due to PLA2 destroying hepatocytes that would have been transfected and produce luciferase. The deaths were most likely caused by digestion of red blood cells. This experiment demonstrated that PLA2 activity must be very carefully controlled and directed not just to specific cells, but to specific membranes in those cells.

To help direct PLA2 activity to the membranes of the nuclear envelope, the SV40 nuclear localizing sequence[146], NLS, peptide was added to PLA2 through either a maleimide or thiopyridine reaction. PLA2 was reacted with 2-Iminothiolane to create free thiols attached to the lysines of the enzyme. Initial activity measurements did not show much loss of activity (**Fig. 5-8**), but later reactions with 2-Iminothiolane showed activity loss (**Fig. 5-12, Fig. 5-13**). This loss was most likely caused by formation of PLA2 dimers, trimers, etc through disulfide bond formation. These higher mass complexes were seen on SDS-PAGE gels prepared without β-

mercaptoethanol, which would have reduced the disulfide bond linking PLA2 to NLS. This also explains why initial measurements showed full activity, since the PLA2-Iminothiolane was tested for enzyme activity immediately after preparation and very little time was given to form aggregates.

NLS peptide was prepared with dithiodipyridine, DTDP, to produce NLS-Thiopyridine, which was verified by LC-MS (**Fig. 5-9**). NLS-Maleimide peptide was provided. Both peptides were used to label PLA2-Iminothiolane (**Fig. 5-10**). When the reaction between PLA2-Iminothiolane and NLS-Thiopyridine or NLS-Maleimide was run for a short amount of time, PLA2 activity was not damaged by addition of NLS. When the reaction allowed to continue for 7 hr, the PLA2-Iminothiolane control lost about half of its acitivity, while PLA2-NLS lost less activity, again suggesting that addition of peptide to PLA2 protected activity, similarly to how the addition of $(Acr\text{-}Lys)_6$-Cys protected PLA2 after modification by GMBS. When PLA2-NLS was analyzed by SDS-PAGE electrophoresis, PLA2-NLS produced with NLS-Thiopyridine did not migrate through the gel, suggesting that large aggregates had been formed through disulfide bonds. However, the PLA2-NLS produced with NLS-Maleimide migrated through the gel, but showed signs of PLA2 dimers and trimers. No visible band shift was seen to suggest PLA2 had been modified by NLS. When PLA2-NLS was treated with TCEP to reduce disulfide bonds, some migration was restored to PLA2-NLS produced with NLS-Thiopyridine, but bands were still faint. PLA2-NLS produced with NLS-Maleimide showed no higher mass bands, suggesting that the PLA2 dimers and trimers had been reduced.

PLA2-NLS produced with either NLS peptide was delivered to mice in 1 μg doses by hydrodynamic dosing with 1 μg doses of pGL3 plasmid DNA (**Fig. 5-10**). Both PLA2-NLS

samples produced slightly less bioluminescent signal than the control DNA dose, and slightly more signal than an unmodified PLA2 control, however no differences were significant. The slight improvement of PLA2-NLS over PLA2 may be explained by the PLA2-NLS having less activity than unmodified PLA2, therefore causing less damage to hepatocytes.

To help direct PLA2 to hepatocytes, bee venom PLA2 was modified by attaching the triantennary oligosaccharide, Tri, isolated from bovine fetuin. Tri contains terminal galactose residues and binds to the Asialogylcoprotien Receptor, ASGPR[198], which is abundant on hepatocytes. Once bound to ASGPR, the receptor and Tri are internalized through endocytosis. Tri can be attached to other molecules to direct them toward hepatocytes and get them into endosomes.

PLA2-Iminothiolane was reacted with Iodoacetamide-Tri, I-Tri (**Fig. 5-11**). At larger excesses of I-Tri, SDS-PAGE analysis showed laddering, with higher mass bands indicating PLA2 modified with 1 or 2 Tri molecules (**Fig. 5-12**). PLA2 activity was severely damaged when PLA2-Iminothiolane was reacted with small amounts of I-Tri, but larger excesses of I-Tri protected PLA2 activity, again demonstrating protection by adding components to the protein. However, most of the PLA2 in the reactions was not labeled with Tri, and attempts were made to drive the reaction further to completion by using larger amounts of 2-Iminothiolane to modify PLA2. However, these larger amounts of 2-Iminothiolane caused greater harm to PLA2 activity, and I-Tri addition was not able to recover activity. When analyzed by SDS-PAGE, PLA2-Iminothiolane without Tri showed dimer formation, while PLA2 with Tri showed bands for singly modified PLA2-Tri. However, these conditions were still unable to drive the reaction toward completion. The reaction was allowed to run for 24 hr, with samples taken at several time

points and analyzed for PLA2 activity and by SDS-PAGE. As the reaction continued, PLA2 activity was lost. Even though single and double modified PLA2-Tri appeared on the gel with increasing time, unmodified PLA2 was not eliminated.

The loss of activity alongside being unable to completely label PLA2 meant this strategy would not work well. The unmodified PLA2 would not be targeted toward hepatocytes and might still be harmful to red blood cells. The addition of Tri to PLA2 might be responsible for the loss of activity depending on where it bound to the protein. If the Tri were added to a lysine on the membrane binding surface of the enzyme, it might not be able to bind to cellular membranes and access the phospholipids.

To produce a PLA2-Tri with a reversible linkage, Tri-Thiopyridine was produced by reacting Tri with DTDP (**Fig. 5-13**). Tri-Thiopyridine was reacted with PLA2-Iminothiolane in 20 fold excess. Again, addition of Tri protected PLA2 activity compared to PLA2-Iminothiolane. SDS-PAGE of PLA2-Tri showed several bands, indicating multiple additions of Tri to PLA2, with smaller amounts of unmodified PLA2. This suggests that the Tri-Thiopyridine is more reactive with PLA2-Iminothiolane than I-Tri. However, not even the improved PLA2-Tri reaction went to completion and some unmodified PLA2 remained.

To separate PLA2-Tri from unmodified PLA2, a lectin column was used to bind PLA2-Tri by the terminal galactose residues and allow unmodified PLA2 to wash through. Though bee venom PLA2 is glycosylated, its oligosaccharides have mostly terminal mannose, with some fucose, and even less N-acetyl-galactosamine instead of galactose[373], and doesn't bind the column. PLA2-Tri could be bound to the column and eluted off with lactose (**Fig. 5-14**), efficiently separating it from unmodified PLA2. The PLA2 in each fraction could be measured

by PLA2 activity assay and SDS-PAGE shows that unmodified PLA2 can be totally removed from PLA2-Tri. However, the lectin column proved to be fragile, and eventually stopped binding PLA2-Tri. Care must be taken to monitor the column for binding ability and the column should be replaced once it no longer separates PLA2-Tri from unmodified PLA2.

Using bee venom PLA2 extracted from bees imposed some limitations on producing modified PLA2. Bee sting allergy is fairly common and potentially dangerous[404], and using bee venom protein could trigger harmful allergic reactions in human patients. It also creates uncertainty in chemical modification, since a lysine modifying reagent could target any of the 12 lysines on the enzyme, and different lysines may have different affects on enzyme activity. Some enzymes may also receive multiple modifications. By expressing recombinant PLA2 in bacterial systems, it is possible to introduce mutations that may allow site specific modification. It also removes the glycosylation normally found on bee venom PLA2, potentially reducing it's allergenic potential. However, bee venom PLA2 is not easy to express in bacteria. The enzyme is usually packaged into inclusion bodies, and must be recovered, unfolded, and refolded[379]. Recombinant expression also allows the production of human forms of PLA2, which should be less likely to cause an allergic reaction.

Several variants of bee venom PLA2 were produced, some with or without the leader peptides responsible for directing the nascent enzyme through the secretion pathway during synthesis and keeping the enzyme inactive in the bee venom gland, some with nuclear localizing sequences, some with cysteines mutated to alanine to break disulfide bonds and create free thiols, and one with an inactive active site. The middle domain of human PLA2 Group III and PLA2 Group X were chosen because their size, sequence, and folding were fairly similar to bee venom

PLA2. These genes were synthesized and inserted into PET28 plasmid for bacterial production.

Bee venom PLA2 C37A and C113A were produced in bacteria as a proof of concept that the enzymes could be produced and purified and chemically modified. While active enzymes could be recovered, yields were lower than desired (**Fig. 5-15**). Chemical modification of the purified refolded recombinant enzymes failed, and they did not show much reactivity with iodoacetamide or maleimide containing compounds (**Fig. 5-16**). It is likely that their poor reactivity can be explained by reducing agents used in the refolding process, such as glutathione and dithiothreitol. If these compounds form disulfide bonds with the free thiols created in the mutant PLA2, then those thiols would not be available for modification with maleimide or iodoacetamide. This hypothesis is supported by the presence of glutathione disulfide and small amounts of free glutathione in samples of purified PLA2 C37A (**Fig. 5-18**).

Attempts to reduce disulfide bonds in PLA2 mutants or wild type bee venom PLA2 with TCEP and then label them with iodoacetamide or maleimide containing reagents were also not successful (**Fig. 5-17**). Wild type PLA2 reduced with TCEP was double labeled with PEG_{5kDa}-Maleimide in one experiment at 37 °C, but was not labeled in another reaction at 42 °C. Recombinant PLA2 was not efficiently labeled under any conditions.

Wild type bee venom Phospholipase A2 was able to be modified with DNA binding $(Acr\text{-}Lys)_6$-Cys peptide, nuclear localizing NLS peptides, Avidin binding biotin, and hepatocyte targeting triantenarry oligosaccharide. However, it was not possible to reliably control how many times a PLA2 was labeled, and heterogeneous labeling was common. Pushing the labeling reactions to completion also proved difficult, and significant amounts of unlabeled PLA2 remained in almost all reactions. Preserving PLA2 activity was also problematic, especially

when labeled with 2-Iminothiolane. PLA2-Iminothiolane would form disulfide bonds and aggregates with no PLA2 activity. PLA2 mutants could be produced in bacteria and refolded, but was not efficiently labeled.

It may be better to produce PLA2 in eukaryotic systems such as yeast or insect cells[388,391,392]. These would be much closer to the environment bee venom PLA2 is normally produced in, and would probably eliminate the need to unfold and refold the enzyme. Alternatively, an artificial amino acid[405] could be used to provide a unique handle for chemical modification while leaving the native disulfide bonds in place. A recent report[406], demonstrated that denatured lysozyme from boiled eggs could be unfolded, then rapidly and efficiently refolded using a "vortex fluid device". This method might be applicable to recombinant PLA2 production.

6 Research Summary

The human liver is vital to the metabolism of many endogenous and exogenous compounds, and the production site for most important proteins in the bloodstream. As such, it is subject to a wide variety of genetic metabolic disorders, infectious diseases, and cancers[5,27]. Liver transplantation is often used to treat these issues, but the number of donor livers available is too low, even with live donor transplantation[407]. Therefore, gene therapy has become an attractive goal for treating liver disease[28].

While viral gene therapy has had some success in vivo[45], it faces significant challenges, such as immune reaction, large scale production, and quality control[408]. Nonviral gene therapy should avoid many of these issues, but has not been nearly as efficient as viral gene therapy in in vivo applications[409].

The research presented in this thesis has focused on improving the nonviral delivery of DNA or mRNA to the liver. Chapter 2 presented work on the in vitro nonviral transfection of HepG2 cells or primary hepatocytes in 384 and 1536 wellplates. Even though in vitro transfections fail to account for biodistribution, pharmacokinetics, circulation, or other phenomenon found in whole animal models, they can be used to study receptor binding, polyplex internalization, endosomal escape, and nuclear entry. Additionally, in vitro transfection can be used to genetically modify cells taken from a patient's tissues before reimplantation, allowing the modified cells to provide the metabolic functions missing from the rest of the tissue[30].

By miniaturizing the transfection assays, more transfection agents can be tested at a time, leveraging the advantages of high-throughput screening for in vitro transfection. This should help

discover new transfection agents that offer more efficient transfection, less toxicity, or more precise targeting to specific cell types.

Mammalian cancer cell lines are used in most in vitro transfection studies. They are easy to obtain and maintain in culture, however they may not accurately represent cells in an in vivo environment. By using primary hepatocytes, more accurate conditions can be studied. This places a higher standard on transfection agents, because the primary cells are more vulnerable to toxicity and do not rapidly divide. Despite issues with nuclear entry, PEI and calcium phosphate were both able to transfect primary hepatocytes, with calcium phosphate DNA nanoparticles being the more effective of the two. Miniaturization of the assay is even more beneficial when using primary cells, where the number of cells that can be obtained from a single animal is limited. The 384 wellplate allows many more samples to be tested from one cell preparation.

Nonviral delivery of DNA in vivo is much more difficult than transfection in vitro. In vivo, the DNA must be protected against degradation by nucleases, must find its target tissues, be taken up by the cells, and enter the nucleus to be expressed. Polyintercalating polyacridine peptides have been shown to protect DNA against degradation by nucleases and increase the time that DNA can circulate in the bloodstream of a mouse while remaining transfection competent through hydrodynamic stimulation. However, the mechanism behind delayed hydrodynamic stimulation was not fully understood.

Chapter 3 presents work that helped to elucidate the mechanism behind delayed hydrodynamic stimulation, while further improving the time that DNA peptide polyplexes could circulate. The polyplexes were shown to bind serum proteins and become negatively charged. These negatively charged particles were susceptible to uptake by scavenger receptors on Kupffer

cells and sinusoidal endothelial cells. By using 50 – 100 μg doses of polyplex, scavenger receptors could be saturated, allowing DNA polyplexes to be hydrodynamically stimulated at times up to 12 hr post-injection. The PEGylated peptides themselves were also able to bind serum proteins and form small nanoparticles capable of inhibiting scavenger receptors and extending DNA polyplex circulation time.

Once scavenger receptors were inhibited, polyplexes showed a delayed uptake into the liver. This suggested that the polyplexes were crossing sinusoidal fenestrae and entering the Space of Disse. Polyplexes in the Space of Disse were protected against scavenger receptor uptake and could be forced into hepatocytes by the high pressure of a hydrodynamic injection of normal saline.

Inhibiting scavenger receptors to extend circulation time should also be applicable to other types of nanoparticles, such as liposomes or viruses[263–267]. By extending circulation time, the particles have more time to find their target tissues and are more likely to be successfully delivered, reducing the number of particles that need to be injected. Since simple PEGylated polylysine peptides were able to inhibit scavenger receptors, they may be useful as general rapid uptake inhibitors with other types of nanoparticles.

While inhibiting scavenger receptors increased the time DNA peptide polyplexes could circulate in the bloodstream, hydrodynamic stimulation was still required to force the DNA into hepatocytes. One problem with DNA delivery research is that in order to see any expression, the DNA must not only enter the cells, but must also escape the endosome and enter the nucleus. If any step fails, there may not be any detectable signal, and it would not be possible to determine which step failed.

In recent years, there has been significant interest in mRNA delivery. mRNA has the advantage of not needing to enter the nucleus to produce protein, eliminating one of the steps and simplifying the delivery process. However, mRNA is much more susceptible to nuclease digestion than DNA, and must be better protected.

Chapter 4 presents work towards using mRNA in hydrodynamic injection. The only other reported uses of hydrodynamic injection for mRNA delivery were able to produce a detectable amount of luciferase in the liver at 4 – 12 hr when a large amount of mRNA was used[174,175]. The work presented here significantly improved the efficiency with the addition of untranslated regions to improve the mRNA's half-life in the cytoplasm and codon optimization to increase the amount of protein the mRNA could make. PEGylated polyacridine peptides were demonstrated to bind mRNA and further enhanced luciferase expression after hydrodynamic injection, so that 1 μg of mRNA peptide polyplex was able to produce 10^9 photons/sec/cm^2/steradian, 10 fold higher signal than a 1 μg dose of pGL3 plasmid DNA. Furthermore, PEGylated polyacridine peptides were able to provide some protection to mRNA against RNases in mouse serum.

However, mRNA could not be protected in the bloodstream for 5 min, and did not work with delayed hydrodynamic stimulation. The extreme vulnerability of mRNA to RNases makes it very difficult to deliver mRNA in vivo. There are two potential general strategies to improve the stability of mRNA peptide polyplexes in the bloodstream, either modify the peptide or modify the RNA. While the polyacridine peptides have been extensively studied[184,185], one structural feature that has not been thoroughly explored is the linker between the acridine and peptide backbone. Currently, the acridine is attached directly to the epsilon amine of a lysine, but this may not be long enough to reach inside the RNA double helix, which is an A type helix[309]. The

base pairs of an A type helix are more steeply tilted than in the B type helix commonly found in DNA, it also has a deeper major groove and shallower minor groove. These structural differences may reduce the peptide's affinity for the RNA double helix. If the acridine were attached to the lysine epsilon amine through a longer, more flexible, linker, it may overcome the different helical structure and improve binding.

Altering the mRNA to improve polyplex stability would involve increasing the amount of double strandedness in the RNA, since the acridines intercalate into double stranded RNA. While mRNA usually adopts a complex secondary structure with some double stranded portions, much of the molecule remains single stranded, especially the 3' polyA tail. The addition of polyuridine or other RNA homopolymers may increase the amount of double stranded RNA by binding to the polyA tail or simply burying the mRNA inside a larger RNA peptide polyplex. Immogenicity and toxicity associated with PolyA·PolyU duplexes may be reduced by replacing uridine with pseudouridine, based on other work using pseudouridine in mRNA[294,296].

If the mRNA stability issues can be solved, mRNA delivery could not only be used as a tool to debug DNA delivery by testing methods to target cells, internalize polyplexes, and escape endosomes, but could be therapeutically useful by itself. While delivered mRNA would only be able to produce proteins temporarily, such short term production may be desirable in situations where the protein product is potentially toxic. Some of these proteins may include anticancer applications[298], or genome editing applications, such as CRISPR/CAS-9[172], TALEN endonucleases[410], zinc finger endonucleases[411], or transposases[174].

One challenge faced by DNA or mRNA delivery is crossing cellular membranes. While endosomal escape is often achieved through the proton sponge effect[61,99,100] or fusogenic

peptides[113], phospholipase enzymes are also capable of disrupting membranes[393] and may be able to be engineered to assist with nuclear entry of DNA. Chapter 5 presented work on the chemical modification of bee venom PLA2 and recombinant expression of mutant forms of PLA2. While the project failed to develop a useful product for enhancing DNA delivery, some progress was made towards developing techniques to label PLA2 with peptides and oligosaccharides, as well as purifying the modified protein away from unmodified enzyme. Attempts to recombinantly produce bee venom PLA2 were difficult and ran into trouble with preserving the free thiols that were needed for site specific labeling. These issues may be overcome by expression in eukaryotic cells[388,391,392], where the proteins can be properly folded and secreted, and with artificial amino acids[405], which would allow the site specific addition of bioorthogonal functional groups that can be labeled without interfering with the protein's lysines or cysteines.

The toxicity observed when large amounts of PLA2 were injected into mice suggests that it may have potential as a cytotoxic agent if properly targeted and controlled. It may be that mRNA delivery could be useful to produce PLA2 inside target cells to disrupt cellular membranes and induce apoptosis. mRNA delivered alongside DNA might be able to produce PLA2 or other proteins that induce the nuclear envelope to break down and allow DNA to enter the nucleus.

Nonviral gene delivery is still a very challenging problem with much work left to do. However, PEGylated polyacridine peptides have greatly improved the stability of DNA in the bloodstream and may play an important role in a future therapeutic nonviral DNA delivery application. This thesis presents significant progress toward that goal, by developing assays for nonviral gene delivery that may be applied toward the high-throughput screening of gene transfer

agents, by demonstrating the importance of scavenger receptors for DNA polyplex delivery and how scavenger receptor inhibition can extend circulation time, and by applying PEGylated polyacridine peptides to mRNA delivery to enhance expression in hydrodynamic injection and provide some protection against nucleases.

Hopefully, this research has helped to build a foundation for further discoveries with applications that improve human health and quality of life.

Works Cited

1. Hesiod. *Hesiod, Homeric Hymns, Epic Cycle, Homerica*. (Loeb Classical Library, 1914).

2. Jeyes, U. The 'Palace Gate' of the Liver: A Study of Terminology and Methods in Babylonian Extispicy. *J. Cuneif. Stud.* **30,** 209–233 (1978).

3. Horowitz, W., Oshima, T. & Winitzer, A. Hazor 17: Another Clay Liver Model. *Isr. Explor. J.* **60,** 133–145 (2010).

4. Jaeschke, H. in *Casarett & Doull's Toxicology: The Basic Science of Poisons* (ed. Klaassen, C. D.) 557–582 (McGraw Hill Medical, 2008).

5. Mccuskey, R. S. in *Zakim and Boyer's Hepatology: a Textbook of Liver Disease* (eds. Boyer, T. D., Manns, M. P. & Sanyal, A. J.) 3–19 (Elsevier, 2012).

6. Juza, R. M. & Pauli, E. M. Clinical and surgical anatomy of the liver: A review for clinicians. *Clin. Anat.* **27**, 764-769 (2014).

7. Wisse, E., Jacobs, F., Topal, B., Frederik, P. & De Geest, B. The size of endothelial fenestrae in human liver sinusoids: implications for hepatocyte-directed gene transfer. *Gene Ther.* **15,** 1193–1199 (2008).

8. Wisse, E., De Zanger, R. B., Charels, K., Van Der Smissen, P. & Mccuskey, R. S. The Liver Sieve: Considerations Concerning the Structure and Function of Endothelial Fenestrae, the Sinusoidal Wall and the Space of Disse. *Hepatology* **5,** 683–692 (1985).

9. Le Couteur, D. G. *et al.* Old Age and the Hepatic Sinusoid. *Anat. Rec. Adv. Integr. Anat. Evol. Biol.* **291,** 672–683 (2008).

10. Brunt, E. M. *et al.* Pathology of the liver sinusoids. *Histopathology* **64,** 907–920 (2014).

11. Sørensen, K. K. *et al.* The scavenger endothelial cell: a new player in homeostasis and immunity. *Am. J. Physiol. - Regul. Integr. Comp. Physiol.* **303,** R1217–R1230 (2012).

12. Tietz, P. S. & Larusso, N. F. Cholangiocyte biology. *Curr. Opin. Gastroenterol.* **22,** 279–287 (2006).

13. Schramm, W. The history of haemophilia – a short review. *Thromb. Res.* **134**, S4-S9 (2014)**.**

14. Bolton-Maggs, P. H. & Pasi, K. J. Haemophilias A and B. *The Lancet* **361,** 1801–1809 (2003).

15. Walsh, C. E. & Batt, K. M. Hemophilia clinical gene therapy: brief review. *Transl. Res.*

161, 307–312 (2013).

16. Qiu, X. *et al.* Implantation of autologous skin fibroblast genetically modified to secrete clotting factor IX partially corrects the hemorrhagic tendencies in two hemophilia B patients. *Chin. Med. J. (Engl.)* **109,** 832–839 (1996).

17. Roth, D. A. *et al.* Nonviral transfer of the gene encoding coagulation factor VIII in patients with severe hemophilia A. *N. Engl. J. Med.* **344,** 1735–1742 (2001).

18. Powell, J. S. *et al.* Phase 1 trial of FVIII gene transfer for severe hemophilia A using a retroviral construct administered by peripheral intravenous infusion. *Blood* **102,** 2038–2045 (2003).

19. Manno, C. S. *et al.* Successful transduction of liver in hemophilia by AAV-Factor IX and limitations imposed by the host immune response. *Nat. Med.* **12,** 342–347 (2006).

20. Nathwani, A. C. *et al.* Long-term safety and efficacy following systemic administration of a self-complementary AAV vector encoding human FIX pseudotyped with serotype 5 and 8 capsid proteins. *Mol. Ther. J. Am. Soc. Gene Ther.* **19,** 876–885 (2011).

21. Pipe, S. W. & Kaufman, R. J. Characterization of a genetically engineered inactivation-resistant coagulation factor VIIIa. *Proc. Natl. Acad. Sci.* **94,** 11851–11856 (1997).

22. Monahan, P. E. & Gui, T. Gene therapy for hemophilia: advancing beyond the first clinical success. *Curr. Opin. Hematol.* **20,** 410–416 (2013).

23. Stoller, J. K. & Aboussouan, L. S. α1-antitrypsin deficiency. *The Lancet* **365,** 2225–2236 (2005).

24. Flotte, T.R. *et al*. Phase I Trial of Intramuscular Injection of a Recombinant Adeno-Associated Virus Alpha 1-Antitrypsin (rAAV2-CB-hAAT) Gene Vector to AAT-Deficient Adults. *Hum. Gene Ther.* **15,** 93–128 (2004).

25. Kanwar, P. & Kowdley, K. V. Metal Storage Disorders: Wilson Disease and Hemochromatosis. *Med. Clin. North Am.* **98,** 87–102 (2014).

26. Anderson, E. R. & Shah, Y. M. Iron Homeostasis in the Liver. *Comprehensive Physiology* **3**, 315-330 (2013)

27. Fagiuoli, S., Daina, E., D'Antiga, L., Colledan, M. & Remuzzi, G. Monogenic diseases that can be cured by liver transplantation. *J. Hepatol.* **59,** 595–612 (2013).

28. Cassiman, D. Gene Transfer for Inborn Errors of Metabolism of the Liver: The Clinical Perspective. *Curr. Pharm. Des.* **17,** 2550–2557 (2011).

29. Schmitt, F. *et al.* Lentiviral Vectors That Express UGT1A1 in Liver and Contain miR-142 Target Sequences Normalize Hyperbilirubinemia in Gunn Rats. *Gastroenterology* **139,** 999–1007. (2010).

30. Ambrosino, G. *et al.* Isolated Hepatocyte Transplantation for Crigler-Najjar Syndrome Type 1. *Cell Transplant.* **14,** 151–157 (2005).

31. Birraux, J. *et al.* A Step Toward Liver Gene Therapy: Efficient Correction of the Genetic Defect of Hepatocytes Isolated From a Patient With Crigler-Najjar Syndrome Type 1 With Lentiviral Vectors. *Transplant.* **87,** 1006–1012 (2009).

32. Hoffmann, G. F. & Kölker, S. in *Handbook of Clinical Neurology* (ed. Olivier Dulac, M. L. and H. B. S.) **113,** 1755–1773 (Elsevier, 2013).

33. Raper, S. E. *et al.* A Pilot Study of In Vivo Liver-Directed Gene Transfer with an Adenoviral Vector in Partial Ornithine Transcarbamylase Deficiency. *Hum. Gene Ther.* **13,** 163–175 (2002).

34. Blau, N., van Spronsen, F. J. & Levy, H. L. Phenylketonuria. *The Lancet* **376,** 1417–1427 (2010).

35. Prick, B. W., Hop, W. C. & Duvekot, J. J. Maternal phenylketonuria and hyperphenylalaninemia in pregnancy: pregnancy complications and neonatal sequelae in untreated and treated pregnancies. *Am. J. Clin. Nutr.* **95,** 374–382 (2012).

36. Yagi, H. *et al.* Recovery of neurogenic amines in phenylketonuria mice after liver-targeted gene therapy. *Neuroreport* **23,** 30–34 (2012).

37. Viecelli, H. M. *et al.* Treatment of phenylketonuria using minicircle-based naked-DNA gene transfer to murine liver. *Hepatology* **60**, 1035-1043 (2014).

38. Scott, C. R. The genetic tyrosinemias. *Am. J. Med. Genet. C Semin. Med. Genet.* **142C,** 121–126 (2006).

39. Aquaron, R. Alkaptonuria: a very rare metabolic disorder. *Indian J. Biochem. Biophys.* **50,** 339–344 (2013).

40. Hicks, J., Wartchow, E. & Mierau, G. Glycogen Storage Diseases: A Brief Review and Update on Clinical Features, Genetic Abnormalities, Pathologic Features, and Treatment. *Ultrastruct. Pathol.* **35,** 183–196 (2011).

41. Chou, J. Y. & Mansfield, B. C. Recombinant AAV-directed gene therapy for type I glycogen storage diseases. *Expert Opin. Biol. Ther.* **11,** 1011–1024 (2011).

42. Koeberl, D. D., Pinto, C., Brown, T. & Chen, Y. T. Gene Therapy for Inherited Metabolic Disorders in Companion Animals. *ILAR J.* **50,** 122–127 (2009).

43. Byrne, B. J. *et al.* Pompe disease gene therapy. *Hum. Mol. Genet.* **20,** R61–R68 (2011).

44. Mah, C. S. *et al.* Adeno-Associated Virus–Mediated Gene Therapy for Metabolic Myopathy. *Hum. Gene Ther.* **24,** 928–936 (2013).

45. Pollack, A. European Agency Recommends Approval of a Gene Therapy. *The New York Times* (2012).

46. Kawabata, K., Takakura, Y. & Hashida, M. The fate of plasmid DNA after intravenous injection in mice: involvement of scavenger receptors in its hepatic uptake. *Pharm. Res.* **12,** 825–830 (1995).

47. Takakura, Y. *et al.* Characterization of plasmid DNA binding and uptake by peritoneal macrophages from class A scavenger receptor knockout mice. *Pharm. Res.* **16,** 503–508 (1999).

48. Lv, H., Zhang, S., Wang, B., Cui, S. & Yan, J. Toxicity of cationic lipids and cationic polymers in gene delivery. *J. Controlled Release* **114,** 100–109 (2006).

49. Jain, K., Kesharwani, P., Gupta, U. & Jain, N. K. Dendrimer toxicity: Let's meet the challenge. *Int. J. Pharm.* **394,** 122–142 (2010).

50. Panté, N. & Kann, M. Nuclear Pore Complex Is Able to Transport Macromolecules with Diameters of ~39 nm. *Mol. Biol. Cell* **13,** 425–434 (2002).

51. Junquera, E. & Aicart, E. Cationic Lipids as Transfecting Agents of DNA in Gene Therapy. *Curr. Top. Med. Chem.* **14,** 649–663 (2014).

52. Zhang, S., Zhi, D. & Huang, L. Lipid-based vectors for siRNA delivery. *J. Drug Target.* **20,** 724–735 (2012).

53. Zhou, T., Llizo, A., Wang, C., Xu, G. & Yang, Y. Nanostructure-induced DNA condensation. *Nanoscale* **5,** 8288–8306 (2013).

54. Mann, A., Thakur, G., Shukla, V. & Ganguli, M. Peptides in DNA delivery: current insights and future directions. *Drug Discov. Today* **13,** 152–160 (2008).

55. Rao, N. M. Cationic lipid-mediated nucleic acid delivery: beyond being cationic. *Chem. Phys. Lipids* **163,** 245–252 (2010).

56. Dass, C. Immunostimulatory activity of cationic-lipid-nucleic-acid complexes against cancer. *J. Cancer Res. Clin. Oncol.* **128,** 177–181 (2002).

57. Semple, S. C. *et al.* Rational design of cationic lipids for siRNA delivery. *Nat. Biotechnol.* **28,** 172–176 (2010).

58. Semple, S. C., Chonn, A. & Cullis, P. R. Interactions of liposomes and lipid-based carrier systems with blood proteins: Relation to clearance behaviour in vivo. *Adv. Drug Deliv. Rev.* **32,** 3–17 (1998).

59. Basha, G. *et al.* Influence of Cationic Lipid Composition on Gene Silencing Properties of Lipid Nanoparticle Formulations of siRNA in Antigen-Presenting Cells. *Mol. Ther.* **19**, 2186-2200 (2011).

60. Heyes, J., Hall, K., Tailor, V., Lenz, R. & MacLachlan, I. Synthesis and characterization of novel poly(ethylene glycol)-lipid conjugates suitable for use in drug delivery. *J. Controlled Release* **112,** 280–290 (2006).

61. Patnaik, S. & Gupta, K. C. Novel polyethylenimine-derived nanoparticles for in vivo gene delivery. *Expert Opin. Drug Deliv.* **10,** 215–228 (2013).

62. Tschiche, A., Malhotra, S. & Haag, R. Nonviral gene delivery with dendritic self-assembling architectures. *Nanomed.* **9,** 667–693 (2014).

63. Tiera, M. J., Shi, Q., Winnik, F. M. & Fernandes, J. C. Polycation-based gene therapy: current knowledge and new perspectives. *Curr. Gene Ther.* **11,** 288–306 (2011).

64. Mansouri, S. *et al.* Chitosan-DNA nanoparticles as non-viral vectors in gene therapy: strategies to improve transfection efficacy. *Eur. J. Pharm. Biopharm. Off. J. Arbeitsgemeinschaft Für Pharm. Verfahrenstechnik EV* **57,** 1–8 (2004).

65. Eliyahu, H., Barenholz, Y. & Domb, A. J. Polymers for DNA delivery. *Mol. Basel Switz.* **10,** 34–64 (2005).

66. Wightman, L. *et al.* Different behavior of branched and linear polyethylenimine for gene delivery in vitro and in vivo. *J. Gene Med.* **3,** 362–372 (2001).

67. Morimoto, K. *et al.* Molecular weight-dependent gene transfection activity of unmodified and galactosylated polyethyleneimine on hepatoma cells and mouse liver. *Mol. Ther. J. Am. Soc. Gene Ther.* **7,** 254–261 (2003).

68. Schelhaas, M. *et al.* Human Papillomavirus Type 16 Entry: Retrograde Cell Surface Transport along Actin-Rich Protrusions. *PLoS Pathog* **4,** e1000148 (2008).

69. Ur Rehman, Z., Sjollema, K. A., Kuipers, J., Hoekstra, D. & Zuhorn, I. S. Nonviral gene delivery vectors use syndecan-dependent transport mechanisms in filopodia to reach the cell surface. *ACS Nano* **6,** 7521–7532 (2012).

70. Rejman, J., Oberle, V., Zuhorn, I. S. & Hoekstra, D. Size-dependent internalization of particles via the pathways of clathrin- and caveolae-mediated endocytosis. *Biochem. J.* **377,** 159 (2004).

71. Parton, R. G. & Simons, K. The multiple faces of caveolae. *Nat. Rev. Mol. Cell Biol.* **8,** 185–194 (2007).

72. Canton, I. & Battaglia, G. Endocytosis at the nanoscale. *Chem. Soc. Rev.* **41,** 2718–2739 (2012).

73. Lam, A. P. & Dean, D. A. Progress and prospects: nuclear import of nonviral vectors. *Gene Ther.* **17,** 439–447 (2010).

74. Maeda, H., Sawa, T. & Konno, T. Mechanism of tumor-targeted delivery of macromolecular drugs, including the EPR effect in solid tumor and clinical overview of the prototype polymeric drug SMANCS. *J. Controlled Release* **74,** 47–61 (2001).

75. Nichols, J. W. & Bae, Y. H. EPR: Evidence and fallacy. *J. Controlled Release* **190,** 451–464 (2014).

76. Tros de Ilarduya, C. & Düzgüneş, N. Delivery of therapeutic nucleic acids via transferrin and transferrin receptors: lipoplexes and other carriers. *Expert Opin. Drug Deliv.* **10,** 1583–1591 (2013).

77. Wagner, E., Zenke, M., Cotten, M., Beug, H. & Birnstiel, M. L. Transferrin-polycation conjugates as carriers for DNA uptake into cells. *Proc. Natl. Acad. Sci.* **87,** 3410–3414 (1990).

78. Cheng, P.-W. Receptor Ligand-Facilitated Gene Transfer: Enhancement of Liposome-Mediated Gene Transfer and Expression by Transferrin. *Hum. Gene Ther.* **7,** 275–282 (1996).

79. Xu, L., Pirollo, K. F. & Chang, E. H. Transferrin–Liposome-Mediated p53 Sensitization of Squamous Cell Carcinoma of the Head and Neck to Radiation In Vitro. *Hum. Gene Ther.* **8,** 467–475 (1997).

80. Seki, M., Iwakawa, J., Cheng, H. & Cheng, P.-W. p53 and PTEN/MMAC1/TEP1 Gene Therapy of Human Prostate PC-3 Carcinoma Xenograft, Using Transferrin-Facilitated Lipofection Gene Delivery Strategy. *Hum. Gene Ther.* **13,** 761–773 (2002).

81. Camp, E. R. *et al.* Transferrin receptor targeting nanomedicine delivering wild-type p53 gene sensitizes pancreatic cancer to gemcitabine therapy. *Cancer Gene Ther.* **20,** 222–228 (2013).

82. Jiang, Q. *et al.* (Coixan polysaccharide)-graft-Polyethylenimine Folate for Tumor-Targeted Gene Delivery. *Macromol. Biosci.* **11,** 435–444 (2011).

83. Xu, Z. *et al.* Comparisons of three polyethyleneimine-derived nanoparticles as a gene therapy delivery system for renal cell carcinoma. *J. Transl. Med.* **9,** 46-55 (2011).

84. Zhang, C. *et al.* Targeted minicircle DNA delivery using folate–poly(ethylene glycol)–polyethylenimine as non-viral carrier. *Biomaterials* **31,** 6075–6086 (2010).

85. Park, J. *et al.* A review of RGD-functionalized nonviral gene delivery vectors for cancer therapy. *Cancer Gene Ther.* **19,** 741–748 (2012).

86. Zhan, C. *et al.* Cyclic RGD–Polyethylene Glycol–Polyethylenimine for Intracranial Glioblastoma-Targeted Gene Delivery. *Chem. – Asian J.* **7,** 91–96 (2012).

87. Lu, Z.-X., Liu, L.-T. & Qi, X.-R. Development of small interfering RNA delivery system using PEI-PEG-APRPG polymer for antiangiogenic vascular endothelial growth factor tumor-targeted therapy. *Int. J. Nanomedicine* **6,** 1661–1673 (2011).

88. Son, S. *et al.* RVG peptide tethered bioreducible polyethylenimine for gene delivery to brain. *J. Controlled Release* **155,** 18–25 (2011).

89. Shir, A., Ogris, M., Roedl, W., Wagner, E. & Levitzki, A. EGFR-Homing dsRNA Activates Cancer-Targeted Immune Response and Eliminates Disseminated EGFR-Overexpressing Tumors in Mice. *Clin. Cancer Res.* **17,** 1033–1043 (2011).

90. Huang, H., Yu, H., Tang, G., Wang, Q. & Li, J. Low molecular weight polyethylenimine cross-linked by 2-hydroxypropyl-γ-cyclodextrin coupled to peptide targeting HER2 as a gene delivery vector. *Biomaterials* **31,** 1830–1838 (2010).

91. Pi, Y. *et al.* Targeted delivery of non-viral vectors to cartilage in vivo using a chondrocyte-homing peptide identified by phage display. *Biomaterials* **32,** 6324–6332 (2011).

92. Rehman, Z. ur, Zuhorn, I. S. & Hoekstra, D. How cationic lipids transfer nucleic acids into cells and across cellular membranes: Recent advances. *J. Controlled Release* **166,** 46–56 (2013).

93. Zhi, D. *et al.* Synthesis and biological activity of carbamate-linked cationic lipids for gene delivery in vitro. *Bioorg. Med. Chem. Lett.* **22,** 3837–3841 (2012).

94. Yan, J., Korolev, N., Eom, K. D., Tam, J. P. & Nordenskiöld, L. Biophysical properties and supramolecular structure of self-assembled liposome/ε-peptide/DNA nanoparticles: correlation with gene delivery. *Biomacromolecules* **13,** 124–131 (2012).

95. Fielden, M. L. *et al.* Sugar-based tertiary amino gemini surfactants with a vesicle-to-micelle transition in the endosomal pH range mediate efficient transfection in vitro. *Eur. J. Biochem.* **268,** 1269–1279 (2001).

96. Wasungu, L., Stuart, M. C. A., Scarzello, M., Engberts, J. B. F. N. & Hoekstra, D. Lipoplexes formed from sugar-based gemini surfactants undergo a lamellar-to-micellar phase transition at acidic pH. Evidence for a non-inverted membrane-destabilizing hexagonal phase of lipoplexes. *Biochim. Biophys. Acta BBA - Biomembr.* **1758,** 1677–1684 (2006).

97. Zhao, Y.-N. *et al.* Novel Gemini cationic lipids with carbamate groups for gene delivery. *J. Mater. Chem. B* **2,** 2920–2928 (2014).

98. Bell, P. C. *et al.* Transfection mediated by gemini surfactants: engineered escape from the endosomal compartment. *J. Am. Chem. Soc.* **125,** 1551–1558 (2003).

99. Nguyen, J. & Szoka, F. C. Nucleic Acid Delivery: The Missing Pieces of the Puzzle? *Acc. Chem. Res.* **45,** 1153–1162 (2012).

100. Shete, H. K., Prabhu, R. H. & Patravale, V. B. Endosomal escape: a bottleneck in intracellular delivery. *J. Nanosci. Nanotechnol.* **14,** 460–474 (2014).

101. Neuberg, P. & Kichler, A. in *Advances in Genetics* (ed. Leaf Huang, D. L. and E. W.) **88,** 263–288 (Academic Press, 2014).

102. Won, Y.-Y., Sharma, R. & Konieczny, S. F. Missing pieces in understanding the intracellular trafficking of polycation/DNA complexes. *J. Controlled Release* **139,** 88–93 (2009).

103. Kichler, A., Leborgne, C., Coeytaux, E. & Danos, O. Polyethylenimine-mediated gene delivery: a mechanistic study. *J. Gene Med.* **3,** 135–144 (2001).

104. Akinc, A., Thomas, M., Klibanov, A. M. & Langer, R. Exploring polyethylenimine-mediated DNA transfection and the proton sponge hypothesis. *J. Gene Med.* **7,** 657–663 (2005).

105. Yue, Y. *et al.* Revisit complexation between DNA and polyethylenimine — Effect of length of free polycationic chains on gene transfection. *J. Controlled Release* **152,** 143–151 (2011).

106. Sonawane, N. D., Thiagarajah, J. R. & Verkman, A. S. Chloride Concentration in

Endosomes Measured Using a Ratioable Fluorescent Cl− Indicator: Evidence for Chloride Accumulation During Acidification. *J. Biol. Chem.* **277,** 5506–5513 (2002).

107. Sonawane, N. D., Szoka, F. C. & Verkman, A. S. Chloride Accumulation and Swelling in Endosomes Enhances DNA Transfer by Polyamine-DNA Polyplexes. *J. Biol. Chem.* **278,** 44826–44831 (2003).

108. Olton, D. *et al.* Nanostructured calcium phosphates (NanoCaPs) for non-viral gene delivery: Influence of the synthesis parameters on transfection efficiency. *Biomaterials* **28,** 1267–1279 (2007).

109. Olton, D. Y. E., Close, J. M., Sfeir, C. S. & Kumta, P. N. Intracellular trafficking pathways involved in the gene transfer of nano-structured calcium phosphate-DNA particles. *Biomaterials* **32,** 7662–7670 (2011).

110. Hu, Y., Haynes, M. T., Wang, Y., Liu, F. & Huang, L. A Highly Efficient Synthetic Vector: Nonhydrodynamic Delivery of DNA to Hepatocyte Nuclei in Vivo. *ACS Nano* **7,** 5376–5384 (2013).

111. Haynes, M. T. & Huang, L. Lipid-coated calcium phosphate nanoparticles for nonviral gene therapy. *Adv. Genet.* **88,** 205–229 (2014).

112. Zhang, Y., Schwerbrock, N. M., Rogers, A. B., Kim, W. Y. & Huang, L. Codelivery of VEGF siRNA and Gemcitabine Monophosphate in a Single Nanoparticle Formulation for Effective Treatment of NSCLC. *Mol. Ther.* **21,** 1559–1569 (2013).

113. Lee, S. H., Castagner, B. & Leroux, J.-C. Is there a future for cell-penetrating peptides in oligonucleotide delivery? *Eur. J. Pharm. Biopharm.* **85,** 5–11 (2013).

114. Marsh, M. & Helenius, A. Virus Entry: Open Sesame. *Cell* **124,** 729–740 (2006).

115. Gruenberg, J. & van der Goot, F. G. Mechanisms of pathogen entry through the endosomal compartments. *Nat. Rev. Mol. Cell Biol.* **7,** 495–504 (2006).

116. Plank, C., Oberhauser, B., Mechtler, K., Koch, C. & Wagner, E. The influence of endosome-disruptive peptides on gene transfer using synthetic virus-like gene transfer systems. *J. Biol. Chem.* **269,** 12918–12924 (1994).

117. Lear, J. D. & DeGrado, W. F. Membrane binding and conformational properties of peptides representing the NH2 terminus of influenza HA-2. *J. Biol. Chem.* **262,** 6500–6505 (1987).

118. Subramanian, A., Ma, H., Dahl, K. N., Zhu, J. & Diamond, S. L. Adenovirus or HA-2 fusogenic peptide-assisted lipofection increases cytoplasmic levels of plasmid in nondividing endothelium with little enhancement of transgene expression. *J. Gene Med.* **4,**

75–83 (2002).

119. Oliveira, S., van Rooy, I., Kranenburg, O., Storm, G. & Schiffelers, R. M. Fusogenic peptides enhance endosomal escape improving siRNA-induced silencing of oncogenes. *Int. J. Pharm.* **331,** 211–214 (2007).

120. Mastrobattista, E. *et al.* Functional Characterization of an Endosome-disruptive Peptide and Its Application in Cytosolic Delivery of Immunoliposome-entrapped Proteins. *J. Biol. Chem.* **277,** 27135–27143 (2002).

121. Parente, R. A., Nir, S. & Szoka, F. C. Mechanism of leakage of phospholipid vesicle contents induced by the peptide GALA. *Biochemistry (Mosc.)* **29,** 8720–8728 (1990).

122. Futaki, S. *et al.* Unique features of a pH-sensitive fusogenic peptide that improves the transfection efficiency of cationic liposomes. *J. Gene Med.* **7,** 1450–1458 (2005).

123. Sasaki, K. *et al.* An artificial virus-like nano carrier system: enhanced endosomal escape of nanoparticles via synergistic action of pH-sensitive fusogenic peptide derivatives. *Anal. Bioanal. Chem.* **391,** 2717–2727 (2008).

124. Kakudo, T. *et al.* Transferrin-Modified Liposomes Equipped with a pH-Sensitive Fusogenic Peptide: An Artificial Viral-like Delivery System†. *Biochemistry (Mosc.)* **43,** 5618–5628 (2004).

125. Simoes, S. *et al.* Mechanisms of gene transfer mediated by lipoplexes associated with targeting ligands or pH-sensitive peptides. *Gene Ther.* **6,** 1798–1807 (1999).

126. Lee, H., Jeong, J. H. & Park, T. G. A new gene delivery formulation of polyethylenimine/DNA complexes coated with PEG conjugated fusogenic peptide. *J. Controlled Release* **76,** 183–192 (2001).

127. Min, S.-H. *et al.* A composite gene delivery system consisting of polyethylenimine and an amphipathic peptide KALA. *J. Gene Med.* **8,** 1425–1434 (2006).

128. Han, J. & Il Yeom, Y. Specific gene transfer mediated by galactosylated poly-l-lysine into hepatoma cells. *Int. J. Pharm.* **202,** 151–160 (2000).

129. Wyman, T. B. *et al.* Design, Synthesis, and Characterization of a Cationic Peptide That Binds to Nucleic Acids and Permeabilizes Bilayers. *Biochemistry (Mosc.)* **36,** 3008–3017 (1997).

130. Parente, R. A., Nir, S. & Szoka, F. C. pH-dependent fusion of phosphatidylcholine small vesicles. Induction by a synthetic amphipathic peptide. *J. Biol. Chem.* **263,** 4724–4730 (1988).

131. Metkar, S. S. *et al.* Cytotoxic cell granule-mediated apoptosis: perforin delivers granzyme B-serglycin complexes into target cells without plasma membrane pore formation. *Immunity* **16,** 417–428 (2002).

132. Jenssen, H., Hamill, P. & Hancock, R. E. W. Peptide Antimicrobial Agents. *Clin. Microbiol. Rev.* **19,** 491–511 (2006).

133. Ogris, M., Carlisle, R. C., Bettinger, T. & Seymour, L. W. Melittin Enables Efficient Vesicular Escape and Enhanced Nuclear Access of Nonviral Gene Delivery Vectors. *J. Biol. Chem.* **276,** 47550–47555 (2001).

134. Dempsey, C. E. The actions of melittin on membranes. *Biochim. Biophys. Acta BBA - Rev. Biomembr.* **1031,** 143–161 (1990).

135. Legendre, J. Y. & Szoka, F. C. Cyclic amphipathic peptide-DNA complexes mediate high-efficiency transfection of adherent mammalian cells. *Proc. Natl. Acad. Sci.* **90,** 893–897 (1993).

136. Meyer, M., Philipp, A., Oskuee, R., Schmidt, C. & Wagner, E. Breathing Life into Polycations: Functionalization with pH-Responsive Endosomolytic Peptides and Polyethylene Glycol Enables siRNA Delivery. *J. Am. Chem. Soc.* **130,** 3272–3273 (2008).

137. Boeckle, S., Fahrmeir, J., Roedl, W., Ogris, M. & Wagner, E. Melittin analogs with high lytic activity at endosomal pH enhance transfection with purified targeted PEI polyplexes. *J. Controlled Release* **112,** 240–248 (2006).

138. Bettinger, T., Carlisle, R. C., Read, M. L., Ogris, M. & Seymour, L. W. Peptide-mediated RNA delivery: a novel approach for enhanced transfection of primary and post-mitotic cells. *Nucleic Acids Res.* **29,** 3882–3891 (2001).

139. Wooddell, C. I. *et al.* Hepatocyte-targeted RNAi Therapeutics for the Treatment of Chronic Hepatitis B Virus Infection. *Mol. Ther.* **21,** 973–985 (2013).

140. Babcock, H. P., Chen, C. & Zhuang, X. Using Single-Particle Tracking to Study Nuclear Trafficking of Viral Genes. *Biophys. J.* **87,** 2749–2758 (2004).

141. Lai, S. K. *et al.* Privileged delivery of polymer nanoparticles to the perinuclear region of live cells via a non-clathrin, non-degradative pathway. *Biomaterials* **28,** 2876–2884 (2007).

142. Welte, M. A. Bidirectional transport along microtubules. *Curr. Biol. CB* **14,** R525–537 (2004).

143. Carlisle, R. C. *et al.* Adenovirus Hexon Protein Enhances Nuclear Delivery and Increases

Transgene Expression of Polyethylenimine/Plasmid DNA Vectors. *Mol. Ther.* **4,** 473–483 (2001).

144. Suomalainen, M., Nakano, M. Y., Boucke, K., Keller, S. & Greber, U. F. Adenovirus□ activated PKA and p38/MAPK pathways boost microtubule□mediated nuclear targeting of virus. *EMBO J.* **20,** 1310–1319 (2001).

145. Kalderon, D., Richardson, W. D., Markham, A. F. & Smith, A. E. Sequence requirements for nuclear location of simian virus 40 large-T antigen. *Nature* **311,** 33–38 (1984).

146. Kalderon, D., Roberts, B. L., Richardson, W. D. & Smith, A. E. A short amino acid sequence able to specify nuclear location. *Cell* **39,** 499–509 (1984).

147. Wagstaff, K. M. & Jans, D. A. Importins and Beyond: Non-Conventional Nuclear Transport Mechanisms. *Traffic* **10,** 1188–1198 (2009).

148. Marfori, M. *et al.* Molecular basis for specificity of nuclear import and prediction of nuclear localization. *Biochim. Biophys. Acta BBA - Mol. Cell Res.* **1813,** 1562–1577 (2011).

149. Pollard, H. *et al.* Polyethylenimine but Not Cationic Lipids Promotes Transgene Delivery to the Nucleus in Mammalian Cells. *J. Biol. Chem.* **273,** 7507–7511 (1998).

150. Collas, P. & Aleström, P. Nuclear localization signals: a driving force for nuclear transport of plasmid DNA in zebrafish. *Biochem. Cell Biol. Biochim. Biol. Cell.* **75,** 633–640 (1997).

151. Ritter, W. *et al.* A novel transfecting peptide comprising a tetrameric nuclear localization sequence. *J. Mol. Med.* **81,** 708–717 (2003).

152. Chan, C. K. & Jans, D. A. Enhancement of Polylysine-Mediated Transferrinfection by Nuclear Localization Sequences: Polylysine Does Not Function as a Nuclear Localization Sequence. *Hum. Gene Ther.* **10,** 1695–1702 (1999).

153. Ludtke, J. J., Zhang, G., Sebestyen, M. G. & Wolff, J. A. A nuclear localization signal can enhance both the nuclear transport and expression of 1 kb DNA. *J. Cell Sci.* **112,** 2033–2041 (1999).

154. Sebestyén, M. G. *et al.* DNA vector chemistry: The covalent attachment of signal peptides to plasmid DNA. *Nat. Biotechnol.* **16,** 80–85 (1998).

155. Ciolina, C. *et al.* Coupling of Nuclear Localization Signals to Plasmid DNA and Specific Interaction of the Conjugates with Importin α. *Bioconjug. Chem.* **10,** 49–55 (1998).

156. Zanta, M. A., Belguise-Valladier, P. & Behr, J.-P. Gene delivery: A single nuclear localization signal peptide is sufficient to carry DNA to the cell nucleus. *Proc. Natl. Acad.*

Sci. **96,** 91–96 (1999).

157. Tanimoto, M., Kamiya, H., Minakawa, N., Matsuda, A. & Harashima, H. No Enhancement of Nuclear Entry by Direct Conjugation of a Nuclear Localization Signal Peptide to Linearized DNA. *Bioconjug. Chem.* **14,** 1197–1202 (2003).

158. Van der Aa, M. a. E. M. *et al.* An NLS peptide covalently linked to linear DNA does not enhance transfection efficiency of cationic polymer based gene delivery systems. *J. Gene Med.* **7,** 208–217 (2005).

159. Dean, D. A., Strong, D. D. & Zimmer, W. E. Nuclear entry of nonviral vectors. *Gene Ther.* **12,** 881–890 (2005).

160. Dean, D. A., Dean, B. S., Muller, S. & Smith, L. C. Sequence Requirements for Plasmid Nuclear Import. *Exp. Cell Res.* **253,** 713–722 (1999).

161. Dean, D. A. Import of Plasmid DNA into the Nucleus Is Sequence Specific. *Exp. Cell Res.* **230,** 293–302 (1997).

162. Dean, D. A., Byrd, J. N. & Dean, B. S. Nuclear targeting of plasmid DNA in human corneal cells. *Curr. Eye Res.* **19,** 66–75 (1999).

163. Vacik, J., Dean, B. S., Zimmer, W. E. & Dean, D. A. Cell-specific nuclear import of plasmid DNA. *Gene Ther.* **6,** 1006–1014 (1999).

164. Young, J. L., Benoit, J. N. & Dean, D. A. Effect of a DNA nuclear targeting sequence on gene transfer and expression of plasmids in the intact vasculature. *Gene Ther.* **10,** 1465–1470 (2003).

165. Mir, B. & Piedrahita, J. A. Nuclear localization signal and cell synchrony enhance gene targeting efficiency in primary fetal fibroblasts. *Nucleic Acids Res.* **32,** e25 (2004).

166. Blomberg, P., Eskandarpour, M., Xia, S., Sylvén, C. & Islam, K. B. Electroporation in combination with a plasmid vector containing SV40 enhancer elements results in increased and persistent gene expression in mouse muscle. *Biochem. Biophys. Res. Commun.* **298,** 505–510 (2002).

167. Young, J. L., Zimmer, W. E. & Dean, D. A. Smooth Muscle-Specific Gene Delivery in the Vasculature Based on Restriction of DNA Nuclear Import. *Exp. Biol. Med.* **233,** 840–848 (2008).

168. DeGiulio, J. V., Kaufman, C. D. & Dean, D. A. The SP-C promoter facilitates alveolar type II epithelial cell-specific plasmid nuclear import and gene expression. *Gene Ther.* **17,** 541–549 (2010).

169. Miller, A. M. & Dean, D. A. Cell-specific nuclear import of plasmid DNA in smooth muscle requires tissue-specific transcription factors and DNA sequences. *Gene Ther.* **15,** 1107–1115 (2008).

170. Zhang, G., Budker, V. & Wolff, J. A. High Levels of Foreign Gene Expression in Hepatocytes after Tail Vein Injections of Naked Plasmid DNA. *Hum. Gene Ther.* **10,** 1735–1737 (1999).

171. Liu, F., Song, Y. & Liu, D. Hydrodynamics-based transfection in animals by systemic administration of plasmid DNA. *Gene Ther.* **6,** 1258–1266 (1999).

172. Xue, W. *et al.* CRISPR-mediated direct mutation of cancer genes in the mouse liver. *Nature* **514,** 380–384 (2014).

173. Yilmazer, A., de Lázaro, I., Bussy, C. & Kostarelos, K. In Vivo Cell Reprogramming towards Pluripotency by Virus-Free Overexpression of Defined Factors. *PLoS ONE* **8,** e54754 (2013).

174. Wilber, A. *et al.* RNA as a Source of Transposase for Sleeping Beauty-Mediated Gene Insertion and Expression in Somatic Cells and Tissues. *Mol. Ther.* **13,** 625–630 (2006).

175. McCaffrey, A. P. *et al.* Determinants of Hepatitis C Translational Initiation in Vitro, in Cultured Cells and Mice. *Mol. Ther.* **5,** 676–284 (2002).

176. Kobayashi, N. *et al.* Hepatic delivery of particulates in the submicron range by a hydrodynamics-based procedure: implications for particulate gene delivery systems. *J. Gene Med.* **6,** 455–463 (2004).

177. Condiotti, R. *et al.* Prolonged liver-specific transgene expression by a non-primate lentiviral vector. *Biochem. Biophys. Res. Commun.* **320,** 998–1006 (2004).

178. Li, J., Yao, Q. & Liu, D. Hydrodynamic cell delivery for simultaneous establishment of tumor growth in mouse lung, liver and kidney. *Cancer Biol. Ther.* **12,** 737–741 (2011).

179. Kamimura, K. *et al.* Safety Assessment of Liver-Targeted Hydrodynamic Gene Delivery in Dogs. *PLoS ONE* **9,** e107203 (2014).

180. Sendra, L. *et al.* Low RNA translation activit limits the efficacy of hydrodynamic gene transfer to pig liver in vivo. *J. Gene Med.* **16,** 179–192 (2014).

181. Hegge, J. O. *et al.* Evaluation of hydrodynamic limb vein injections in nonhuman primates. *Hum. Gene Ther.* **21,** 829–842 (2010).

182. Chen, C. *et al.* Synthetic PEGylated Glycoproteins and Their Utility in Gene Delivery. *Bioconjug. Chem.* **18,** 371–378 (2007).

183. Fernandez, C. A. *et al.* Metabolically stabilized long-circulating PEGylated polyacridine peptide polyplexes mediate hydrodynamically stimulated gene expression in liver. *Gene Ther.* **18,** 23–37 (2011).

184. Kizzire, K., Khargharia, S. & Rice, K. G. High-affinity PEGylated polyacridine peptide polyplexes mediate potent in vivo gene expression. *Gene Ther.* **20,** 407–416 (2013).

185. Khargharia, S., Kizzire, K., Ericson, M. D., Baumhover, N. J. & Rice, K. G. PEG length and chemical linkage controls polyacridine peptide DNA polyplex pharmacokinetics, biodistribution, metabolic stability and in vivo gene expression. *J. Controlled Release* **170,** 325–333 (2013).

186. Rettig, G. R., McAnuff, M., Liu, D., Kim, J.-S. & Rice, K. G. Quantitative bioluminescence imaging of transgene expression in vivo. *Anal. Biochem.* **355,** 90–94 (2006).

187. McKenzie, D. L., Kwok, K. Y. & Rice, K. G. A Potent New Class of Reductively Activated Peptide Gene Delivery Agents. *J. Biol. Chem.* **275,** 9970–9977 (2000).

188. McKenzie, D. L., Smiley, E., Kwok, K. Y. & Rice, K. G. Low Molecular Weight Disulfide Cross-Linking Peptides as Nonviral Gene Delivery Carriers. *Bioconjug. Chem.* **11,** 901–909 (2000).

189. Park, Y., Kwok, K. Y., Boukarim, C. & Rice, K. G. Synthesis of Sulfhydryl Cross-Linking Poly(Ethylene Glycol)-Peptides and Glycopeptides as Carriers for Gene Delivery. *Bioconjug. Chem.* **13,** 232–239 (2002).

190. Kwok, K. Y. *et al.* In vivo gene transfer using sulfhydryl cross-linked PEG-peptide/glycopeptide DNA co-condensates. *J. Pharm. Sci.* **92,** 1174–1185 (2003).

191. Chen, C.-P., Kim, J., Steenblock, E., Liu, D. & Rice, K. G. Gene Transfer with Poly-Melittin Peptides. *Bioconjug. Chem.* **17,** 1057–1062 (2006).

192. Ericson, M. D. & Rice, K. G. Synthesis of homogenous disulfide cross-linked polypeptides by iterative reducible ligation. *Pept. Sci.* **98,** 510–517 (2012).

193. Ericson, M. D. & Rice, K. G. Iterative Reducible Ligation to form Homogeneous Penicillamine Cross-linked Polypeptides. *Tetrahedron Lett.* **54,** (2013).

194. Ericson, M. D. & Rice, K. G. A Convergent Synthesis of Homogeneous Reducible Polypeptides. *Tetrahedron Lett.* **54,** 4746–4748 (2013).

195. Fernandez, C. A., Baumhover, N. J., Anderson, K. & Rice, K. G. Discovery of Metabolically Stabilized Electronegative Polyacridine-PEG Peptide DNA Open Polyplexes. *Bioconjug. Chem.* **21,** 723–730 (2010).

196. Anderson, K., Fernandez, C. & Rice, K. G. N-Glycan Targeted Gene Delivery to the Dendritic Cell SIGN Receptor. *Bioconjug. Chem.* **21,** 1479–1485 (2010).

197. Baumhover, N. J., Anderson, K., Fernandez, C. A. & Rice, K. G. Synthesis and In Vitro Testing of New Potent Polyacridine−Melittin Gene Delivery Peptides. *Bioconjug. Chem.* **21,** 74–83 (2010).

198. Ramadugu, S. K., Chung, Y.-H., Fuentes, E. J., Rice, K. G. & Margulis, C. J. In Silico Prediction of the 3D Structure of Trimeric Asialoglycoprotein Receptor Bound to Triantennary Oligosaccharide. *J. Am. Chem. Soc.* **132,** 9087–9095 (2010).

199. Smith, M. C. *et al.* OctreoTher: ongoing early clinical development of a somatostatin-receptor-targeted radionuclide antineoplastic therapy. *Digestion* **62**, 69–72 (2000).

200. Mayr, L. M. & Bojanic, D. Novel trends in high-throughput screening. *Curr. Opin. Pharmacol.* **9,** 580–588 (2009).

201. Current Trends in High-Throughput Screening. *ASSAY Drug Dev. Technol.* **6,** 491–504 (2008).

202. Gao, X., Kim, K.-S. & Liu, D. Nonviral gene delivery: What we know and what is next. *AAPS J.* **9,** E92–E104 (2007).

203. Midoux, P., Pichon, C., Yaouanc, J.-J. & Jaffrès, P.-A. Chemical vectors for gene delivery: a current review on polymers, peptides and lipids containing histidine or imidazole as nucleic acids carriers. *Br. J. Pharmacol.* **157,** 166–178 (2009).

204. Barua, S. *et al.* Discovery of Cationic Polymers for Non-Viral Gene Delivery Using Combinatorial Approaches. *Comb. Chem. High Throughput Screen.* **14,** 908–924 (2011).

205. Bonner, D. K., Zhao, X., Buss, H., Langer, R. & Hammond, P. T. Crosslinked linear polyethylenimine enhances delivery of DNA to the cytoplasm. *J. Controlled Release* **167,** 101–107 (2013).

206. Boussif, O. *et al.* A versatile vector for gene and oligonucleotide transfer into cells in culture and in vivo: polyethylenimine. *Proc. Natl. Acad. Sci.* **92,** 7297–7301 (1995).

207. Gonzalez, H., Hwang, S. J. & Davis, M. E. New Class of Polymers for the Delivery of Macromolecular Therapeutics. *Bioconjug. Chem.* **10,** 1068–1074 (1999).

208. Cryan, S.-A., Holohan, A., Donohue, R., Darcy, R. & O'Driscoll, C. M. Cell transfection with polycationic cyclodextrin vectors. *Eur. J. Pharm. Sci.* **21,** 625–633 (2004).

209. Liu, Y. & Reineke, T. M. Hydroxyl stereochemistry and amine number within poly(glycoamidoamine)s affect intracellular DNA delivery. *J. Am. Chem. Soc.* **127,** 3004–3015 (2005).

210. Kwok, A., Eggimann, G. A., Reymond, J.-L., Darbre, T. & Hollfelder, F. Peptide Dendrimer/Lipid Hybrid Systems Are Efficient DNA Transfection Reagents: Structure–Activity Relationships Highlight the Role of Charge Distribution Across Dendrimer Generations. *ACS Nano* **7,** 4668–4682 (2013).

211. Bayele, H. K. *et al.* Versatile peptide dendrimers for nucleic acid delivery. *J. Pharm. Sci.* **94,** 446–457 (2005).

212. Sanclimens, G. *et al.* Synthesis and screening of a small library of proline-based biodendrimers for use as delivery agents. *Pept. Sci.* **80,** 800–814 (2005).

213. Laemmli, U. K. Characterization of DNA condensates induced by poly(ethylene oxide) and polylysine. *Proc. Natl. Acad. Sci. U. S. A.* **72,** 4288–4292 (1975).

214. Midoux, P. & Monsigny, M. Efficient Gene Transfer by Histidylated Polylysine/pDNA Complexes. *Bioconjug. Chem.* **10,** 406–411 (1999).

215. De Raad, M., Teunissen, E. A., Lelieveld, D., Egan, D. A. & Mastrobattista, E. High-content screening of peptide-based non-viral gene delivery systems. *J. Controlled Release* **158,** 433–442 (2012).

216. Van Vliet, L. D., Chapman, M. R., Avenier, F., Kitson, C. Z. & Hollfelder, F. Relating Chemical and Biological Diversity Space: A Tunable System for Efficient Gene Transfection. *ChemBioChem* **9,** 1960–1967 (2008).

217. Li, L. *et al.* A biomimetic lipid library for gene delivery through thiol-yne click chemistry. *Biomaterials* **33,** 8160–8166 (2012).

218. Anderson, D. G., Lynn, D. M. & Langer, R. Semi-Automated Synthesis and Screening of a Large Library of Degradable Cationic Polymers for Gene Delivery. *Angew. Chem. Int. Ed.* **42,** 3153–3158 (2003).

219. Akinc, A., Lynn, D. M., Anderson, D. G. & Langer, R. Parallel Synthesis and Biophysical Characterization of a Degradable Polymer Library for Gene Delivery. *J. Am. Chem. Soc.* **125,** 5316–5323 (2003).

220. Zugates, G. T. *et al.* Rapid Optimization of Gene Delivery by Parallel End-modification of

Poly(β-amino ester)s. *Mol. Ther.* **15,** 1306–1312 (2007).

221. Ovcharenko, D., Jarvis, R., Hunicke-Smith, S., Kelnar, K. & Brown, D. High-throughput RNAi screening in vitro: From cell lines to primary cells. *RNA* **11,** 985–993 (2005).

222. Borawski, J., Lindeman, A., Buxton, F., Labow, M. & Gaither, L. A. Optimization procedure for small interfering RNA transfection in a 384-well format. *J. Biomol. Screen.* **12,** 546–559 (2007).

223. Sunshine, J. C., Akanda, M. I., Li, D., Kozielski, K. L. & Green, J. J. Effects of Base Polymer Hydrophobicity and End-Group Modification on Polymeric Gene Delivery. *Biomacromolecules* **12,** 3592–3600 (2011).

224. Garyantes, T. K. 1536-well assay plates: when do they make sense? *Drug Discov. Today* **7,** 489–490 (2002).

225. Kariv, I. *et al.* Identification of inhibitors of bacterial transcription/translation machinery utilizing a miniaturized 1536-well format screen. *J. Biomol. Screen.* **6,** 233–243 (2001).

226. Maffia, Kariv & Oldenburg. Miniaturization of a Mammalian Cell-Based Assay: Luciferase Reporter Gene Readout in a 3 Microliter 1536-Well Plate. *J. Biomol. Screen.* **4,** 137–142 (1999).

227. Rajasarkka, J. & Virta, M. Miniaturization of a Panel of High Throughput Yeast-Cell-Based Nuclear Receptor Assays in 384- and 1536-Well Microplates. *Comb. Chem. High Throughput Screen.* **14,** 47–54 (2011).

228. Gomez-Lechon, M., Donato, M., Lahoz, A. & Castell, J. Cell Lines: A Tool for In Vitro Drug Metabolism Studies. *Curr. Drug Metab.* **9,** 1–11 (2008).

229. Zhou, R., Geiger, R. C. & Dean, D. A. Intracellular trafficking of nucleic acids. *Expert Opin. Drug Deliv.* **1,** 127–140 (2004).

230. Pichon, C., Billiet, L. & Midoux, P. Chemical vectors for gene delivery: uptake and intracellular trafficking. *Curr. Opin. Biotechnol.* **21,** 640–645 (2010).

231. Gaunitz, F., Papke, M. & Gebhardt, R. Transient transfection of primary cultured hepatocytes using CaPO4/DNA precipitation. *BioTechniques* **20,** 826–830, 832 (1996).

232. Edwards, M. *et al.* Transfection of primary cultures of rat hepatocytes. *Methods Mol. Biol. Clifton NJ* **320,** 273–282 (2006).

233. Park, J.-S., Surendran, S., Kamendulis, L. M. & Morral, N. Comparative nucleic acid transfection efficacy in primary hepatocytes for gene silencing and functional studies. *BMC*

Res. Notes **4,** 8 (2011).

234. Watanabe, Y., Nomoto, H., Takezawa, R., Miyoshi, N. & Akaike, T. Highly Efficient Transfection into Primary Cultured Mouse Hepatocytes by Use of Cation-Liposomes: An Application for Immunization. *J. Biochem. (Tokyo)* **116,** 1220–1226 (1994).

235. Jarnagin, W. R., Debs, R. J., Wang, S. S. & Bissell, D. M. Cationic lipid-mediated transfection of liver cells in primary culture. *Nucleic Acids Res.* **20,** 4205–4211 (1992).

236. Letrou-Bonneval, E. *et al.* Galactosylated multimodular lipoplexes for specific gene transfer into primary hepatocytes. *J. Gene Med.* **10,** 1198–1209 (2008).

237. Mukthavaram, R. *et al.* Cationic glycolipids with cyclic and open galactose head groups for the selective targeting of genes to mouse liver. *Biomaterials* **30,** 2369–2384 (2009).

238. Gardmo, C., Kotokorpi, P., Helander, H. & Mode, A. Transfection of adult primary rat hepatocytes in culture. *Biochem. Pharmacol.* **69,** 1805–1813 (2005).

239. Li, W., Ralphs, K. L. & Tosh, D. Isolation and Culture of Adult Mouse Hepatocytes. *Mouse Cell Culture* (eds. Ward, A. & Tosh, D.) 185–196 (Humana Press, 2010).

240. McAnuff, M. A., Rettig, G. R. & Rice, K. G. Potency of siRNA versus shRNA mediated knockdown in vivo. *J. Pharm. Sci.* **96,** 2922–2930 (2007).

241. Fasbender, A., Zabner, J., Zeiher, B. G. & Welsh, M. J. A low rate of cell proliferation and reduced DNA uptake limit cationic lipid-mediated gene transfer to primary cultures of ciliated human airway epithelia. *Gene Ther.* **4,** 1173–1180 (1997).

242. Godbey, W. T., Wu, K. K. & Mikos, A. G. Poly(ethylenimine) and its role in gene delivery. *J. Control. Release Off. J. Control. Release Soc.* **60,** 149–160 (1999).

243. Creusat, G. *et al.* Proton Sponge Trick for pH-Sensitive Disassembly of Polyethylenimine-Based siRNA Delivery Systems. *Bioconjug. Chem.* **21,** 994–1002 (2010).

244. Richard, I., Thibault, M., De Crescenzo, G., Buschmann, M. D. & Lavertu, M. Ionization Behavior of Chitosan and Chitosan–DNA Polyplexes Indicate That Chitosan Has a Similar Capability to Induce a Proton-Sponge Effect as PEI. *Biomacromolecules* **14,** 1732–1740 (2013).

245. Benjaminsen, R. V., Mattebjerg, M. A., Henriksen, J. R., Moghimi, S. M. & Andresen, T. L. The Possible 'Proton Sponge ' Effect of Polyethylenimine (PEI) Does Not Include Change in Lysosomal pH. *Mol. Ther.* **21,** 149–157 (2013).

246. Zhang, J.-H., Chung, T. D. Y. & Oldenburg, K. R. A Simple Statistical Parameter for Use in

Evaluation and Validation of High Throughput Screening Assays. *J. Biomol. Screen.* **4,** 67–73 (1999).

247. Khargharia, S., Baumhover, N. J., Crowley, S. T., Duskey, J. & Rice, K. G. The uptake mechanism of PEGylated DNA polyplexes by the liver influences gene expression. *Gene Ther.* **21,** 1021-1028 (2014).

248. Ziady, A.-G., Ferkol, T., Dawson, D. V., Perlmutter, D. H. & Davis, P. B. Chain Length of the Polylysine in Receptor-targeted Gene Transfer Complexes Affects Duration of Reporter Gene Expression Both in Vitro and in Vivo. *J. Biol. Chem.* **274,** 4908–4916 (1999).

249. Merdan, T. *et al.* PEGylation of Poly(ethylene imine) Affects Stability of Complexes with Plasmid DNA under in Vivo Conditions in a Dose-Dependent Manner after Intravenous Injection into Mice. *Bioconjug. Chem.* **16,** 785–792 (2005).

250. Ogris, M., Brunner, S., Schüller, S., Kircheis, R. & Wagner, E. PEGylated DNA/transferrin-PEI complexes: reduced interaction with blood components, extended circulation in blood and potential for systemic gene delivery. *Gene Ther.* **6,** 595–605 (1999).

251. Khargharia, S., Kizzire, K., Ericson, M. D., Baumhover, N. J. & Rice, K. G. PEG length and chemical linkage controls polyacridine peptide DNA polyplex pharmacokinetics, biodistribution, metabolic stability and in vivo gene expression. *J. Controlled Release* **170,** 325–333 (2013).

252. Peracchia, M. T. *et al.* Stealth® PEGylated polycyanoacrylate nanoparticles for intravenous administration and splenic targeting. *J. Controlled Release* **60,** 121–128 (1999).

253. Mosqueira, V. C. *et al.* Biodistribution of long-circulating PEG-grafted nanocapsules in mice: effects of PEG chain length and density. *Pharm. Res.* **18,** 1411–1419 (2001).

254. Pun, S. H. & Davis, M. E. Development of a Nonviral Gene Delivery Vehicle for Systemic Application. *Bioconjug. Chem.* **13,** 630–639 (2002).

255. Sung, S.-J. *et al.* Effect of Polyethylene Glycol on Gene Delivery of Polyethylenimine. *Biol. Pharm. Bull.* **26,** 492–500 (2003).

256. Mao, S. *et al.* Influence of Polyethylene Glycol Chain Length on the Physicochemical and Biological Properties of Poly(ethylene imine)-graft-Poly(ethylene glycol) Block Copolymer/SiRNA Polyplexes. *Bioconjug. Chem.* **17,** 1209–1218 (2006).

257. Burke, R. S. & Pun, S. H. Extracellular Barriers to in Vivo PEI and PEGylated PEI Polyplex-Mediated Gene Delivery to the Liver. *Bioconjug. Chem.* **19,** 693–704 (2008).

258. Khare, R., Reddy, V. S., Nemerow, G. R. & Barry, M. A. Identification of Adenovirus

Serotype 5 Hexon Regions That Interact with Scavenger Receptors. *J. Virol.* **86,** 2293–2301 (2012).

259. Kwok, K. Y., Mckenzie, D. L., Evers, D. L. & Rice, K. G. Formulation of highly soluble poly(ethylene glycol)-peptide DNA condensates. *J. Pharm. Sci.* **88,** 996–1003 (1999).

260. Collard, W. T., Yang, Y., Kwok, K. Y., Park, Y. & Rice, K. G. Biodistribution, metabolism, and in vivo gene expression of low molecular weight glycopeptide polyethylene glycol peptide DNA co-condensates. *J. Pharm. Sci.* **89,** 499–512 (2000).

261. Beaumier, P. L., Hwang, K. J. & Slattery, J. T. Effect of liposome dose on the elimination of small unilamellar sphingomyelin/cholesterol vesicles from the circulation. *Res. Commun. Chem. Pathol. Pharmacol.* **39,** 277–289 (1983).

262. Smith, J. S., Xu, Z., Tian, J., Stevenson, S. C. & Byrnes, A. P. Interaction of Systemically Delivered Adenovirus Vectors with Kupffer Cells in Mouse Liver. *Hum. Gene Ther.* **19,** 547–554 (2008).

263. Nishikawa, K., Arai, H. & Inoue, K. Scavenger receptor-mediated uptake and metabolism of lipid vesicles containing acidic phospholipids by mouse peritoneal macrophages. *J. Biol. Chem.* **265,** 5226–5231 (1990).

264. Lee, K.-D., Hong, K. & Papahadjopoulos, D. Recognition of liposomes by cells: In vitro binding and endocytosis mediated by specific lipid headgroups and surface charge density. *Biochim. Biophys. Acta BBA - Biomembr.* **1103,** 185–197 (1992).

265. Lee, K.-D., Pitas, R. E. & Papahadjopoulos, D. Evidence that the scavenger receptor is not involved in the uptake of negatively charged liposomes by cells. *Biochim. Biophys. Acta BBA - Biomembr.* **1111,** 1–6 (1992).

266. Rigotti, A., Acton, S. L. & Krieger, M. The Class B Scavenger Receptors SR-BI and CD36 Are Receptors for Anionic Phospholipids. *J. Biol. Chem.* **270,** 16221–16224 (1995).

267. Fukasawa, M. *et al.* SRB1, a Class B Scavenger Receptor, Recognizes both Negatively Charged Liposomes and Apoptotic Cells. *Exp. Cell Res.* **222,** 246–250 (1996).

268. Chow, D. D., Essien, H. E., Padki, M. M. & Hwang, K. J. Targeting small unilamellar liposomes to hepatic parenchymal cells by dose effect. *J. Pharmacol. Exp. Ther.* **248,** 506–513 (1989).

269. Scherphof, G. L. & Kamps, J. A. A. M. Receptor versus non-receptor mediated clearance of liposomes. *Adv. Drug Deliv. Rev.* **32,** 81–97 (1998).

270. Yoshida, M., Mahato, R. I., Kawabata, K., Takakura, Y. & Hashida, M. Disposition

characteristics of plasmid DNA in the single-pass rat liver perfusion system. *Pharm. Res.* **13,** 599–603 (1996).

271. Takagi, T. *et al.* Involvement of Specific Mechanism in Plasmid DNA Uptake by Mouse Peritoneal Macrophages. *Biochem. Biophys. Res. Commun.* **245,** 729–733 (1998).

272. Hisazumi, J., Kobayashi, N., Nishikawa, M. & Takakura, Y. Significant role of liver sinusoidal endothelial cells in hepatic uptake and degradation of naked plasmid DNA after intravenous injection. *Pharm. Res.* **21,** 1223–1228 (2004).

273. Liu, F., Shollenberger, L. M., Conwell, C. C., Yuan, X. & Huang, L. Mechanism of naked DNA clearance after intravenous injection. *J. Gene Med.* **9,** 613–619 (2007).

274. Xu, Z., Tian, J., Smith, J. S. & Byrnes, A. P. Clearance of Adenovirus by Kupffer Cells Is Mediated by Scavenger Receptors, Natural Antibodies, and Complement. *J. Virol.* **82,** 11705–11713 (2008).

275. Manickan, E. *et al.* Rapid Kupffer Cell Death after Intravenous Injection of Adenovirus Vectors. *Mol. Ther.* **13,** 108–117 (2006).

276. Liu, Y.-P. *et al.* Polyinosinic acid decreases sequestration and improves systemic therapy of measles virus. *Cancer Gene Ther.* **19,** 202–211 (2012).

277. Piccolo, P. *et al.* SR-A and SREC-I Are Kupffer and Endothelial Cell Receptors for Helper-dependent Adenoviral Vectors. *Mol. Ther.* **21,** 767–774 (2013).

278. Koski, A. *et al.* Systemic adenoviral gene delivery to orthotopic murine breast tumors with ablation of coagulation factors, thrombocytes and Kupffer cells. *J. Gene Med.* **11,** 966–977 (2009).

279. Kamps, J. A. A. M., Morselt, H. W. M., Swart, P. J., Meijer, D. K. F. & Scherphof, G. L. Massive targeting of liposomes, surface-modified with anionized albumins, to hepatic endothelial cells. *Proc. Natl. Acad. Sci.* **94,** 11681–11685 (1997).

280. Haisma, H. J. *et al.* Polyinosinic acid enhances delivery of adenovirus vectors in vivo by preventing sequestration in liver macrophages. *J. Gen. Virol.* **89,** 1097–1105 (2008).

281. Van Dijk, R. *et al.* Polyinosinic Acid Blocks Adeno-Associated Virus Macrophage Endocytosis In Vitro and Enhances Adeno-Associated Virus Liver-Directed Gene Therapy In Vivo. *Hum. Gene Ther.* **24,** 807–813 (2013).

282. Tung, C. H., Zhu, T., Lackland, H. & Stein, S. An acridine amino acid derivative for use in Fmoc peptide synthesis. *Pept. Res.* **5,** 115–118 (1992).

283. Terebesi, J., Kwok, K. Y. & Rice, K. G. Iodinated Plasmid DNA as a Tool for Studying Gene Delivery. *Anal. Biochem.* **263,** 120–123 (1998).

284. Adami, R. C. & Rice, K. G. Metabolic stability of glutaraldehyde cross-linked peptide dna condensates. *J. Pharm. Sci.* **88,** 739–746 (1999).

285. Oja, C. D., Semple, S. C., Chonn, A. & Cullis, P. R. Influence of dose on liposome clearance: critical role of blood proteins. *Biochim. Biophys. Acta* **1281,** 31–37 (1996).

286. Wisse, E. Fixation methods for electron microscopy of human and other liver. *World J. Gastroenterol.* **16,** 2851 (2010).

287. Tavernier, G. *et al.* mRNA as gene therapeutic: How to control protein expression. *J. Controlled Release* **150,** 238–247 (2011).

288. Van Tendeloo, V. F. I., Ponsaerts, P. & Berneman, Z. N. mRNA-based gene transfer as a tool for gene and cell therapy. *Curr. Opin. Mol. Ther.* **9,** 423–431 (2007).

289. Wolff, J. A. *et al.* Direct gene transfer into mouse muscle in vivo. *Science* **247,** 1465–1468 (1990).

290. Deering, R. P., Kommareddy, S., Ulmer, J. B., Brito, L. A. & Geall, A. J. Nucleic acid vaccines: prospects for non-viral delivery of mRNA vaccines. *Expert Opin. Drug Deliv.* **11,** 885–899 (2014).

291. Ulmer, J. B., Mason, P. W., Geall, A. & Mandl, C. W. RNA-based vaccines. *Vaccine* **30,** 4414–4418 (2012).

292. Ljungberg, K. & Liljeström, P. Self-replicating alphavirus RNA vaccines. *Expert Rev. Vaccines* **14,** 177-194 (2014).

293. Kallen, K.-J. *et al.* A novel, disruptive vaccination technology: Self-adjuvanted RNActive® vaccines. *Hum. Vaccines Immunother.* **9,** 2263–2276 (2013).

294. Karikó, K., Muramatsu, H., Keller, J. M. & Weissman, D. Increased Erythropoiesis in Mice Injected With Submicrogram Quantities of Pseudouridine-containing mRNA Encoding Erythropoietin. *Mol. Ther.* **20,** 948-953 (2012).

295. Anderson, B. R. *et al.* Nucleoside modifications in RNA limit activation of 2′-5′-oligoadenylate synthetase and increase resistance to cleavage by RNase L. *Nucleic Acids Res.* **39,** 9329–9338 (2011).

296. Karikó, K. *et al.* Incorporation of Pseudouridine Into mRNA Yields Superior Nonimmunogenic Vector With Increased Translational Capacity and Biological Stability.

Mol. Ther. **16,** 1833–1840 (2008).

297. Kormann, M. S. D. *et al.* Expression of therapeutic proteins after delivery of chemically modified mRNA in mice. *Nat. Biotechnol.* **29,** 154–157 (2011).

298. Wang, Y. *et al.* Systemic Delivery of Modified mRNA Encoding Herpes Simplex Virus 1 Thymidine Kinase for Targeted Cancer Gene Therapy. *Mol. Ther.* **21,** 358–367 (2013).

299. Kobayashi, N., Kuramoto, T., Yamaoka, K., Hashida, M. & Takakura, Y. Hepatic Uptake and Gene Expression Mechanisms following Intravenous Administration of Plasmid DNA by Conventional and Hydrodynamics-Based Procedures. *J. Pharmacol. Exp. Ther.* **297,** 853–860 (2001).

300. Suda, T., Suda, K. & Liu, D. Computer-assisted Hydrodynamic Gene Delivery. *Mol. Ther.* **16,** 1098–1104 (2008).

301. Yokoo, T. *et al.* Novel electric power-driven hydrodynamic injection system for gene delivery: safety and efficacy of human factor IX delivery in rats. *Gene Ther.* **20,** 816–823 (2013).

302. Russell, J. E. & Liebhaber, S. A. The stability of human beta-globin mRNA is dependent on structural determinants positioned within its 3' untranslated region. *Blood* **87,** 5314–5323 (1996).

303. Cohen, A. R., Galanello, R., Pennell, D. J., Cunningham, M. J. & Vichinsky, E. Thalassemia. *ASH Educ. Program Book* **2004,** 14–34 (2004).

304. Karikó, K., Muramatsu, H., Ludwig, J. & Weissman, D. Generating the optimal mRNA for therapy: HPLC purification eliminates immune activation and improves translation of nucleoside-modified, protein-encoding mRNA. *Nucleic Acids Res.* **39,** e142–e142 (2011).

305. Baumhover, N. J. *et al.* Simple PEGylated Polylysine Peptides Mediate Potent Stimulated Gene Expression in Liver. In Progress.

306. Meyer, C. *et al.* Stabilized Interleukin-6 receptor binding RNA aptamers. *RNA Biol.* **11,** 57–65 (2013).

307. Ibach, J. *et al.* Identification of a T7 RNA polymerase variant that permits the enzymatic synthesis of fully 2′-O-methyl-modified RNA. *J. Biotechnol.* **167,** 287–295 (2013).

308. Khargharia, S., Baumhover, N. J., Crowley, S. T., Duskey, J. & Rice, K. G. The uptake mechanism of PEGylated DNA polyplexes by the liver influences gene expression. *Gene Ther.* (2014). doi:10.1038/gt.2014.81

309. Lescrinier, E., Froeyen, M. & Herdewijn, P. Difference in conformational diversity between nucleic acids with a six□membered 'sugar' unit and natural 'furanose' nucleic acids. *Nucleic Acids Res.* **31,** 2975–2989 (2003).

310. Balagopal, V., Fluch, L. & Nissan, T. Ways and means of eukaryotic mRNA decay. *Biochim. Biophys. Acta BBA - Gene Regul. Mech.* **1819,** 593–603 (2012).

311. Leis, J. P., Berkower, I. & Hurwitz, J. Mechanism of Action of Ribonuclease H Isolated from Avian Myeloblastosis Virus and Escherichia coli. *Proc. Natl. Acad. Sci. U. S. A.* **70,** 466–470 (1973).

312. Cerritelli, S. M. & Crouch, R. J. Ribonuclease H: the enzymes in Eukaryotes. *FEBS J.* **276,** 1494–1505 (2009).

313. Champoux, J. J. & Schultz, S. J. Ribonuclease H: Properties, Substrate Specificity, and Roles in Retroviral Reverse Transcription. *FEBS J.* **276,** 1506–1516 (2009).

314. Heppel, L. A., Ortiz, P. J. & Ochoa, S. Studies on Polynucleotides Synthesized by Polynucleotide Phosphorylase I. Structure of Polynucleotides with One Type of Nucleotide Unit. *J. Biol. Chem.* **229,** 679–694 (1957).

315. Brummond, D. O., Staehelin, M. & Ochoa, S. Enzymatic Synthesis of Polynucleotides Ii. Distribution of Polynucleotide Phosphorylase. *J. Biol. Chem.* **225,** 835–850 (1957).

316. Hunt, J. A. Interaction between polyuridylic acid and rabbit globin messenger ribonucleic acid. *Biochem. J.* **131,** 327–333 (1973).

317. Bishop, J. O. & Rosbash, M. Polynucleotide sequences in eukaryotic DNA and RNA that form ribonuclease-resistant complexes with polyuridylic acid. *J. Mol. Biol.* **85,** 75–86 (1974).

318. Hoerter, J. A. H., Krishnan, V., Lionberger, T. A. & Walter, N. G. siRNA-Like Double-Stranded RNAs Are Specifically Protected Against Degradation in Human Cell Extract. *PLoS ONE* **6,** e20359 (2011).

319. Rich, A., Davies, D. R., Crick, F. H. C. & Watson, J. D. The molecular structure of polyadenylic acid. *J. Mol. Biol.* **3,** 71–86 (1961).

320. Pattabiraman, N. Can the double helix be parallel? *Biopolymers* **25,** 1603–1606 (1986).

321. Safaee, N. *et al.* Structure of the Parallel Duplex of Poly(A) RNA: Evaluation of a 50 Year-Old Prediction. *Angew. Chem. Int. Ed.* **52,** 10370–10373 (2013).

322. Ramadan, A. *et al.* Activation of basophils by the double-stranded RNA poly(A:U)

exacerbates allergic inflammation. *Allergy* **68,** 732–738 (2013).

323. Sugiyama, T. *et al.* Immunoadjuvant effects of polyadenylic:polyuridylic acids through TLR3 and TLR7. *Int. Immunol.* **20,** 1–9 (2008).

324. Hilleman, M. R. *et al.* Double-Stranded RNA's in Relation to Interferon Induction and Adjuvant Activity. *Biological Effects of Polynucleotides* (eds. Beers, RF and Braun, W) 27-44 (Springer-Verlag, 1971).

325. Ducret, J. P. *et al.* A Phase I Clinical Tolerance Study of Polyadenylic-Polyuridylic Acid in Cancer Patients. *J. Biol. Response Mod.* **4,** 129–133 (1985).

326. Hovanessian, A. G. *et al.* Enhancement of natural killer cell activity and 2-5A synthetase in operable breast cancer patients treated with polyadenylic; polyuridylic acid. *Cancer* **55,** 357–362 (1985).

327. Youn, J. K., Hovanessian, A. G., Riviere, Y., Hue, G. & Lacour, F. Enhancement of natural killer cell activity and 2-5A synthetase in mice treated with polyadenylic · polyuridylic acid. *Cell. Immunol.* **79,** 298–308 (1983).

328. Liang, S.-L., Quirk, D. & Zhou, A. RNase L: its biological roles and regulation. *IUBMB Life* **58,** 508–514 (2006).

329. Hornung, V., Hartmann, R., Ablasser, A. & Hopfner, K.-P. OAS proteins and cGAS: unifying concepts in sensing and responding to cytosolic nucleic acids. *Nat. Rev. Immunol.* **14,** 521–528 (2014).

330. Huang, Z. & Szostak, J. W. A Simple Method for 3′-Labeling of RNA. *Nucleic Acids Res.* **24,** 4360–4361 (1996).

331. Yehudai-Resheff, S. & Schuster, G. Characterization of the E.coli poly(A) polymerase: nucleotide specificity, RNA-binding affinities and RNA structure dependence. *Nucleic Acids Res.* **28,** 1139–1144 (2000).

332. Chen, L. S., Plunkett, W. & Gandhi, V. Polyadenylation inhibition by the triphosphates of deoxyadenosine analogues. *Leuk. Res.* **32,** 1573–1581 (2008).

333. Chen, L. S. *et al.* Chain termination and inhibition of mammalian poly(A) polymerase by modified ATP analogues. *Biochem. Pharmacol.* **79,** 669–677 (2010).

334. Martin, G. & Keller, W. Tailing and 3'-end labeling of RNA with yeast poly(A) polymerase and various nucleotides. *RNA* **4,** 226–230 (1998).

335. Martin, G., Möglich, A., Keller, W. & Doublié, S. Biochemical and Structural Insights into

Substrate Binding and Catalytic Mechanism of Mammalian Poly(A) Polymerase. *J. Mol. Biol.* **341,** 911–925 (2004).

336. Aa, M. A. E. M. van der *et al.* The Nuclear Pore Complex: The Gateway to Successful Nonviral Gene Delivery. *Pharm. Res.* **23,** 447–459 (2006).

337. Varkouhi, A. K., Scholte, M., Storm, G. & Haisma, H. J. Endosomal escape pathways for delivery of biologicals. *J. Controlled Release* **151,** 220–228 (2011).

338. Girod, A. *et al.* The VP1 capsid protein of adeno-associated virus type 2 is carrying a phospholipase A2 domain required for virus infectivity. *J. Gen. Virol.* **83,** 973–978 (2002).

339. Canaan, S. *et al.* Interfacial Enzymology of Parvovirus Phospholipases A2. *J. Biol. Chem.* **279,** 14502–14508 (2004).

340. Lupescu, A. *et al.* Phospholipase A2 Activity-Dependent Stimulation of Ca2+ Entry by Human Parvovirus B19 Capsid Protein VP1. *J. Virol.* **80,** 11370–11380 (2006).

341. Grieger, J. C., Johnson, J. S., Gurda-Whitaker, B., Agbandje-McKenna, M. & Samulski, R. J. Surface-Exposed Adeno-Associated Virus Vp1-NLS Capsid Fusion Protein Rescues Infectivity of Noninfectious Wild-Type Vp2/Vp3 and Vp3-Only Capsids but Not That of Fivefold Pore Mutant Virions. *J. Virol.* **81,** 7833–7843 (2007).

342. Burke, J. E. & Dennis, E. A. Phospholipase A2 structure/function, mechanism, and signaling. *J. Lipid Res.* **50,** S237–S242 (2008).

343. Lambeau, G. & Gelb, M. H. Biochemistry and Physiology of Mammalian Secreted Phospholipases A2. *Annu. Rev. Biochem.* **77,** 495–520 (2008).

344. Martelli, A. M. *et al.* Metabolism and signaling activities of nuclear lipids. *Cell. Mol. Life Sci. CMLS* **61,** 1143–1156 (2004).

345. Uthe, J. F. & Magee, W. L. Phospholipase A2: action on purified phospholipids as affected by deoxycholate and divalent cations. *Can. J. Biochem.* **49,** 776–784 (1971).

346. Cummings, B. S., McHowat, J. & Schnellmann, R. G. Phospholipase A2s in Cell Injury and Death. *J. Pharmacol. Exp. Ther.* **294,** 793–799 (2000).

347. Shinzawa, K. & Tsujimoto, Y. PLA2 activity is required for nuclear shrinkage in caspase-independent cell death. *J. Cell Biol.* **163,** 1219–1230 (2003).

348. Shipolini, R. A., Callewaert, G. L., Cottrell, R. C. & Vernon, C. A. The Amino-Acid Sequence and Carbohydrate Content of Phospholipase A2 from Bee Venom. *Eur. J. Biochem.* **48,** 465–476 (1974).

349. Xin, Y. *et al.* Molecular cloning and characterization of a venom phospholipase A2 from the bumblebee Bombus ignitus. *Comp. Biochem. Physiol. B Biochem. Mol. Biol.* **154,** 195–202 (2009).

350. Li, J.-H., Zhang, C.-X., Shen, L., Tang, Z.-H. & Cheng, J.-A. Expression and regulation of phospholipase A2 in venom gland of the chinese honeybee, Apis cerana cerana. *Arch. Insect Biochem. Physiol.* **60,** 1–12 (2005).

351. Rivers, D. B., Rocco, M. M. & Frayha, A. R. Venom from the ectoparasitic wasp Nasonia vitripennis increases Na+ influx and activates phospholipase C and phospholipase A2 dependent signal transduction pathways in cultured insect cells. *Toxicon* **40,** 9–21 (2002).

352. Nagaraju, S., Mahadeswaraswamy, Y. H., Girish, K. S. & Kemparaju, K. Venom from spiders of the genus Hippasa: biochemical and pharmacological studies. *Comp. Biochem. Physiol. Toxicol. Pharmacol. CBP* **144,** 1–9 (2006).

353. Usmanov, P. B. & Nuritova, F. A. The anticoagulant action of phospholipase A from Eresus niger spider venom. *Toxicon Off. J. Int. Soc. Toxinology* **32,** 625–628 (1994).

354. Ettinger, K., Cohen, G., Momic, T. & Lazarovici, P. The Effects of a Chactoid Scorpion Venom and Its Purified Toxins on Rat Blood Pressure and Mast Cells Histamine Release. *Toxins* **5,** 1332–1342 (2013).

355. González-Morales, L., Diego-García, E., Segovia, L., Carmen Gutiérrez, M. del & Possani, L. D. Venom from the centipede Scolopendra viridis Say: Purification, gene cloning and phylogenetic analysis of a phospholipase A2. *Toxicon* **54,** 8–15 (2009).

356. Laing, G. D., Kamiguti, A. S., Wilkinson, M. C., Lowe, G. M. & Theakston, R. D. Characterisation of a purified phospholipase A2 from the venom of the Papuan black snake (Pseudechis papuanus). *Biochim. Biophys. Acta* **1250,** 137–143 (1995).

357. Gomez, F. *et al.* Purification and characterization of five variants of phospholipase A2 and complete primary structure of the main phospholipase A2 variant in Heloderma suspectum (Gila Monster) venom. *Eur. J. Biochem.* **186,** 23–33 (1989).

358. Cornet, V. *et al.* Dual role of the cuttlefish salivary proteome in defense and predation. *J. Proteomics* **108,** 209–222 (2014).

359. Del Monte-Martínez, A. *et al.* Improved purification and enzymatic properties of a mixture of Sticholysin I and II: Isotoxins with hemolytic and phospholipase A2 activities from the sea anemone Stichodactyla helianthus. *Protein Expr. Purif.* **95,** 57–66 (2014).

360. Safavi-Hemami, H. *et al.* Combined Proteomic and Transcriptomic Interrogation of the

Venom Gland of Conus geographus Uncovers Novel Components and Functional Compartmentalization. *Mol. Cell. Proteomics* **13,** 938–953 (2014).

361. Fry, B. G. *et al.* The Toxicogenomic Multiverse: Convergent Recruitment of Proteins Into Animal Venoms. *Annu. Rev. Genomics Hum. Genet.* **10,** 483–511 (2009).

362. Valentin, E. & Lambeau, G. What can venom phospholipases A2 tell us about the functional diversity of mammalian secreted phospholipases A2? *Biochimie* **82,** 815–831 (2000).

363. Rouault, M. *et al.* Recombinant Production and Properties of Binding of the Full Set of Mouse Secreted Phospholipases A2 to the Mouse M-Type Receptor. *Biochemistry (Mosc.)* **46,** 1647–1662 (2007).

364. Nicolas, J.-P. *et al.* Localization of Structural Elements of Bee Venom Phospholipase A2 Involved in N-type Receptor Binding and Neurotoxicity. *J. Biol. Chem.* **272,** 7173–7181 (1997).

365. Beisson, F., Tiss, A., Rivière, C. & Verger, R. Methods for lipase detection and assay: a critical review. *Eur. J. Lipid Sci. Technol.* **102,** 133–153 (2000).

366. Price III, J. A. A colorimetric assay for measuring phospholipase A2 degradation of phosphatidylcholine at physiological pH. *J. Biochem. Biophys. Methods* **70,** 441–444 (2007).

367. Sharko, O. & Kisel, M. 1-Acyl-2-[N-(2,4-dinitrophenyl)aminopropionyl]-sn-glycero-3-phosphocholine as a chromogenic substrate for phospholipase A2 assay. *Anal. Biochem.* **413,** 69–71 (2011).

368. Hendrickson, H. S. Fluorescence-Based Assays of Lipases, Phospholipases, and Other Lipolytic Enzymes. *Anal. Biochem.* **219,** 1–8 (1994).

369. Wichmann, O., Gelb, M. H. & Schultz, C. Probing Phospholipase A2 with Fluorescent Phospholipid Substrates. *ChemBioChem* **8,** 1555–1569 (2007).

370. Feng, L. *et al.* A real-time fluorogenic phospholipase A(2) assay for biochemical and cellular activity measurements. *Chem. Biol.* **9,** 795–803 (2002).

371. Wichmann, O., Wittbrodt, J. & Schultz, C. A Small-Molecule FRET Probe To Monitor Phospholipase A2 Activity in Cells and Organisms. *Angew. Chem. Int. Ed.* **45,** 508–512 (2006).

372. Hendrickson, H. S., Hendrickson, E. K., Johnson, I. D. & Farber, S. A. Intramolecularly Quenched BODIPY-Labeled Phospholipid Analogs in Phospholipase A2 and Platelet-Activating Factor Acetylhydrolase Assays and in Vivo Fluorescence Imaging. *Anal.*

Biochem. **276,** 27–35 (1999).

373. Kubelka, V. *et al.* Primary structures of the N-linked carbohydrate chains from honeybee venom phospholipase A2. *Eur. J. Biochem.* **213,** 1193–1204 (1993).

374. Ameratunga, R. V., Hawkins, R., Prestidge, R. & Marbrook, J. A high efficiency method for purification and assay of bee venom phospholipase A2. *Pathology (Phila.)* **27,** 157–160 (1995).

375. Annand, R. R. *et al.* Active Site of Bee Venom Phospholipase A2: The Role of Histidine-34, Aspartate-64 and Tyrosine-87. *Biochemistry (Mosc.)* **35,** 4591–4601 (1996).

376. Scott, D. L., Otwinowski, Z., Gelb, M. H. & Sigler, P. B. Crystal structure of bee-venom phospholipase A2 in a complex with a transition-state analogue. *Science* **250,** 1563–1566 (1990).

377. Yunes, R., Goldhammer, A. R., Garner, W. K. & Cordes, E. H. Phospholipases: Melittin facilitation of bee venom phospholipase A2-catalyzed hydrolysis of unsonicated lecithin liposomes. *Arch. Biochem. Biophys.* **183,** 105–112 (1977).

378. Prenner, C., Mach, L., Glössl, J. & März, L. The antigenicity of the carbohydrate moiety of an insect glycoprotein, honey-bee (Apis mellifera) venom phospholipase A2. The role of alpha 1,3-fucosylation of the asparagine-bound N-acetylglucosamine. *Biochem. J.* **284,** 377–380 (1992).

379. Dudler, T. *et al.* High-level expression in Escherichia coli and rapid purification of enzymatically active honey bee venom phospholipase A2. *Biochim. Biophys. Acta BBA - Lipids Lipid Metab.* **1165,** 201–210 (1992).

380. Shen, L.-R. *et al.* Expression of a bee venom phospholipase A2 from Apis cerana cerana in the baculovirus-insect cell. *J. Zhejiang Univ. Sci. B* **11,** 342–349 (2010).

381. Chang, L., Wu, P.-F. & Chang, C.-C. Expression of Taiwan Banded Krait Phospholipase A2 in Escherichia coli, a Fully Active Enzyme Generated by Hydrolyzing with Aminopeptidase. *Biochem. Biophys. Res. Commun.* **225,** 990–996 (1996).

382. Armugam, A. *et al.* Group IB phospholipase A2 from Pseudonaja textilis. *Arch. Biochem. Biophys.* **421,** 10–20 (2004).

383. Liang, N.-S., Pungerčar, J., Križaj, I., Štrukelj, B. & Gubenšek, F. Expression of fully active ammodytoxin A, a potent presynaptically neurotoxic phospholipase A2, in Escherichia coli. *FEBS Lett.* **334,** 55–59 (1993).

384. Chen, Y. & Dennis, E. A. Expression and characterization of human group V phospholipase

A2. *Biochim. Biophys. Acta BBA - Lipids Lipid Metab.* **1394,** 57–64 (1998).

385. Franken, P. A. *et al.* Purification and characterization of a mutant human platelet phospholipase A2 expressed in Escherichia coli. *Eur. J. Biochem.* **203,** 89–98 (1992).

386. Valentin, E. *et al.* Cloning and Recombinant Expression of Human Group IIF-Secreted Phospholipase A2. *Biochem. Biophys. Res. Commun.* **279,** 223–228 (2000).

387. Han, S. K., Yoon, E. T. & Cho, W. Bacterial expression and characterization of human secretory class V phospholipase A2. *Biochem. J.* **331,** 353–357 (1998).

388. Kawauchi, Y., Takasaki, J., Matsuura, Y. & Masuho, Y. Preparation and Characterization of Human Rheumatoid Arthritic Synovial Fluid Phospholipase A2 Produced by Recombinant Baculovirus-Infected Insect Cells. *J. Biochem. (Tokyo)* **116,** 81–87 (1994).

389. Seilhamer, J. J. *et al.* Cloning and recombinant expression of phospholipase A2 present in rheumatoid arthritic synovial fluid. *J. Biol. Chem.* **264,** 5335–5338 (1989).

390. Rice, S. Q. *et al.* Expression, purification and characterization of a human serine-dependent phospholipase A2 with high specificity for oxidized phospholipids and platelet activating factor. *Biochem. J.* **330,** 1309–1315 (1998).

391. Lefkowitz, L. J., Deems, R. A. & Dennis, E. A. Expression of Group IA Phospholipase A2 in Pichia pastoris: Identification of a Phosphatidylcholine Activator Site Using Site-Directed Mutagenesis. *Biochemistry (Mosc.)* **38,** 14174–14184 (1999).

392. Zhang, F. & Wang, Y. Cloning, expression, and purification of lipoprotein-associated phospholipase A(2) in Pichia pastoris. *Mol. Biotechnol.* **33,** 29–36 (2006).

393. Afrin, R., Zohora, U. S., Uehara, H., Watanabe-Nakayama, T. & Ikai, A. Atomic force microscopy for cellular level manipulation: imaging intracellular structures and DNA delivery through a membrane hole. *J. Mol. Recognit.* **22,** 363–372 (2009).

394. Le, H. T., Rao, G. A., Hirko, A. C. & Hughes, J. A. Polymeric Nanoparticles Containing Conjugated Phospholipase A2 for Nonviral Gene Delivery. *Mol. Pharm.* **7,** 1090–1097 (2010).

395. Toita, S., Sawada, S. & Akiyoshi, K. Polysaccharide nanogel gene delivery system with endosome-escaping function: Co-delivery of plasmid DNA and phospholipase A2. *J. Controlled Release* **155,** 54–59 (2011).

396. Nagahara, N., Matsumura, T., Okamoto, R. & Kajihara, Y. Protein Cysteine Modifications: (1) Medicinal Chemistry for Proteomics. *Curr. Med. Chem.* **16,** 4419–4444 (2009).

397. Kim, Y. *et al.* Efficient Site-Specific Labeling of Proteins via Cysteines. *Bioconjug. Chem.* **19,** 786–791 (2008).

398. Valentin, E., Ghomashchi, F., Gelb, M. H., Lazdunski, M. & Lambeau, G. Novel Human Secreted Phospholipase A2 with Homology to the Group III Bee Venom Enzyme. *J. Biol. Chem.* **275,** 7492–7496 (2000).

399. Melville, D. B. Biotin Sulfoxide. *J. Biol. Chem.* **208,** 495–502 (1954).

400. Wu, A. M. *et al.* Differential affinities of Erythrina cristagalli lectin (ECL) toward monosaccharides and polyvalent mammalian structural units. *Glycoconj. J.* **24,** 591–604 (2007).

401. Cummings, R. D. Use of Lectins in Analysis of Glycoconjugates. *Methods in Enzymology* (ed. William J. Lennarz, G. W. H.) **230,** 66–86 (Academic Press, 1994).

402. Mechref, Y., Madera, M. & Novotny, M. V. Glycoprotein Enrichment Through Lectin Affinity Techniques. *2D PAGE: Sample Preparation and Fractionation* (ed. Posch, A.) 373–396 (Humana Press, 2008).

403. Porwal, M. *et al.* Parvoviruses Cause Nuclear Envelope Breakdown by Activating Key Enzymes of Mitosis. *PLoS Pathog* **9,** e1003671 (2013).

404. Brown, T. C. Reactions to honeybee stings: an allergic prospective. *Curr. Opin. Allergy Clin. Immunol.* **13,** 365–371 (2013).

405. Kim, C. H., Axup, J. Y. & Schultz, P. G. Protein conjugation with genetically encoded unnatural amino acids. *Curr. Opin. Chem. Biol.* **17,** 412–419 (2013).

406. Yuan, T. Z. *et al.* Shear-Stress-Mediated Refolding of Proteins from Aggregates and Inclusion Bodies. *ChemBioChem* **16,** 393–396 (2015).

407. Ojo, A. O. *et al.* Organ donation and utilization in the USA. *Am. J. Transplant. Off. J. Am. Soc. Transplant. Am. Soc. Transpl. Surg.* **4,** 27–37 (2004).

408. Kotterman, M. A. & Schaffer, D. V. Engineering adeno-associated viruses for clinical gene therapy. *Nat. Rev. Genet.* **15,** 445–451 (2014).

409. Wang, W., Li, W., Ma, N. & Steinhoff, G. Non-viral gene delivery methods. *Curr. Pharm. Biotechnol.* **14,** 46–60 (2013).

410. Nakajima, K. & Yaoita, Y. Highly efficient gene knockout by injection of TALEN mRNAs into oocytes and host transfer in Xenopus laevis. *Biol. Open* 1-6 (2015). Electronically Published Ahead of Print.

411. Salabi, F. *et al.* Myostatin knockout using zinc-finger nucleases promotes proliferation of ovine primary satellite cells in vitro. *J. Biotechnol.* **192A,** 268–280 (2014).

Appendix

A.1 Luciferase mRNA Sequences

Start Codons are highlighted in Green, stop codons in Red, and UTRs in Blue

A.1.1 Luc mRNA Without Untranslated Regions

5′GGGAGACCCAAGCUGGCUAGCGUUUAAACGGGCCCUCUAGACUCGAGCGGCCGCUCUAGGAAG
CUUUCCAUGGAAGACGCCAAAAACAUAAAGAAAGGCCCGGCGCCAUUCUAUCCGCUGGAAGAUGG
AACCGCUGGAGAGCAACUGCAUAAGGCUAUGAAGAGAUACGCCCUGGUUCCUGGAACAAUUGCUU
UUACAGAUGCACAUAUCGAGGUGGACAUCACUUACGCUGAGUACUUCGAAAUGUCCGUUCGGUUG
GCAGAAGCUAUGAAACGAUAUGGGCUGAAUACAAAUCACAGAAUCGUCGUAUGCAGUGAAAACUC
UCUUCAAUUCUUUAUGCCGGUGUUGGGCGCGUUAUUUAUCGGAGUUGCAGUUGCGCCCGCGAACG
ACAUUUAUAAUGAACGUGAAUUGCUCAACAGUAUGGGCAUUUCGCAGCCUACCGUGGUGUUCGUU
UCCAAAAAGGGGUUGCAAAAAAUUUUGAACGUGCAAAAAAAGCUCCCAAUCAUCCAAAAAAUUAU
UAUCAUGGAUUCUAAAACGGAUUACCAGGGAUUUCAGUCGAUGUACACGUUCGUCACAUCUCAUC
UACCUCCCGGUUUUAAUGAAUACGAUUUUGUGCCAGAGUCCUUCGAUAGGGACAAGACAAUUGCA
CUGAUCAUGAACUCCUCUGGAUCUACUGGUCUGCCUAAAGGUGUCGCUCUGCCUCAUAGAACUGC
CUGCGUGAGAUUCUCGCAUGCCAGAGAUCCUAUUUUUGGCAAUCAAAUCAUUCCGGAUACUGCGA
UUUUAAGUGUUGUUCCAUUCCAUCACGGUUUUGGAAUGUUUACUACACUCGGAUAUUUGAUAUGU
GGAUUUCGAGUCGUCUUAAUGUAUAGAUUUGAAGAAGAGCUGUUUCUGAGGAGCCUUCAGGAUUA
CAAGAUUCAAAGUGCGCUGCUGGUGCCAACCCUAUUCUCCUUCUUCGCCAAAAGCACUCUGAUUG
ACAAAUACGAUUUAUCUAAUUUACACGAAAUUGCUUCUGGUGGCGCUCCCCUCUCUAAGGAAGUC
GGGGAAGCGGUUGCCAAGAGGUUCCAUCUGCCAGGUAUCAGGCAAGGAUAUGGGCUCACUGAGAC
UACAUCAGCUAUUCUGAUUACACCCGAGGGGGAUGAUAAACCGGGCGCGGUCGGUAAAGUUGUUC
CAUUUUUUGAAGCGAAGGUUGUGGAUCUGGAUACCGGGAAAACGCUGGGCGUUAAUCAAAGAGGC
GAACUGUGUGUGAGAGGUCCUAUGAUUAUGUCCGGUUAUGUAAACAAUCCGGAAGCGACCAACGC
CUUGAUUGACAAGGAUGGAUGGCUACAUUCUGGAGACAUAGCUUACUGGGACGAAGACGAACACU
UCUUCAUCGUUGACCGCCUGAAGUCUCUGAUUAAGUACAAAGGCUAUCAGGUGGCUCCCGCUGAA
UUGGAAUCCAUCUUGCUCCAACACCCCAACAUCUUCGACGCAGGUGUCGCAGGUCUUCCCGACGA
UGACGCCGGUGAACUUCCCGCCGCCGUUGUUGUUUUGGAGCACGGAAAGACGAUGACGGAAAAAG
AGAUCGUGGAUUACGUCGCCAGUCAAGUAACAACCGCGAAAAAGUUGCGCGGAGGAGUUGUGUUU
GUGGACGAAGUACCGAAAGGUCUUACCGGAAAACUCGACGCAAGAAAAAUCAGAGAGAUCCUCAU
AAAGGCCAAGAAGGGCGGAAAGAUCGCCGUGUAAUUCUAGACCAGGCGCCUGGAUCCGAGCUCGG
UACCAAG 3′

A.1.2 Luc-UTR, With Untranslated Regions

5′GGGAGACCCAAGCUGGCUAGCGUUUAAACGGGCCCUCUAGAACAUUUGCUUCUGACACAACUG
UGUUCACUAGCAACCUCAAACAGACACCGCCGCCACCAUGGAGGACGCCAAGAAUAUCAAGAAAG
GCCCCGCUCCCUUCUACCCCCUGGAAGACGGCACAGCCGGCGAACAACUCCACAAGGCCAUGAAG
AGGUAUGCCCUGGUCCCCGGAACCAUCGCCUUCACCGAUGCCCAUAUCGAGGUCGACAUCACCUA
CGCUGAGUACUUCGAGAUGUCCGUCAGGCUCGCCGAGGCUAUGAAGAGAUAUGGCCUCAACACCA
ACCACAGGAUCGUGGUCUGCUCCGAGAACUCCCUGCAGUUUUUCAUGCCCGUGCUGGGCGCCCUG
UUUAUCGGAGUCGCCGUCGCCCCCGCUAACGACAUCUACAACGAGAGAGAGCUCCUGAACAGCAU
GGGCAUUUCCCAGCCUACCGUGGUCUUCGUGAGCAAGAAAGGCCUCCAGAAGAUCCUGAACGUCC

AAAAGAAGCUGCCCAUUAUCCAGAAGAUCAUCAUCAUGGAUAGCAAGACCGACUACCAGGGAUUC
CAGUCCAUGUACACCUUCGUGACAAGCCAUCUGCCCCCCGGCUUCAACGAGUAUGACUUCGUCCC
CGAGUCCUUCGACAGAGACAAGACCAUCGCCCUGAUCAUGAACUCCUCCGGAAGCACCGGACUGC
CCAAAGGCGUGGCUCUCCCUCACAGGACCGCUUGUGUCAGGUUCAGCCACGCCAGGGACCCCAUC
UUCGGCAACCAGAUCAUCCCCGACACAGCUAUCCUCAGCGUGGUGCCCUUCCACCACGGCUUCGG
AAUGUUCACCACCCUCGGCUACCUCAUCUGUGGCUUCAGAGUGGUGCUCAUGUACAGAUUCGAGG
AGGAGCUGUUUCUGAGGUCCCUCCAGGACUACAAAAUCCAAUCCGCUCUGCUCGUCCCCACCCUG
UUCAGCUUCUUCGCCAAAAGCACCCUGAUCGACAAGUAUGACCUCUCCAACCUGCAUGAGAUCGC
CAGCGGAGGAGCCCCUCUGUCCAAGGAGGUCGGCGAAGCCGUGGCUAAGAGGUUUCACCUCCCUG
GCAUUAGGCAAGGAUACGGCCUGACCGAAACCACAAGCGCUAUCCUGAUCACCCCUGAGGGAGAC
GACAAACCCGGAGCCGUCGGAAAGGUCGUCCCCUUCUUCGAGGCCAAGGUGGUCGACCUGGACAC
CGGCAAGACCCUGGGCGUGAACCAAAGGGGCGAACUCUGUGUGAGGGGCCCUAUGAUCAUGAGCG
GCUACGUCAACAACCCUGAGGCUACCAACGCUCUCAUCGACAAGGAUGGCUGGCUGCACUCCGGA
GAUAUCGCCUACUGGGACGAGGAUGAGCAUUUUUUUAUCGUCGAUAGGCUCAAGAGCCUGAUCAA
GUACAAGGGCUACCAGGUGGCCCCUGCUGAGCUCGAAUCCAUCCUGCUCCAGCACCCUAACAUCU
UUGACGCUGGCGUGGCUGGACUGCCUGACGACGACGCUGGCGAACUCCCUGCCGCUGUCGUGGUC
CUCGAACACGGCAAGACAAUGACCGAGAAGGAGAUCGUGGACUACGUGGCCUCCCAAGUGACAAC
AGCCAAGAAGCUGAGAGGCGGAGUGGUGUUCGUGGACGAGGUGCCCAAGGGCCUGACAGGCAAGC
UCGACGCUAGAAAGAUCAGGGAGAUUCUGAUUAAAGCCAAAAAGGGCGGAAAGAUUGCCGUGUGA
UGAGCUCGCUUUCUUGCUGUCCAAUUUCUAUUAAAGGUUCCUUUGUUCCGUAAGUCCAACUACUA
AACUGGGGGAUAUUAUGAAGGGCCUUGAGCAUCUGGAUUCUGCCUAAUAAAAAACAUUUAUUUUC
AUUGCGGAUCCGAGCUCGGUACCAAG 3′

A.2 PLA2 Gene Sequences

Pre- and Pro-Peptides are highlighted in Yellow, the Active Site Histidine is highlighted in Green, Nuclear Localizing Sequences are highlighted in Blue. Translated amino acid sequences are provided below the DNA sequence.

A.2.1 BVM Bee Venom PLA2, Mature Sequence

ATGGTCATCTACCCCGGCACCCTGTGGTGCGGCCACGGCAACAAAAGCAGCGGCCCTAATGAG
 M V I Y P G T L W C G H G N K S S G P N E
CTGGGCCGGTTCAAGCACACCGACGCCTGCTGCAGAACCCACGACATGTGCCCCGACGTGATG
 L G R F K H T D A C C R T H D M C P D V M
TCTGCCGGCGAGTCTAAGCACGGCCTGACCAATACCGCCAGCCACACCAGACTGAGCTGCGAC
 S A G E S K H G L T N T A S H T R L S C D
TGCGACGACCAGTTCTACGACTGCCTGAAGAACAGCGCCGACACCATCAGCAGCTACTTCGTG
 C D D Q F Y D C L K N S A D T I S S Y F V
GGCAAGATGTACTTCAACCTGATCGACACCAAGTGCTACAAGCTGGAACACCCCGTGACCGGC
 G K M Y F N L I D T K C Y K L E H P V T G
TGCGGCGAGAGAACAGAGGGAAGATGCCTGCACTACACCGTGGACAAGAGCAAGCCCAAGGTG
 C G E R T E G R C L H Y T V D K S K P K V
TACCAGTGGTTCGACCTGCGGAAGTACTAA
 Y Q W F D L R K Y

A.2.2 BVM-NLS, Mature Bee Venom PLA2, With Nuclear Localizing Sequence

```
ATGGTCATCTACCCCGGCACCCTGTGGTGCGGCCACGGCAACAAAAGCAGCGGCCCTAATGAG
 M  V  I  Y  P  G  T  L  W  C  G  H  G  N  K  S  S  G  P  N  E
CTGGGCCGGTTCAAGCACACCGACGCCTGCTGCAGAACCCACGACATGTGCCCCGACGTGATG
 L  G  R  F  K  H  T  D  A  C  C  R  T  H  D  M  C  P  D  V  M
TCTGCCGGCGAGTCTAAGCACGGCCTGACCAATACCGCCAGCCACACCAGACTGAGCTGCGAC
 S  A  G  E  S  K  H  G  L  T  N  T  A  S  H  T  R  L  S  C  D
TGCGACGACCAGTTCTACGACTGCCTGAAGAACAGCGCCGACACCATCAGCAGCTACTTCGTG
 C  D  D  Q  F  Y  D  C  L  K  N  S  A  D  T  I  S  S  Y  F  V
GGCAAGATGTACTTCAACCTGATCGACACCAAGTGCTACAAGCTGGAACACCCCGTGACCGGC
 G  K  M  Y  F  N  L  I  D  T  K  C  Y  K  L  E  H  P  V  T  G
TGCGGCGAGAGAACAGAGGGAAGATGCCTGCACTACACCGTGGACAAGAGCAAGCCCAAGGTG
 C  G  E  R  T  E  G  R  C  L  H  Y  T  V  D  K  S  K  P  K  V
TACCAGTGGTTCGACCTGCGGAAGTACCCCAAGAAAAAGCGGAAGGTGTAA
 Y  Q  W  F  D  L  R  K  Y  P  K  K  K  R  K  V
```

A.2.3 BV-NLS, Immature Bee Venom PLA2, With Nuclear Localizing Sequence

```
ATGGAGGTGGTGCTGGGCAGCCTGTTCCTGCTGCTGCTGAGCACATCTCACGGCTGGCAGATC
 M  E  V  V  L  G  S  L  F  L  L  L  L  S  T  S  H  G  W  Q  I
CGGGACCGGATCGGCGACAACGAGCTGGAAGAGAGAATCATCTACCCCGGCACCCTGTGGTGC
 R  D  R  I  G  D  N  E  L  E  E  R  I  I  Y  P  G  T  L  W  C
GGCCACGGCAACAAAAGCAGCGGCCCTAATGAGCTGGGCCGGTTCAAGCACACCGACGCCTGC
 G  H  G  N  K  S  S  G  P  N  E  L  G  R  F  K  H  T  D  A  C
TGCAGAACCCACGACATGTGCCCCGACGTGATGTCTGCCGGCGAGTCTAAGCACGGCCTGACC
 C  R  T  H  D  M  C  P  D  V  M  S  A  G  E  S  K  H  G  L  T
AATACCGCCAGCCACACCAGACTGAGCTGCGACTGCGACGACAAGTTCTACGACTGCCTGAAG
 N  T  A  S  H  T  R  L  S  C  D  C  D  D  K  F  Y  D  C  L  K
AACAGCGCCGACACCATCAGCAGCTACTTCGTGGGCAAGATGTACTTCAACCTGATCGACACC
 N  S  A  D  T  I  S  S  Y  F  V  G  K  M  Y  F  N  L  I  D  T
AAGTGCTACAAGCTGGAACACCCCGTGACCGGCTGCGGCGAGAGAACAGAGGGAAGATGCCTG
 K  C  Y  K  L  E  H  P  V  T  G  C  G  E  R  T  E  G  R  C  L
CACTACACCGTGGACAAGAGCAAGCCCAAGGTGTACCAGTGGTTCGACCTGCGGAAGTACCCC
 H  Y  T  V  D  K  S  K  P  K  V  Y  Q  W  F  D  L  R  K  Y  P
AAGAAAAAGCGGAAGGTGTAA
 K  K  K  R  K  V
```

A.2.4 H34Q, Mature Bee Venom PLA2 With Nuclear Localizing Sequence and Active Site Mutation

```
ATGGTCATCTACCCCGGCACCCTGTGGTGCGGCCACGGCAACAAAAGCAGCGGCCCTAATGAG
 M  V  I  Y  P  G  T  L  W  C  G  H  G  N  K  S  S  G  P  N  E
CTGGGCCGGTTCAAGCACACCGACGCCTGCTGCAGAACCCAGGACATGTGCCCCGACGTGATG
 L  G  R  F  K  H  T  D  A  C  C  R  T  Q  D  M  C  P  D  V  M
TCTGCCGGCGAGTCTAAGCACGGCCTGACCAATACCGCCCGCCACACCAGACTGAGCTGCGAC
 S  A  G  E  S  K  H  G  L  T  N  T  A  R  H  T  R  L  S  C  D
TGCGACGACCAGTTCTACGACTGCCTGAAGAACAGCGCCGACACCATCAGCAGCTACTTCGTG
```

```
 C  D  D  Q  F  Y  D  C  L  K  N  S  A  D  T  I  S  S  Y  F  V
GGCAAGATGTACTTCAACCTGATCGACACCAAGTGCTACAAGCTGGAACACCCCGTGACCGGC
 G  K  M  Y  F  N  L  I  D  T  K  C  Y  K  L  E  H  P  V  T  G
TGCGGCGAGAGAACAGAGGGAAGATGCCTGCACTACACCGTGGACAAGAGCAAGCCCAAGGTG
 C  G  E  R  T  E  G  R  C  L  H  Y  T  V  D  K  S  K  P  K  V
TACCAGTGGTTCGACCTGCGGAAGTACCCCAAGAAAAAGCGGAAGGTGTAA
 Y  Q  W  F  D  L  R  K  Y  P  K  K  K  R  K  V
```

A.2.5 C37A, Mature Bee Venom PLA2 With Nuclear Localizing Sequence and Cysteine 37 Mutated to Alanine

```
ATGGTCATCTACCCCGGCACCCTGTGGTGCGGCCACGGCAACAAAAGCAGCGGCCCTAATGAG
 M  V  I  Y  P  G  T  L  W  C  G  H  G  N  K  S  S  G  P  N  E
CTGGGCCGGTTCAAGCACACCGACGCCTGCTGCAGAACCCACGACATGGCCCCCGACGTGATG
 L  G  R  F  K  H  T  D  A  C  C  R  T  H  D  M  A  P  D  V  M
TCTGCCGGCGAGTCTAAGCACGGCCTGACCAATACCGCCAGCCACACCAGACTGAGCTGCGAC
 S  A  G  E  S  K  H  G  L  T  N  T  A  S  H  T  R  L  S  C  D
TGCGACGACCAGTTCTACGACTGCCTGAAGAACAGCGCCGACACCATCAGCAGCTACTTCGTG
 C  D  D  Q  F  Y  D  C  L  K  N  S  A  D  T  I  S  S  Y  F  V
GGCAAGATGTACTTCAACCTGATCGACACCAAGTGCTACAAGCTGGAACACCCCGTGACCGGC
 G  K  M  Y  F  N  L  I  D  T  K  C  Y  K  L  E  H  P  V  T  G
TGCGGCGAGAGAACAGAGGGAAGATGCCTGCACTACACCGTGGACAAGAGCAAGCCCAAGGTG
 C  G  E  R  T  E  G  R  C  L  H  Y  T  V  D  K  S  K  P  K  V
TACCAGTGGTTCGACCTGCGGAAGTACCCCAAGAAAAAGCGGAAGGTGTAA
 Y  Q  W  F  D  L  R  K  Y  P  K  K  K  R  K  V
```

A.2.6 C113A, Mature Bee Venom PLA2 With Nuclear Localizing Sequence and Cysteine 113 Mutated to Alanine

```
ATGGTCATCTACCCCGGCACCCTGTGGTGCGGCCACGGCAACAAAAGCAGCGGCCCTAATGAG
 M  V  I  Y  P  G  T  L  W  C  G  H  G  N  K  S  S  G  P  N  E
CTGGGCCGGTTCAAGCACACCGACGCCTGCTGCAGAACCCACGACATGTGCCCCGACGTGATG
 L  G  R  F  K  H  T  D  A  C  C  R  T  H  D  M  C  P  D  V  M
TCTGCCGGCGAGTCTAAGCACGGCCTGACCAATACCGCCAGCCACACCAGACTGAGCTGCGAC
 S  A  G  E  S  K  H  G  L  T  N  T  A  S  H  T  R  L  S  C  D
TGCGACGACCAGTTCTACGACTGCCTGAAGAACAGCGCCGACACCATCAGCAGCTACTTCGTG
 C  D  D  Q  F  Y  D  C  L  K  N  S  A  D  T  I  S  S  Y  F  V
GGCAAGATGTACTTCAACCTGATCGACACCAAGTGCTACAAGCTGGAACACCCCGTGACCGGC
 G  K  M  Y  F  N  L  I  D  T  K  C  Y  K  L  E  H  P  V  T  G
TGCGGCGAGAGAACAGAGGGAAGAGCCCTGCACTACACCGTGGACAAGAGCAAGCCCAAGGTG
 C  G  E  R  T  E  G  R  A  L  H  Y  T  V  D  K  S  K  P  K  V
TACCAGTGGTTCGACCTGCGGAAGTACCCCAAGAAAAAGCGGAAGGTGTAA
 Y  Q  W  F  D  L  R  K  Y  P  K  K  K  R  K  V
```

A.2.7 G3, Human Group III Secreted PLA2, Middle Domain

```
ATGGGATGGACCATGCCTGGCACACTGTGGTGTGGAGTTGGAGATTCTGCTGGGAACTCCTCG
 M  G  W  T  M  P  G  T  L  W  C  G  V  G  D  S  A  G  N  S  S
GAGCTGGGGGGTCTTCCAGGGACCTGATCTCTGTTGCCGGGAACATGACCGCTGCCCACAGAAC
 E  L  G  G  V  F  Q  G  P  D  L  C  C  R  E  H  D  R  C  P  Q  N
ATCTCACCCTTGCAGTACAACTATGGCATCCGAAACTACCGATTCCACACCATCTCCCACTGT
 I  S  P  L  Q  Y  N  Y  G  I  R  N  Y  R  F  H  T  I  S  H  C
GACTGTGACACCAGGTTTCAGCAATGCCTACAGAATCAGCACGACTCCATCTCGGACATCGTG
 D  C  D  T  R  F  Q  Q  C  L  Q  N  Q  H  D  S  I  S  D  I  V
GGCGTGGCCTTCTTCAACGTGCTGGAGATCCCCTGCTTTGTGCTGGAGGAGCAGGAGGCGTGT
 G  V  A  F  F  N  V  L  E  I  P  C  F  V  L  E  E  Q  E  A  C
GTGGCGTGGTACTGGTGGGGCGGGTGTAGGATGTACGGCACAGTGCCCCTCGCTCGCCTGCAG
 V  A  W  Y  W  W  G  G  C  R  M  Y  G  T  V  P  L  A  R  L  Q
CCCAGGACCTTCTACAATGCCTCCTGGAGCTCCCGGGCCACCTCCCCAACTTAA
 P  R  T  F  Y  N  A  S  W  S  S  R  A  T  S  P  T
```

A.2.8 G10, Immature Human Group X Secreted PLA2, With Nuclear Localizing Sequence

```
ATGGGTCCGCTGCCGGTTTGTCTGCCGATTATGTTATTACTGCTGCTGCCGAGCCTTCTTTTG
 M  G  P  L  P  V  C  L  P  I  M  L  L  L  L  L  P  S  L  L  L
CTTCTGCTGCTGCCTGGTCCGGGTAGCGGTGAAGCAAGCCGTATTCTGCGTGTTCATCGTCGT
 L  L  L  L  P  G  P  G  S  G  E  A  S  R  I  L  R  V  H  R  R
GGTATTCTGGAACTGGCAGGCACCGTTGGTTGTGTTGGTCCGCGTACCCCGATTGCATATATG
 G  I  L  E  L  A  G  T  V  G  C  V  G  P  R  T  P  I  A  Y  M
AAATATGGTTGTTTTTGTGGCCTGGGTGGTCATGGTCAGCCTCGTGATGCAATTGATTGGTGT
 K  Y  G  C  F  C  G  L  G  G  H  G  Q  P  R  D  A  I  D  W  C
TGCCATGGTCATGATTGTTGTTATACCCGTGCAGAAGAAGCAGGTTGTAGCCCGAAAACCGAA
 C  H  G  H  D  C  C  Y  T  R  A  E  E  A  G  C  S  P  K  T  E
CGTTATAGCTGGCAGTGTGTTAATCAGAGCGTTCTGTGTGGTCCGGCAGAAAACAAATGTCAA
 R  Y  S  W  Q  C  V  N  Q  S  V  L  C  G  P  A  E  N  K  C  Q
GAACTGCTGTGTAAATGCGATCAAGAAATTGCAAATTGTCTGGCCCAGACCGAATATAATCTG
 E  L  L  C  K  C  D  Q  E  I  A  N  C  L  A  Q  T  E  Y  N  L
AAATACCTGTTTTATCCGCAGTTTCTGTGTGAACCGGATAGTCCGAAATGTGATGGATCCCCC
 K  Y  L  F  Y  P  Q  F  L  C  E  P  D  S  P  K  C  D  G  S  P
AAAAAGAAGCGGAAGGTATAA
 K  K  K  R  K  V
```